DESIGN METHODS FOR LARGE RECTANGULAR INDUSTRIAL DUCTS

By

THARANI THANGA B.Sc.(Hons.), M.A.Sc., P.Eng., P.E.

A Thesis

Submitted to the School of Graduate Studies in Partial Fulfillment of the Requirements for the Degree

Doctor of Philosophy

McMaster University

DOCTOR OF PHILOSOPHY (2012)
(Civil Engineering)

McMaster University
Hamilton, Ontario

TITLE: Design Methods for Large Rectangular Industrial Ducts

AUTHOR: Tharani Thanga

B.Sc. Eng.(Hons) (University of Peradeniya), M.A.Sc. (McMaster University)

ADVISORS: Prof. Ken Siva Sivakumaran

Dr. Bassam Halabieh

NUMBER OF PAGES: xiii, 328

ABSTRACT

A large rectangular industrial duct consists of plates stiffened with parallel wide flange sections. The plates along with stiffeners acts to resist the pressure loads and to carry other loads to the supports. The behaviours of the components of large industrial ducts are significantly different from the behaviours on which the current design methods are based on. Investigation presented herein deals with the design methods for spacing stiffeners, proportioning stiffeners and calculating shear resistance of side panel.

Current method of spacing stiffeners is based on large deflection plate theory. A parametric study was conducted on dimensionless parameters identified in order to benefit from membrane action in partially yielding plate for spacing stiffeners. Design equations were established in terms of dimensionless pressure, plate slenderness and normalized out-of-plane deflection for three cases namely; 0%, 16.5% and 33% of through thickness yielding of the plate. Results show that approximately 50% increase in stiffener spacing when yielding of 16.5% of thickness is permitted.

Under suction type pressure load, the unsupported compression flange and restrained tension flange lead to distortional buckling of the stiffeners. The current methods do not address distortional buckling adequately. A parametric study on dimensionless parameters governing the behaviour and strength of stiffened plat panels was conducted. The study indicated that the behaviour and strength of the stiffened panels could be a function of web slenderness and overall slenderness of the stiffener. The study also identified the slenderness limit of stiffener web for which the stiffener reaches the yield moment capacity. This study demonstrated the conservatism of current method. Finally a method was established to calculate the strength of stiffened plate panel subjected lateral pressure.

Side panels adjacent to the supports transfer large amount of shear to the supports and, in addition, resist internal pressure. Currently the design of side panels for shear is based on the methods used for the web of fabricated plate girders. The behaviour and the characteristics between the web of plate girder and the thin side panels are significantly different. A parametric study was conducted on dimensionless parameters identified. It was concluded that the plate slenderness dominates the normalized shear strength of stockier side panels. The aspect ratio and plate slenderness influence the normalized shear strength of slender side panels. Design methods to calculate the shear strength of side panels were proposed.

ACKNOWLEDGEMENTS

First and foremost I wish to extend my sincere thank to my co-advisor **Dr. Bassam Halabieh** for guiding and sharing his immense experiences and knowledge in this subject. His many years of practical experiences in analysing and designing large industrial ducts raised the scopes of this study and were valuable inputs for successfully completing this study. His readiness and willingness to apply the findings of this study inspire me to keep busy myself for the rest of my life.

I especially want to acknowledge and thank my advisor **Prof. Ken Siva Sivakumaran** for his patient, precious guidance, valuable advice and systematic approach during this study. Furthermore, without Prof. Sivakumaran's gracious acceptance of my research interests during my master's and doctoral studies, I could never have had a chance to achieve a successful career in structural engineering.

Lastly and most importantly, a big thank to my wife, **Usitha**, for her understanding, support and endless love and a great thank to my sons, **Vipul** and **Sayal**, for many sacrifices they have made.

Tharani Thanga

To my elder brother **Thaya**:

For his Love, Support and Strength that have always been for me

TABLE OF CONTENTS

LIST OF TABLES

LIST OF FIGURES

Chapter 1: Introduction

1.1 Introduction

Many industrial processes such as coal power stations, industrial boiler applications and furnace off-gas systems, require a series of large rectangular duct system to transport large amount of air and flue-gases. Recent flue-gas emission reduction measures by national governments raised the requirements of the large duct systems for many existing and new industrial processes. As flue gas emission requirements add large precipitators and scrubbers to become part of duct systems, the design pressure increases significantly and large duct design becomes more complicated. In the last ten years, several large duct systems have been constructed. This unique structure is formed by plate surfaces stiffened with often parallel stiffeners.

The investigation presented herein deals with the design methods for components of the large rectangular duct systems. The design of large industrial ducts is not covered by any design standard. In addition, very little technical information has been published describing suitable analysis and design techniques for such structures. Current design methods commonly used for the duct components are adapted from other standards and limited previous publications. The major difficulty for an engineer in the analysis and design procedures of this unique structure is the uncertainty as to how the components should be designed. The behaviours of the components of large industrial ducts are significantly different from the behaviours on which the current design methods are based on.

The purpose of this chapter is to briefly describe the large rectangular duct system and the analysis and design methods currently used to design its components. The main chapters present the details associated with the investigations of the each component.

1.2 Large Rectangular Industrial Duct System

Large industrial processes require to transport large volume of hot air and flue gases in controlled manner between process equipments through a series of ducts system. Figure 1.1 illustrates the arrangement of a sample large rectangular duct structural system for an industrial process. The duct structural system associated with industrial applications are significantly large and in some ways unique structures. Though ducts having circular or rectangular cross sections are feasible, the large industrial ducts are often rectangular. The cross sectional dimensions of such industrial ducts may be in the range of 5m to 15m, sometimes even larger. Figure 1.2 shows an industrial duct during fabrication.

The large rectangular ducts are air tight conduits to transport air or flue gases under positive or negative pressure. The ducts are sometimes exposed to high temperature as well as the air or flue gases are transported at elevated temperature. In order to accommodate the expansion due to the temperature, expansions joints are introduced along the duct length. This creates independent pieces of ducts with own floating supports. Figure 1.3 illustrates a typical piece of large rectangular duct between two expansion joints.

A segment of rectangular duct is formed by welding together four flat side plate panels. Each side duct panel consists of a thin steel plate generally stiffened with stiffeners as shown in Figure 1.4. The thin plates that are stabilized in one direction by the stiffeners to form an integral part of large rectangular system in which a high strength-to-weight ratio is important. The plates of those large industrial ducts are generally stiffened with wide flange stiffeners in parallel configuration by wrapping around the duct as shown in Figure 1.3. The stiffeners are generally oriented perpendicular to flow direction. The typical connection between stiffener and plate is generally made by intermittent fillet welds that are staggered on either side of the stiffener as shown in Figure 1.5.

The duct system is designed to resist the following loads: (1) internal positive or negative pressure, (2) weight of the duct, insulation and lugging, (3) live loads such as wind, snow, seismic and ash loads (4) other loads such as thermal expansion or support reactions. The internal pressure load consists of two components; operating pressure, which is the expected pressure continuously acting on the wall, and transient pressure, which is the very high pressure for relatively very short period of time during an abnormal event.

The duct side panels are often joined longitudinally with angles or bent plates at the corner of the duct as shown in Figure 1.6. Corner angles provide air tight seal in addition to strength and stiffness. The stiffener and the plate act as one composite section to jointly resist the loads. In order to be a complete composite section, the attachment between the stiffener and the plate must have adequate strength enough to transfer horizontal shear arising between them due to bending. End connections of the wrapping

stiffeners on each ring are either pinned or fixed. The most common end connection would be pinned. There are many alternative ways to make a pinned connection and Figure 1.6 shows the typical end stiffener pinned connection. The large industrial duct should be able to transfer lateral loads to supports and keep the shape of the cross section. This can be achieved by internal bracings and struts members. Figure 1.7 shows the details of the bracing connection at support ring.

The support system of the duct should be able to accommodate the thermal expansion and contraction. Therefore, the supports associated a duct segment generally consist of pinned support, guide supports and roller support. Figure 1.8 shows typical support arrangement for a rectangular duct. The pinned support and the guide supports resist the lateral loads while maintaining the lateral stability and accommodating the thermal expansion. Figure 1.9, Figure 1.10 and Figure 1.11 show the typical pinned, guided and roller supports used in large industrial ducts.

1.3 Current Design Methods

The design process of the large rectangular ducts and their supports generally involves local structural analysis (stiffener and plate level) and global analysis (entire structure level) to predict their performance and verify their structural integrity. Determining the duct plate thickness, stiffener spacing, and proportioning of stiffener section are done based on local structural analysis. The global analysis of the large rectangular ducts is related to the methods of transferring all external and system loads to the supports by flexural behaviour. The duct cross section provides flexural stiffness in resisting bending stresses. The side panels of the duct segment transfer the gravity loads to the supports by shear. Therefore, the global analysis involves with flexural stiffness and strength of the duct cross section and shear resistance of the side panels.

In large rectangular ducts, the side plates act along with stiffener to resist the pressure forces and to carry gravity and external loads to the supports. The plate between parallel stiffeners is assumed to span and be supported by those stiffeners as shown in Figure 1.12. The stiffener spacing and plate thickness are determined by considering allowable stress and deflection of a unit width of plate strip between stiffeners subjected to the pressure load. The transient pressure load governs the plate design. The stress and deflection of the strip of the plate is generally calculated by considering large deflection plate theory to include the bending stress and diaphragm stress. Based on previous analytical studies, Roark's Formulas for Stress and Strain by Young (1989) provide simplified design tables which are currently used in the industry to establish stiffener spacing and plate thickness.

Having defined the stiffener spacing, the stiffener member is chosen to resist the governing load. The pressure inside the ducts may be positive or negative. The stiffener design is generally governed by the combination of transient internal pressure and wind load. The beam section is chosen by determining the capacity of the stiffened plate panel in composite action. In large industrial duct, the long stiffener span (5m to 15m or even larger) due and high internal pressure generally result in wide flanged beam stiffeners. As noted earlier, the pressure inside the duct may be positive or negative. Negative pressure acts to pull the stiffeners in, resulting in tension to flange attached to the plate and compression in outstanding flange. As the compression flange is not braced, the full span of the beam length is taken as unsupported length in the current design practice. On the other hand, under the positive pressure, the flange not connected to plate will be in tension and the plate in compression.

In the current design practice, a certain portion of plate and the corresponding stiffener is considered to act together as one composite section to resist pressure. The typical combined section due to the composite action between the plate and stiffener is shown in Figure 1.13. The design methods commonly used in industry for proportioning stiffeners are based on the steel structural member design method adapted from the standards. The method are somewhat modified to account the composite action between the stiffeners and plate and other unusual service conditions.

The global bending behavior of large rectangular duct is related to the cross sectional strength and stiffness of the duct to resist mainly the longitudinal stresses. Because of high slenderness ratio (height to thickness ratio) of the plate in rectangular duct, only portion of the plate at the corners would be effective in providing stiffness for the global behavior of the cross section. As mentioned before, the side panels are connected at corners usually with embedded longitudinal angles. Therefore, the effective area of the plate and the area of the angles are used to calculate the axial and flexural cross sectional properties for the global analysis. For this purpose, in industry, the effective section is usually assumed to be a plate width of certain times of plate thickness from the edge of the corner angles as shown in Figure 1.14.

Duct side walls consist of thin plate panels between parallel stiffeners. The vertical and other system related loads must be transferred to the side walls and then to the supports. The side panels transfer the loads to the supports by shear. For a long span duct, significant shear accumulates near the supports. In the current design method, the side plate panel between the stiffeners is considered as the web of a large fabricated plate girder with transverse stiffener in resisting shear. Therefore, the shear capacity of the side plate panels is calculated using the methods in the structural steel building design standards for the web of large fabricated plate girders. In this method, the contribution of shear buckling and diagonal tension field of the plate between stiffeners is considered in resisting shear.

1.4 Motivation

The questions arose during practical experiences gained in designing large rectangular industrial duct gave rise to the scope of this study. Although the large industrial duct has been designed for many years, the behavior and strength of its elements are still not understood well. Current analytical methods and provisions used to design large rectangular duct were found to be inadequate, inconsistent and very conservative in many cases. When working on some of the mega projects, it was found that many questions remained unanswered.

During the recent design of ducting for Ohio Sammis Coal Power plant in OH, USA, being the largest duct retro-fit known to date, tipping the scales at 44 million lbs of structural steel, reaching 2.8 km (1.75 linear miles) across Ohio's horizon and consisting ducts with the cross sectional dimensions up to 12.8 m (44 feet) in height and 6 m (20 feet) in width, it was observed proper understanding the behavior of the elements of large industrial duct may lead optimum design resulting huge capital savings in future mega projects.

The main drawback deterring engineers from using available design methods is uncertainty as to how the components of the large industrial rectangular ducts should be analyzed and designed. It is because the behaviours of the components of large industrial ducts are significantly different when compared to the behaviours on which the current design methods from the building design and bridge design standards are based on. The structural design and analysis of the components of large industrial duct system is not

covered by any specific standard. In addition, very little research studies has been published describing suitable analysis and design methods for large rectangular ducts. In short, the overall motivation of this research is to increase the understanding of the behavior of the components and to develop comprehensive methods to estimate their load carrying capacities.

1.5 Scope and Objectives

The primary objectives of the study are to understand the behaviour of the components of large rectangular industrial ducts and to propose effective design and analysis methods for such systems. Although the components of large rectangular industrial ducts have been designed over past several years, the stability aspects of the components are still not well understood. The structural analysis and design of these large industrial duct systems is not governed by any design standard and a little publication on structural analysis and design procedures is available. Number of parameters that dictate the behaviour of the components is too large to do limited tests. Therefore, there is a need to do large scale parametric study for each component. With the current finite element tools, more precise modeling of the components can be achieved. The residual stresses, initial geometric imperfections, boundary conditions, nonlinearities and other factors can be explicitly incorporated into numerical models. In this study, experimentally verified finite element modeling techniques will be used to perform extensive parametric studies for the behaviour of the components of industrial ducts and to derive method to calculate their strength. In this study, ADINA 8.5 has been selected to model and analyze the rectangular stiffened steel plate duct.

In this study, the scopes of the work include:

- Investigate the method of spacing stiffeners and the design of plating
- Investigate the behaviour and strength of plate stiffened with general steel sections by parametric studies
- Derive a method to calculate the flexural capacity of stiffened plate panels under negative pressure
- Study the behaviour of the side plate panels subjected to support shear and to propose a comprehensive method of estimating shear capacity of plate panels between stiffeners

The verified finite element modeling techniques are to be used extensively to study the behaviour and strength of the components of large rectangular industrial duct through the parametric studies. In order to assess all the parameters involved and reduce the number of parameters for the parametric studies, dimensional analysis will be done. However, the parametric studies would require hundreds of finite element analysis models. Therefore, in addition to above primary scopes, there are number of secondary scopes.

- Verify the finite element modeling techniques with the experimental and theoretical results available in literature.
- Develop external programming tools that will generate the numerical models instantly with basic information such as physical dimensions, material model type, analysis type , residual stress and initial geometric imperfection patterns, etc.

These studies considered only the static pressure loading conditions and the components are assumed to be at ambient temperature.

1.5 Organization of Thesis

This section provides an overview of the remaining thesis. The thesis consists of six chapters. Chapter 2 presents the details of study on the strength of plate and stiffener spacing and describes the proposed optimum method of spacing stiffeners. An example on stiffener spacing based on the proposed method is also presented. These results are valid for plate

Chapter 3 provides the review of the previously published researches in a chronological order and evaluates the methods for stiffener capacity in the literature and describes the nonlinear finite element modeling techniques applied for the model of stiffened plate panel. Finally, the modeling techniques are verified with full scale experimental results.

Chapter 4 presents the method of dimensional analysis in order to do a manageable parametric study. Two dimensionless parameters are identified to be dominant in affecting the behaviour of the stiffened plate panel subjected to lateral pressure load. Based on the results of the parametric study, a method to evaluate the bending capacity of the plate panel is presented.

Chapter 5 firstly describes a chronological review of earlier researches on plate subjected uniform shear, secondly presents the finite element model developed and the dimensionless parameters affecting the behaviour of the side panel subjected to shear and finally provides design methods to evaluate the shear capacity of the side panel based on the parametric study.

Chapter 6 provides a summary of the research conducted and presents the conclusions.

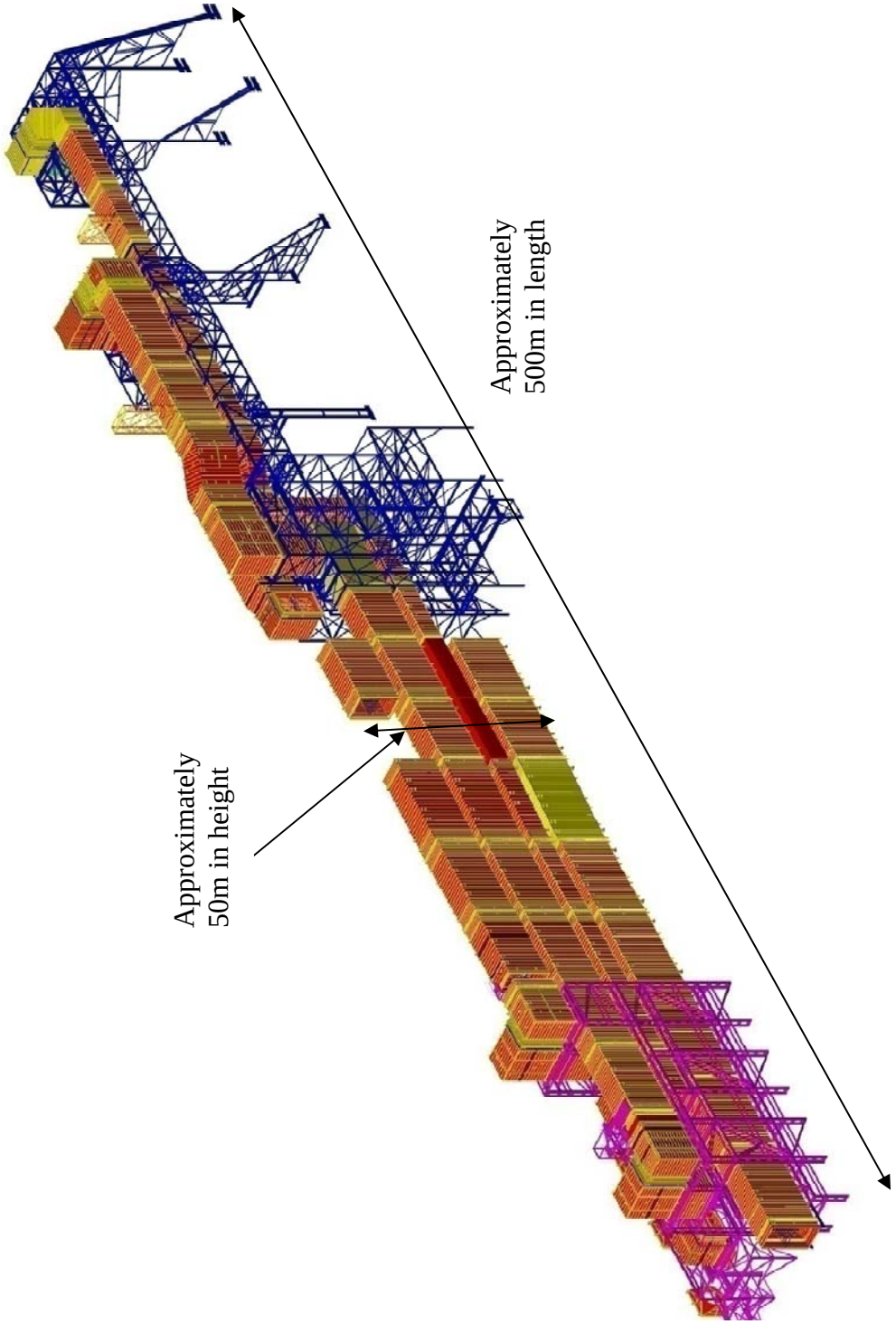

Figure 1.1 Sample Large Rectangular Industrial Duct System

Figure 1.2 Large Rectangular Industrial Duct During Fabrication

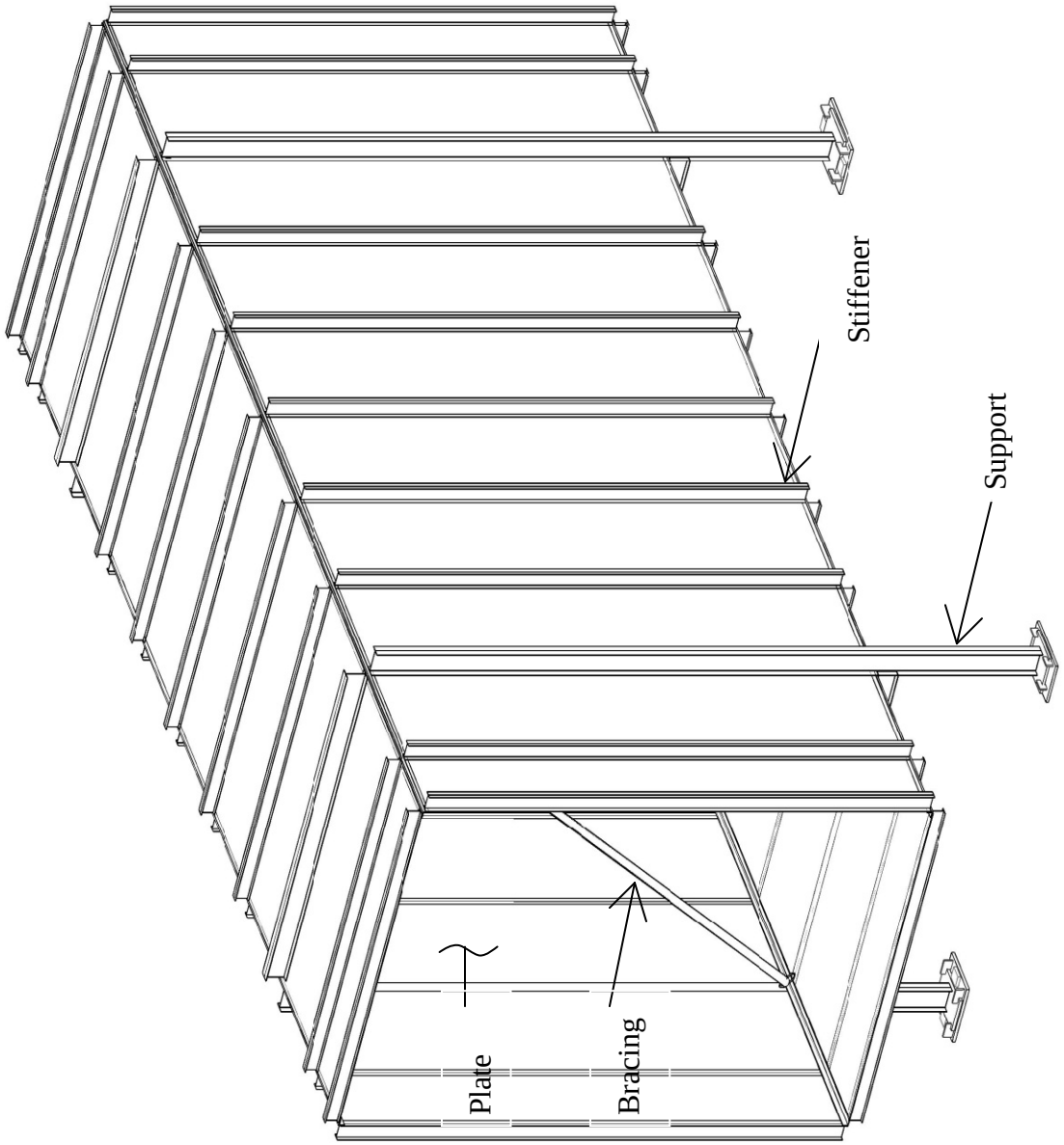

Figure 1.3 Isometric View of an Industrial Duct between Expansion Joints

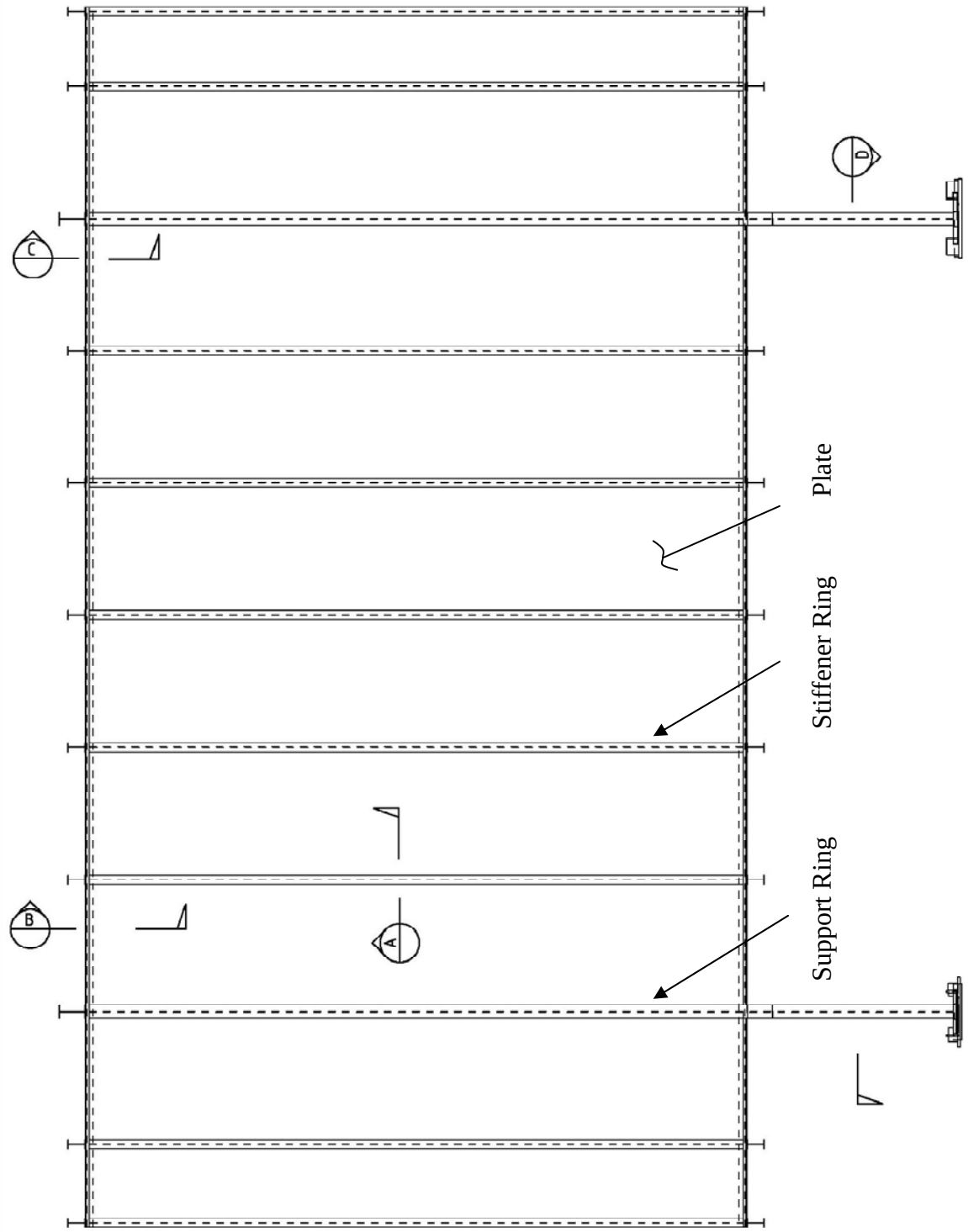

Figure 1.4 Elevation View of a Duct Segment

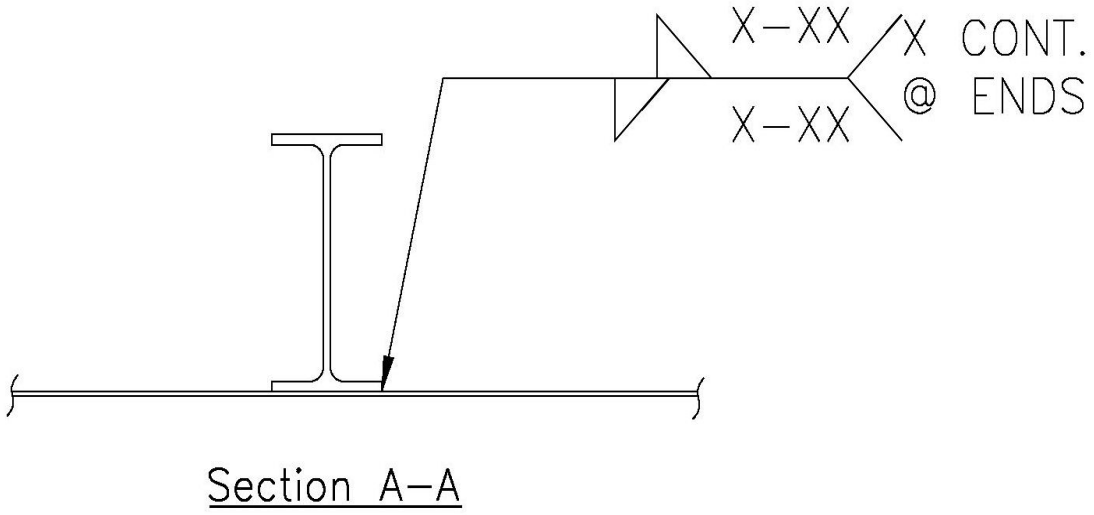

Figure 1.5 Typical Plate-Stiffener Welds

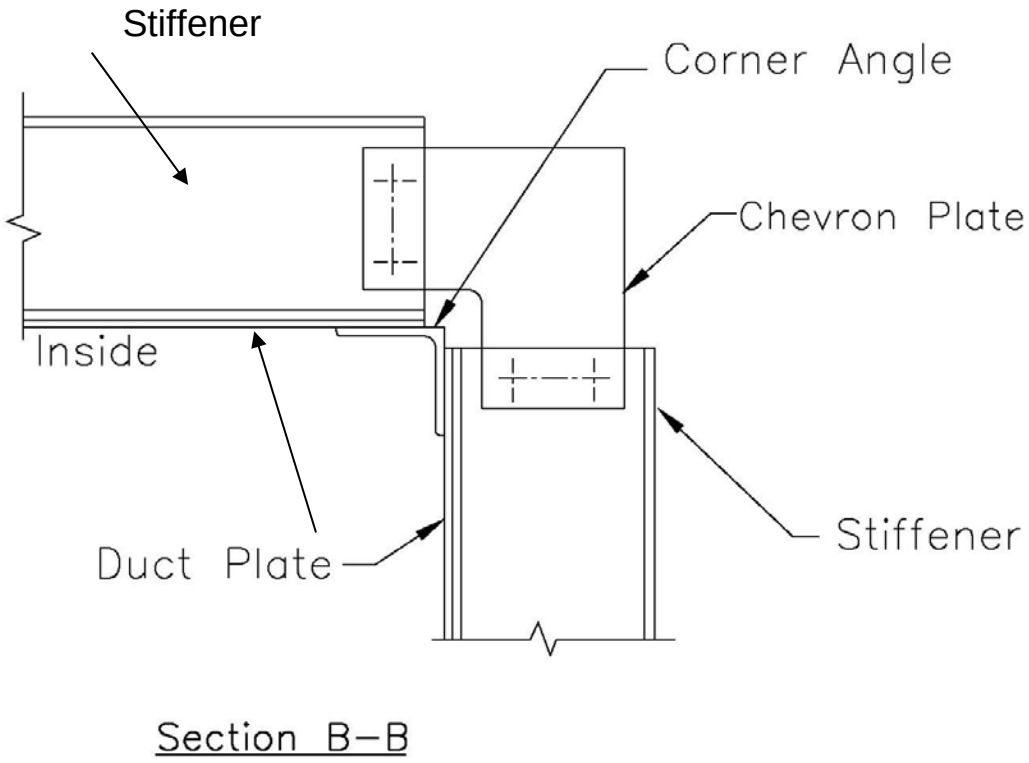

Figure 1.6 Typical Corner Detail

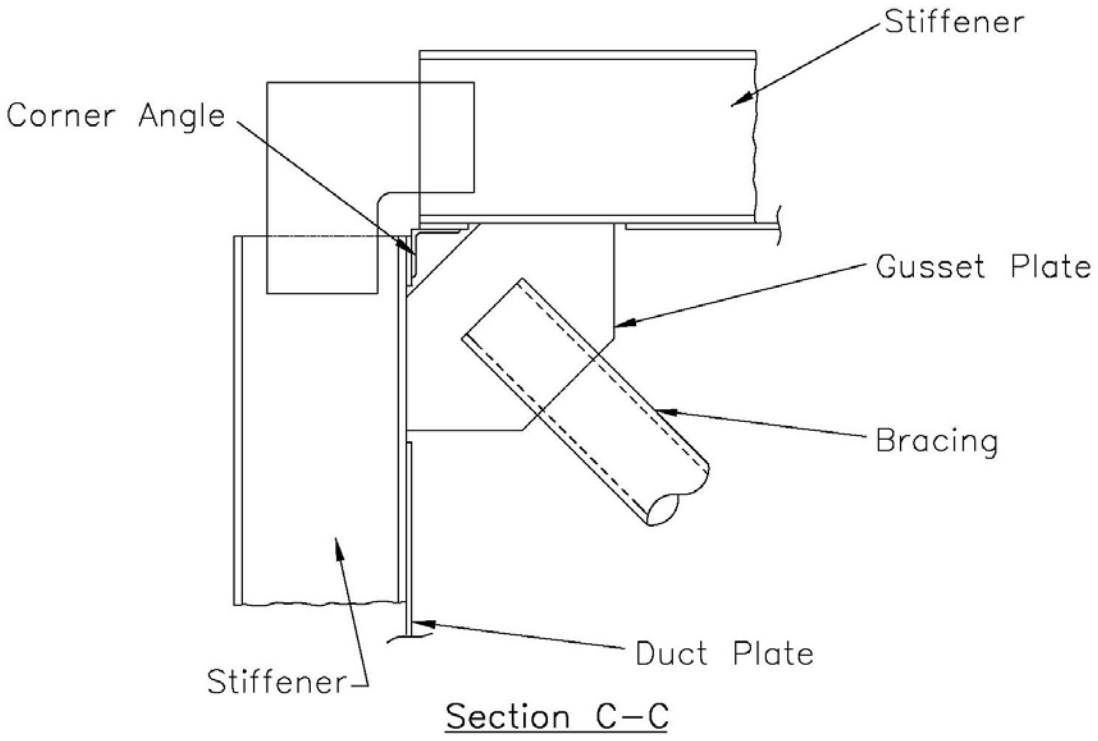

Figure 1.7 Corner Detail at a Support Ring Including Bracing

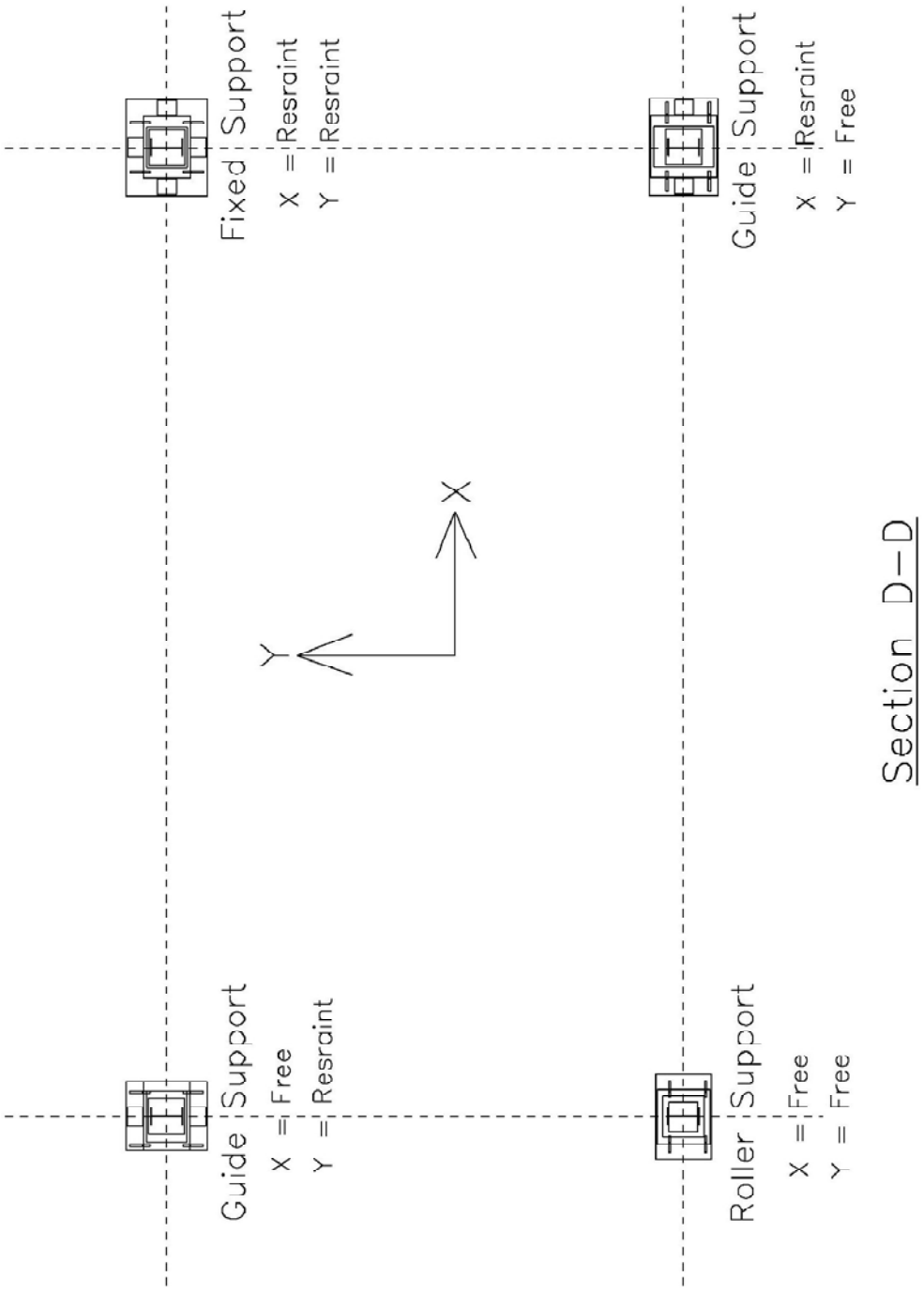

Figure 1.8 Support Arrangements

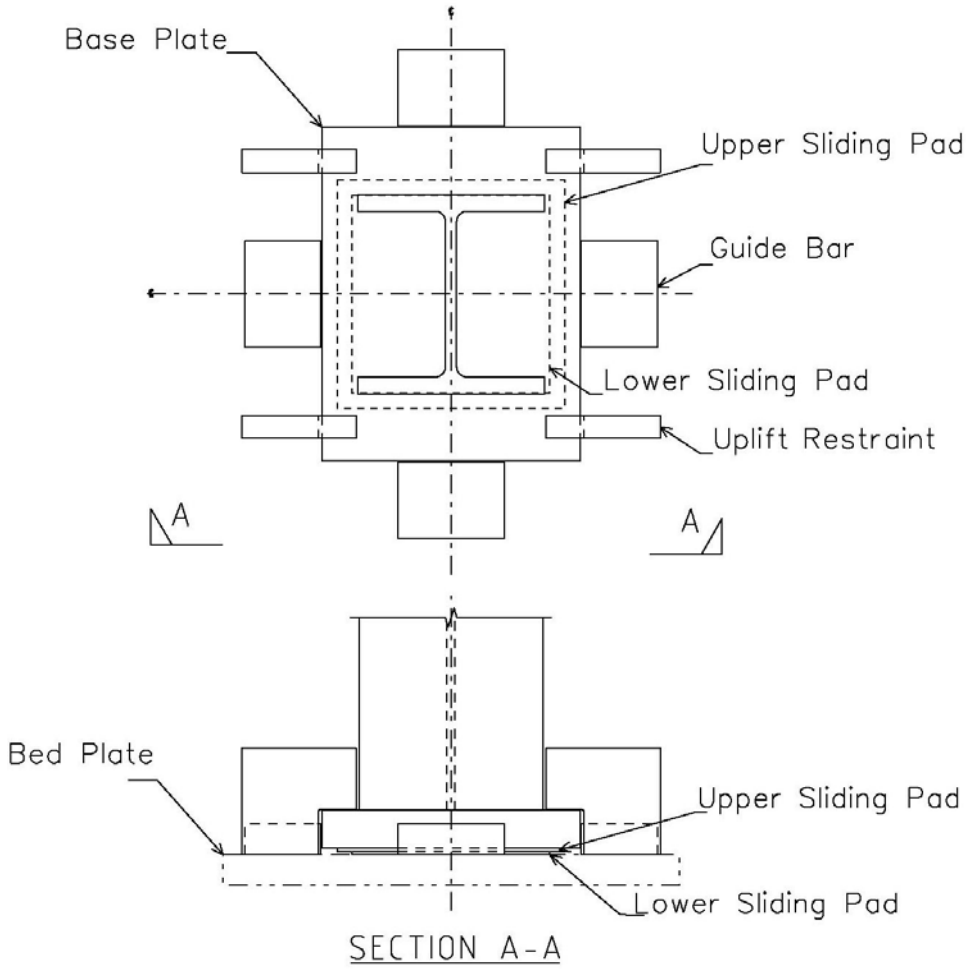

Figure 1.9 Typical Fixed Support

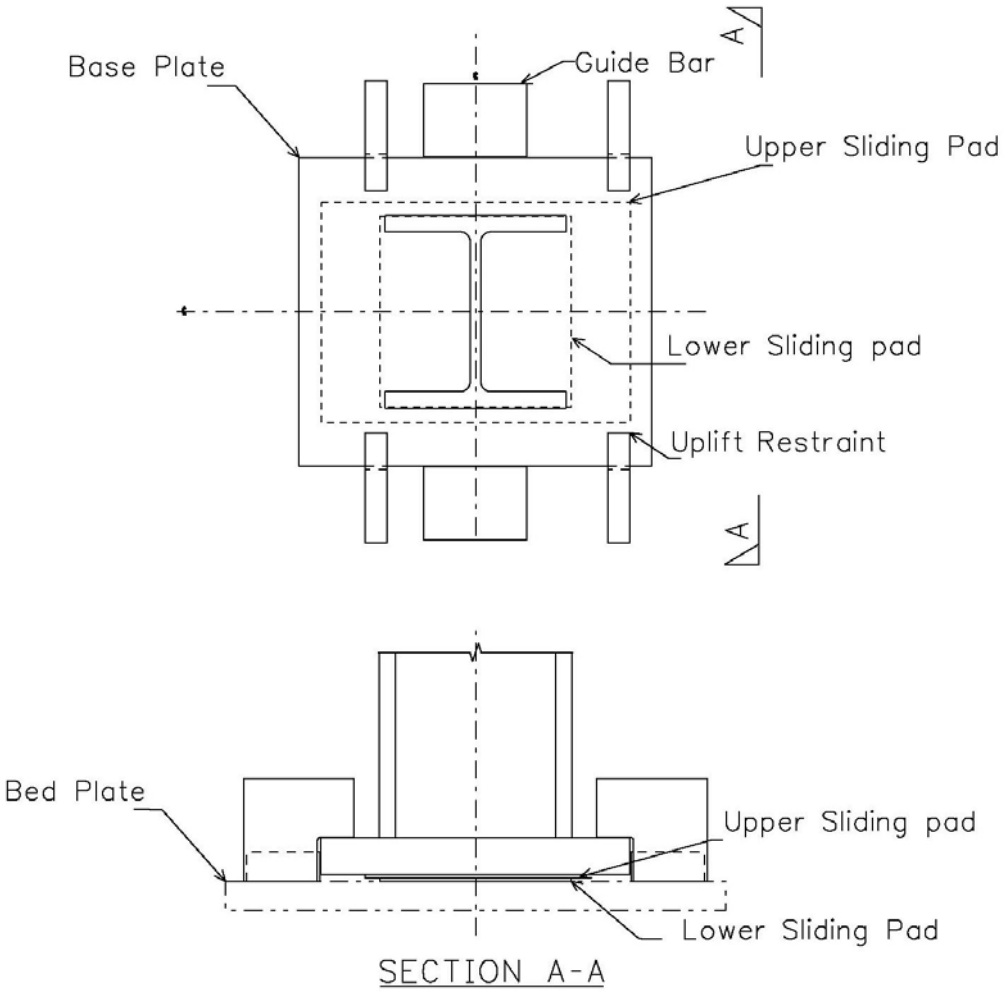

Figure 1.10 Typical Guide Support

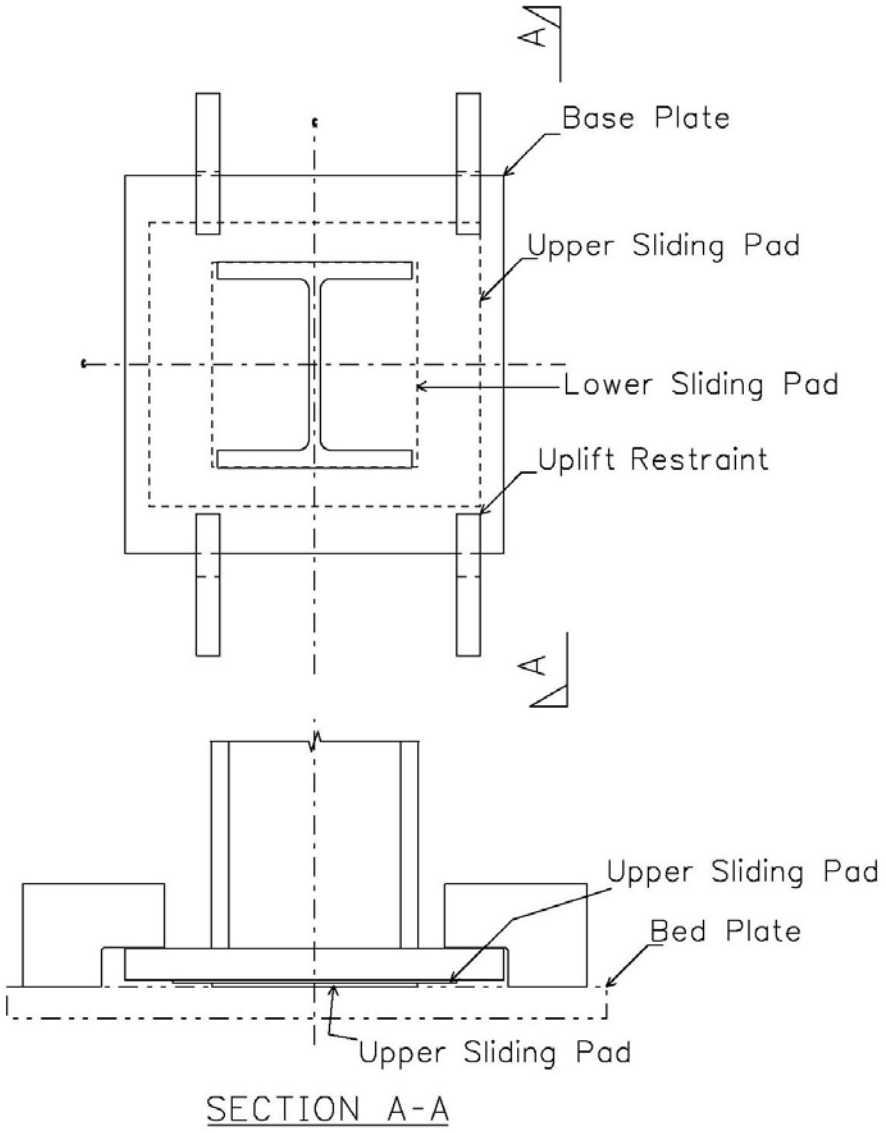

Figure 1.11 Typical Roller Support

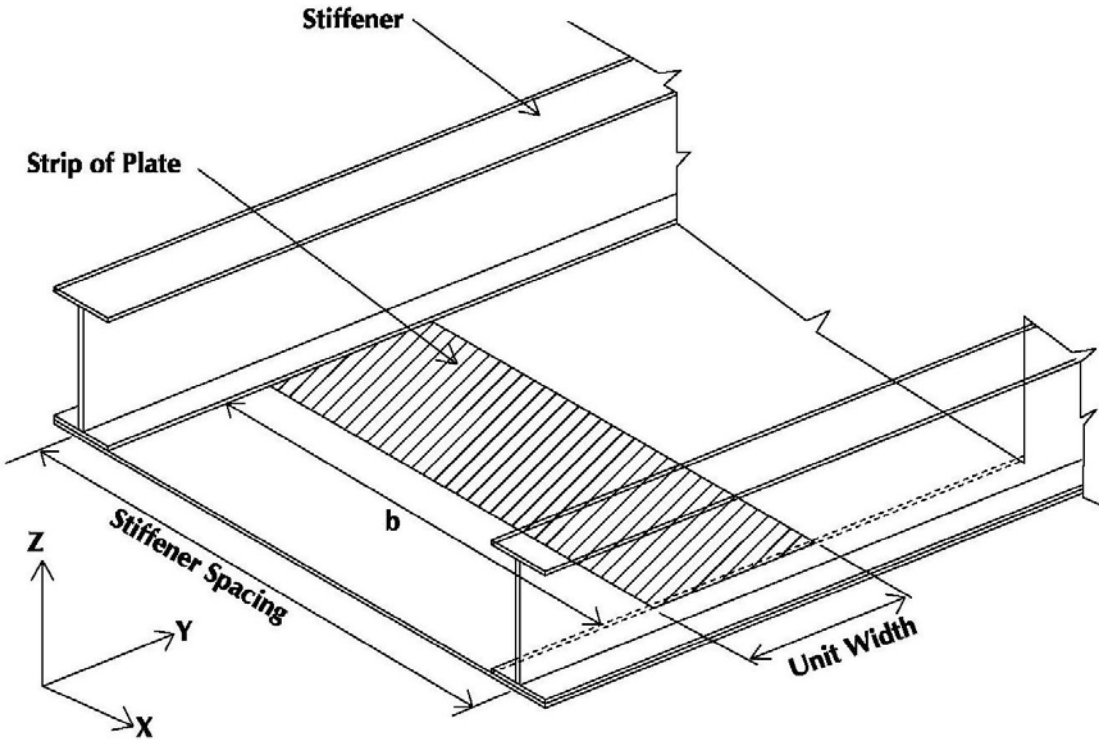

Figure 1.12 Plate between Stiffeners

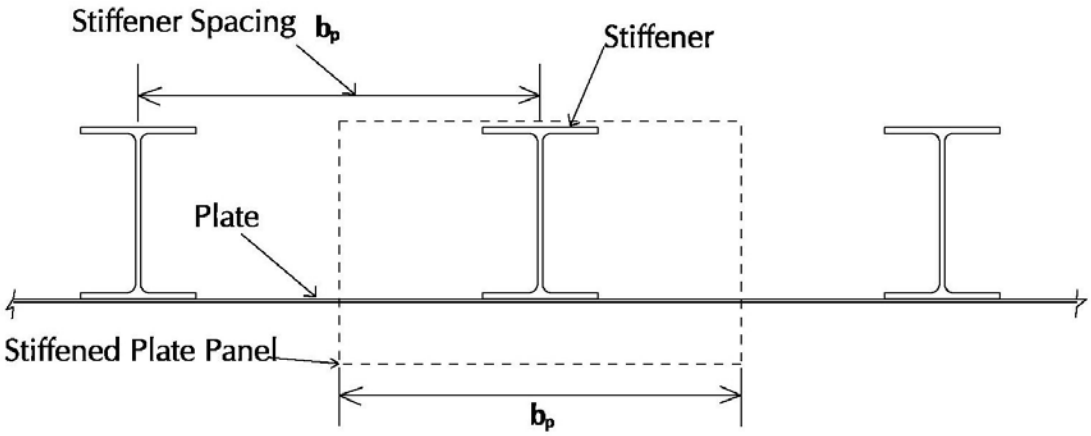

Figure 1.13 Composite Action between Plate and Stiffeners

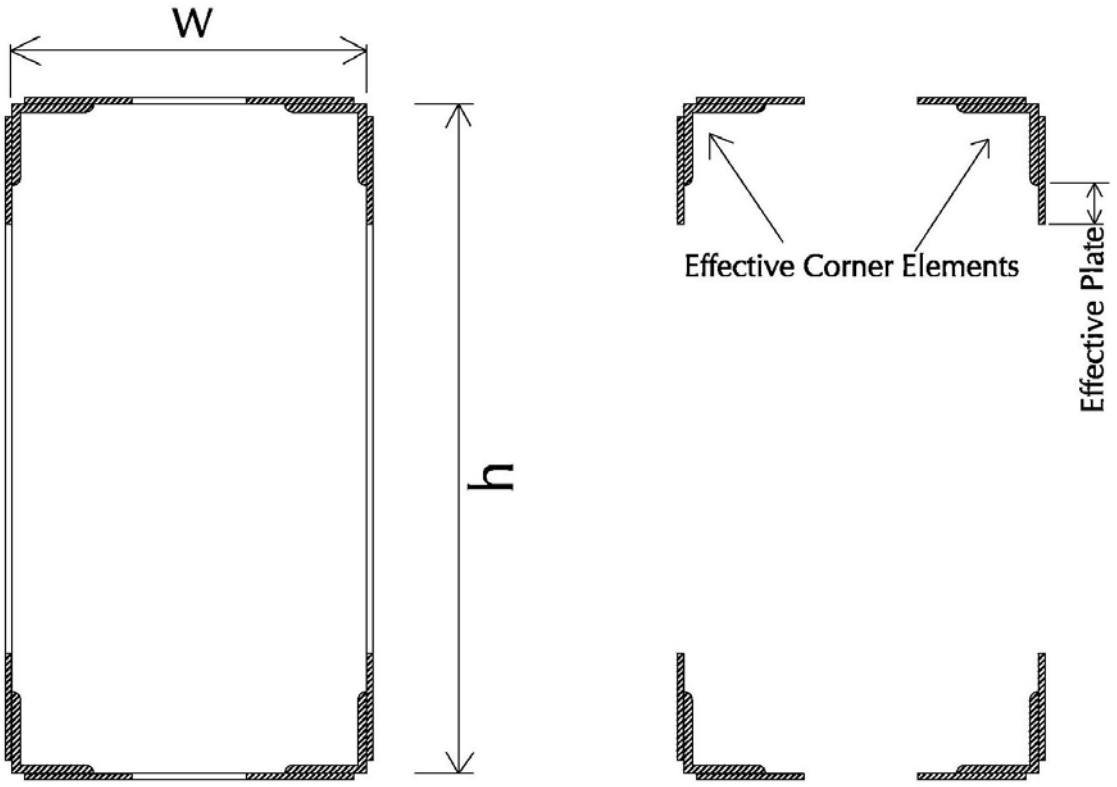

(a) Physical Cross Section (b) Effective Cross Section

Figure 1.14 Effective Corner Elements on Cross Section of Duct

Chapter 2: Strength of Plate and Stiffener Spacing of Large Rectangular Industrial Duct

Abstract

A large industrial duct is often rectangular and consists of stiffened plates, where the plates along with stiffeners act to resist the pressure loads and carry other loads to the supports. The plates of these ducts are generally stiffened with wide flange stiffeners in a parallel configuration. The plate between parallel stiffeners is assumed to span and be supported by those stiffeners. The load carrying capacity and the serviceability of the plate determine the plate thickness and the stiffener spacing. The current method of plate design and spacing of stiffeners are based on the large deflection plate theory in which bending and membrane actions contribute to elastic strength and deflection of the plate between stiffeners. The purpose of this study is to determine how partial yielding of the plate can result in economical stiffener spacing by benefiting from membrane action.

A numerical parametric study was conducted on the dimensionless parameters identified to characterize the behavior of laterally loaded long plates. The results were established for dimensionless pressure versus plate slenderness, and normalized out-of-plane deflection versus plate slenderness relations for three yielding cases namely; 0%, 16.5% and 33% of through thickness yielding of the plate. Design equations were established for the three cases above. Results show that approximately 55% and 110% increase in load carrying capacities when 16.5% and 33% yielding is permitted. However, such yielding results in 30% and 40% increase in deflections as well. Partially yielding plates can easily satisfy the serviceability limits states and lead to economical stiffened plate

systems for large industrial ducts. Also, results show approximately a 50% increase in stiffener spacing when 16.5% yielding is permitted. This study proposes design equations for plating and for spacing stiffeners for three different scenarios namely; 0%, 16.5% and 33% of through thickness yielding of the plate.

Keywords: Rectangular industrial duct, Stiffened plate, Finite element analysis, Large deflection, Partial yielding

2.1 Introduction

Many heavy industrial processes require transport of large amounts of air or flue gases through series of steel ducts. The duct systems in industrial applications are significantly large and, in some ways, are quite unique structures. Ducts with rectangular cross section are commonly used in large industrial applications. The cross sectional dimensions of industrial rectangular ducts are in the range of 5 to 15 m, sometimes even larger. The rectangular cross section is formed by welding together relatively thin steel plates. Stiffeners should be added to a plate to reinforce the thin plate. The plate is generally stiffened with stiffeners in a parallel configuration as shown in Figure 2.1. Figure 2.2 shows a similar industrial duct during fabrication.

The plate and the stiffeners act together as one composite section to resist the pressure loads. The plate is the most important structural element in a duct, but it could not economically function without its stiffeners. The plate between two parallel stiffeners is assumed to span between the stiffeners and be supported by those stiffeners. Thus, the

duct structural system develops the load path from the plate to the stiffeners. The load carrying capacity of the plate element is obviously determined by the plate thickness, i.e., the stiffener spacing.

In the past, the analysis and design of the plate thickness, i.e., the stiffener spacing, was done in accordance with pure plate bending behavior known as elastic small deflection theory. The small deflection theory generally leads to a thicker plate or smaller stiffener spacing. Currently, engineering firms have adopted the design process of determining the spacing of stiffeners based on elastic large deflection plate theory. Based on previous analytical studies for uniformly loaded rectangular plates with large deflections, various publications, such as Roark's Formulas for Stress and Strain (Roark's Formula) by Young (1989), provide simplified design tables which are widely used in the industry. For example, Young (1989) has provided tabulated numerical values for dimensionless coefficients for the relations among pressure load, deflection and stresses for rectangular plates under uniform load producing large deflections.

A close observation of the numerical values in the table mentioned above (Young 1989) and the practical experience gained in designing large industrial ducts raised the scope of this study. The range of the dimensionless coefficients does not cover the cases of laterally loaded slender plates with large pressure loads. Furthermore, these dimensionless coefficients were derived for the elastic state of analysis of rectangular plates subjected to transverse pressure and are not valid at the onset of yielding in plates.

In that sense, these approximate elastic solutions do not establish the true limit state capacity of the plate element.

Also, the pinned edge support condition leads to a larger stiffener spacing compared to the fixed edge support condition for a given pressure load and plate thickness. This is due to the fact that the deflection of a pinned edge plate is larger than the deflection of a fixed edge plate. This larger deflection causes higher membrane stresses and a higher proportion of the pressure load is supported by membrane stress rather than by bending stress. This illustrates that membrane action requires some deflection. Therefore, it is anticipated to benefiting from the partial yielding which rises the deflection. The structural analysis and design of the large rectangular duct systems is not governed by any design standard and very little publication on structural analysis and design procedures is available. Therefore, there is a need to conduct a study to derive a comprehensive method for plating and spacing stiffener for large industrial ducts.

2.2 Objectives

The primary objective of this part of the study is to establish relations between loads, plate thickness and stiffener spacing, recognizing the benefit of yielding and the true capacity of steel plates associated with large industrial ducts. In order to achieve this primary objective, a nonlinear finite element model was developed to accurately simulate the plate behavior in the inelastic range. The model was validated using results from theoretical solution and the values from "Roark's Formulas" by Young (1989). Another objective was to identify the fundamental parameters that dictate the behavior of laterally loaded plates for the numerical study. The final objective was to obtain dimensionless parameters to conduct a manageable parametric study to achieve the primary objective. The plate subjected to static pressure loading and under ambient temperature was only considered in this study.

Section 2.3 provides the background theory on the bending of long rectangular plates undergoing large deflection. Section 2.4 describes the finite element model developed for this study. Section 2.5 describes the determination of the dimensionless parameters that completely simulate the response of a long plates subjected to lateral pressure. Section 2.6 describes the parametric study conducted and presents the summary of study and the proposed method of plating or stiffener spacing for large industrial ducts. Section 2.7 presents an example for applying the proposed method to space the stiffeners. Section 2.8 provides recommendations for future studies.

2.3. Bending of Long Rectangular Plate

The classic theory of laterally loaded plate bending is often classified into small and large deflection plate theory, based on the out of plane deflection as compared to the plate thickness. Regardless, the out of plane deflection is small compared with other plate dimensions. The small deflection theory does not consider the membrane (diaphragm) stress that arises when deflection becomes large and when the edges are prevented from pulling in. If the deflections are sufficiently smaller than 10-20 % percent of plate thickness, the stretching of the plate can be negligible. The relationship between pressure and deflection will be linear during small deflection. The linear small deflection theory is generally attributed to Kirchoff (Ugural 1981).

Large deflection behavior occurs when the magnitude of the out of plane deflection becomes equal to or greater than half the thickness of the plates subjected lateral pressure. The large out of plane deflection causes stretching of the plate resulting in membrane stresses in addition to bending stresses. If the edges are prevented from pulling in, membrane action becomes significant. The plate behavior when carrying lateral load by bending and membrane action is referred to as nonlinear large deflection plate theory, as the relationship between pressure, stresses and deflection becomes nonlinear due to membrane action.

The use of small deflection theory leads to excessive thickness or smaller stiffener spacing. Solutions based on the small deflection theory are readily available. The solutions for large deflections theory in plate design are complicated. However, the

analysis of rectangular plates subjected to uniform lateral pressure and undergoing large out of plane deflection, received increasing attention in the 1940s (Levy 1942a, 1942b, Levy et al 1944). In large industrial ducts, the plate between stiffeners can undergo large deflection while performing safely and satisfying the serviceability limit. This leads to a need for a method of analysis that can trace the behavior of plates after undergoing large deflection.

The nonlinear differential equations for large deflection plate theory were developed by von Karman (Ugural 1981). The differential equations, namely the compatibility and equilibrium equations, are as follows:

$$\frac{\partial^4 \emptyset}{\partial^4 x} + 2\frac{\partial^4 \emptyset}{\partial^2 x \partial^2 y} + \frac{\partial^4 \emptyset}{\partial^4 y} = E\left[\left(\frac{\partial^4 w}{\partial^2 x \partial^2 y}\right)^2 - \frac{\partial^2 w}{\partial^2 x}\frac{\partial^2 w}{\partial^2 y}\right] \tag{2.1}$$

$$\frac{\partial^4 w}{\partial^4 x} + 2\frac{\partial^4 w}{\partial^2 x \partial^2 y} + \frac{\partial^4 w}{\partial^4 y} = \frac{t}{D}\left[\frac{p}{t} + \frac{\partial^2 \emptyset}{\partial^2 y}\frac{\partial^2 w}{\partial^2 x} + \frac{\partial^2 \emptyset}{\partial^2 x}\frac{\partial^2 w}{\partial^2 y} - 2\frac{\partial^2 \emptyset}{\partial x \partial y}\frac{\partial^2 w}{\partial x \partial y}\right] \tag{2.2}$$

Where $w(x, y)$ = Out of plane deflection, $\emptyset(x, y)$ = Stress function which defines in-plane forces N_x, N_y *and* N_{xy}, E = Young's modulus, p = Pressure load and D = Flexural rigidity of the plate. There were several attempts to solve these differential equations (Levy 1942a., Levy et al 1944), which resulted in lengthy mathematical procedures for limited boundary support cases. The approximate solutions were derived in terms of Fourier series for the von Karman equations (Levy 1942a., Levy et al 1944). Some of the other methods for limited cases are based on the energy method that assumes

a deflection in advance. To solve these two fourth-order and second-order partial differential Von Karman equations relating the lateral deflection and applied load, a lengthy mathematical solution for this long standing plate problem of simply supported plate was presented by Wang et al (2005). This solution was facilitated by benefiting from current computing facilities in solving equations.

In order to obtain a solution for the plates of large industrial ducts, the width of the plate between stiffeners can be assumed to be small compared to the length of the plate. The plate analysis can, therefore, be assumed to be bending of a long plate that is subjected to transverse load. The deflected shape of the plate can then be assumed to be cylindrical. Therefore, the investigation of the plate bending can be restricted to bending of an elemental strip cut from the plate by two planes perpendicular to the stiffener direction as shown in Figure 2.3. The x axis is perpendicular to the stiffener direction and the y axis is parallel to the stiffener direction. In this case, $w(x)$, $\frac{\partial^2 \emptyset}{\partial^2 x}$ and $\frac{\partial^2 \emptyset}{\partial^2 y}$ are constant along the y axis. Therefore, $N_y \; and \; N_{xy}$ can be taken as zero.

Currently in the design of duct plating, the stiffener spacing is determined by considering the allowable stress and the allowable deflection of a strip of plate between the stiffeners. The stiffener spacing is the distance between the centre lines of the stiffeners. However, the length of the strip of the plate under consideration is distance which is equal to the stiffener spacing minus one flange width as shown in Figure 2.4.

The bending of an elemental strip of the long plate can be assumed to be one way bending. For an elemental plate strip of length b, thickness t and having a unit width, the governing Equation 2.1 is satisfied identically while Equation 2.2 can be reduced to:

$$D\frac{d^4w}{d^4x} - N_x\frac{d^2w}{d^2x} = p \tag{2.3}$$

Because, in stiffened duct plating, the elemental plate strip is attached to the stiffeners and its edges are not free to pull in, a tension in the plate is produced depending on the magnitude of lateral deflection $w(x)$. The tensile forces in the plate carry part of the lateral loading through membrane action. The relative magnitude of membrane forces depends on two factors: the degree of lateral deflection due to lateral pressure and the degree of lateral restraint from pulling in.

2.3.1. Fixed Plate Strip

Assure the edges of the elemental strip to be fixed in such a manner that they cannot rotate and pull in. Considering an elemental strip with a bending moment M_o per unit length along the fixed edges, the forces acting on the strip are shown in Figure 2.4.

The bending moment M at any cross section of the strip is

$$M = \frac{pb}{2}x - \frac{px^2}{2} - N_x w + M_o \tag{2.4}$$

Substituting this bending moment into, $\frac{d^2y}{d^2x} = -\frac{M}{D}$, the modified Equation 2.2 in terms of moment, Equation 2.3 becomes:

$$\frac{d^2w}{d^2x} - \frac{N_x}{D}w = -\frac{pb}{2D}x + \frac{px^2}{2D} - \frac{M_o}{D} \tag{2.5}$$

Observing the symmetrical deflection curve and other boundary conditions, the general solution for this equation given in Timeshenko (1959) is:

$$w = \frac{pb^4}{16u^3 D \tanh(u)}\left\{\frac{\cosh\left[u\left(1-\frac{2x}{b}\right)\right]}{\cosh(u)} - 1\right\} + \frac{pb^2(l-x)x}{8u^2 D} \tag{2.6}$$

Where u is defined as: $u^2 = \frac{N_x}{D}\frac{b^2}{4}$. Thus, the deflection of elemental strip depends on u, which is a function of the membrane stress. This stress can be determined from the extension of the elemental plate strip produced by the membrane stress. The extension due to the deflection curve and the strain in the x direction can be equated as shown below:

$$\frac{1}{2}\int_0^b \left(\frac{dw}{dx}\right)^2 dx = \frac{N_x(1-\nu^2)b}{Et} \tag{2.7}$$

Substituting the above in Equation 2.6 for w and performing integration, the following equation for calculating u can be obtained:

$$\frac{E^2t^8}{(1-\nu^2)^2p^2b^8} = -\frac{81}{16u^7\tanh(u)} - \frac{27}{16u^6\sinh^2(u)} + \frac{27}{4u^8} + \frac{9}{8u^6} \quad (2.8)$$

Having calculated u, the membrane stress σ_m at any point and the bending stress σ_b at edge point can be obtained as follows.

$$\sigma_m = \frac{N_x}{t} = \frac{4u^2D}{tb^2} = \frac{Eu^2}{3(1-\nu^2)}\left(\frac{t}{b}\right)^2 \quad (2.9)$$

$$\sigma_b = \frac{6M_0}{t^2} = \frac{-3p}{2}\left(\frac{b}{t}\right)^2\left[\frac{1}{u^2} - \frac{\coth(u)}{u}\right] \quad (2.10)$$

The current method used to space the stiffeners is based on the numerical values of coefficients in the table found in "Roarks' Formula" by Young (1989). The relations among pressure load, deflection, plate characteristics and stresses are expressed by numerical values of dimensionless coefficients. Those dimensionless coefficients are $\frac{\sigma b^2}{Et^2}$, $\frac{\sigma_m b^2}{Et^2}$ and $\frac{\Delta}{t}$. These dimensionless coefficients were obtained from the approximate elastic solution of uniformly loaded rectangular plates (Levy 1942a, 1942b, Levy et al 1944). Also, it is evident from Equations 2.6, 2.9 and 2.10 that the relations among pressure load, deflection, plate characteristics and stress can be expressed by the same dimensionless coefficients.

From our observation during recent design of large industrial ducts and review of these dimensionless coefficients from "Roark's Formula" by Young (1989), it can be noted that the calculated membrane stress σ_m for pinned edge plate is significantly higher than the membrane stress σ_m in a similar fixed edged plate. Nevertheless, the total stress, the

summation of the membrane stress σ_m and the bending stress σ_b, is significantly lower for pinned edge plate. This is due to the fact that at a given pressure the out-of-plane deflection of pinned edge plates is higher than the deflection of fixed edge plates. This higher deflection of pinned edge plates causes higher membrane stress, indicating that a high proportion of the pressure load is supported by membrane stress σ_m rather than by bending stress σ_b. This means that the design of large industrial duct plates allowing for large deflections would lead to economical design.

One approach to reduce the edge rotational restraint and to increase the membrane action would be to permit yielding of the plate element at the supported edges. The edge condition of the plate between stiffeners is generally taken as fixed edge because the stiffeners are welded on a continuous plate and the plate thickness generally is smaller than the thickness of stiffener flange. In addition, the uniform pressure load acting on adjacent plate panels prevents any rotation of the stiffeners and leads to a fixed boundary condition. Therefore, yielding first occurs at the boundaries of the plate as the pressure load increases. This marks the beginning of the transition from fixed edge boundary to pinned edge boundary conditions. Furthermore, it can be argued that it is not mandatory to prevent local yielding of the duct. As the load is further increased, the yielding gradually penetrates through thickness. At the same time, a higher portion of the increased load will be taken by the increasing membrane stress σ_m. Therefore, the use of membrane stress can lead to economical design. Also the pressure load that results in the onset of yielding does not represent the limiting load. The plate can be further loaded until the serviceability becomes a governing factor. The purpose of this study is to

determine how the plate can take the advantage of yielding beyond the elastic range and the membrane stress σ_m for spacing the plate between stiffeners.

To continue, the properties that characterize the plate behavior should be identified. The bending of the plate usually occurs in two orthogonal directions. The plate between stiffeners is a very long and narrow rectangular plate. A plate that is infinitely long in one direction will bend in one direction. Therefore, the unit width of a plate strip perpendicular to the stiffener direction can be used to represent the behavior of the plate between stiffeners as shown in Figure 2.3. From the plate stress Equations 2.9 and 2.10, it is clear that stresses depend strongly on the ratio $\frac{b}{t}$. The ratio $\frac{b}{t}$ is measures the slenderness of the plate strip. The dimensionless coefficients in "Roark's Formula" by Young (1989) further prove that the deflections and the plate stresses depend strongly on plate slenderness $\frac{b}{t}$. Other fundamental properties that characterize a plate strip are yield stress F_y and Young's modulus E. While the yield stress F_y defines the elastic range of a plate, Young's modulus E characterizes its elastic flexibility. For the purpose of this study, the parameters that characterize the behavior of the plate strip are the plate slenderness $\frac{b}{t}$, the yield stress F_y and Young's modulus E.

The purpose of this study is to derive a comprehensive method that estabilishes the plate thickness t and the stiffener spacing b of rectangular long plates subjected to a uniform lateral pressure p. Equations 2.9 and 2.10 are based on the elastic theory in which

materials do not yield. However, the lateral pressure load applied to the plate which results in the onset of yield does not represent the limit of the lateral pressure load that the plate can support. The plate can withstand a lateral load several times greater than the elastic load before it fails in limiting stress level or in acceptable deformation. When the lateral load becomes very large, the edge of plate strip gradually yields. The elastic large deflection plate theory is somewhat complicated. The theories relating the behavior of the plate following the onset of yield is then quite complicated due to the different sources of nonlinearities such as yielding, large deflections and restraint from the edge pulling in. Therefore, it is not so easy to derive closed form solutions when the plate is partially yielding due to difficulties associated with the incorporation of nonlinearities. An accurate and general solution requires the use of numerical techniques such as the incremental finite element method. Several numerical studies for plate problems have been done satisfactorily. Therefore, the powerful finite element analysis can be used to study the solution of large deflections of thin plates beyond the elastic range, as several commercially available finite element programs now have material and geometric nonlinear analysis capability.

2.4. Finite Element Model

The nonlinear finite element method is applied to determine the stresses and maximum deflection of a long rectangular plate subjected transverse pressure in the inelastic range. The aim of this portion of the study is to develop a reliable finite element model to trace the stresses and the deflection of a long plate under uniform pressure. The model will be validated using theoretical results after the mesh density is refined so that it can be analyzed for the rest of the study.

A numerical model for the long plate was developed using the commercial multi-purpose nonlinear finite element program ADINA (2009). In this investigation, since the nonlinearity may come from the material properties and the kinematic assumption of large deflection, nonlinear static analysis was performed using the structural analysis module of ADINA. ADINA contains an extensive element library that can model variety of geometry and boundary conditions.

The large deflection of a laterally loaded plate involves in-plane and out-of-plane displacements. Therefore, a shell element was used to study the behavior of the laterally loaded plate. Figure 2.6 shows a 4-node rectangular shell element with the shell mid-surface nodal points. In addition, the 4-node rectangular shell element makes it easier to obtain the stresses in the direction of the plate edges for this nonlinear plate analysis. The shell element is formulated with the assumptions used in the Mindlin/Reissner plate theory and can be employed to model thick and thin general shell structures.

This shell element can be used with elastic-isotropic, plastic-bilinear and plastic-multilinear material models. It can also be used in a large displacement/small strain problem. This type of element is suitable for the present application since the magnitudes of the strains are generally not very large. To predict material behaviour under multi-axial loading, a yield criterion, that indicates for which combination of stress components transition from elastic to plastic deformations occur occur, should be used. The applicable yield criterion for metal plasticity is the von Mises yield criterion. The von Mises yield criterion has been interpreted physically as implying that plastic flow occurs when shear strain energy exceeds a critical value. The von Mises criterion is often used to estimate the yielding of ductile materials. Also, this criterion is largely based on the experimental observation that most polycrystalline metals are isotropic. Steel is an isotropic and ductile material. A flow rule relates the plastic strain rates to the current stresses and the stress increments subsequent to yielding and a hardening rule specifies how the yield condition is modified during the plastic flow. ADINA's metal plasticity model is characterized as an associated flow plasticity model with the isotropic hardening rule being used as the default hardening rule. An associated plasticity model is a plastic flow rule. It is observed experimentally that metals such as steel obey the associated flow rule. Also, in other numerical studies on the behaviour of steel structural members, it is common practice to use the isotropic hardening rule to track the yield surface. Therefore, the default ADINA metal plasticity features were used in the present study. These features are based on an associated flow plasticity model that uses the von Mises yield criterion as the failure surface. Evolution of this failure surface was restricted in the current study to the isotropic hardening rule.

In this study, it is necessary to obtain the nonlinear equilibrium path in order to study the laterally loaded plate beyond the elastic limit. When the response is nonlinear, the equilibrium path should be obtained by incremental methods. In this study, the increment is done by automatic step increment. This automatic increment can be carried out by the Automatic Time Stepping (ATS) method to obtain a converged solution. The basic approach used in ADINA to solve for the nonlinear equilibrium path is the Modified Newton iterative method applied at each incremental load. In this iterative method, the solution seeks the equilibrium through a horizontal path at a constant load vector. In this method, the stiffness matrix is updated at the end of every iteration. It should be noted that this method fails to converge in the neighborhood of unstable response as this ATS method uses the load-control iterative method.

2.4.1. Numerical Integration through Thickness

This study attempts to capture the behavior of steel plates beyond the elastic limit. Therefore, it is necessary to capture the onset and spread of the material yielding accurately. In finite element analysis, material yielding is established at the integrations points of the elements. In members subjected to bending, yielding occurs first at the surface of the elements and it may spread through the thickness. Thus, it is necessary to perform through thickness integration to trace the partial yielding. In addition the integration points should preferably lie on the top and bottom surfaces of the element. Therefore, a Gauss quadrature rule for numerical integration is inappropriate because its sampling points lie within the thickness of the plate and no integration point is at either surface, where yielding begins first. This consideration leads to conclude that the

Newton-Cotes integration scheme, simply the Simpson rule, is very effective to perform through thickness integration because this method has integration points on the boundaries. Figure 2.7 shows the integration points. The number of integration points through the thickness was chosen to be available was a maximum of seven for this study in order to trace the yielding of plate through thickness.

2.4.2. Statement of the Problem

This part of the study attempts to establish the maximum possible stiffener spacing based on the allowable stress and the allowable deflection of a long plate supported between stiffeners. To simplify the modeling and computation, only a portion of the long plate can be used for the satisfactory solution. With respect to the symmetry of the deflected shape of a long plate, a strip of plate can be modeled. Figure 2.3 shows the overview of the strip of the plate under consideration. This is a strip of plate of length, thickness t and having a unit width.

Figure 2.8 shows the finite element model and the coordinate system for the strip of plate considered. The x-y plane coincides with the middle plane of the plate. The z-axis is perpendicular to the plate. Unless otherwise shown, all nodal degrees of freedom for all nodes were set to freely displace and rotate. The strip of the plate should satisfy the artificial boundary formed when it is cut from the long plate. This artificial boundary represents the symmetric continuous edges that link the adjacent strips of plate. In order to provide the symmetric continuous edges (L_1 and L_3), the rotations about the x direction and the translation along the y direction are restrained. This edge condition represents the

situation of the strip of plate cut from long plate. The strip of plate is assumed to be fixed along the edges (L_2 and L_4) connected to stiffeners in such a manner that it cannot rotate or pull in from the two edges along the stiffeners. The boundary edges and the corresponding boundary conditions for the model are shown in Figure 2.8. The plate is subjected to uniform lateral pressure.

This nonlinear analysis involved material nonlinearity in association with yielding and plasticity. For the current practice of ultimate limit state design, the effects of strain hardening are not often considered. The simplified elastic-perfectly plastic material can be satisfactorily used for this study. The plate material is chosen to be carbon steel Grade A36. The Grade A36 carbon steel has an Elastic modulus E of 200,000 MPa, Poisson ratio v of 0.3 and yield strength F_y of 250 MPa. However, it should be noted here that the parametric study will be conducted on dimensionless parameters that are independent of geometric and material characteristics.

2.4.3 Validation of Modeling Techniques

Before the analysis of the strip of plate begins, it is necessary to verify that the proposed finite element modeling techniques are adequate. This can be accomplished through comparison of theoretical and experimental results available. However, a convergence study should be done before the validation study in order to establish a suitable mesh density.

Figure 2.8 shows the plate model used in this convergence study. In this convergence study, a 200 mm wide and 1000 mm long strip (b) of plate was used. A thickness t of 5mm, i.e., a width to thickness ratio $\frac{b}{t}$ = 200, was chosen to perform this mesh validation analysis. The convergence study was based on an elastic analysis. In order to do an elastic analysis, the elastic material model with a Young's modulus of 200 GPa was assumed. The load control increment method with a 60 kPa total pressure load was applied. The percentage change in total stresses at the top side of the clamped edges was compared as the mesh was being refined. The mesh validation was performed on five different runs with the same physical and material plate properties and the same uniform pressure loading condition. The only variable was the mesh size. Table 2.1 shows the mesh detail and the results from the analysis. Five different finite element mesh configurations were considered in this convergence study. The coarse mesh contained only 40 shell elements, whereas the most refined mesh contained 800 elements.

In order to find the suitable mesh density, the percentage change in total stresses between different mesh refinements was compared. The total stresses were obtained at top surface of the fixed edge. The percentage change in total stress from mesh density of 1 to 2, 2 to 3 and 3 to 4 were 8.87%, 5.91% and 3.61%, respectively. The percentage change in the total stress between mesh densities of 4 and 5 was only 1.14%. In general, a percentage change of less than 5% may be considered acceptable. Thus, mesh densities 4 and 5 may be acceptable. However, due to the severe nature of the material and geometric nonlinearities involved in later analyses, a very dense mesh of shell elements was desirable in order to trace the nonlinear equilibrium path. Thus, mesh 5 was selected as

the most suitable mesh and its mesh density 50x16 was used for rest of the studies presented in this chapter. In physical dimensions, each element is of size 20 x 15 mm.

As found in the above convergence study, the accuracy of the finite element model increases with the number of elements used. In this study, the stresses across the thickness at different depth are to be obtained in order to calculate the diaphragm stresses and to trace the partial yielding of plate through its thickness. Therefore, smaller elements are desired at the clamped edges when compared to the size of the element at the middle of the plate model. A graded mesh is then adopted to provide more elements at the clamped edges as shown in Figure 2.9.

In order to verify the accuracy of the final finite element model, the same model with the refined mesh used for the convergence study was used for the comparisons with theoretical results found in the literature. The pressure load was reduced to 10kPa for this validation study as the available dimensionless coefficients in "Roark's Formula" by Young (1989) is limited for lower pressure loads. The bending stress σ_b and the membrane stress σ_m of a laterally loaded elemental strip of plate were compared in order to determine the validity of the current finite element model. The theoretical results were calculated from the method explained in Section 2.2 and from the values in the book by Young (1989).

2.4.4 Comparison of the Bending Stress, Membrane Stresses and Deflection

The bending stresses σ_b, the membrane stresses σ_m and the deflections Δ from the theoretical and the numerical analysis are presented in Table 2.2. Two cases with clamped edge and pinned edge boundary conditions were considered for this comparison. The stresses and the deflections obtained for both boundary conditions were in very close agreement to the theoretical values. However, the membrane stress of numerical results shows around 4% less than theoretical and the results of "Roark's Formula" (Young 1989). Also, the bending stress is around 2% higher than theoretical and the results of "Roark's Formula". Despite these minor differences in the stresses, the deflection agrees well as the deflection generally converges faster than stresses in numerical analysis. From the above observations, it can be concluded that the accuracy of the finite element model developed in this study to analyze the laterally loaded strip of long plate is reasonable.

2.5 Dimensionless Parameters

Before a parametric study can be carried out, it is necessary to identify the dimensionless parameters that influence the bending stress σ_b, the diaphragm stress σ_m and the out-of-plane deflection Δ of laterally loaded long plates. Ideally these parameters should be independent of scale and material characteristics. First the fundamental parameters that govern the strength and the out-of-plane deflection of laterally loaded plates are defined. Then, a set of dimensionless parameters are identified. Finally, these dimensionless parameters will be used to perform a parametric study.

The geometric parameters that affect the strength and deformation of laterally loaded long plate are the plate length b and the plate thickness t. The material parameters for the plate are Young's modulus E, Poisson ratio v and yield strength F_y. The Poisson ratio v is dimensionless. The lateral pressure p is the loading parameter and the maximum lateral deflection Δ , the total stress σ_t, the diaphragm stress σ_m are other parameters measuring the response . Therefore, a total of 8 fundamental parameters, b, t, E, F_y, p, Δ, σ_t and σ_m, affects the behavior of laterally loaded plate. This is a complete and independent set. The above set of fundamental parameters with the practical range of each parameter will result an unmanageable number of finite element models. Therefore, it is necessary to reduce the number of variables to do a manageable parametric study. Dimensional analysis offers a method for reducing the number of variables that must be specified for a physical problem. This can be done by using Buckingham Pi-theorem (Harris 1999).

If the behavior of a physical problem can be defined by a set of n complete and independent variables, the relationship among them can be expressed by a homogeneous function of n variables. Then, Buckingham Pi-theorem is stated as (Lanhaar 1951)

When a complete relationship between dimensional physical quantities is expressed in dimensionless form, the number of independent quantities that appear in it is reduced from the original n to n-k, where k is the rank of the dimensional matrix of the n physical quantities

These parameters have the dimensions: M = mass, L = length and T = time. To apply the Buckingham Pi-theorem, the matrix by the fundamental parameters and their dimensions is formed as shown below.

Fundamental Parameters	b	t	Δ	p	F_y	E	σ_t	σ_m
M	0	0	0	1	1	1	1	1
L	1	1	1	-1	-1	-1	-1	-1
T	0	0	0	-2	-2	-2	-2	-2

The rank of above matrix is 2. Therefore, the number of dimensionless parameters expected in this case would be 6.

The Buckingham Pi-theorem simply identifies the number of dimensionless parameters and does not form the dimensionless parameters. From the theoretical method in Section 2.2 and the "Roark's Formula" by Young (1989), It can be shown that the surface stresses and the deflections for such long plates strongly depend on the $\frac{b}{t}$ ratio which measures the slenderness of the long plates. The material parameter Young's modulus E governs the elastic flexibility and the other material parameter that characterizes the elastic range is yield strength F_y. Therefore, another dimensionless parameter $\frac{F_y}{E}$ can be defined. Similarly, the total stress σ_t and the diaphragm stress σ_m can also be normalized by yield stress F_y of the plate material.

A preliminary study was carried out to identify other dimensionless parameters that can be used to study a laterally loaded long plate beyond the elastic range. First, the basis for the selection of the parameters is explained below as per Hughes (1981).

In order to determine the dimensionless parameters that govern the strength of the long plate, the pure bending of a laterally loaded strip of plate with unit width between stiffeners is considered. The edge surface stress along the strip length is $\sigma_x = \frac{1}{2} p \left(\frac{b}{t}\right)^2$ (longitudinal stress). In the long plate, a transverse deformation due to the longitudinal stress does not occur, i.e. $\varepsilon_y = 0$. The zero transverse strain causes a transverse stress $\sigma_y = \nu\, \sigma_x$ as seen from the strain equation $\varepsilon_y = \frac{\sigma_y}{E} - \nu \frac{\sigma_x}{E} = 0$. The third principal stress is zero at the free surface and p at the loaded surface. The third principal stress p at

the loaded surface is very small compared to the principal stresses σ_x and σ_y. Therefore, the σ_x at yielding as per the von Mises yield criterion is $\sigma_x = \frac{F_y}{\sqrt{1-\upsilon+\upsilon^2}}$. The bending moment at initial yielding M_y would be $M_y = \frac{F_y}{\sqrt{1-\upsilon+\upsilon^2}} \frac{t^2}{6}$. Therefore, the pressure at which the initial yielding occurs is

$$p = \frac{2F_y}{\sqrt{1-\upsilon+\upsilon^2}} \left(\frac{t}{b}\right)^2 \tag{2.11}$$

In the above case, it was assumed that only pure bending of long plate occurs without stretching of plate.

In order to make the plate slenderness $\frac{b}{t}$ material independent, a dimensionless parameter that combines the $\frac{b}{t}$ and $\frac{F_y}{E}$ can be derived by defining a dimensionless load parameter $\frac{pE}{{F_y}^2}$ from Equation 2.11. Therefore Equation 2.11 can be rewritten as follows

$$\frac{pE}{{F_y}^2} = \frac{2}{\sqrt{1-\upsilon+\upsilon^2}} \left(\frac{t}{b}\sqrt{\frac{E}{F_y}}\right)^2 \tag{2. 12}$$

From Equation 2.12, $\frac{pE}{{F_y}^2}$ and $\frac{b}{t}\sqrt{\frac{F_y}{E}}$ can be identified as dimensionless parameters that make the laterally loaded long plate independent of material characteristic when first yield occurs by pure bending only. In the literature, $\beta = \frac{b}{t}\sqrt{\frac{F_y}{E}}$ was defined as the plate slenderness parameter. Also, it can be shown from the deflection equation of the long

plate under pure bending that the normalized deflection $\frac{\Delta}{t}$ depends on the plate slenderness $\beta = \frac{b}{t}\sqrt{\frac{F_y}{E}}$. Therefore, the dimensionless parameters that define the behavior of laterally loaded plates are named as follows:

$Q = \frac{pE}{{F_y}^2}$ = Load parameter

$\beta = \frac{b}{t}\sqrt{\frac{F_y}{E}}$ = Plate slenderness

$\frac{\Delta}{t}$ = Normalized deflection

$\frac{\sigma_t}{F_y}$ = Normalized total stress

$\frac{\sigma_m}{F_y}$ = Normalized diaphragm stress

Before a parametric study can be carried out, it is important to determine that these dimensionless parameters are still independent from scale and material characteristics when the long plate undergoes stretching in addition to pure bending beyond the elastic range. In order to establish the independence of these dimensionless parameters for the above mentioned case, a numerical study was performed. In this investigation, two models each having the same plate slenderness $\beta = 8.367$ from two different combinations of geometric and material parameters were analyzed. The first, Model-1, was a 200 mm wide, 1000 mm long and 5 mm thick plate with elastic perfectly plastic material with yield strength of 350 MPa. The second, Model-2, was 200 mm width, 1000 mm long and 4.22 mm thickplate with elastic-perfectly-plastic material with yield strength of 250 MPa. The results for each of above two models were presented in Figure

2.10. The normalized total stress $\frac{\sigma_t}{F_y}$ versus the dimensionless loading history $\frac{pE}{{F_y}^2}$ of the analysis results is presented. The plot of normalized total stress $\frac{\sigma_t}{F_y}$ versus dimensionless load parameter $\frac{pE}{{F_y}^2}$ showed the independency of the dimensionless parameters β and $\frac{pE}{{F_y}^2}$ even for the case of stretching and bending of the plate in the inelastic range. The other useful information that is extracted from the results was the load parameter $\frac{pE}{{F_y}^2}$ at the onset of yielding, at yielding of 16.5% and 33% of plate thickness for both models. Those load parameters were also found to be same for all three cases of both models as shown in Table 2.3. Therefore, it can be concluded that these dimensionless parameters β and $\frac{pE}{{F_y}^2}$ are independent of any scale and material characteristics.

Similarly, the normalized diaphragm stress $\frac{\sigma_m}{F_y}$ versus the loading history $\frac{pE}{{F_y}^2}$ of the analysis results is presented in Figure 2.11. The graph of the normalized diaphragm stress $\frac{\sigma_m}{F_y}$ versus the dimensionless load parameter $\frac{pE}{{F_y}^2}$ showed the independency of dimensionless parameters β and $\frac{pE}{{F_y}^2}$ even for the case of stretching and bending of the plate in the inelastic range.

Further, the results of same models were used to verify the independency of the normalized centre deflection. The normalized deflection $\frac{\Delta}{t}$ against the dimensionless

pressure $\frac{pE}{{F_y}^2}$ for both models were plotted in Figure 2.12. The graph showed the independency of the normalized deflection $\frac{\Delta}{t}$ with respect to the dimensionless parameters β and $\frac{pE}{{F_y}^2}$ even for the case of stretching and bending of the plate in the inelastic range.

It can be concluded from the analysis above that the dimensionless parameters $\frac{b}{t}\sqrt{\frac{F_y}{E}}$, $\frac{pE}{{F_y}^2}$, $\frac{\Delta}{t}$, $\frac{\sigma_t}{F_y}$ and $\frac{\sigma_m}{F_y}$ can be used to define the behavior of a laterally loaded long plate beyond the elastic range and have no scale effect. Therefore, these parameters can be used for the parametric study.

2.6 Parametric Study

To determine the plate thickness or the stiffener spacing, it is evident that plate can be loaded beyond the elastic limit. However, the inelastic plate theory is more complex than the elastic plate theory. The stiffener spacing or the plate thickness for industrial ducts is generally governed by serviceability rather than limit states. Therefore, it will be helpful to study how much lateral pressure can be applied beyond the elastic range while satisfying the serviceability requirements. The boundary condition of the long plate between stiffeners is considered to be clamped and restrained to pull in. Therefore, yielding will first occur at the boundaries of the plate along the stiffeners. As the load is further increased, the yielding gradually penetrates through the thickness of plate. In order to determine the basic relations between the lateral pressures loads, the plate characteristics, the spread of yielding through the thickness and the deflection, a parametric study was conducted in this portion of this study.

In practice, the ratio of stiffener spacing to plate thickness $\frac{b}{t}$ is generally in the range of 125 to 350. For these slender plates, the deflection will be large and hence membrane effects may become significant. It will be seen that as the pressure increases for slender plates, the bending causes more deflection, thus membrane effects become significant.

Figure 2.9 shows the model of the strip of long plate used for this parametric study. The plate is assumed to be made of carbon steel Grade A36, which is the common steel material used in the ductwork. An idealized elastic perfectly plastic material model was used for plate material. Young`s modulus, Poisson ratio v and yield strength F_y of the

material were taken as 200 GPa, 0.3 and 250MPa, respectively. Since the concern with this study is the load carrying capacity of the plate in the inelastic range for spacing the stiffeners, plate models with different slenderness ratios ranging from 125 to 350 were considered. Strip of plate models having $\frac{b}{t} =$ 125, 150, 175, 200, 225, 250, 275, 300, 325 and 350 were analyzed. Therefore, these plate models have dimensionless plate slenderness: $\beta = \frac{b}{t}\sqrt{\frac{F_y}{E}} =$ 4.419, 5.303, 6.187, 7.071, 7.955, 8.839, 9.723, 10.607, 11.490 and 12.374. In this study, an incremental nonlinear static analysis was done, as it was necessary to trace the yielding of the plate through its thickness. From the results of the analysis, the x -directional stresses and strains at the support for each time step and for all integration points through the thickness were obtained. The maximum deflections for each time step at the middle of the plate models were also obtained. From the results, the time step for the first yielding was identified. The corresponding lateral pressure and deflection for that time step were then obtained. The membrane stresses for each time step were calculated from the stresses obtained at seven integration points through thickness. The membrane stress will be the resultant stress obtained by adding all the stresses at seven integration points through thickness as the algebraic summation of bending stresses become zero. In order to estimate the possible load increments beyond the elastic limits, the time steps for the first yield stress at the first, second and third integration points through thickness from the top were identified. The yield stresses at the first, second and third integration points from the top indicate the yielding of 0%, 16.5% and 33% of plate thickness. The corresponding pressure, deflections and

membrane stresses were identified for each model. The results obtained were tabulated in Table 2.4.

As shown in Table 2.4, it is demonstrated that higher lateral loads can be carried by the plate if partial yielding is permitted. It can be observed that, as the slenderness increased, the membrane stress became significant. As the load is further increased, the yielding gradually penetrates through thickness. It should be noted that the percentage increment of the load to yield one sixth of the thickness (16.5% of the thickness) was approximately 50% of the load required for onset of yielding. At the same time, the percentage increment in the out-of-plane deflection was approximately 20%. Similarly, the percentage increment of the load to yield one third of thickness (33% of the thickness) was approximately 100% of the load required to begin yielding and the percentage increment in the deflection is approximately 35 to 40%. Therefore, the rate of increase in deflection compared to the rate of increase in loading as yielding penetrates through the thickness is not significant enough to affect the serviceability design requirement. Generally the allowable limit for out-of-plane deflections of a plate between stiffeners is one hundredth of the length b of the plate. Nevertheless the forgoing analysis showed that for a long plate, the load can be even doubled from the load at first yield without affecting the serviceability design requirement.

In this section, the results obtained from the parametric study for the selected range of slenderness of plates made of carbon steel Grade A36 have been analyzed in order to study the relations between the lateral pressure load, deflection, plate thickness , stiffener

spacing and partial yielding. In order to analyze the results, the results in Table 2.4 were converted into dimensionless parameters identified in Section 2.5 and that are independent of the geometric and the material characteristics. Table 2.5 summarizes the values of the dimensionless parameters obtained from the finite element analyses for the range of plate slenderness considered.

To derive the relationship between the plate slenderness $\frac{b}{t}\sqrt{\frac{F_y}{E}}$ and the dimensionless load parameter $\frac{pE}{{F_y}^2}$, the dimensionless load parameter was plotted against the plate slenderness as shown in Figure 2.13 for the cases of onset of top fibre yielding and 16.5% and 33% of plate thickness yielding. The horizontal and vertical axes are associated with the plate slenderness $\frac{b}{t}\sqrt{\frac{F_y}{E}}$ and the dimensionless load parameter $\frac{pE}{{F_y}^2}$, respectively. This graph is useful in illustrating, in a general way, how the dimensionless load parameter varies with the plate slenderness when 0%, 16.5% and 33% of plate thickness yields. From Figure 2.14, it is obvious that the percentage of the pressure load increment from the onset of yielding to the yielding of one sixth (16.5%) of the thickness for the whole range of slenderness under consideration is nearly constant at about 55%. Similarly, an additional 33% increase in load carrying capacity can be observed between 16.5% of the thickness yielding and 33% of the thickness yielding.

At the same time, to check the serviceability of the plate between stiffeners, the normalized deflection $\frac{\Delta}{t}$ was plotted against the plate slenderness $\frac{b}{t}\sqrt{\frac{F_y}{E}}$ as shown in

Figure 2.14. The generally accepted deflection limit for these types of duct plate is one hundredth of the stiffener spacing $\left(\frac{b}{100}\right)$. Figure 2.14 indicates that the deflections satisfy the serviceability limit of the plate between stiffeners even for the case of 33% of the plate thickness yielding. On the other hand, the increments of deflection for the cases of yielding of 16.5% and 33% of plate thickness are within the serviceability requirement. Therefore, the design of plates between stiffeners for higher pressure loads will not be governed by serviceability limit but would be by the strength limit. Even though the above general conclusions can be reached, it will be meaningful and useful to establish practical design equations incorporating the degree of yielding. These design equations should be able to quantify the stiffener spacing and deflection for a given plate thickness and design pressure. The graphs provided herein can be used for manual calculation. Also, it is necessary to derive some relations that can be used in spreadsheet applications.

A close inspection of these plots reveals that the trend of each line in Figure 2.13 represents a portion of a power law distribution. Therefore, three power equations for each line on the graph were established such that each line would represent all the data points. The power equations represent the relations between the plate slenderness $\frac{b}{t}\sqrt{\frac{F_y}{E}}$ and the dimensionless load parameter $\frac{pE}{{F_y}^2}$ for the following cases: the onset of top fibre yielding, 16.5% plate thickness yielding and 33% plate thickness yielding. Similarly, another three linear equations were established for the relation between the normalized out-of-plane deflections $\frac{\Delta}{t}$ and the plate slenderness $\frac{b}{t}\sqrt{\frac{F_y}{E}}$ for the cases of top fibre

yielding, 16.5% percent and 33% percent of plate thickness yielding. The proposed equations are shown in each graph. The summaries of the proposed equations to obtain the limiting lateral pressure load and lateral deflection for various plate slenderness are provided in Table 2.6. It should be noted that these results are valid only for the plate subjected to static pressure loading and ambient temperature.

2.6.1 Forces due to Membrane Stresses

The plating or the spacing of stiffeners based on the large deflection plate theory considers the contribution of the membrane stresses σ_m in addition to the contribution of bending stress σ_b in carrying lateral pressure p. The membrane stresses σ_m develops in-plane reactions at the plate edges. The in-plane forces due to the membrane stresses σ_m are balanced by the adjacent plates on either side of the plate considered. Thus, the plate is prevented from pulling in by the in-plane forces. However, the membrane stresses σ_m of the plates adjacent to the end stiffener-rings are not restrained as the plates discontinue at the end stiffener-rings. Therefore, in the current design practice, the stiffener spacing for the end panels are closely spaced based on the small deflection plate theory. The in-plane forces developed in the middle plate panels are expected to be transmitted to the end panels and resisted by the deep beam action formed by the end plate panels and the adjacent end ring stiffeners. In this deep beam action, the end plate panel acts as a web and the stiffeners act as flanges in resisting the in-plane forces developed by the membrane stresses σ_m. The in-plane forces are transferred by shear V_m to the duct corners by this deep beam action as shown in Figure 2.15.

In large rectangular ducts, as a consequence of the larger plate height to thickness $\left(\frac{h}{t}\right)$ ratio, only a portion of the corner duct becomes more effective and is considered in contributing to the stiffness for global bending. The four effective corner elements of the duct at corners experience compressive and tension force due to the global bending of the duct. Therefore, the shear V_m due to the membrane stresses σ_m causes additional compressive force on the effective corner elements. Thus, the equilibrium between in-plane forces due to the membrane stresses σ_m and the additional compressive forces on the effective corner elements is maintained.

The analysis method proposed in this study is also based on large deflection plate theory, while benefiting from partial yielding of the plate edges. This method increases the contribution of diaphragm stress σ_m in carrying the lateral pressure p. Therefore, the additional compressive forces on the effective corner elements are also increased. From the parametric study, the relations between the normalized membrane stresses $\frac{\sigma_m}{F_y}$ and the plate slenderness $\frac{b}{t}\sqrt{\frac{F_y}{E}}$ were established for the cases namely; 0%, 16.5% and 33% of through thickness yielding as shown in Table 2.5. Therefore, for an industrial duct with given plate slenderness $\frac{b}{t}\sqrt{\frac{F_y}{E}}$ and height h, the additional compressive force due the in-plane forces can be calculated for above cases using the corresponding normalized diaphragm stress $\frac{\sigma_m}{F_y}$ from Table 2.5. The effective corner elements should be designed for the compressive force due to the global bending and the additional compressive force due to increased diaphragm stresses σ_m from the proposed method of spacing stiffeners.

2.7 Design Example

An example calculation is done to verify and compare the proposed design method for spacing stiffeners. This example uses only a single pressure load. It is assumed that this pressure load is the result of combinations of primary load cases. The first step in the design process of industrial ducts is to determine the stiffener spacing. The stiffeners are spaced to minimize the plate stress and deflection. In the conventional design process, generally the maximum stress and the deflection of the plate for a given pressure and predetermined plate thickness are calculated for an assumed stiffener spacing b. If the maximum stress and the deflection of the plate are within allowable limits, the assumed stiffener spacing will be accepted. The design parameters used for this calculation are:

Pressure load	$p = 15\ MPa$
Plate Thickness	$t = 5\ mm$
Modulus of elasticity	$E = 200\ GPa$
Yield stress of plate material	$F_y = 200\ MPa$

Initially the maximum stress and the deflection were calculated from the large deflection plate theory described in "Roark`s Formula" by Young (1989) where the relation among the load, deflection and stresses are expressed by numerical values of normalized parameters $\frac{\sigma b^2}{Et^2}$, $\frac{\sigma_m b^2}{Et^2}$ and $\frac{\Delta}{t}$ in a table form. The variables σ_m, σ_t and Δ represent the membrane stress, the total stress found by adding the membrane stress and the bending stress and the deflection respectively. These parameters are tabulated for different pressure coefficients $\frac{qb^4}{Et^4}$ ranging from 0 to 250 in step of 25. Therefore, the pressure

coefficient $\frac{qb^4}{Et^4}$ for the above design parameters was first calculated for a trial stiffener spacing $= 1005\ mm$.

$\frac{qb^4}{Et^4} = 122.42$ Pressure coefficient

The corresponding values for $\frac{\sigma_t b^2}{Et^2}$ and $\frac{\Delta}{t}$ were obtained by interpolating the values of the coefficients in the table linearly. The obtained values are:

$\frac{\sigma_t b^2}{Et^2} = 40.38$

$\frac{\Delta}{t} = 1.38$

Therefore, the maximum total stress and deflection are:

$\sigma_t = 199.9\ MPa$ Maximum total stress

$\Delta = 6.92\ mm$ Maximum Deflection

The trial stiffener spacing $b = 1005\ mm$ was purposely selected in order for the total stress σ reach the assumed yield stress of the material $F_y = 200\ MPa$. Hereafter, the relations derived in this study will be used to compare the results from the conventional method and the method (derived) in this study. Therefore, the corresponding dimensionless parameter $\beta = \frac{b}{t}\sqrt{\frac{F_y}{E}}$ defined in this study was calculated for the design parameters.

$\beta = \frac{b}{t}\sqrt{\frac{F_y}{E}} = 6.92$

Using the obtained relations when the top fiber yields as given in Table 2.6, the corresponding load parameter $Q = \frac{pE}{{F_y}^2}$ can be calculated.

$$Q = 0.580.\left(\frac{b}{t}\sqrt{\frac{F_y}{E}}\right)^{-1.10}$$

$$Q = \frac{pE}{{F_y}^2} = 0.08$$

$$\frac{\Delta}{t} = 0.288\left(\frac{b}{t}\sqrt{\frac{F_y}{E}}\right) - 0.399 = 1.38$$

Therefore, the required pressure load and maximum deflection when top fiber yields:

$P = \frac{Q\,{F_y}^2}{E} = 15.17kPa$ Required pressure

$\Delta = 6.9\ mm$ Maximum deflection

It is now clear through the examination of the proposed design method that it predicts the same pressure load and maximum deflection when the top fiber of the plate begins to yield.

However, the pressure load that results in onset of yielding does not represent the limit of the pressure load that the plate can withstand. As stated in the purpose of the study, the plate beyond the elastic range can be exploited the benefits of yielding and membrane action in spacing the stiffeners. To take these benefits, the required plate slenderness $\beta = \frac{b}{t}\sqrt{\frac{F_y}{E}}$ was calculated for the same load parameter $Q = \frac{pE}{{F_y}^2} = 0.08$ for the case of 16.6% of plate thickness yielding. Using the obtained relations for the case of 16.5% thickness of top fiber yielding as given in Table 2.6.

$$Q = 0.864.\left(\frac{b}{t}\sqrt{\frac{F_y}{E}}\right)^{-1.08}$$

Therefore, the $\beta = \frac{b}{t}\sqrt{\frac{F_y}{E}}$ is computed for the known Q as:

$$\beta = e^{\frac{ln(0.864) - \ln(Q)}{1.08}}$$

$$\beta = \frac{b}{t}\sqrt{\frac{F_y}{E}} = 9.49$$

Therefore, for the same pressure load $P = 15kPa$ and the same plate thickness $= 5mm$, the stiffener spacing b for which 16.5% plate thickness yields can be computed as:

$$b = \beta t\sqrt{\frac{E}{F_y}} = 9.49t\sqrt{\frac{E}{F_y}}$$

$b = 1500\ mm$ Stiffener spacing

The corresponding maximum deflection, when 16.5% of the plate thickness yields, can be computed for the case of a laterally loaded plate with the same pressure load $P = 15\ kPa$, the same plate thickness $t = 5mm$ for the stiffener spacing $b = 1500mm$.

$$\frac{\Delta}{t} = 0.330\left(\frac{b}{t}\sqrt{\frac{F_y}{E}}\right) - 0.356 = 2.77$$

$\Delta = 13\ mm$ Maximum Deflection

The span to deflection ratio is $\frac{1500}{13} = 115$. This is within the allowable limit of one hundredth of the span (Span/100) (ASCE 1995).

Therefore, the example calculation presented in this portion of the study indicates that the stiffener spacing obtained from conventional method can be increased by 50% for just yielding one sixth of plate thickness while satisfying the serviceability limit.

2.8 Recommendations for Further Research

This parametric study focuses only on geometric and material parameters alone. The scope of this study should be extended to include other parameters affecting the capacity of plates subjected to lateral pressure beyond the elastic limit.

There will be a geometric imperfection in the plate between stiffeners as the welding of stiffeners to steel plates affects the geometry of the plate. Generally, the distribution of imperfection due to welding is some degree of inwards dishing of the plate bound by the stiffeners. It is obvious that even a small initial deformation allows membrane effects to occur as soon as the load is applied. Therefore, it is better to incorporate the effects of the initial geometry imperfections for further study.

During the process of welding the stiffeners on the plate, significant residual stresses are introduced into the plate between the stiffeners. If the plate has already acquired some residual stress, the pressure may cause initial yielding earlier than with a residual stress free plate. Therefore, it is important to incorporate the effect of the residual stress in the future study.

The effects of other loading conditions such as compression, shear, lateral pressure and their combinations need to be investigated.

Table 2.1 Mesh Density and Convergence Study

Total Stress (σ_T) for Different Trial Meshes				
Mesh Number	Mesh Density	Number of Elements	σ_T (MPa)	Percentage Change / (%)
1	10x4	40	424	
				8.87
2	15x6	90	465	
				5.91
3	25x8	200	494	
				3.61
4	40x12	480	513	
				1.14
5	50x16	800	519	

Table 2.2 Comparison of Bending Stress, Membrane Stress and Deflection

Clamped Edged Elemental Strip of Plate			
	Membrane Stress σ_m (MPa)	Bending Stress σ_b (MPa)	Max. Deflection (mm)
Roark's Formula (Young 1989)	17.45	129.05	5.52
Method in Section 2.3	17.94	131.18	5.78
Present Study	16.70	132.00	5.84
Pinned Edged Elemental Strip of Plate			
	Membrane Stress σ_m (MPa)	Bending Stress σ_b (MPa)	Max. Deflection (mm)
Roark's Formula (Young 1989)	29.35	35.65	7.36
Method in Section 2.3	27.96	37.73	7.80
Present Study	27.57	35.06	7.53

Table 2.3 Dimensionless Load Parameters

Dimensionless Load Parameter	$pE/F_y{}^2$	
	Model-1	Model-2
Onset of yielding	0.0552	0.0556
16.5% of thickness yielding	0.0855	0.0851
33.0% of thickness yielding	0.1151	0.1151

Table 2.4 Loads and Deflections of Yielding Long Plates

Width to Thickness Ratio	(b/t)	**125**	**150**	**175**	**200**	**225**	**250**	**275**	**300**	**325**	**350**
Pressure at onset of top fibre yielding	(kPa)	36.4	28.6	23.8	20.4	18.0	16.0	14.6	13.4	12.4	11.5
Deflection at onset of top fibre yielding	(mm)	6.90	7.50	7.90	8.23	8.50	8.67	8.80	8.90	8.94	9.01
Membrane stress at onset of top fibre yielding	(MPa)	22.0	25.0	29.3	31.8	33.9	35.2	36.6	37.8	38.6	39.4
Pressure at which 16.5% of thickness yields	(kPa)	55.4	44.2	36.8	31.7	27.9	25.0	22.8	20.8	19.3	18.0
Percentage Increment in Load to yield 16.5% of thickness		52.2%	54.5%	54.6%	55.4%	55.0%	56.3%	56.2%	55.2%	55.9%	56.5%
Deflection at which 16.5% of thickness yields	(mm)	8.70	9.28	9.68	9.93	10.15	10.29	10.43	10.52	10.55	10.63
Membrane stress at which 16.5% of thickness yields	(MPa)	32.5	37.5	41.2	43.6	46.0	47.7	48.3	50.5	51.6	52.7
Pressure at which 33% of thickness yields	(kPa)	74.6	60.0	50.0	43.3	38.2	34.4	32.0	28.7	26.7	24.9
Percentage Increment in Load to yield 33% of thickness		104.9%	109.8%	110.1%	112.3%	112.4%	115.0%	119.2%	114.2%	116.2%	116.5%
Deflection at which 33% of thickness yields	(mm)	10.30	10.78	11.10	11.34	11.54	11.68	11.78	11.91	11.96	12.01
Membrane stress at which 33% of thickness yields	(MPa)	52.9	57.7	60.9	63.3	65.6	67.4	68.4	70.4	71.6	72.4

Table 2.5 Dimensionless Strengths and Deflections of Yielding Long Plates

$\beta = \frac{b}{t}\sqrt{\frac{F_y}{E}}$		***4.419***	***5.303***	***6.187***	***7.071***	***7.955***	***8.839***	***9.723***	***10.607***	***11.490***	***12.374***
Dimensionless Load at onset of top fibre yielding	$\frac{pE}{{F_y}^2}$	0.116	0.092	0.076	0.065	0.058	0.051	0.047	0.043	0.040	0.037
Normalized Diaphragm Stress at onset of yielding	$\frac{\sigma_m}{F_y}$	0.088	0.104	0.117	0.127	0.136	0.141	0.146	0.151	0.154	0.158
Normalized Deflection at onset of top fibre yielding	$\frac{\Delta}{t}$	0.86	1.13	1.38	1.65	1.91	2.17	2.42	2.67	2.91	3.15
Dimensionless Load at which 16.5% of thickness yields	$\frac{pE}{{F_y}^2}$	0.177	0.141	0.118	0.101	0.089	0.080	0.073	0.067	0.062	0.058
Normalized Diaphragm Stress at which 16.5% of thickness yields	$\frac{\sigma_m}{F_y}$	0.130	0.150	0.165	0.176	0.184	0.191	0.193	0.202	0.206	0.211
Normalized Deflection at which 16.5% of thickness yields	$\frac{\Delta}{t}$	1.09	1.39	1.69	1.99	2.28	2.57	2.87	3.16	3.43	3.72
Dimensionless Load at which 33% of thickness yields	$\frac{pE}{{F_y}^2}$	0.239	0.192	0.160	0.139	0.122	0.110	0.102	0.092	0.085	0.080
Normalized Diaphragm Stress at which 33% of thickness yields	$\frac{\sigma_m}{F_y}$	0.212	0.231	0.244	0.253	0.262	0.270	0.274	0.282	0.286	0.290
Normalized Deflection at which 33% of thickness yields	$\frac{\Delta}{t}$	1.29	1.62	1.94	2.27	2.60	2.92	3.24	3.57	3.89	4.20

Table 2.6 Summary of Proposed Equations for Dimensionless Pressure and Deflection

Cases	Limiting Load Parameter $Q = \frac{pE}{{F_y}^2}$	Normalized Deflection $\frac{\Delta}{t}$
Onset of yielding	$Q = 0.580.\left(\frac{b}{t}\sqrt{\frac{F_y}{E}}\right)^{-1.10}$	$\frac{\Delta}{t} = 0.288\left(\frac{b}{t}\sqrt{\frac{F_y}{E}}\right) - 0.399$
16.5% of thickness yields	$Q = 0.864.\left(\frac{b}{t}\sqrt{\frac{F_y}{E}}\right)^{-1.08}$	$\frac{\Delta}{t} = 0.330\left(\frac{b}{t}\sqrt{\frac{F_y}{E}}\right) - 0.356$
33% of thickness yields	$Q = 1.112.\left(\frac{b}{t}\sqrt{\frac{F_y}{E}}\right)^{-1.05}$	$\frac{\Delta}{t} = 0.367\left(\frac{b}{t}\sqrt{\frac{F_y}{E}}\right) - 0.328$

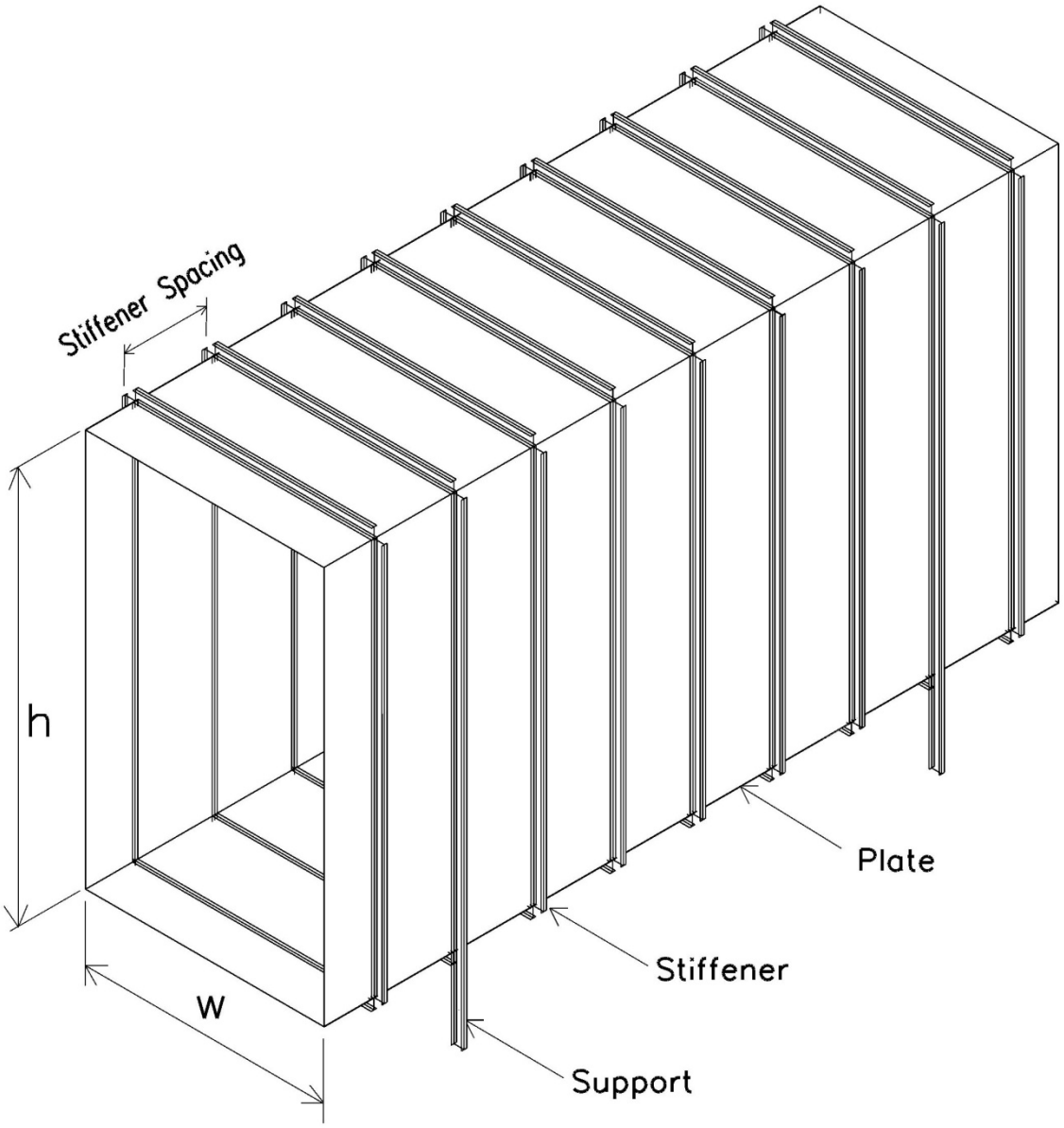

Figure 2.1 Typical Large Rectangular Industrial Duct

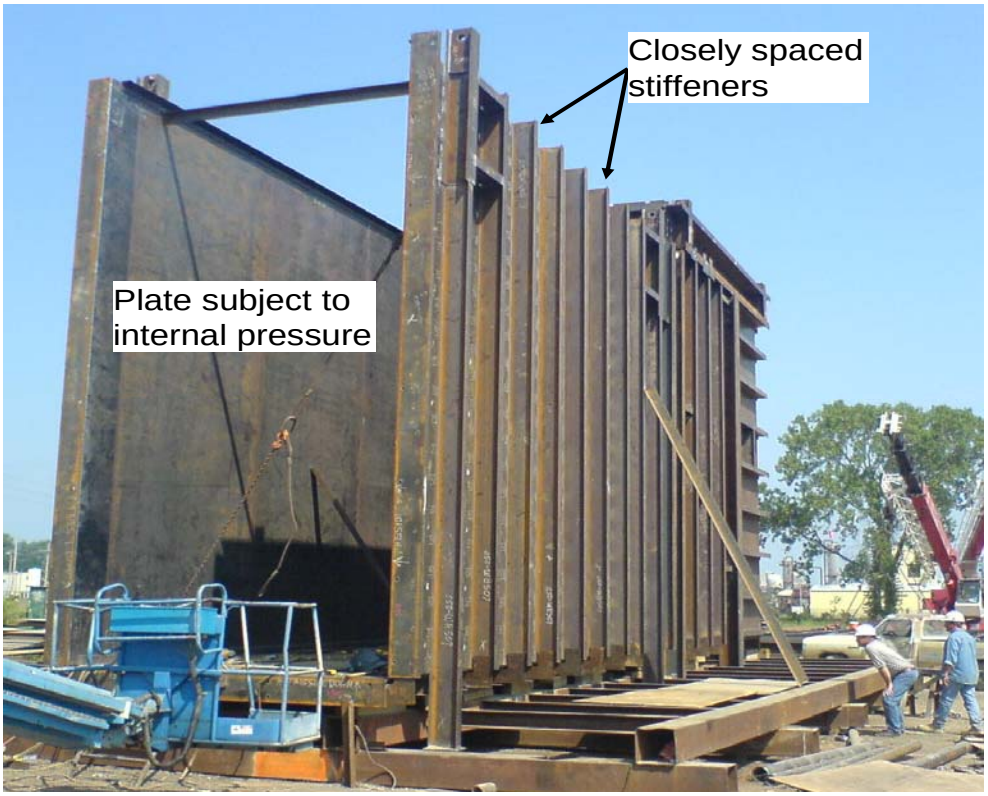

Figure 2.2 Large Rectangular Industrial Duct During Fabrication

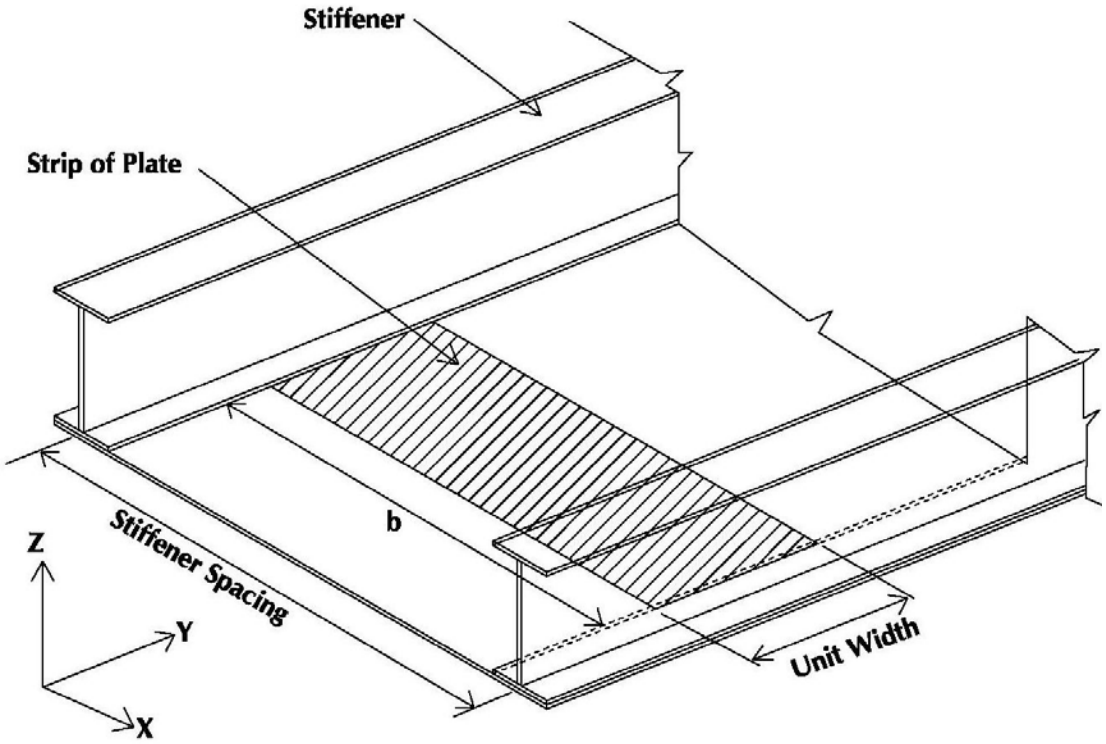

Figure 2.3 Elemental Strip of Long Plate

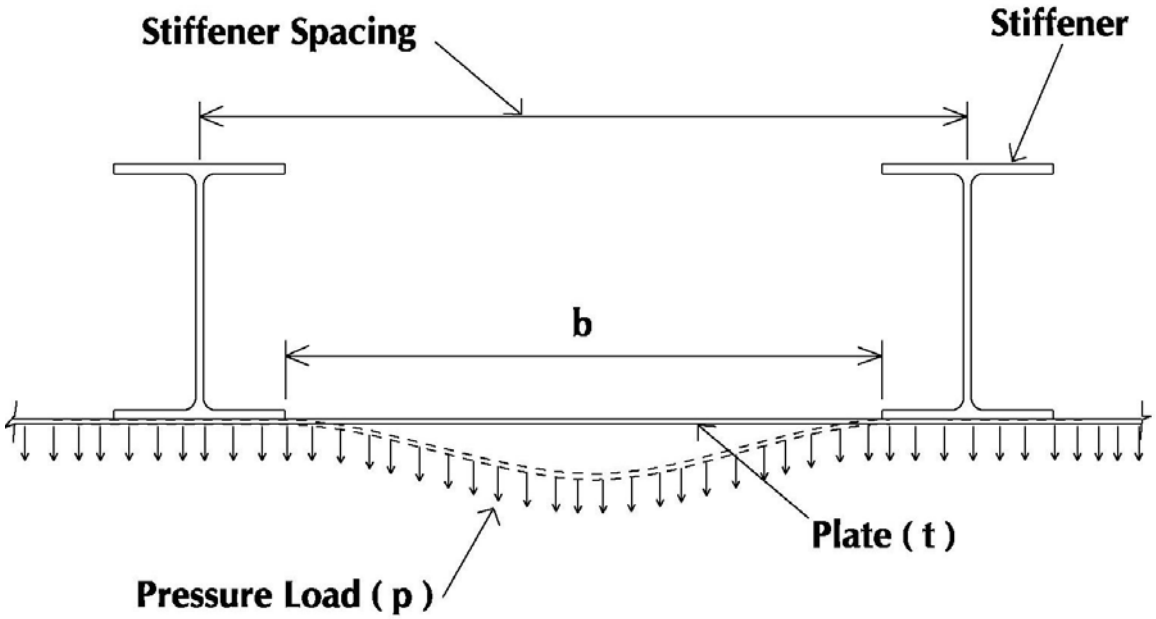

Figure 2.4 Long Plate between Stiffeners

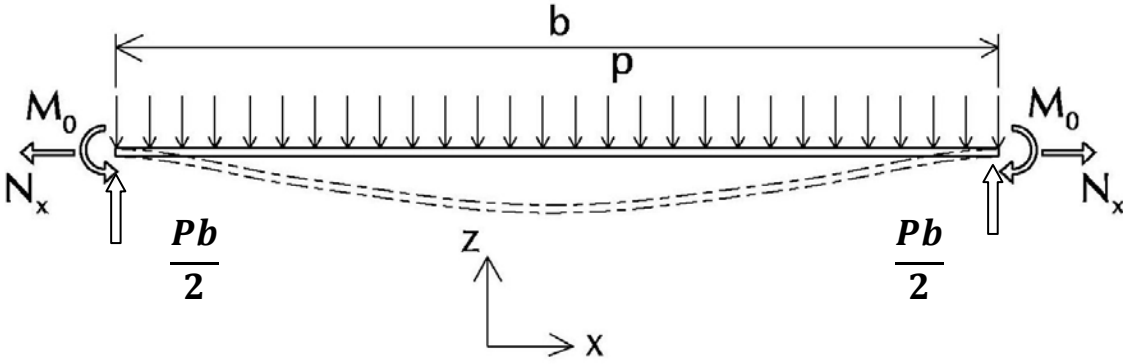

Figure 2.5 Free Body Diagram of Strip of Plate

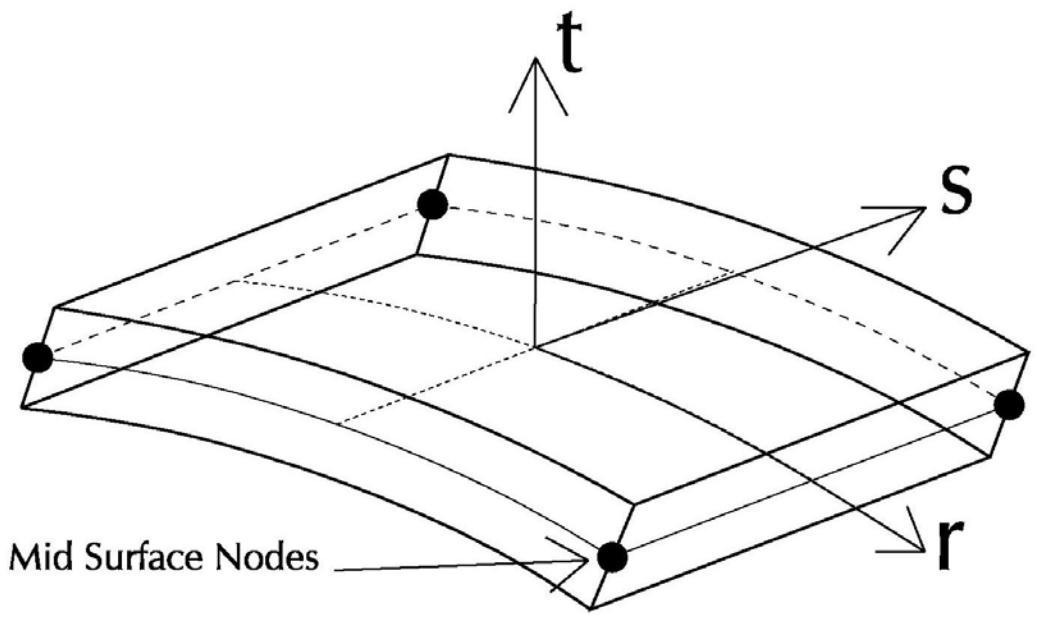

Figure 2.6 Four Node Shell Element for Thick and Thin Shells

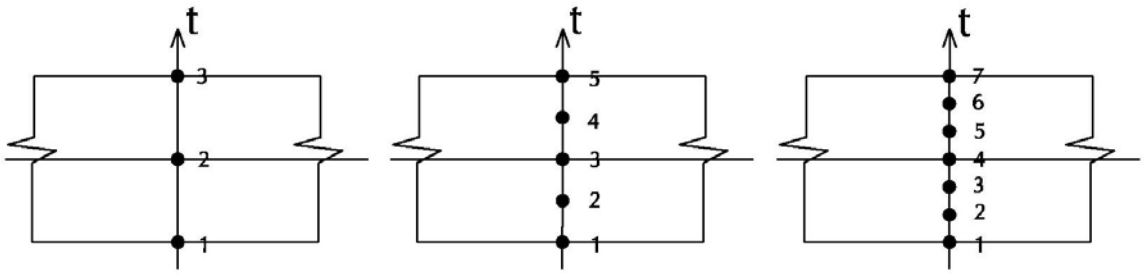

Figure 2.7 Newton-Cotes Integration Points in the Thickness Direction

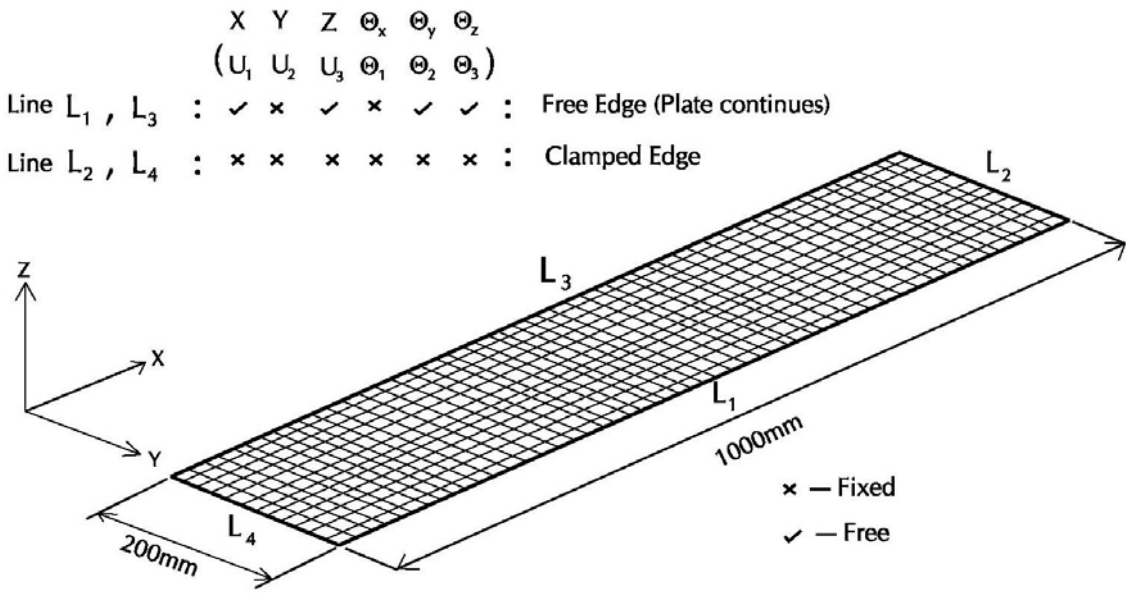

Figure 2.8 Elemental Strip of Long Plate -Convergence Study

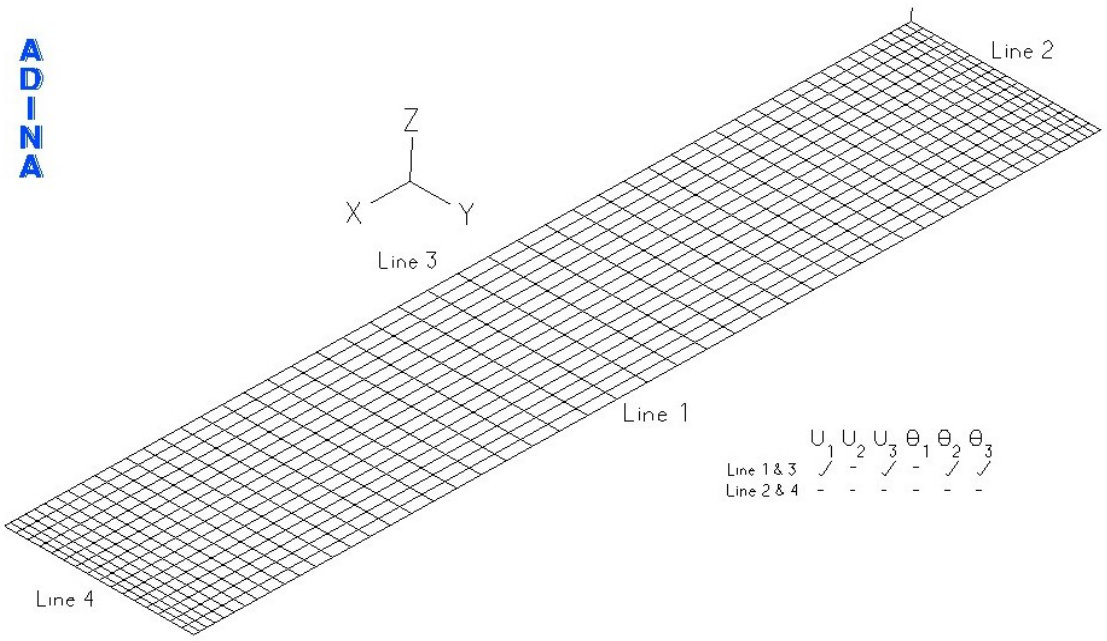

Figure 2.9 Finite Element Model -Plate Analysis

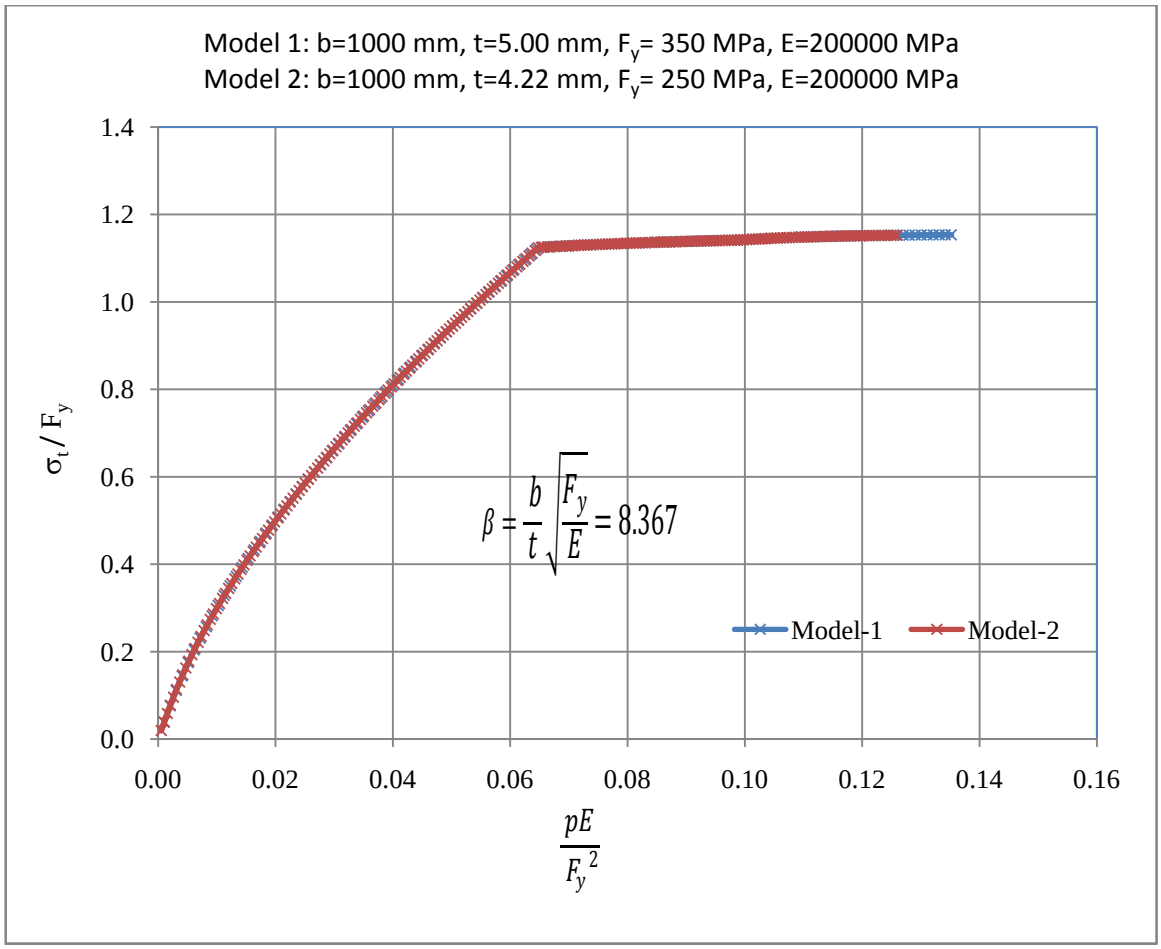

Figure 2.10 Normalized Total Stress versus Dimensionless Pressure

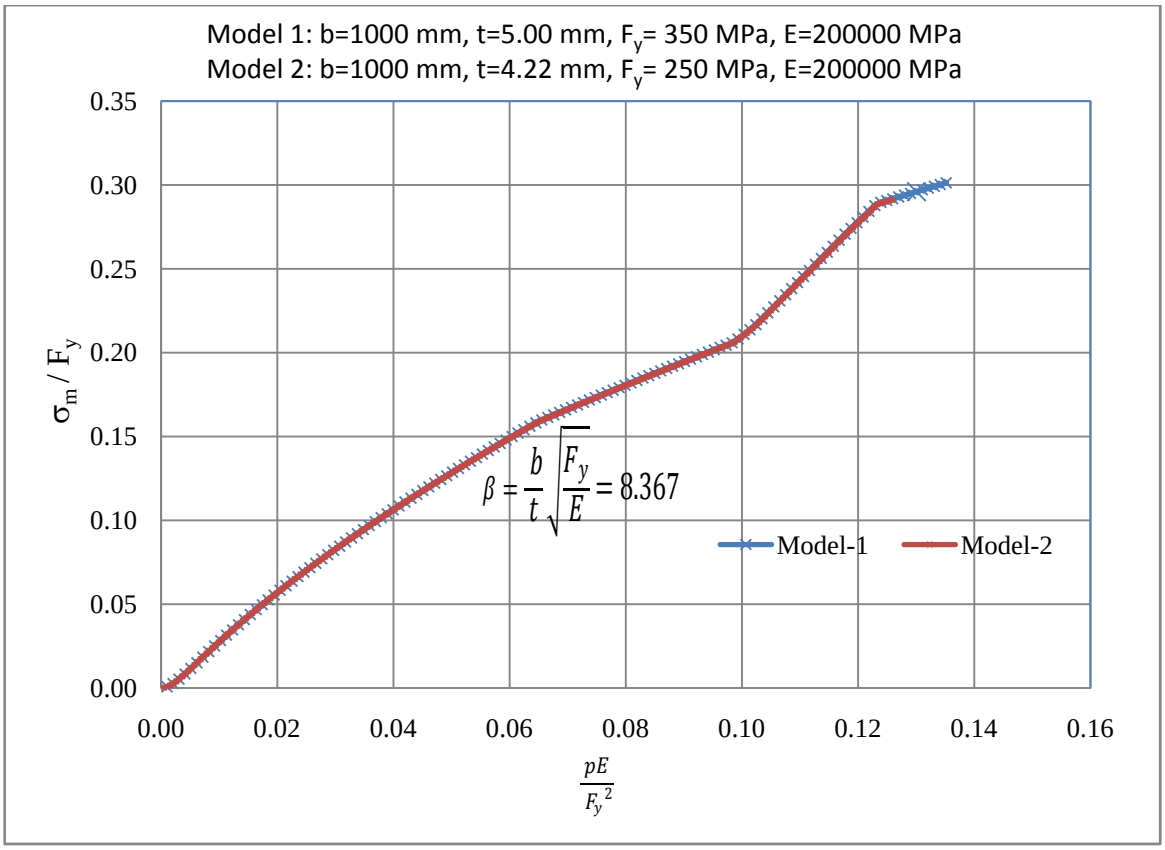

Figure 2.11 Normalized Diaphragm Stress versus Dimensionless Pressure

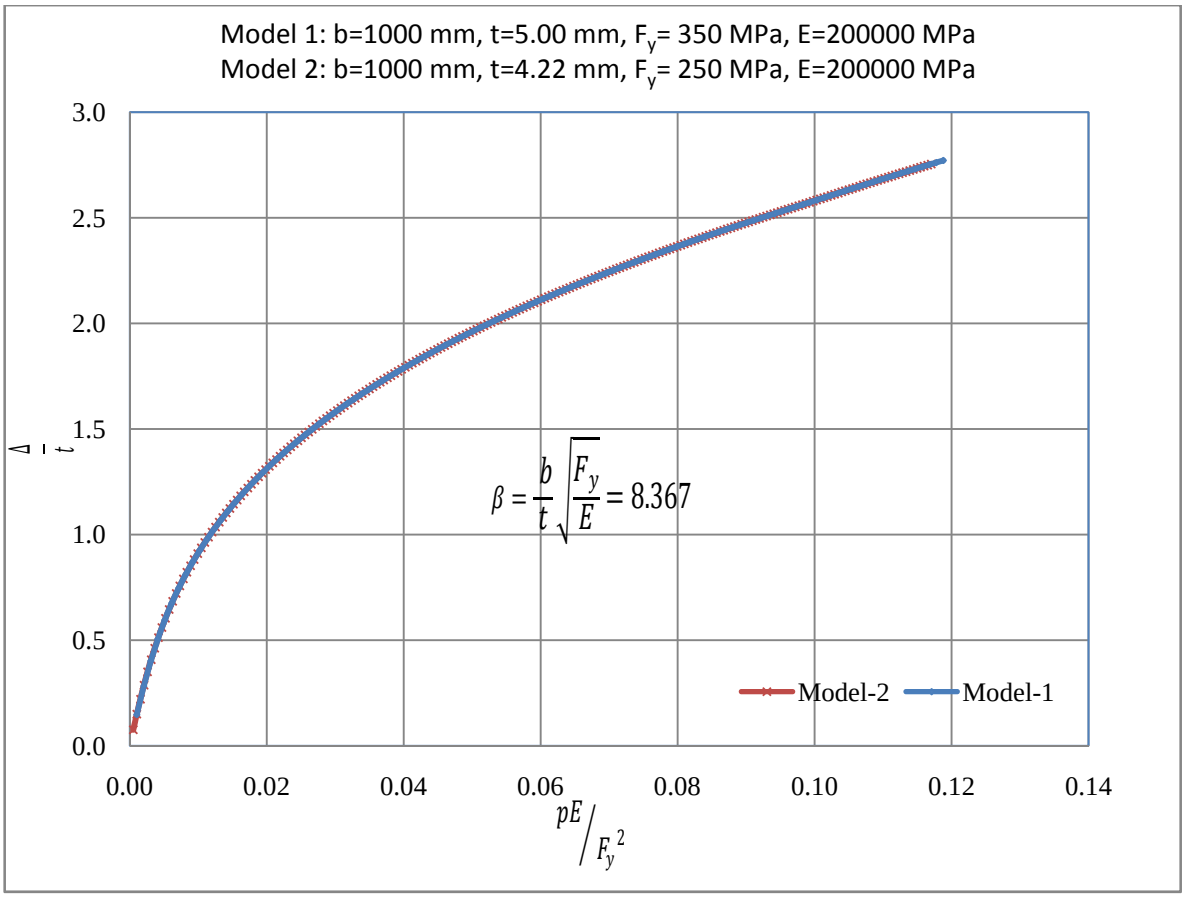

Figure 2.12 Normalized Deflection versus Dimensionless Pressure

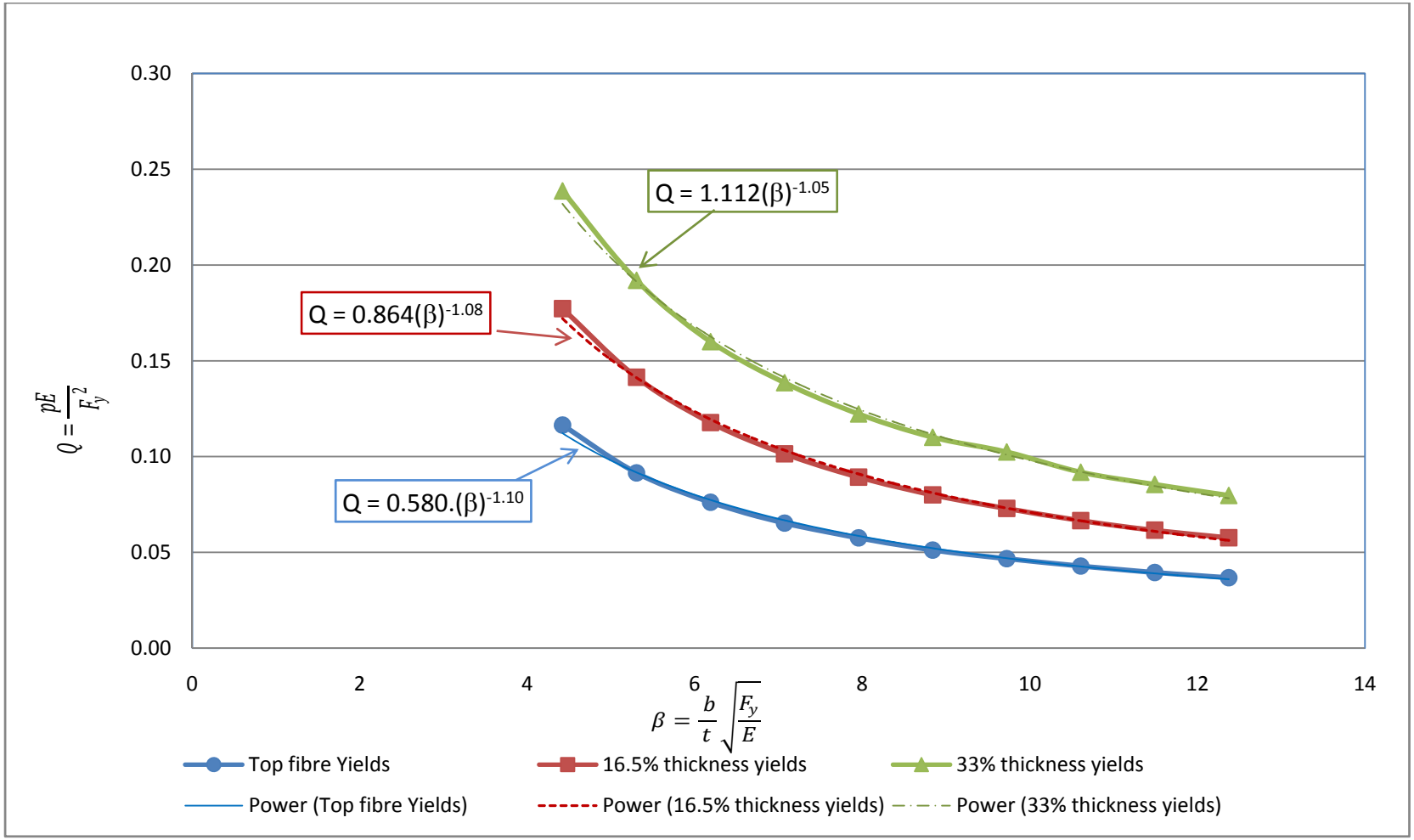

Figure 2.13 Dimensionless Load Parameter versus Plate Slenderness

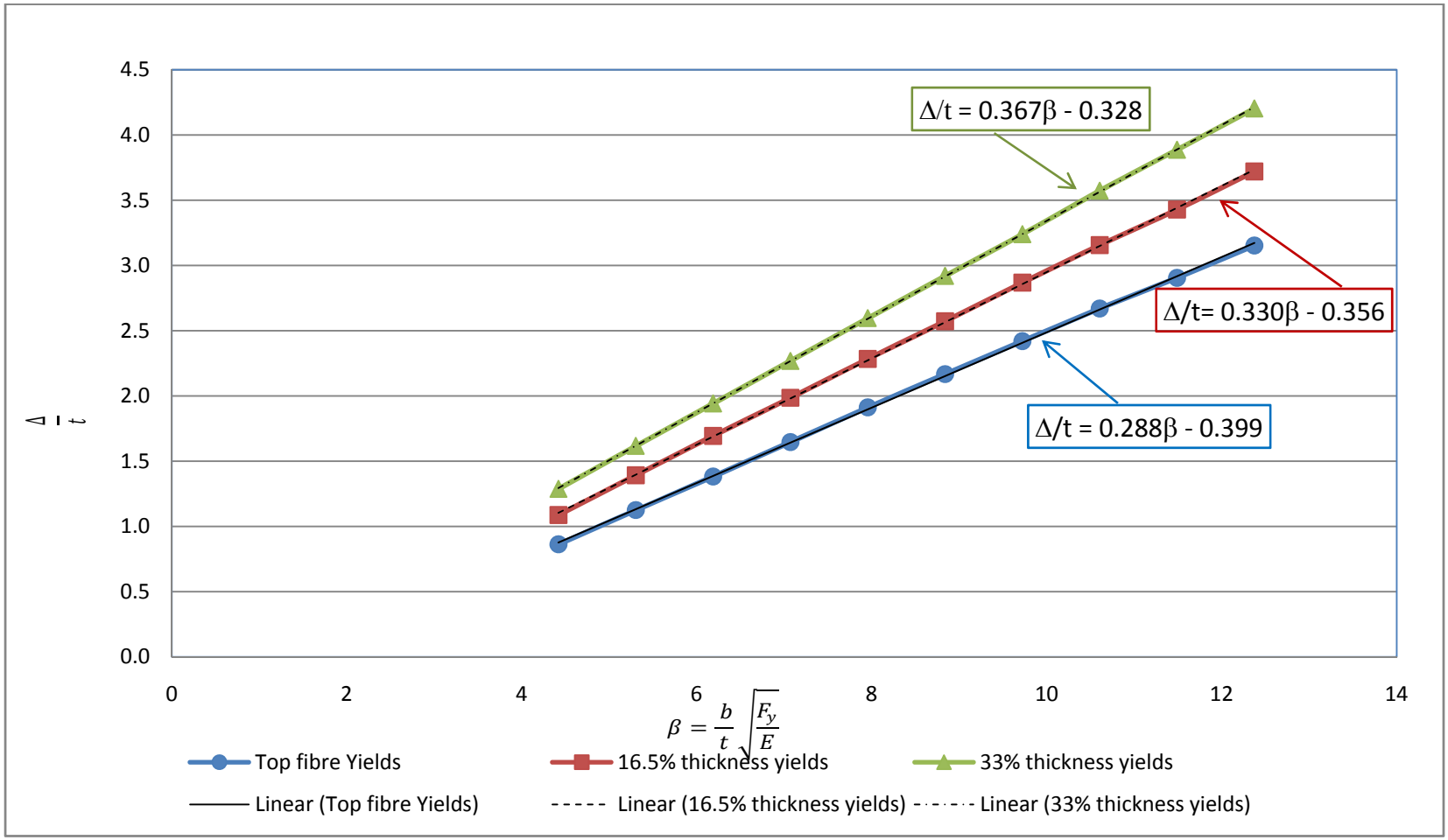

Figure 2.14 Normalized Deflection versus Plate Slenderness

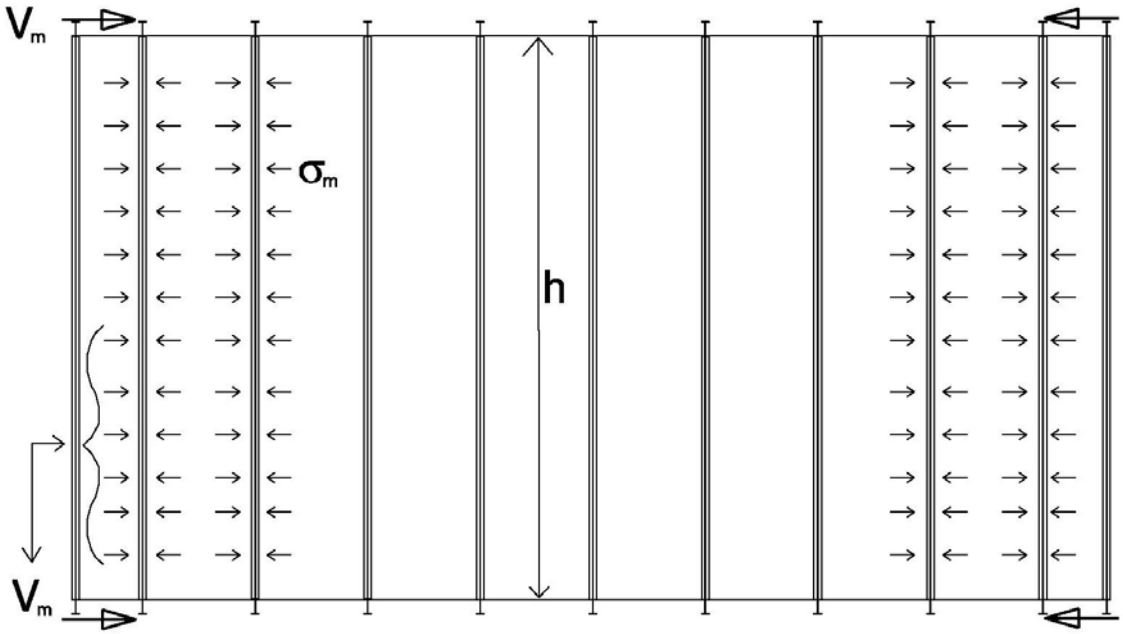

Figure 2.15 In-Plane Forces Due to Membrane Stresses

Appendix 2. 1 Notations

The following symbols are used in this chapter

b = Stiffener spacing

D = Flexural rigidity of plate

E = Young's Modulus

F_y = Yield stress of plate material

h = Height of duct

L = Length

M = Mass

M_o = Bending moment at end of fixed plate

p = Pressure load

$Q = \frac{pE}{{F_y}^2}$ = Load parameter

t = Thickness of plate

T = Time

u = Function of membrane stress

V_m = Shear forces due to membrane stress

$w(x, y)$ = Out of plane deflection of laterally loaded plate

$\beta = \frac{b}{t}\sqrt{\frac{F_y}{E}}$ = Plate slenderness

Δ= Mid span lateral deflection

$\emptyset(x, y)$ = Stress function which defines in-plane forces

σ_m = Membrane stress

σ_b = Bending stress

σ_t = Total stress

v = Poisson's ratio

Appendix 2. 2 References

ADINA , (2009), "ADINA 8.5 user manual." ADINA R & D Inc, Watertown, MA, USA.

ASCE, (1995), "The structural Design of Air and Gas Ducts for Power Stations and Industrial Boiler Applications." Air and Gas Structural Design Committee of the Energy Division of the ASCE, Reston.

Bakker, M.C.M., Rosmanit, M., Hofmyer, H., (2008), "Approximate Large-deflection Analysis of Simply Supported Rectangular Plates under Transverse Loading Using Plate Post-buckling Solutions." Thin Walled Structures, 46, 1224-1235.

Harris, H.G., Sabnis, G., (1999), "Structural Modeling and Experimental Techniques." 2nd edition. CRC Press, New York.

Hughes, O.F., (1981), "Design of Laterally Loaded Plating –Uniform Pressure Load." Journal of Ship Research, 25(2), 77-89.

Langhaar, H.L., (1951), "Dimensional Analysis and Theory of Models." John Wiley, N.Y

Levy, S., (1942a), "Bending of Rectangular Plates with Large Deflections." T.N. No. 737, National Advisory Committee for Aeronautics, Washington, D.C.

Levy, S., (1942b), "Square Plates with Clamped Edges under Normal Pressure Producing Large Deflections." T.N. No. 847, National Advisory Committee for Aeronautics, Washington, D.C.

Levy, S., Greenman, S.,(1942), "Bending with Large Deflection of a Clamped Rectangular Plate with Length-width ratio 1.5 under Normal Pressure." T.N. No. 853, National Advisory Committee for Aeronautics, Washington, D.C.

Timoshenko, S., Krieger, S.W.,(1959), "Theory of Plates and Shells." McGraw-Hill, Tokyo.

Udall, J.D., (2007), "Effective Design of Stiffener on Industrial Ducts." Master Thesis, McMaster University, Hamilton.

Ugural, A. C., (1981), "Stresses in Plates and Shells." Mcgraw Hill Companies. FL. USA.

Wang, D., EI-Sheikh, A.I., (2005), "Large Deflection Mathematical Analysis of Rectangular Plates, Journal of Engineering Mechanics." ASCE, 131(8), 809-821.

Young, W.C., (1989), "Roark's Formulas for Stress and Strain." 6th edition, McGraw Hill, New York.

Chapter 3: Literature Review and Finite Element Modeling Techniques Applied to Stiffened Plate Panels

Abstract

In large rectangular industrial ducts, parallel stiffeners are attached to outside of the plate in order to maintain the structural integrity and to increase the plate strength in the out of plate direction. High pressure loading conditions and the length of the stiffener dictate the use of wide flange steel sections as stiffeners. Under a suction type pressure load, the flange not connected to the plate will be in compression whereas the tension flange is restrained by the plates. The unsupported compression flange may lead to lateral distortional buckling of the stiffeners. The current methods of practice to proportion the stiffeners are derived from standard beam instability design methods. Considering the differences in the instabilities between the general beam and the stiffened panels, the current method is not applicable and very conservative. A better understanding of the parameters associated with the behavior and strength of stiffened plate panels is therefore necessary. A parametric study may be conducted to determine the behavior and strength of laterally loaded stiffened plate panels. An extensive literature review on the buckling behavior of beams with different restraint conditions was completed. The finite element modeling techniques used to simulate the stiffeners in large rectangular industrial duct were compared to experimental results. It was concluded that the bahaviour and strength of laterally loaded stiffened plate can be predicted very well with the proposed modeling techniques. Subsequently, a parametric study, presented in Chapter 4, was conducted using the finite element techniques.

Keywords: Stiffener, Plate, Initial Imperfection, Finite Element, Distortional Buckling

3.1 Introduction

As heavy industrial processes, such as in industrial furnace and boiler applications and power plants, require a large supply of air and gas, duct systems in industrial applications are significantly larger compared with those in residential and HVAC applications. Ducts with rectangular cross sections are commonly used in large industrial applications. A typical rectangular duct with stiffeners is shown in Figure 3.1. The width and the length of the duct are labeled as w and h, respectively.

Common sizes of industrial rectangular ducts are in the range of 5m to 15 m in cross sectional dimensions, sometimes even larger. As flue gas emission requirements become more stringent over the years, and as the use of precipitators, fabric filters and scrubbers becomes part of a duct system, the design pressure magnitudes have increased considerably. Therefore, additional reinforcements that stabilize thin steel plates are necessary in order to minimize the plate thickness and increase the strength-to-weight ratio. A stiffener functions as a plate reinforcement. In large rectangular ducts, the plate is generally stiffened with stiffeners in a parallel configuration. The plate and stiffeners act together as one composite section to resist the loads. The plate is probably the most important structural element in duct, but it could not economically function without its stiffeners.

The design process of ducts generally consists of global and local structural analyses. Determination of the stiffener spacing, as shown in Figure 3.2, and the selection of the stiffener section are the local structural analysis. The stiffener spacing is determined by

considering the allowable stress and the allowable deflection of a unit width of a plate strip between the stiffeners. The allowable stress and deflection of the strip of plate is generally calculated by considering large deflection plate theory which includes the bending stress and diaphragm stress. If the maximum deflection of plates exceeds half the plate thickness, the plate changes to shallow shell and withstands much of the lateral load as a membrane member, rather than as a flexural member. A method of spacing stiffeners using the large deflection plate theory and partial yielding was proposed in Chapter 2.

Once the stiffener spacing is defined, the stiffener member is chosen to resist the governing load. The pressure inside the ducts may be positive or negative. The transient negative and positive pressures are often in the range of 10 to 15 kPa. The stiffener design is generally governed by the combination of transient internal pressure and wind load. The critical load combination of transient pressure, wind load and other loads will be in the range of 15 to 20 kPa. The beam section is chosen by determining the capacity of the stiffened steel plate in composite action. The long stiffener span (5m to 15m or even larger) due to the quite large size of industrial ducts and high internal pressure generally result in using wide flanged steel section stiffeners. Under negative pressure (suction), the flange not connected to the plate is in compression and the plate is in tension. As the compression flange is not directly braced, the full span of the stiffener length is taken as an unsupported length. On the other hand, under the positive pressure, the flange not connected to plate will be in tension and the plate in compression. In the current design practice, a certain portion of plate and the corresponding stiffener is considered to act together as one composite section to resist positive pressure.

Although the design of stiffened steel plates has been done over the past several years, some of the stability aspects are still not understood. The structural analysis and the design of these large duct systems are not governed by any design standards and little publication on structural analysis and design procedures is available. Therefore, there is a need to conduct a study on the behavior and the strength of stiffened steel plates subjected to a lateral pressure load. This chapter focuses on the behavior of stiffened steel plates subjected to a negative pressure load. In this case, the flange not connected to the plate will be in compression and the whole tributary area of plate will in tension. The width of tributary area is the distance between centerline of adjacent stiffeners. Therefore, a representative stiffened plate panel consists of a stiffener and the tributary area. A typical cross section of stiffened plate panel is shown Figure 3.2.

3.2 Objectives

In this part of the study, a nonlinear finite element model is to be developed in order to accurately simulate the behavior of a stiffened plate panel subjected to a negative pressure load. The finite element model was built using the commercially available software ADINA (2009). ADINA is chosen because of its ability to perform geometric and material non-linear bucking analysis. The modeling efficiency is also evaluated against the accuracy of the solution with the experimental results.

In order to achieve this objective, it is necessary to incorporate the initial imperfections in the form of initial geometric imperfections and residual stresses. A comprehensive study of this plate panel requires an analysis of hundreds of finite element models which cover all the parameters affecting the behavior and capacity of stiffened plate panels. Each model would take a considerable amount of time to build. Therefore, it is necessary to develop an external computer program that can create a model based on values of the basic parameters provided.

This chapter is also to review and evaluate extensively the existing experimental and analytical work performed in the earliest work of Timoshenko (1961) on the buckling behavior of beams for different restraint conditions.

This chapter consists of three parts. In the first part, an extensive literature review related to the capacity of stiffener sections for which the tension flange is restrained is presented. In the second part, the numerical modeling techniques used to develop the finite element

model, including initial conditions and methods of analysis, are discussed. In the third part, the numerical analysis results are compared with the experimental test results to validate the modeling techniques used in the finite element models.

3.3 Literature Review

The current methods used to proportion the stiffeners are applications of standard code formulae used to design regular steel beams. These formulae are somewhat modified to accommodate the composite action formed by the stiffener and the duct plate. In standard design practice, the capacity of steel beams depends on the unbraced length of the compression flange. If the unbraced length of the beam is kept below the critical unbraced length, the section will fail by yielding rather than buckling. Bracing is therefore specified at certain intervals in order to maximize the beam capacity.

The failure of a beam by overall buckling is generally called lateral torsional buckling. At this failure mode, lateral movement and twist of the cross section occur. The closed form solution (Timoshenko and Gere 1961) for lateral torsional buckling of a simply supported doubly symmetric beam bent about strong axis by uniform moment M_o is:

$$M_o = \frac{\pi}{L_b}\sqrt{EI_yGJ + \left(\frac{\pi E}{L_b}\right)^2 I_y C_w} \qquad (3.1)$$

Where L_b = distance between braced points; E = Young's modulus; G = shear modulus; I_y = weak axis moment of inertia; J = torsional constant and C_w = warping constant. It should be noted that Equation 3.1 was derived using no twist but free to warp conditions at each end of the doubly symmetric beam. However, the lateral torsional buckling of a beam is a failure mode that involves lateral movement and twist of the cross section, but the cross section does not distort as shown in Figure 3.3. This means the flanges still lie

in parallel planes and the web remains straight and lies in the plane perpendicular to flanges at the buckling mode. However, it should be noted the flanges may twist at different angles and the web may involve distortion on its length during buckling as shown in Figure 3.3. In this mode of failure, the cross section of the beam gets distorted during buckling.

Bracing a beam is more complicated mainly due to the fact that the lateral torsional buckling of a beam involves both flexure and torsion. Effective beam bracing should resist the twist and lateral movement of the cross section. In general, bracing is divided into two categories; lateral and torsional bracings. The lateral and torsional bracings can restrain the twist and lateral movement fully or elastically. The lateral bracing restrains lateral movement. The effectiveness of a lateral brace is related to the degree of cross sectional twist prevented. For an I-beam subjected to uniform moment, the centre of twist is located at a point outside the tension flange; the lateral movement of the top flange is much bigger than that of the bottom flange. Therefore, a lateral brace restrains the twist best when it is located at the top flange (compression). Lateral bracing attached to the bottom flange (tension) is totally ineffective (Yura 2001). A torsional bracing can be different from a lateral bracing as the twist of the cross section is restrained directly. An example of a torsional bracing system is the twin beams with cross frame.

Generally, the span of a stiffened plate panel is the width w or the height h of the industrial duct. Therefore, the unbraced length of the compression flange of the stiffener of a duct under a negative transient pressure is assumed to be the span of the stiffened plate panel. However, the duct casing provides lateral restraint to the tension flange. The web of the stiffener and the duct casing may also provide some rotational restraint to the compression flange of the stiffener. Therefore, assuming the unbraced length of the outer compression flange to be the full span of the stiffened plate panel is uneconomical.

Taylor and Ojalvo (1966) addressed the use of torsional restraint as bracing. The authors gave the following exact equation for the critical moment of a doubly symmetric beam under uniform moment with continuous torsional bracing

$$M_{cr} = \sqrt{{M_o}^2 + \beta E I_y} \tag{3.2}$$

Where β is the torsional stiffness of the bracing per unit length. Equation 3.2 also assumes no cross section distortion. It should be noted that cross section distortion causes poor agreement with this equation (Yura 2001). In the case of a duct stiffener, the web of the stiffener and the plate attached to the stiffener will provide similar torsional restraint causing distortion of the cross section. Milner (1977) showed that cross section distortion could be approximated by considering the rotational stiffness of the web. Milner (1977) proposed the effective stiffness of bracing β_t in place of the β in Equation 3.2. The effective stiffness of the bracing β_t is defined by:

$$\frac{1}{\beta_t} = \frac{1}{\beta_b} + \frac{1}{\beta_{sec}} \tag{3.3}$$

Where β_b is the rotational stiffness of the external bracing and β_{sec} is the rotational stiffness of the web stiffener. Milner (1977) defined the rotational stiffness $\beta_{sec}$of the web as below:

$$\beta_{sec} = \frac{CEt^3w}{d} \tag{3.4}$$

Where C = a constant, t = thickness of the web, d = height of the web and w = width of the web beneath the support. This rotational stiffness β_{sec} was derived by assuming that a section of the web acts like a cantilever beam with height equal to the stiffener depth. This stiffness is equal to the end-moment of the cantilever divided by the end rotation. It should be noted that Equation 3.3 which is for discrete torsional braces could be adapted for continuous torsional braces. For continuous bracing, a unit width of web instead of the width of the web w beneath the support can be used.

In stiffened plate panels, the rotational stiffness provided by the duct casing can be considered as the rotational stiffness of the external bracing member β_b in Equation 3.3. According to Equation 3.3, the total effective stiffness β_t will be less than the rotational stiffness of the stiffener web or the duct plate. However, the application of this effective brace stiffness β_t into Equation 3.2 is based on the assumption that no cross section distortion occurs. In the case of a torsional restraint of the web to the compression flange, the web may bend to accommodate lateral movement of the compression flange and cause distortion of the cross section.

Since the stiffener section is welded to the duct plate, a singly symmetric composite section is created as shown in Figure 3.5. The lateral torsional formulae for doubly symmetric beams given in Equation 3.1 or Equation 3.2 cannot be used for a singly symmetric section where the smaller flange is in compression as in the case of stiffened plate panels. For the singly symmetric sections where bending is in the plane of symmetry, the shear centre and centroid do not coincide and the general formula for the lateral torsional buckling moment is given by Galambos (1968) as follows:

$$M_{cr} = \frac{C_b \pi^2 E I_y \beta_x}{2(K_y L_b)^2}\left[1 \pm \sqrt{1 + \frac{4}{{\beta_x}^2}\left[\frac{C_w {K_y}^2}{I_y {K_z}^2} + \frac{GJ\left(K_y L_b\right)^2}{\pi^2 E I_y}\right]}\right] \tag{3.5}$$

Where K_y and K_z are the effective length factors for the end restraint and $\beta_x =$ coefficient of monosymmetry. The general expression for β_x is:

$$\beta_x = \frac{1}{I_x}\int y(x^2 + y^2)dA - 2y_o \tag{3.6}$$

Where $I_x =$ major axis moment of inertia, $y_o =$ shear centre distance which is positive when the smaller flange is in compression, x and y are centroidal coordinates and integration is over the whole sectional area A. For practical purpose β_x of the section can be approximated by (Kitipornchai and Trahair 1980)

$$\beta_x = 0.9d'\left(\frac{2I_{yc}}{I_y} - 1\right)\left(1 - \left(\frac{I_y}{I_x}\right)^2\right) \tag{3.7}$$

Where d' = distance between the centres of areas of the flanges, I_{yc} = minor axis moment of inertia of the compression flange and I_y = minor axis moment of inertia of the whole cross section.

For torsionally braced singly symmetric girders, Yura (2001) showed that effective moment of inertia, I_{eff} of Equation 3.8 should be substituted for I_y in the bracing term of Equation 3.2, where I_{yt} = second moment of inertia of the tension flange and t and c are distances from the centroidal axis to the tension and compression flanges respectively as shown in Figure 3.5.

$$I_{eff} = I_{yc} + \left(\frac{t}{c}\right) I_{yt} \tag{3.8}$$

Equation 3.2 shows that the buckling load increases without limit as the continuous torsional brace stiffness increases. When enough bracing is provided, yielding will control the beam strength, and therefore M_{cr} cannot exceed the yielding or plastic strength of the section.

In the case of the industrial duct stiffener under consideration, the stiffener is fully restrained against translation and elastically restrained against twist. Therefore, the closed form solution (Timoshenko and Gere 1961) for lateral torsional buckling which assumes no cross section distortion is not applicable, since the stiffener will not buckle in a global mode as a lateral torsional buckling. In reality, the stiffener will buckle by distortion of web in either elastic or inelastic mode depending on its slenderness.

Whereas the distortion of the web was identified in some of the relatively early work on lateral stability (Cherry 1964, Bradford et al. 1984, Svensson 1985 and Bradford 1992), however, it was not able to derive any closed form solutions similar to Equation 3.1 or Equation 3.5 because of complexity of distorted cross sections. This problem is compounded by many effects which have a significant influence, including those of moment distribution, member slenderness, cross-section slenderness, continuity, restraints and interaction of local and global buckling. Therefore, a solution does not become itself to a closed form. It should also be noted that the concept of bi-moment-induced warping during buckling arises from the derivation of closed form solution for lateral torsional buckling by Timoshenko and Gere(1961). The bi-moment is formed from a pair of equal and opposite flange moments which lie in parallel to the flange planes. In distortional buckling, the flanges twist at different angles during buckling, so that the planes in which these flange moment are, are no longer parallel. Because of this, the concept of a bimoment has questionable meaning when applied to distortional buckling, although warping displacement occur during this mode of buckling.

Distortional buckling in a beam is characterized as a simultaneous occurrence of lateral deflections and a cross sectional distortion which arise only from the web distortion as shown in Figure 3.6 (Bradford 1997). It is assumed that the rigid top and bottom flanges displace by U_T and U_B and twist by $\emptyset_T$ and $\emptyset_B$, respectively and that the web distorts into a cubic curve(U_W), and that all deflections and twists vary sinusoidally along the length of the member. When the wave lengths of both the lateral torsional and local buckling of the compression flange are the same, then the mode is defined as lateral distortional

buckling. Early methods of analyzing web distortion were based on the assumption that the compression flange is a uniformly stressed strut restrained by a continuous translational restraint corresponding to the web, for which the elastic critical load can be calculated quite easily. This method was used in design codes as a U-frame approach, especially for distortional buckling of half-through girders. In this approach, the uniformly stressed flange is translationally restrained by a continuous restraint of web stiffness, α, per unit length. Then, the elastic buckling load N_{cr} was given as:

$$N_{cr} = \frac{\pi^2 EI_F}{L^2} + \frac{\alpha L^2}{\pi^2} \tag{3.9}$$

Where EI_F = flexural rigidity of compression flange and L = length of the strut. The minimum value of N_{cr} may be obtained by differentiating Equation 3.9 with respect to L. The elastic buckling load of the strut (compression flange) can then be used to determine the elastic critical moment M_o. Finally this critical moment is used to calculate the bending strength M_b for the limit state of overall buckling using standard code formula. This method was revised by Svensson (1985) to include a varying axial force on the compressed flange, which corresponds to the moment distribution on the beam. This method was proposed for deep bridge girders which have slender webs and very stocky flanges. However, this method had been shown to provide inaccurate predictions of the elastic critical loads of general rolled beams (Bradford 1997).

An approximate solution for the distortional buckling of I-sections which have comparatively stocky flanges and slender webs was presented by Hancock et al. (1980). During the distortional buckling the web distorts when flanges buckle as rigid bodies. Figure 3.6 shows a wide flange beam which buckles in such a fashion. During buckling, the plate elements of the section deflect and twist and a strain energy associated with the curvatures and twists of these elements is stored. These curvatures and twists can be derived from the assumed deformations and the strain energies can be obtained by using usual energy expressions. To simplify the calculation, some terms were neglected to get the modified energy expression. During buckling, as the energy is conserved, the determination of the stiffness matrix is zero. This yields a quadratic equation in terms of uniform bending moment applied and stiffness of the plate element. However, this was based on the assumption that stocky flanges rotate as rigid body. Therefore, it does not predict the local flange buckling behaviour, which accompanies global buckling during the distortional buckling.

The above method was extended to obtain a beam type finite element for a linear eigenvalue problem by Bradford and Trahair (1981). This element has six nodal out of plane buckling degrees of freedom, comprising the two flange translations U_T and U_B, two flange rotations U_T' and U_B' with respect to longitudinal axis and two flange twists about vertical axis $\emptyset_T$ and $\emptyset_B$. Thus, this beam type finite element has six degrees of freedom at each longitudinal node.

(Bradford 1988) was able to extent this method to monosymmetric beams as top and bottom flange strain energies due to the warping and twisting of flanges were calculated separately. This method predicts the buckling strength for longer and slender members adequately, but inaccuracy arises in shorter and stockier beams for which the interaction between elastic buckling and yielding becomes significant (Bradford 1988). The inelasticity also becomes significant due to the level of residual stress.

Therefore, the above elastic method was extended to incorporate the inelasticity using an incremental and iterative solution of the buckling equation to determine the lowest load factor. In this extended method, a tri-linear stress-strain curve was assumed for the structural steel, in addition to linear a residual stress pattern.

The inelastic method of analysis of the distortional buckling of I-beam sections was later modified to include the effects of continuous elastic restraints against translation, minor axis rotation, torsion and warping (Bradford 1997). In this method, a model of elastic restraints appropriate to chosen displacement fields was introduced. These restraints for top and bottom flange were two translational restraints, two rotational restraints, two torsional restraints and two warping restraints. This method yielded a beam type finite element that incorporates eight degree of freedom at each longitudinal node that is augmented to handle elastic restraints. The vectors of buckling displacements are U_T, U_B , $U_T{}'$, $U_B{}'$, $\emptyset_T$, $\emptyset_B$, $\emptyset_T{}'$ and $\emptyset_B{}'$, where prime indicate the rate of change with respect the longitudinal axis.

In the case of stiffeners in industrial ducts, a stiffener can be considered as a beam fully restrained against lateral displacement and twist along its tension flange. The compression flange is restrained elastically by the stiffness of the web. The effect of elastic restraint, particularly the torsional restraint, on the buckling mode of the stiffener is obviously distortional as shown in Figure 3.6. To include the full translational and elastic twist restraint of the tension flange, the inelastic method presented by Bradford (1988) was modified by Bradford (1998a). Here, it was assumed that a continuous restraint of stiffness per unit length inhibits the twist of the tension flange, while a continuous restraint of stiffness per unit length inhibits the rate of change of twist. The latter stiffness is related to a warping type restraint. The top flange is assumed to be completely free from restraint. These restraints against twist and rate of change of twist correspond to the torque per unit length and warping bi-moment contribution per unit length.

In a recent study by Udall (2007), a method to calculate the flexural capacity of a stiffened panel was proposed. Udall's (2007) proposal was based on standard elastic lateral torsional buckling beam formula; Equation 3.1. Udall (2007) considered test results on six stiffened plates panels and a parametric study for twelve stiffened panels. The parametric study was an Eigen value elastic buckling analysis. The proposal was a modification of the elastic solution (Equation 3.1) of the lateral torsional buckling of a doubly symmetric beam. The primary requirement in the development of Equation 3.1 is that the cross section should involve a lateral translation, while remaining a rigid body when the beam buckles. As a result of that lateral displacement, the applied bending

moment gives a torsional component which causes torsional buckling. The twisting of the beam occurs when the compression of flange become unstable as a result of its being subjected to a flexurally induced axial stress. To the contrary, the bottom flange of the stiffener that is connected to duct plate is in tension and the top flange is in compression when the duct is under negative pressure. The duct plate provides lateral restraint to the tension flange. Because of this lateral restraint, the lateral torsional buckling theory predicts that the beam should reach its plastic moment capacity. Stiffeners with full restraint in the tension flange, however, buckle in a lateral distortional mode, in which the web distorts in order for the compression flange to displace and twist during buckling.

Udall (2007) proposed that the effective width of a duct plate is equal to 128 times of the duct plate thickness on either side of stiffener flange edge. However, less than half of this effective width provides the second moment of area about weaker axis nearly equal to second moment of area about stronger axis. According to derivation of beam elastic buckling Equation 3.1, the second moment of area of the stronger axis must be large compared to second moment of area about weak axis so that the lateral displacement U is not linked to twist. This is clearly the case for general beam sections. But, this is not the case for stiffened plate panels with the proposed effective width. Udall's (2007) modified lateral torsional buckling Equation 3.1 to calculate the section properties of composite section ignored the tension portion of composite section. Udall (2007) used an equivalent section whose depth is equal to twice the distance between the neutral axis and compression flange of the stiffened plate panel. It was supported by the fact that the terms A_f and r_t of the compressive portion are employed by AISC ASD (1989) in calculating

bending stresses. In the codification of elastic beam buckling in AISC ASD (1989), the warping stiffness in Equation 3.1, neglecting the uniform torsional stiffness $EI_y GJ$ in Equation 3.1, was only used to derive the bending stress. During the simplification of this warping stiffness, it was assumed that $r_T = 1.2r_y$.

This design method by Udall (2007) only focuses on the peak strength of a stiffened panel and does not correctly predicts the behavior of stiffened plate panels. Grondin et al. (1999) did a numerical analysis to investigate the strength and behaviour of a plate panel stiffened with a T-section and identified the conditions that may lead to failure by tripping of stiffeners. Stiffener tripping is characterized by the rotation of the stiffener about the stiffener plate junction. Compared with other modes of failure, stiffener tripping generally results in a sudden drop of load carrying capacity (Grondin et al 1999). The dominant force in their study was longitudinal compression as they investigated stiffened plate panels that form the hull of a ship or a box girder of a bridge. But, the dominant force in stiffened plate panels of industrial duct is bending moment. The ultimate and post buckling strength depend on the failure mode of stiffened plate panels (Grondin et al. 1999). Therefore, it is necessary to identify the behaviour of stiffened plate panels that dictates their strength.

The methods of designing steel beams use a conversion of the beam's resistance to elastic buckling strength that allows for the effects of residual stresses and initial imperfections. Thus, when the influence on the elastic buckling resistance of the brace stiffness can be included with those effects of beam geometry, moment distribution and load height, then the conversion allows the beam design strength to be estimated (Valentino and Trahair 1998).

The review of literature has indicated that the parameters that dictate the behaviour and strength of stiffened plate panels are cross sectional slenderness, stiffener overall slenderness, support restraint conditions, load height and location relative to the shear centre and material characteristics (Bradford 1997). In a duct, the critical loading for the stiffened plate panel is the lateral negative pressure. Then, the load height and type of load will be out of focus from the list of parameters. Also, the stiffened panel is generally designed and detailed for construction as a simply supported beam. The material characteristics can also be out of focus as industrial ducts are constructed using general structural steel members that are made of general steel grade. However, the material characteristics will be considered. The geometric parameters that affect the behaviour and strength of stiffened plate panels are cross sectional slenderness and member overall slenderness. The effect of these factors on stiffened plate panels subjected negative pressure load, however, did not receive much attention in research studies. Therefore, the effect of these parameters on the behavior and strength of stiffened plate panels needs to be investigated.

With the current analysis tools and computing power, more precise modeling of stiffened steel plate panels can be achieved. Factors such as residual stresses and initial imperfections can be explicitly incorporated into numerical models. Grondin et al (1999) showed that the magnitude and distribution of initial imperfections have an influence on the capacity of stiffened plates failing by plate buckling, but little influence on failing by overall buckling. Grondin et al (1999) also showed that residual stresses have an influence on the compressive strength of stiffened plates failing by plate buckling.

3.4 Finite Element Model

A review of the literature indicated that number of tests conducted on stiffened plate panels subjected to negative pressure load is very limited. To fully understand the behavior of stiffened plate panels, a large number of tests are required in order to incorporate a wide range of the parameters that affect the behavior of stiffened plate panels. However, it is uneconomical to conduct a large experimentally based investigation. At the present time, one of the most popular methods used to analyze a structural problem is the finite element method. The finite element method has been proven to offer an efficient analytical approach while providing reliable results (Bathe 1996). In order to cover all the parameters, a finite element method based numerical model was used to investigate the full range of parameters.

The numerical modeling techniques employed should be adequate in simulating the stiffened plate panel subjected to lateral pressure load. The accuracy of the model depends on the ability of the modeling techniques to simulate the material and geometric properties, loading, boundary conditions and initial imperfections. Therefore, this chapter focuses on the techniques used to build the model and analyze the numerical model successfully. The performance of this model was first verified by comparing the predicted strength with corresponding tests results.

In this numerical simulation, finite element analysis software ADINA (2009) has been used. ADINA is a commercially available multi-purpose finite element software package. The structural analysis module of ADINA was used for this study. In this investigation,

since the nonlinearity comes from the material properties and buckling behavior of stiffened panels, the nonlinear finite element method was done using ADINA. ADINA contains an extensive element library, material models and modeling capabilities.

The large deflection of laterally loaded thin-walled stiffened plate panels involves in-plane and out-of-plane displacements. Therefore, a shell element was used to study the behavior of the laterally loaded stiffened plate. Figure 3.7 shows a 4-node nonlinear shell element with the shell mid-surface nodal points. In order to simulate the nonlinear buckling behaviour, the flanges and the web were modeled with the shell element. The 4-node shell element is based on the updated Lagrangian formulation (Bathe 1996). The nodal coordinates are updated to reflect the current position in space and all the shape functions and derivatives are updated based on current updated coordinates. Each node has six degrees of freedom: three translations and three rotations. The 4-node shell element used in this study can be employed to model thick and thin general shell structures. The shell element is formulated with the assumptions used in the Mindlin/Reissner plate theory. This shell element can be used with elastic-isotropic, plastic-bilinear and plastic-multilinear material models. This shell element can also be used in a large displacement/small strain problem. This type of element is suitable for the present application since the magnitudes of the strains are generally not very large. In order to capture the onset and spread of material yielding accurately, the Newton-Cotes rule, also known as the Simpson rule, was chosen with seven integration points. Further information was given in Chapter 2,

In order to study the laterally loaded plate panel beyond the elastic limit, it is necessary to obtain the nonlinear equilibrium path even into the unloading region. In the nonlinear finite element analysis, the equilibrium along the loading and unloading path can be obtained by incremental methods. In order to obtain the equilibrium path after each increment, an iteration technique is needed. In this study, the increment is done by automatic step increment by Load Displacement Control (LDC) method. The LDC method can be used to solve for the nonlinear equilibrium path of a model until its collapse. In the LDC method, a prescribed displacement for the first solution step and an expected maximum displacement have to be defined. The main feature of this method is that the level of the externally applied loads is adjusted automatically by the program even during the iteration process to eliminate unbalanced forces. This method uses the arch length method for the iteration to solve highly nonlinear problems including snap-through response problems. This method will terminate at the solution that satisfies the user defined displacement. In spite of computational challenges arising from incremental nature of the solution process and the highly refined finite element models, a personal computer was used to satisfactorily carry out this study.

An experimentally verified finite element model will be extensively used in a parametric study to investigate the behaviour and strength of stiffened plate panels subjected to lateral pressure loads. This parametric study would require hundreds of different models. In the finite element program ADINA, the model can be built either by entering the model parameters through the ADINA User Interface (AUI) dialog boxes or by entering the commands into the AUI command window. These commands can be a text batch file

containing all commands and parameters needed for constructing the model. Then, this text batch file, with file extension ".cmd", can be entered through standard input. This batch file contains the commands to create the geometry including initial geometric imperfection, to create the residual stress pattern, and to define the material model, loading information, boundary conditions, analysis options and post processing options. Each batch file may contain thousands of command lines. Each model takes a considerable amount of time to build. An effective way of creating the finite elements models for a parametric study must utilize quick and effortless manipulation of the input data. The analyst must be capable of altering the model quickly without any costly changes in all model parameters. Also, it is important to guarantee the accuracy of models and solutions for each parametric model by keeping general parameters unchanged. Therefore, it was decided to automate the process of creating the command batch file. An external program using Visual Basic for Application was developed for this automation. All the general basic data for the model, such as the stiffener's dimensions, plate width, plate thickness, material information, boundary types, analysis options, element sizes and density, amplitude of geometric imperfection and residual stress, etc, will be entered in a table form. The external program will generate the necessary coordinate points and the geometry of the stiffened plate panel and then the batch file containing thousands of command lines is generated instantly, based on the above basic data in the table. This automation helps keeping the similarities between models by avoiding accidental error during manual modeling. Also, this automation enables quick post processing as the user can identify the element and node numbers easily anywhere in the model to obtain results.

3.4.1 Initial Geometric Imperfections

The initial geometric imperfections may exist in the plate elements of stiffened plate panels. The geometric imperfections arise during the production of stiffeners and the fabrication of stiffened plate panels by welding. It may also be noted that in order to initiate the buckling response, the finite element buckling analysis needs some disturbance. This disturbance may be a geometric imperfection or a load disturbance. It should be noted that both the magnitude and shape of the initial geometric imperfections play an important role in buckling behavior. An initial geometric imperfection similar to expected buckling mode or the shape of existing geometric imperfection is generally applied on finite element models. In this study, the shape of the buckling mode was assumed to be the initial geometric imperfection as this imperfection will lead to lower bound until and after the ultimate limit state is reached. The stiffened plate panel under consideration may experience local buckling on its plate elements and overall distortional buckling in its stiffener. Therefore, each local buckling type and overall buckling mode of initial geometric imperfections should be included and amplified by the maximum amplitude and the resulting pattern should be superimposed to incorporate the complete initial geometric imperfection.

In order to incorporate the local buckling modes on the plate elements of the stiffened plate panel, in the current study, a double sine wave distribution of the initial geometric imperfection was assumed. Carlsen and Czujko (1978) studied the distribution of post-welding initial geometric imperfection in the plates used in ship structures and suggested that the initial deformed shape could be expressed by a double trigonometric function. To

incorporate the initial imperfections in the flanges, the lines along the flange-to-web joint and the lines along both ends of the member were defined to be straight, but the free edges of the flanges were defined to form a number of half sine waves along the member length. For the web, all edges were defined to be straight, but the middle line along the member length was defined to form a number of half sine waves. To incorporate the initial imperfections in the flanges, web and plate, the lengths of the half sine waves were taken as the half the width of the flanges, the depth of the web, and half the width of the flange respectively. Therefore, the distribution of such assumed imperfection in the flanges, the web and the plates can be calculated using the following curved line equations:

For the geometric imperfection of the flanges and the plate:

$$\delta = \delta_o \sin\left(\pi \frac{2x}{b}\right) sin\left(\pi \frac{2y}{b}\right) \tag{3.10}$$

For the geometric imperfection of the web:

$$\delta = \delta_o \sin\left(\pi \frac{x}{h}\right) sin\left(\pi \frac{z}{h}\right) \tag{3.11}$$

Where δ_o is the maximum imperfection amplitude, and b and h are the width of the flange and the web respectively. The exaggerated initial imperfection for the local buckling of the plate elements is illustrated in Figure 3.8. x, y and z axes are along the longitudinal, transverse and vertical directions, respectively.

In order to incorporate the overall distortional buckling mode of the stiffeners, the initial geometric imperfection of the stiffener can be modeled with following sinusoidal wave (Paik at el. 1998) :

$$\delta = \delta_{os} \frac{\mathrm{z}}{\mathrm{h}} \sin\left(\pi \frac{x}{L}\right) \tag{3.12}$$

Where δ_{os} = maximum amplitude of the sinusoidal sweep of the stiffeners and L = length of the stiffener. Figure 3.9 illustrates the exaggerated shape of sinusoidal sweep applied to the stiffener.

The amplitudes of the imperfections such as the cross sectional geometry and sinusoidal sweep, based on standard mill practice, are outlined in CSA (2010) and AISC (2005). The maximum amplitudes of the imperfections used in this present study are limited to those values associated with the cross sectional geometry and the sinusoidal sweep. The maximum permissible variation in the cross sectional geometry of the flanges is 3mm to 4mm depending on the width of the flange as given in CSA (2010) and AISC (2005). For the inelastic failure of high strength steel wide flange beams, Earls(1999) used the maximum amplitude for the plate elements based on the mill practice as outlined in AISC (2005). Thus, the present study also assumes the maximum imperfection magnitude δ_o of 3 mm for plate elements.

The maximum amplitudes of the permissible sinusoidal sweep are 0.001 times the length of the W shape with flange width greater than 150mm and 0.002 times the length of the

W shape with flange width less than 150 mm CSA (2010) and AISC (2005). Paik at el. (1998) investigated numerically the characteristics of tripping failure in flat bar stiffened plate panels subjected to an axial compressive force. In their study, the amplitude of the global initial deflection was taken in the flat bar stiffener as 0.0015 times the stiffener length. Therefore, the maximum amplitude δ_{os} of the sinusoidal sweep was assumed to be 0.001 times the length of the stiffener. In the current study, the above mentioned initial imperfections were superimposed into the numerical model as illustrated in the exaggerated Figure 3.10.

3.4.2 Residual Stresses

Structural wide flange shapes are manufactured by hot rolling where hot steel is shaped by being forced through a system of rollers. When the structural shape is allowed to cool in the air, the tips of the flanges and the centre portion of the web cool more rapidly than the areas adjacent to the flange-to-web junction. Then, when the central portion of the flanges is restrained by already cooled stiffer areas near the flange tips and centre portion of the web, this causes a self equilibrating stress pattern, known as the residual stress. In W-shaped steel sections, it is typical for the tips of the flanges and the web centre to be in compression while the flange-to-web junction areas are in tension. The residual stress in structural shapes varies along the width of the web and flanges, but not significantly across the thickness of the plate. The distribution of the residual stress across the flange and web of the stiffener can be idealized linearly as shown in Figure 3.11. The magnitude of the compressive and tensile residual stress was assumed to be equivalent to $0.3F_y$ (Arasaratnam 2008 and Grondin et al 1999).

The presence of residual stress in stiffened plates is primarily attributable to the welding of stiffener elements to the plate. The distribution of residual stress due to welding is generally quite different from that due to hot rolling. During welding, metal reaches the plastic range. Due to the different cooling rates and the interaction between different plate fibres, the area nearest to the weld is in tension. Faulkner (1975) measured the residual stress in stiffened plates and proposed a tension block vicinity of weld region. The tension block is extended to three to six times thickness of the plate on either side of the

weld. The following relationship was proposed for the maximum compressive residual stress on the plate.

$$\frac{f_r}{f_y} = \frac{2\mu}{\frac{b}{t} - 2\mu} \tag{3.13}$$

Here f_r= magnitude of compressive residual stress in the plate, f_y= yield strength of the plate, b= width of the plate, t= thickness of the plate and, μ = constant that depends on type of welding. The recommended μ was 4.5 to 3. The welding of stiffeners to the plate introduces tension residual stresses close to the yield stress. As these residual stresses are self equilibrating, residual stresses generally have little effect on the ultimate strength of compressive elements (Grondin et al 1999).

In industrial ducts, the typical connection between the stiffener and the plate in order to have composite action fully is made by using intermittent fillet welds that are staggered on either side of the stiffener. The intermittent welding adds less heat to the plate, thus it reduces the amount of residual stress in the plate. Therefore, the maximum welding tensile residual stress was assumed to be $0.5f_y$. The welding residual stresses in the plate and the bottom flange are accounted for in this numerical study by assuming an idealized linearly varying residual stress pattern as shown in Figure 3.11. The resultant residual stress on the bottom flange due to forming and welding was incorporated in the finite element model. The residual stress was applied at the nodal points as initial strains in the

finite element models. ADINA (2009) provides facilities for allocating the initial stresses and strains in the nodal points of the finite elements.

3.4.3 Material Models

The stiffened plate panels subjected to a negative pressure loads involves material nonlinearity beyond the yielding. Therefore, for the nonlinear finite element analysis, characteristics of the material behavior should be defined precisely in terms of stress versus strain. The realistic relationship between stress and strain can be estimated through the standard tensile coupon testing which covers linear elastic region, yielding, yield plateau, strain hardening, ultimate strength and necking effect.

In the experimental test (Udal 2007), the plate was made of mild carbon steel 44W and the material of the wide flange stiffeners was mild carbon steel A992. During the experiment, the stress-strain relationships were not established for the material of the stiffeners and the plates through the tensile coupon test. Numerical analysis found in the literature generally employ simpler idealized material models as the effects of strain softening and necking for the ultimate limit state of structural limit state design are often unaccounted for. However, numerical simulations of structural steel require accurate yield stress and ultimate tensile stress in order to predict the ultimate strength of the structural member. Generally, ASTM specification provides one minimum yield stress and one minimum ultimate tensile stress for all available grades of structural steels, except for steel grade A992. The steel grade A992 has a range of minimum yield stress from 345 MPa to 450 MPa. Therefore, it is necessary to use realistic yield stress and

ultimate tensile stress for the stiffener material (A992) used in the experimental tests. Recently, Arasaratnam (2008) established stress-strain relation for steel grade A992 using specimens obtained from plate elements of wide flange structural shape. The average yield stress F_y of flange coupons was established to be 444 MPa.

In this verification study, therefore, the material model was assumed to be an idealized tri-linear representation of mild carbon steels A992 and 44W. The tri-linear elastic-plastic-strain hardening models are shown in Figure 3.12. These material models are idealized considering three distinct material stress-strain relationship features; initial linear portion, presence of a yield plateau, magnitude of strain hardening. The Young Modulus E of all three models was taken as 200 GPa. The nominal yield stresses of mild carbon steel A992 and 44W were assumed to be 440 MPa and 300 MPa, respectively. The nominal strain at yield ε_y is $\frac{F_y}{E}$. The strain hardening is anticipated at strains that are somewhere between 10 to 20 times ε_y. The strain hardening slope E_{st} was considered to be $\frac{E}{30}$. The minimum specified ultimate stress for the steel A992 and 44W are 540 MPa and 400 MPa respectively. The values of the strain-stress relation of mild carbon steel A992 and 44W were presented in Figure 3.12. These relationships will be applied in the material models. For both of mild carbon steels, the value of ultimate strain is specified to be large so that it can never be reached in the analysis. The other parameter considered herein is Poisson's ratio, υ. The accepted Poisson's ratio values for steel in generally 0.3.

To predict material behaviour under multi-axial loading, a yield criterion that indicates the combination of stress components for which transition from elastic to plastic deformations occur should be used. The applicable yield criterion for metal plasticity is the von Mises yield criterion. The von Mises yield criterion has been interpreted physically as implying that plastic flow occurs when shear strain energy exceeds a critical value. The von Mises criterion is often used to estimate the yielding of ductile materials. Also, this criterion is largely based on the experimental observation that most polycrystalline metals are isotropic. Steel is also an isotropic and ductile material. A flow rule relates the plastic strain rates to the current stresses and the stress increments subsequent to yielding, and a hardening rule specifies how the yield condition is modified during plastic flow. ADINA metal plasticity model is characterized as an associated flow plasticity model with the isotropic hardening rule being used as the default hardening rule. An associated plasticity model is a plastic flow rule. It was observed experimentally that metals such as steel obey the associated flow rule. Also, in other numerical studies on the behaviour of steel structural members, it is common practice to use the isotropic hardening rule to track the yield surface. Therefore, the default ADINA metal plasticity features were used in the present study. These features are based on an associated flow plasticity model that uses von Mises yield criterion as the failure surface. Evolution of this failure surface was restricted in the current study to isotropic hardening rule.

The finite element analysis method can be used accurately to trace the nonlinear equilibrium path, even into the unloading region, in the buckling behaviour of stiffened plate panels. Thus, the finite element method can be used to obtain the applied pressure

load and corresponding deformations and stresses of stiffened plate panels, in addition to obtaining their buckling and collapse modes. In this portion of the study, finite element models for stiffened plate panels were developed to verify the accuracy of the model techniques with available experimental results in literature. This model incorporates initial imperfections in the plate elements forming the cross section and in overall length of the stiffener and an idealized distribution of residual stresses for the cross section.

3.5 Statement of Problem

Nonlinear finite element methods are powerful tools in analyzing nonlinear structural responses that involve geometric and material nonlinearities. Current nonlinear finite element methods are widely accepted for their ability to predict structural behaviour and strength accurately. However, the numerical modeling techniques employed should be able to idealize adequately the structural problem under consideration. Therefore, it is necessary to verify the modeling techniques used. This is generally accomplished through comparison with experimental or existing theoretical results. Before the verification study, first a convergence study is usually carried out to identify the best size of mesh in order to achieve this verification. Therefore, in this portion of the study, an experimental verification study, followed by a convergent study, is done.

3.5.1 Mesh Density and Convergence Study

In order to get a sufficient level of accuracy with less computational cost, generally similar nonlinear finite element models with a variety of element mesh densities are analyzed to obtain the best mesh density. However, due to the local and global distortional buckling in the flange and the web, which arise during the analysis of stiffened plate panels, it is required to reflect the deformation behavior. The element size should be able to represent the geometry and the deformation behavior. Although a coarser mesh can generally yield the required degree of accuracy, the initial imperfection, specially the residual stress pattern, dictate the finer element sizes in this study in order to incorporate them into the model.

However, in this numerical study, a convergence study was performed in order to establish a suitable mesh density. Figure 3.13 shows the geometry of the stiffened plate panel model used in this mesh size convergent study. The thickness of the plate in the stiffened plate panel was 5mm and the plate was assumed to be made of steel grade 44W having 300MPa nominal yield strength. The depth of the stiffener was chosen to be 240mm as shown in Figure 3.13. The stiffened plate panel was subjected to a lateral negative pressure. The stiffener section was assumed to be made of steel grade A992 having a yield strength of 440 MPa. The stress-strain relation of both material were idealized to be tri-linear as described in Section 3.3.3. The geometric imperfection for plate elements and the stiffener was incorporated as described in Section 3.3.1. The residual stress was not applied for this convergent study. The percentage change in ultimate load was compared as the mesh was being refined. The mesh validation was

performed on five different runs with the same physical properties of stiffened plate model and the same loading conditions. The only variable changing was the mesh size. Table 3.1 shows the mesh detail and the analysis results. As shown in this Table 3.1, four different finite element mesh configurations were considered in this convergence study. The coarse mesh contained only 441 shell elements, whereas the most refined mesh contained 1201 elements.

The results from the convergence study are also shown in Table 3.1. Table 3.1 also shows the percentage change associated with ultimate moment capacity between different mesh refinements. The percentage change in ultimate moment capacities from a mesh density of 1 to 2 and 2 to 3 were 2.65 % and 1.5 %, respectively. The percentage change in the ultimate moment between mesh densities of 3 and 4 was only 0.75 %. In general, the percentage change less than 5 % may be considered acceptable. Thus, mesh densities 1, 2, 3 and 4 may be acceptable. As seen from the above results, a reasonable degree of accuracy can be obtained with a coarse mesh. However, due to the severe nature of the material and geometric nonlinearities involved in later analyses, a very dense mesh of shell elements was desirable in order to trace the nonlinear equilibrium path into the unloading region. Thus, mesh 3 was selected as the most suitable mesh and this mesh density was used for rest of the studies presented in Chapter 3 and Chapter 4. In Physical dimensions, each element is of size 50 x 30 mm. Although this mesh density results in more accurate solutions, a further finer mesh was required to incorporate the residual stress pattern considered for this study.

3.5.2 Verification of Numerical Modeling Techniques

The finite element model developed herein would be used to study the buckling strength of stiffened plate panels. As part of this study, before performing the analysis, it is necessary to validate the finite element modeling techniques used in the present study. This can be accomplished through the application of above developed element modeling techniques and the comparison of the results obtained from these finite element models with available experimental results. This portion presents a comparison between test results and the predictions from the finite element numerical analysis. It is interest of here to determine the behaviour and strength of a stiffened plate panel subjected to lateral pressure load. Therefore, the applied load versus displacement along with the buckling modes of the experimental results and the numerical results will be compared.

Description of Experiment: Due to the severe nature of both material and geometric nonlinearities involved, the finite element model should be able to adequately trace the nonlinear equilibrium path of a laterally loaded stiffened plate. Therefore a similar experimental tests are needed so as to compare the validity of the finite element model. Because of the very limited research study in this area, it was difficult to find experimental results to validate the numerical model. The experimental test results on stiffened plates subjected to lateral pressure by Udall (2007) were selected as a basis of comparison with the numerical results. The scope of Udall (2007) experimental test was to estimate the capacity of the stiffened plate panel. To simulate the loading and the boundary condition of stiffened plates of a large industrial duct, a shallow box with a removable top was made. The removable top contained the plate with a stiffener attached.

The box was made reasonably air tight and the pressure load was applied by vacuum pump. This arrangement simulated a single stiffener and plate between two adjacent stiffeners subjected to lateral pressure. The vacuum pressure was increased until the stiffener collapsed. The test results from these tests (Udall 2007) were used to validate the finite element techniques employed in this study.

A schematic diagram of the test specimen is shown in Figure 3.14. In his study, the size of the box was 4572 x 2438 mm in plan area and 152 mm in depth. A 76X76X7.9 angle frame around the perimeter of the box acted as flange for the removable stiffened plate panel. As reported by Udall (2007), the plate thickness of stiffened panel was 4.76mm and made of ASTM 44W steel with the nominal yield strength of 300MPa . The test stiffeners were W310X21 (W12X14) and W200X27 (W8X18) wide flange sections made of steel grade A992 with the nominal yield strength of 440 MPa. The W310X21 (W12X14) and W200X27 (W8X18) stiffeners were slender and compact sections respectively. Therefore, different failure modes were expected. The experiment consisted of six test specimens using three W200X27 (W8X18) stiffeners and three W310X21 (W12X14) stiffeners.

Description of Numerical Model: Based on the investigation by Udall (2007), two finite element models for the stiffened plate panels, for each W310X21 (W12X14) and W200X27 (W8X18) stiffeners, were developed to determine how accurately the proposed modeling techniques are able to predict the buckling behavior and the strength of stiffened plate panels. The modeling techniques used to develop the models were

presented in Section 3.3. The geometrical details are shown in Figure 3.14. The geometry of the finite element models was created incorporating the geometric imperfection as described in Section 3.3.1. The initial imperfections were modeled at the time of defining mesh. This enabled incorporating the known magnitude and distribution of imperfections in the models. Several thicknesses were specified in each model corresponding to the plate, stiffener flange, stiffener web, angle frame and box. A tri-linear elastic-plastic-strain hardening material model with a von Mises yield criterion was used to model the material's constitutive behavior. Since large out of plane deformations and finite strains were expected in the model during analysis, particularly after buckling, the large displacement and small strain formulation was used. The yield strengths of the plate and the stiffener were assumed to be 300 MPa and 440 MPa, respectively. The yield stress of stiffener obtained by Arasaratnam (2008) was used for this nonlinear numerical analysis as no material characteristics were established by Udall (2007) for his experiments or numerical studies. In this verification study, the modulus of elasticity of 200 GPa was assumed for both plate and stiffener. The only residual stress introduced in the model was the longitudinal stress arising from cold forming and welding process as described in Section 3.3.2. The residual stresses were incorporated into the model as initial strains at nodal points. ADINA uses automatic step increment to carry out the nonlinear incremental analysis for predicting the load-displacement path into unloading region.

In order to simulate the stiffened plate panel edges supported by the angle frame and the box, the vertical faces of box including the angle frame were modeled. Figure 3.15 shows the finite element model of the stiffened plate panels including the angle frame and

support box. The boundary conditions along the plate boundary are now realistically represented by the stiffness of the box with angle frame flange. The bottom edges of the box vertical faces were fixed. Although out-of-plane and in-plane lateral translation of the flange and the web of the stiffeners are not prevented during the experiment as it is usually the case in an actual stiffener of the industrial duct. It should be noted, unless otherwise shown, all degrees of freedom for all nodes were set to freely translate and rotate.

The automatic step incrementing was carried out by the Load Displacement Control (LDC) method in which a prescribed displacement for the first solution time step and expected maximum displacement are defined. The maximum displacement (50mm) was specified at the middle of bottom flanges. The main feature of this method is that the level of the externally applied pressure load is automatically adjusted by ADINA. The Load Displacement Control method was used to follow the nonlinear equilibrium path of the model until and after its collapse.

The characteristics of the stiffened plate panel behavior which were used to compare the results of finite element model were obtained from the numerical analysis. The characteristics were the failure deformation shapes of stiffened plate panels and the applied pressure versus vertical deformation. A quick observation indicates that the failure deformation shapes and the associated load versus deformation patterns are clearly similar.

It should also be noted that the ability of the finite element models to predict the failure modes are consistent with buckling modes observed during the experiments. A comparison of the buckling modes between experimental and numerical results is shown in Figures 3.16, 3.17, 3.18, 3.19, 3.20 and 3.21. The web of the stiffeners got distorted to accommodate the lateral movement of the compression flanges. This mode is clearly similar to the buckling mode seen in numerical results.

Figures 3.16 and 3.17 compare the failure modes of a plate panel with stiffener W200X27 (W8X18) obtained from the test and the numerical simulation respectively. The deformed shape obtained from the finite element analysis is very similar to the one observed during the test. Both have same configuration and web distortional buckling wave at the middle of the plate panel. Also, it should be noted the wave lengths of the distortional buckling modes for the test and numerical simulation are same.

Figure 3.18 and Figure 3.19 depict the deformed configurations numerically predicted and experimentally obtained for the steel plate panel stiffened by W310X21 (W12X14). Both have the same configuration and similar distortional buckle waves. During the deformation in both numerical and experimental tests, the both ends of the top flanges move slightly in opposite direction with respect to the original location of the centre line the top middle flanges. This is because the wave lengths of the case with stiffener W310X21 (W12X14) is higher than that of the case with stiffener W200X27 (W8X18). It should be noted that the cases with stiffener W200X27 (W8X18) do not experience the opposite movement of top end flanges because of the shorter wave length of their

distortional buckling mode. The buckling deformation shapes between the numerical analysis and experiments are in good agreement. Also, it can be concluded that higher web depths lead to higher wave lengths of the distortional buckling mode.

For further comparison, close up views of the middle portion of the stiffened plate panel with stiffeners W310X21 (W12X14) from both the test and the finite element analysis are also depicted in Figure 3.20 and Figure 3.21. Both experience local buckling type deformations in the flanges following the distortional buckling of the stiffener. This indicates that the numerical model is able to predict the behavior of the stiffener correctly even after the collapse.

The next step in the validation process was to compare the predicted pressure load-vertical displacement response with the reported test results. The analytical and experimental results for stiffened plate panel with stiffener W200X27 (W8X18) was presented in Figure 3.22. The vertical and horizontal axes represent the pressure load in kPa and mid-span vertical deflection in mm, respectively. It could be observed that the numerical analysis results agree well with the experimental results. The following observations can be made. The shapes of the curves are similar and the measured and the predicted peak strengths are almost the same. The differences between the predicted capacities and measured capacities are only 1.5% for the case of stiffener W200X27 (W8X18).

Although the finite element models successfully predicted the failure modes for both stiffeners and the model with stiffener W200X27 (W8X18) very closely matched the experimental load versus deformation response, comparison of the load versus deformation response from numerical result of the model with stiffener W310X21 (W12X14) does not closely matched that of the test as shown in Figure 3.23. The numerical model of the stiffener W310X21 (W12X14) predicted 12% smaller strength than predicted by experimental analysis. However, the numerical model of stiffener W310X21 (W12X14) buckles when the mid-span vertical deflection reaches around 20mm, while buckling in one of the experiments also occurs gradually after the mid-span vertical deflection passes the same 20mm, even though the numerical model of stiffened plate penal for the stiffener W310X21 (W12X14) predicts the strength 12% less. In order to explain the difference between the observed and predicted strength of the stiffened plate penal with stiffener W310X21 (W12X14), the following observations were made. Firstly, it should be noted that minimum yield stress of A992 steel has a range of values. The actual yield stress of the stiffener W310X21 (W12X14) may not be truly representative of the material model used. Since the slopes of the elastic portion of the response curves are predicted accurately, the lower strength can reasonably attributed to the difference in material properties, mainly yield strength, between finite element model and the test specimen. Secondly, it is important to remember that both magnitude and shape of initial geometric imperfections dictate the ultimate strength in buckling collapse behaviour. Considering the uncertainty involved in fabrication related initial imperfections, average magnitudes are often assumed for initial geometric imperfections. In numerical simulations, generally the shape of the geometric imperfections is assumed

to be the expected buckling modes, which lead lower bound of ultimate strengths. Therefore, it is reasonable to assume that the higher strength observed in experiment of stiffened plate panel with stiffener W310X21 (W12X14) may have unfavorable imperfections in the stiffener. This is further strengthened by the reported fact that the stiffened panels with stiffener W310X21 (W12X14) experienced sudden collapse, instead of progressive collapse as expected.

The finite element modeling techniques are employed successfully to simulate the buckling behavior and predict the strength of the stiffened plate panels, despite the 12% difference between measured and predicted strength of stiffener W310X21 (W12X14). The finite element models were able to exactly capture the failure modes. The finite element model for the stiffener W200X27 (W8X18) predicted exactly the load versus deformation response of the experiment. In addition, the slopes of elastic portions and the shape of response curves were identical. The finite element models could be relied on the response of loading and unloading branch very well. Therefore, it can be concluded that the behavior and strength of the stiffened plate panels subjected to negative pressure can be reliably predicted with the proposed modeling techniques developed in Section 3.4. These validated modeling techniques will be applied in Chapter 4 for an extensive parametric study.

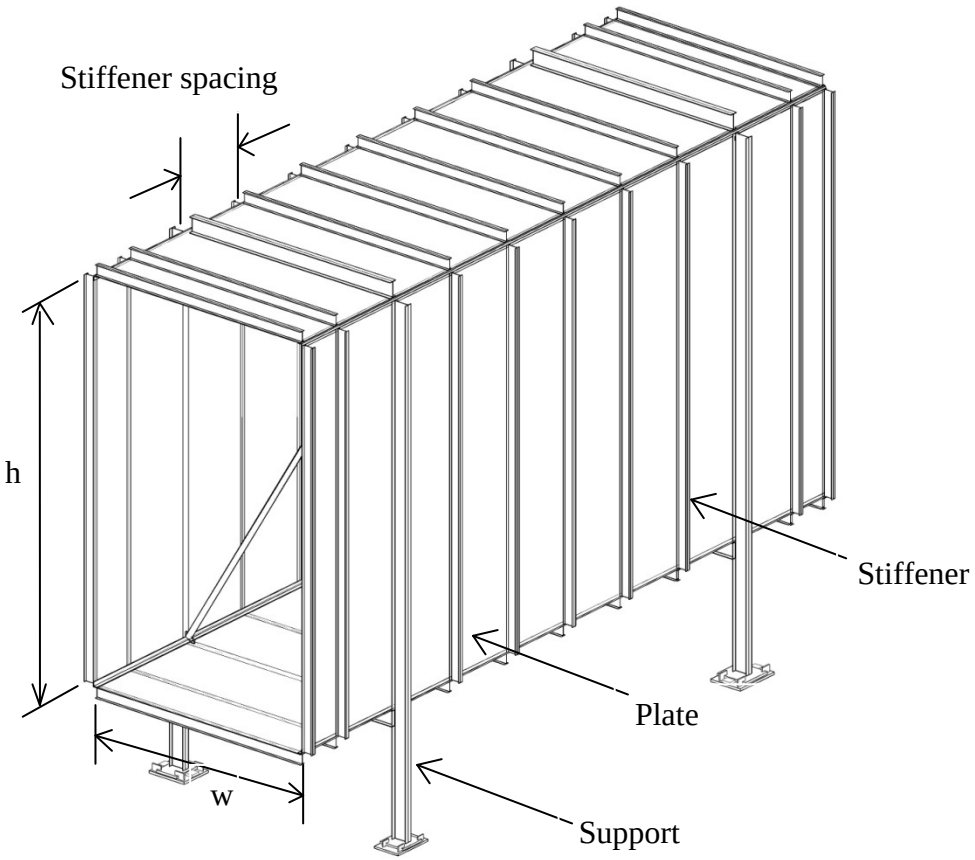

Figure 3.1 Typical Large Rectangular Industrial Duct

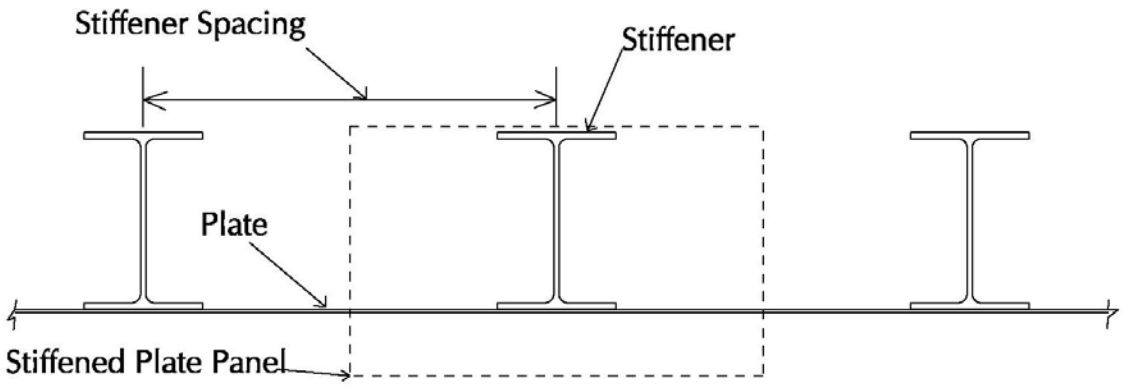

Figure 3.2 Stiffened Plate Panels

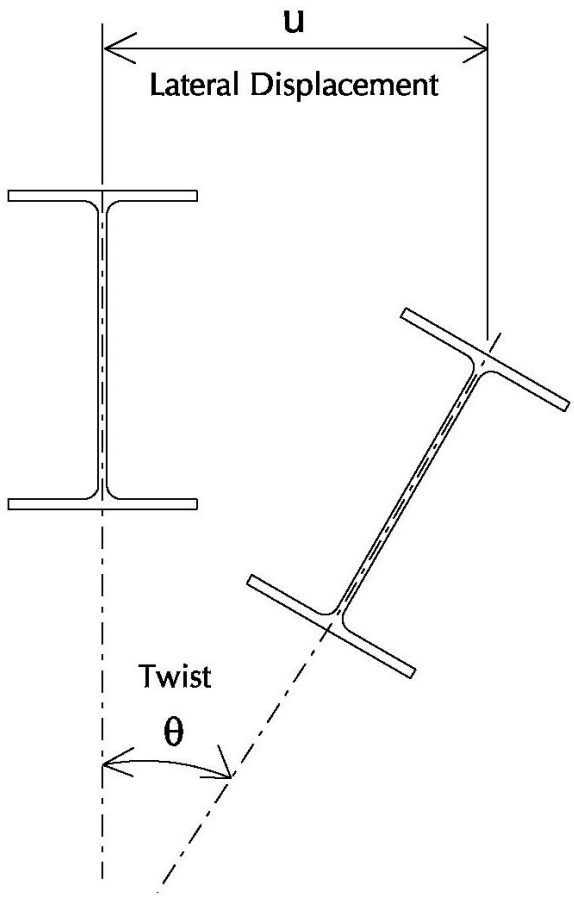

Figure 3.3 Lateral Torsional Buckling

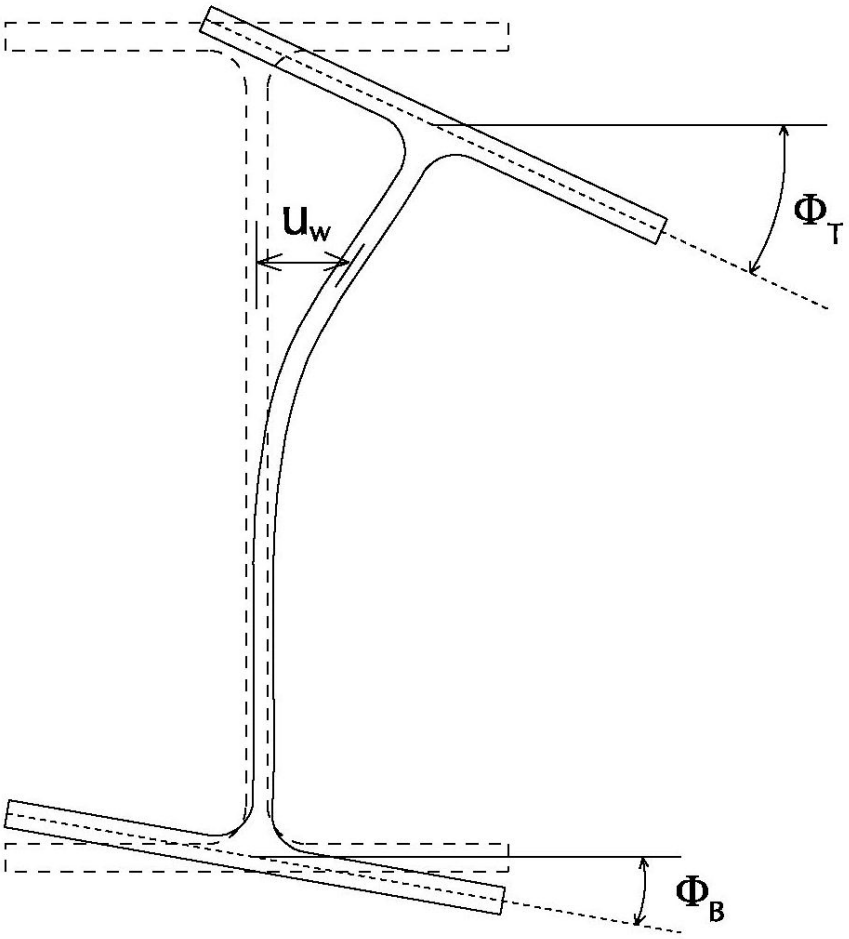

Figure 3.4 Web Distortion of a Cross Section

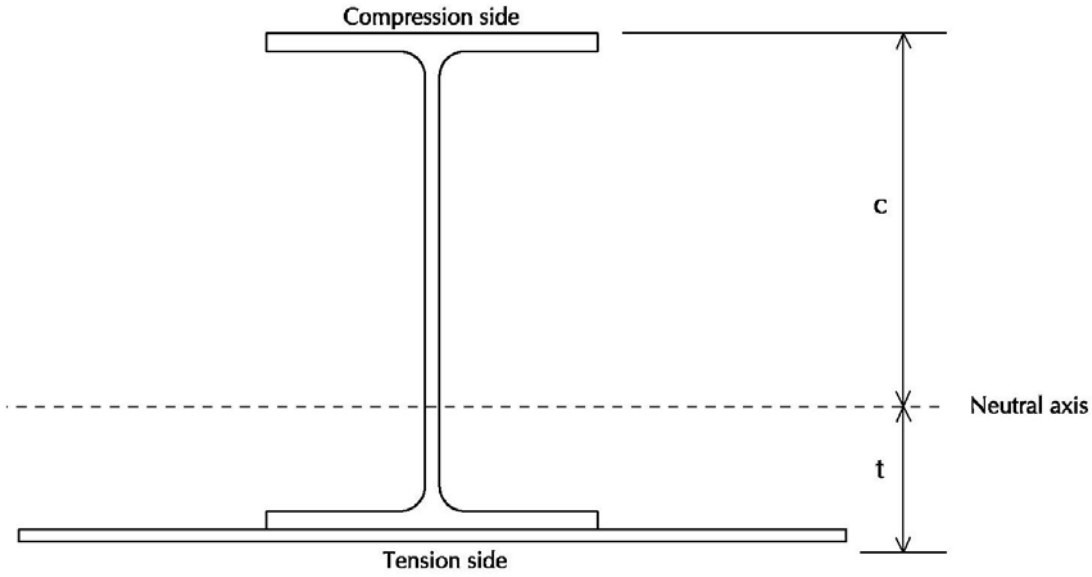

Figure 3.5 Cross Section of Singly Symmetric Beam

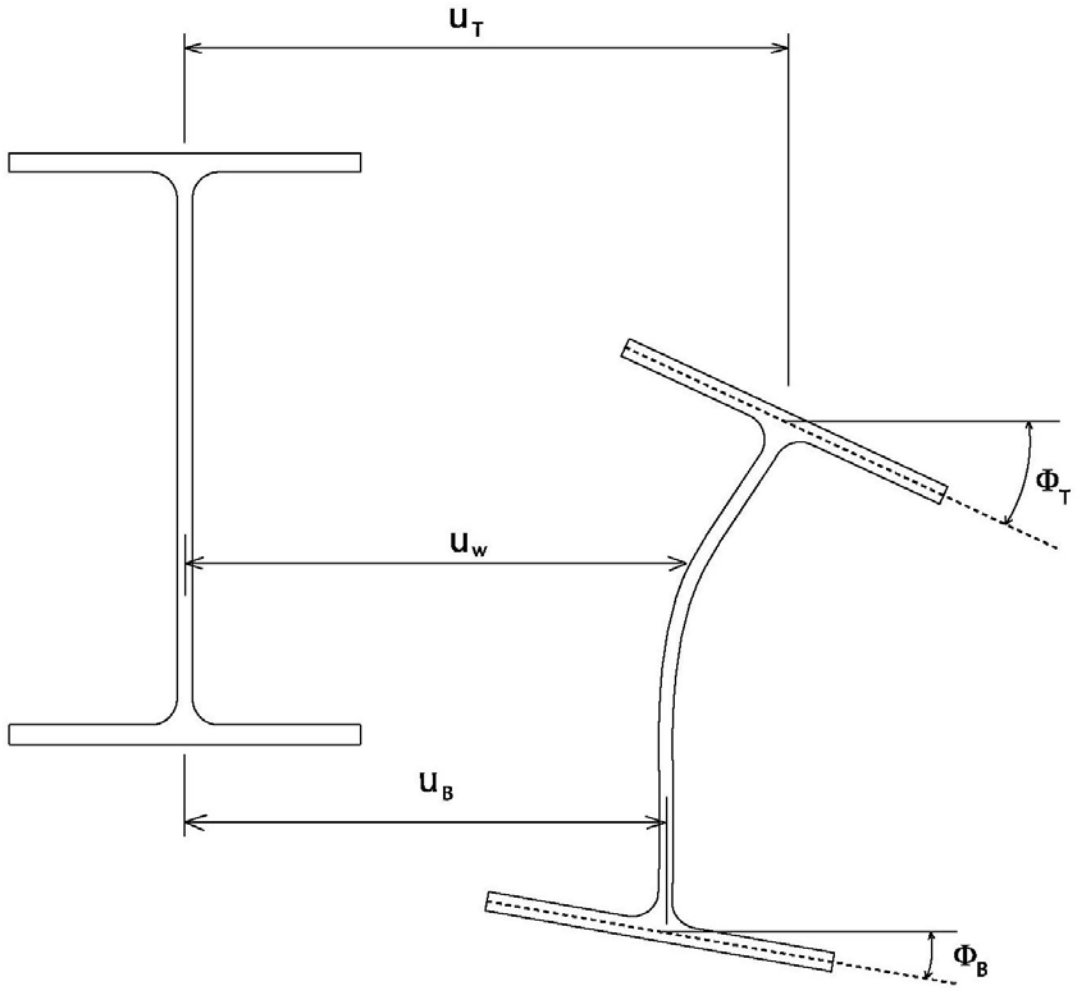

Figure 3.6 Lateral Distortional Buckling

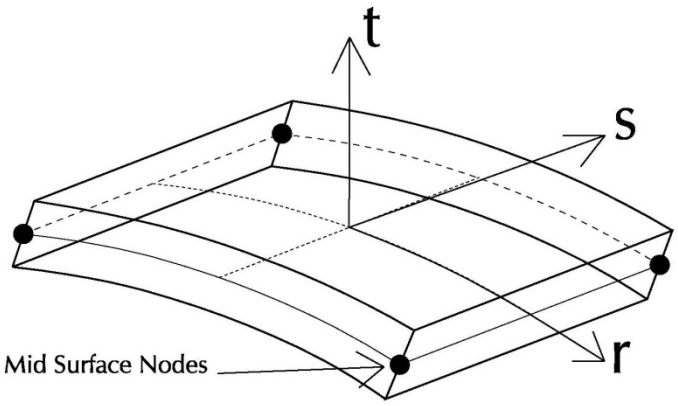

Figure 3.7 Four Node Shell Element for Thick and Thin Shells

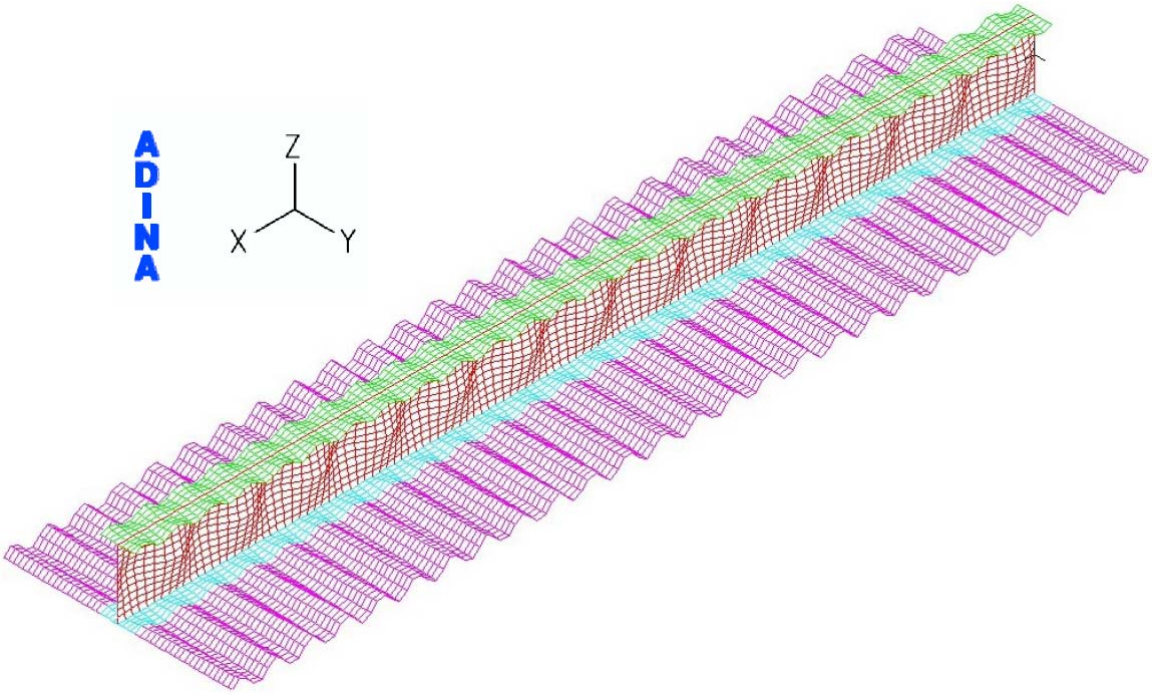

Figure 3.8 Exaggerated Initial Geometric Imperfection in Plate Elements

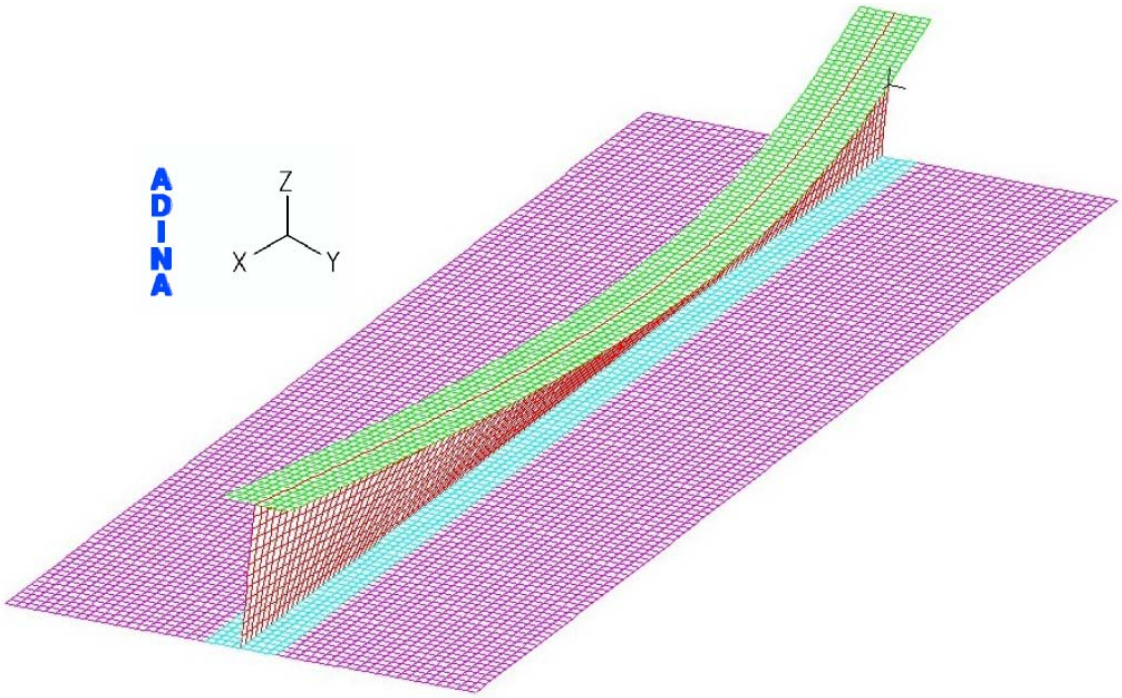

Figure 3.9 Exaggerated Initial Geometric Imperfection in Stiffeners

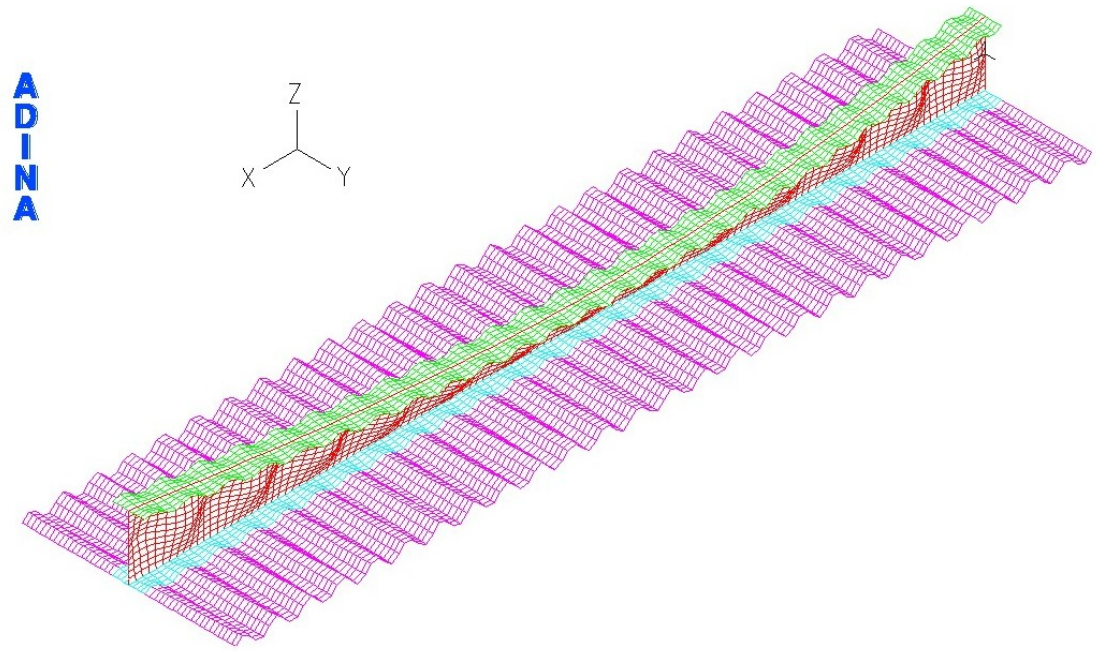

Figure 3.10 Exaggerated Combined Initial Geometric Imperfections for Models

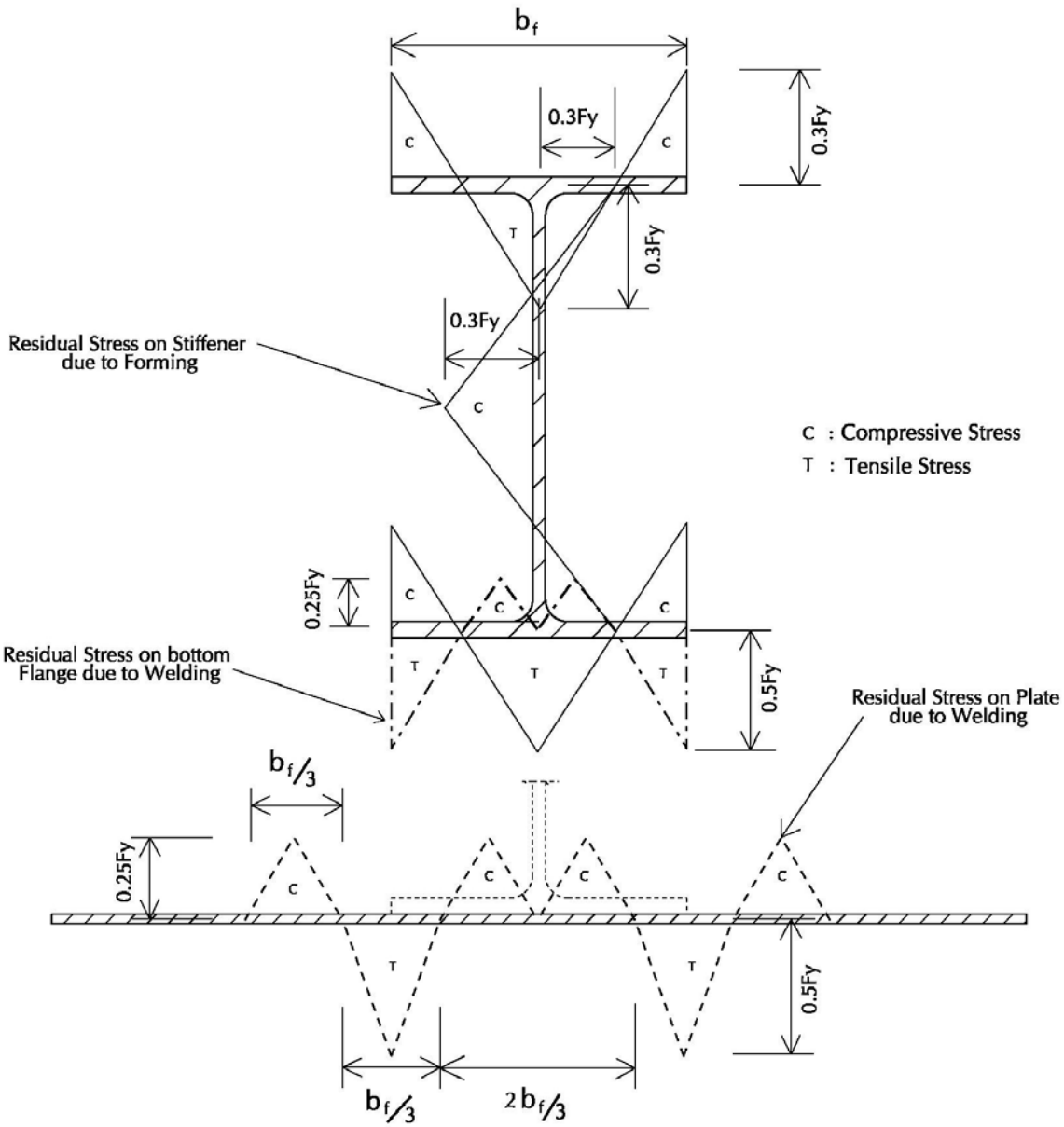

Figure 3.11 Exploded Residual Stress Pattern

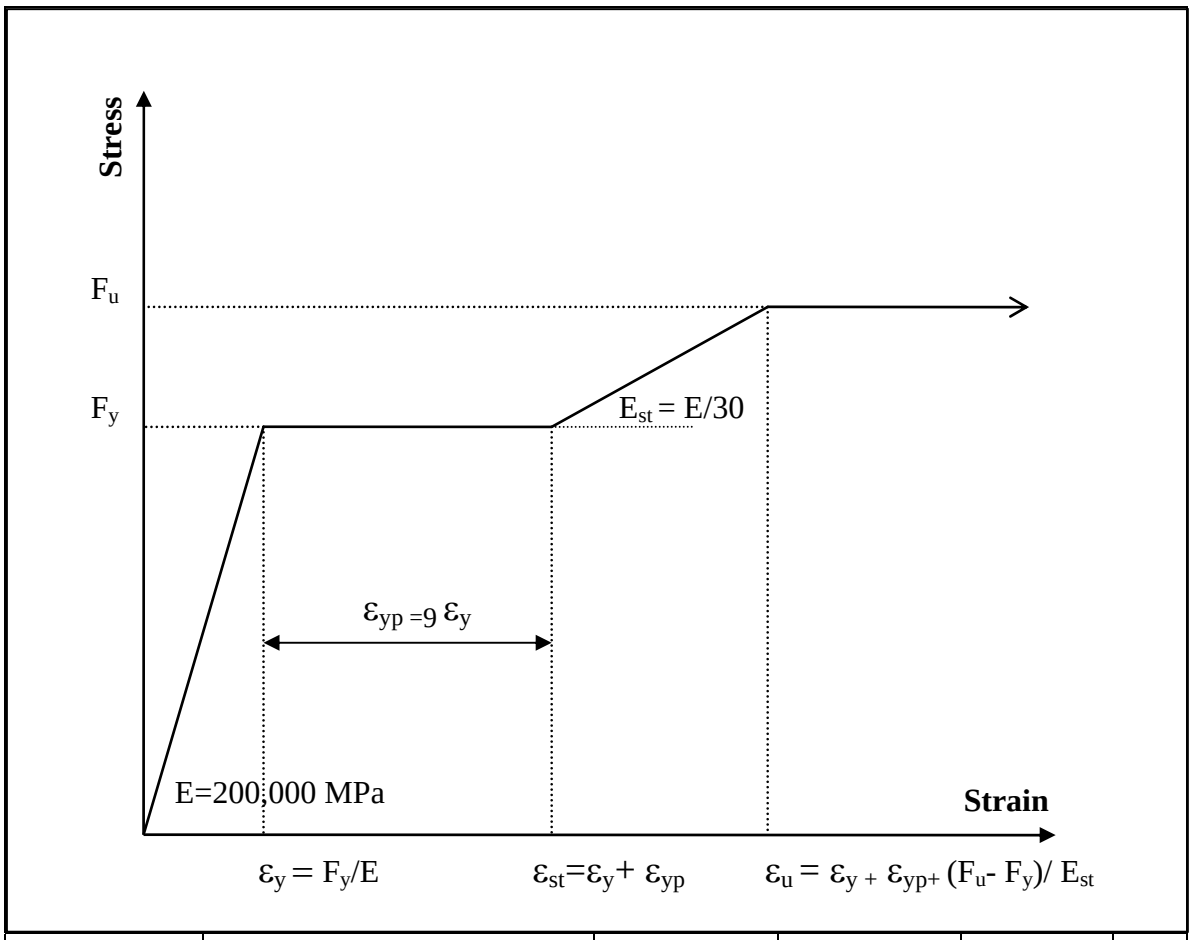

A992	Strain	ε_y	ε_{st}	ε_u	ε_l
		0.0022	0.022	0.0357	0.1
	Stress (MPa)	F_y	F_{st}	F_u	F_u
		440	440	540	540
44W	Strain	ε_y	ε_{st}	ε_u	ε_l
		0.0015	0.015	0.03	0.1
	Stress (MPa)	F_y	F_{st}	F_u	F_u
		300	300	400	400

Figure 3.12 Idealized Material Models

Table 3.1 Results of Mesh Convergence Study

Mesh Number	Element Physical Size	P_{ult} (kPa)	Percentage Change / (%)
1	100x60	69.8	
			2.65
2	80x60	68.0	
			1.50
3	50x30	67.0	
			0.76
4	30X15	66.5	

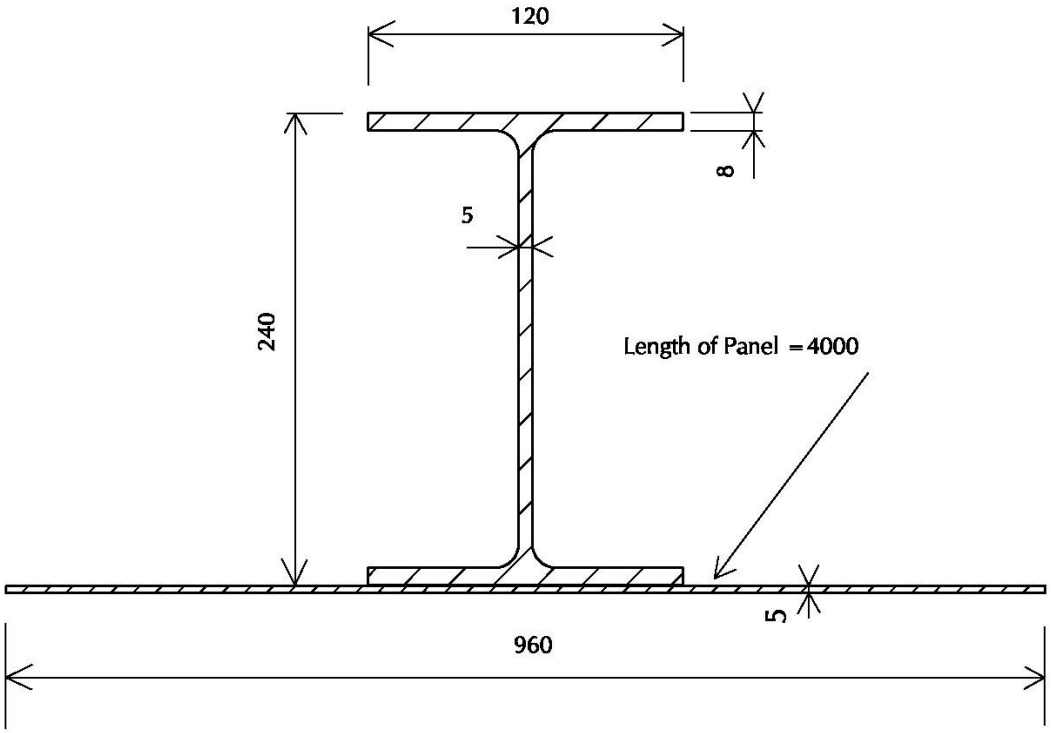

Figure 3.13 Geometry of Model for Convergence Study

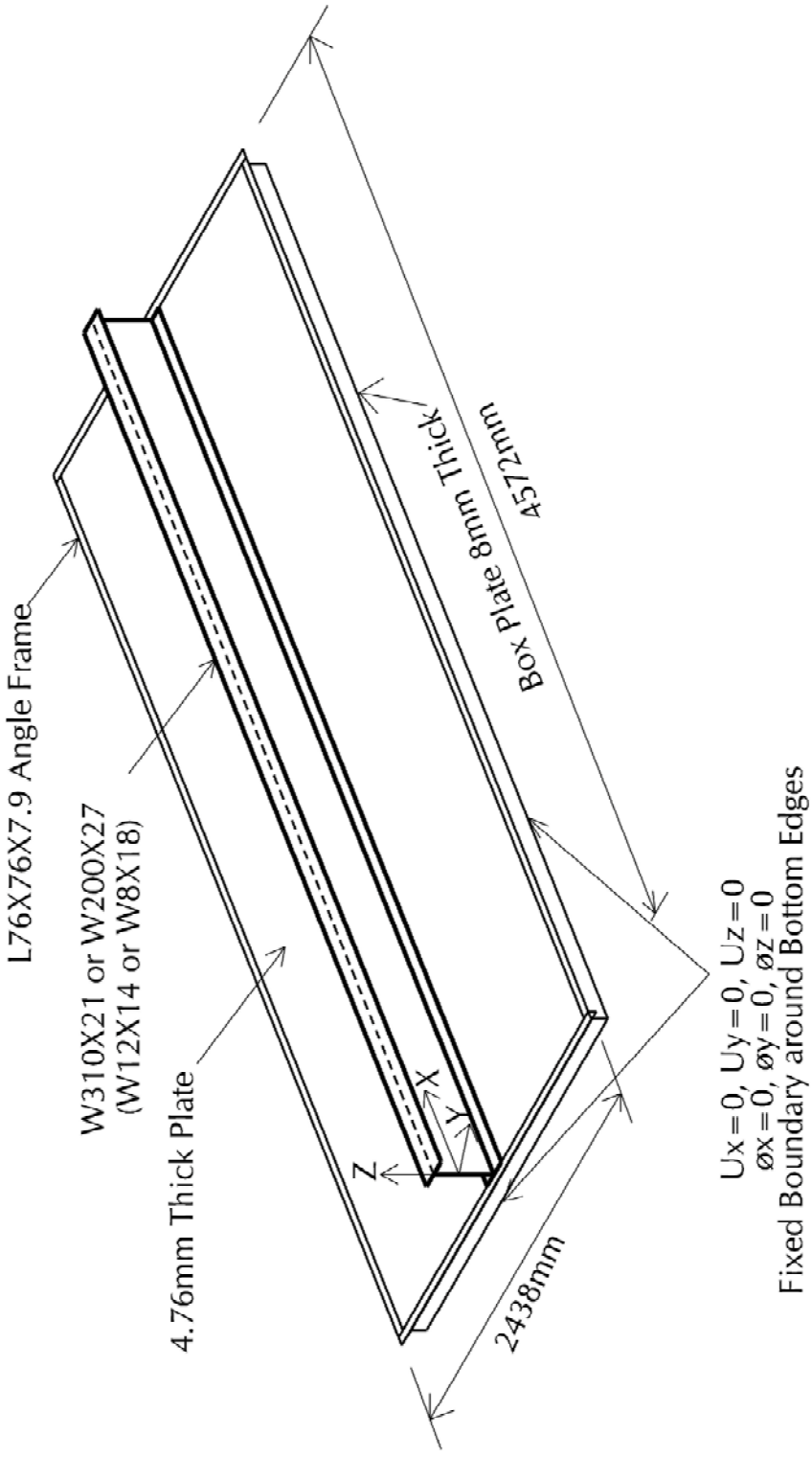

Figure 3.14 Verification Model

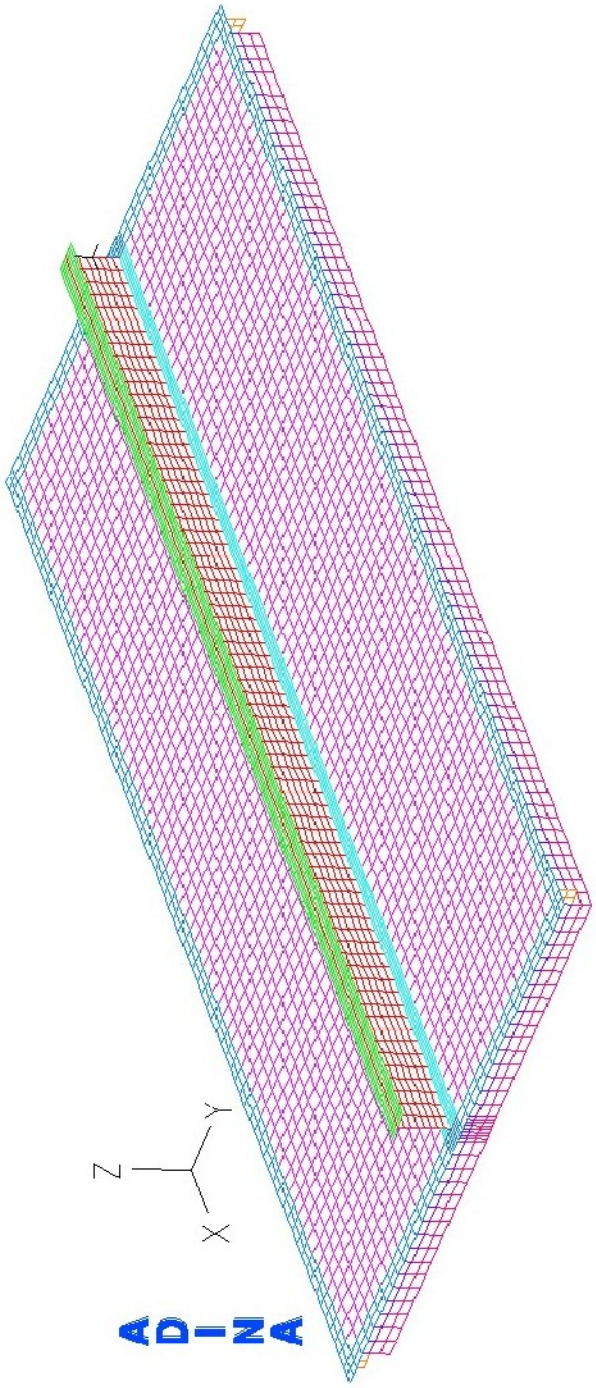

Figure 3.15 Finite Element Model

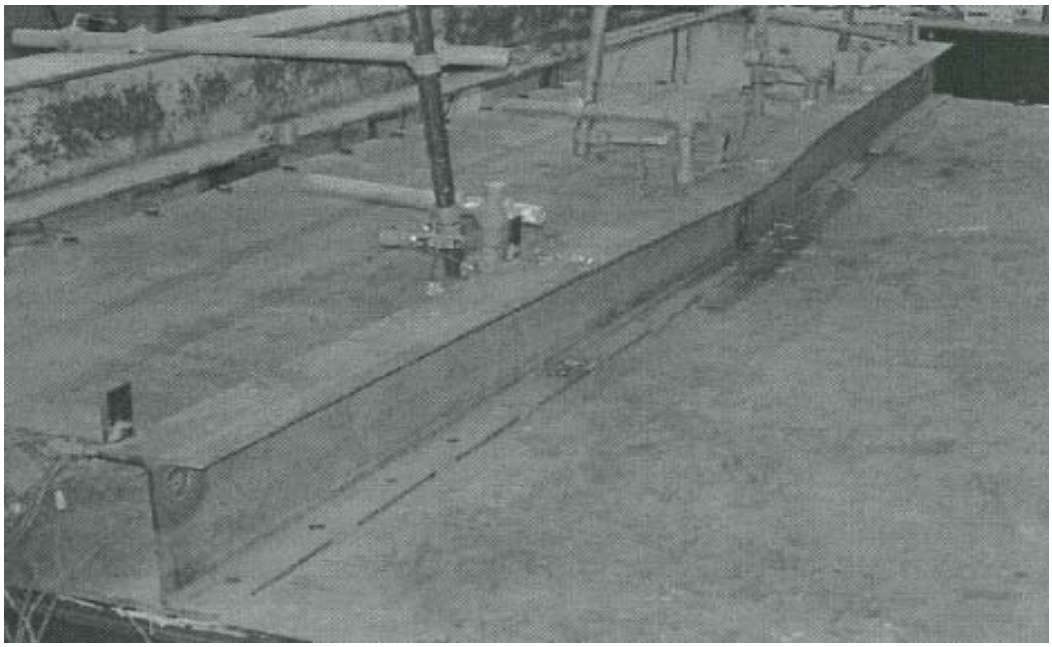

Figure 3.16 Buckling Mode of Stiffener W200X27 from Experiment

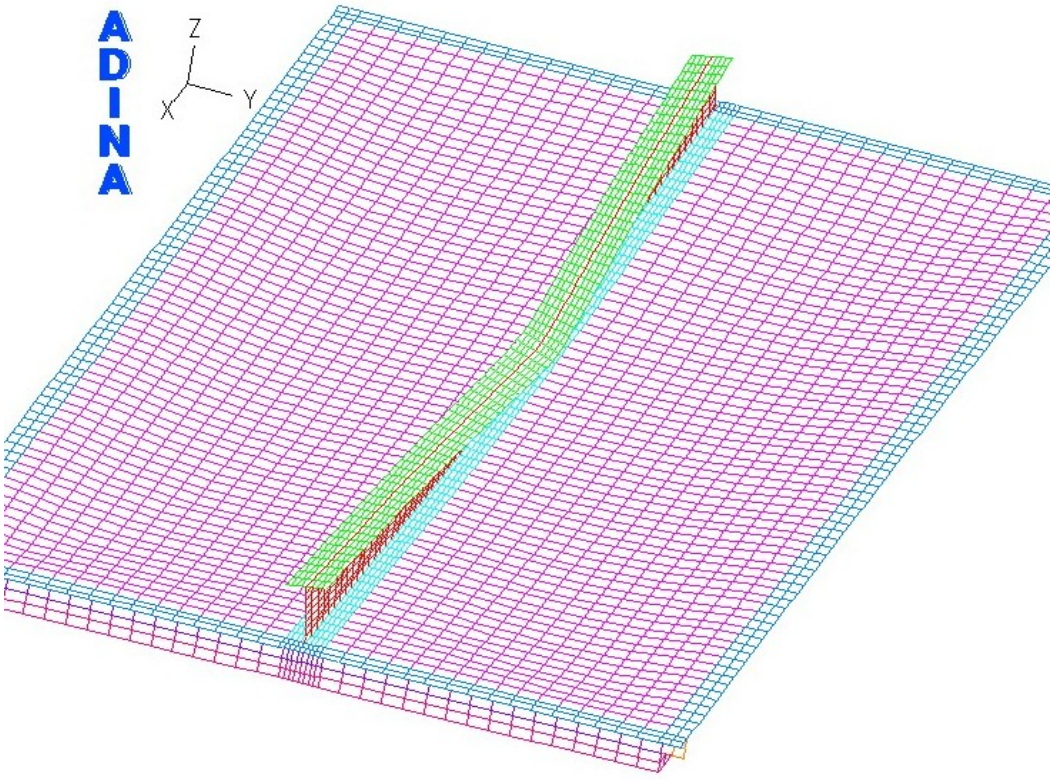

Figure 3.17 Buckling Mode of Stiffener W200X27 from Numerical Analysis

Figure 3.18 Buckling Mode of Stiffener W310X21 from Experiment

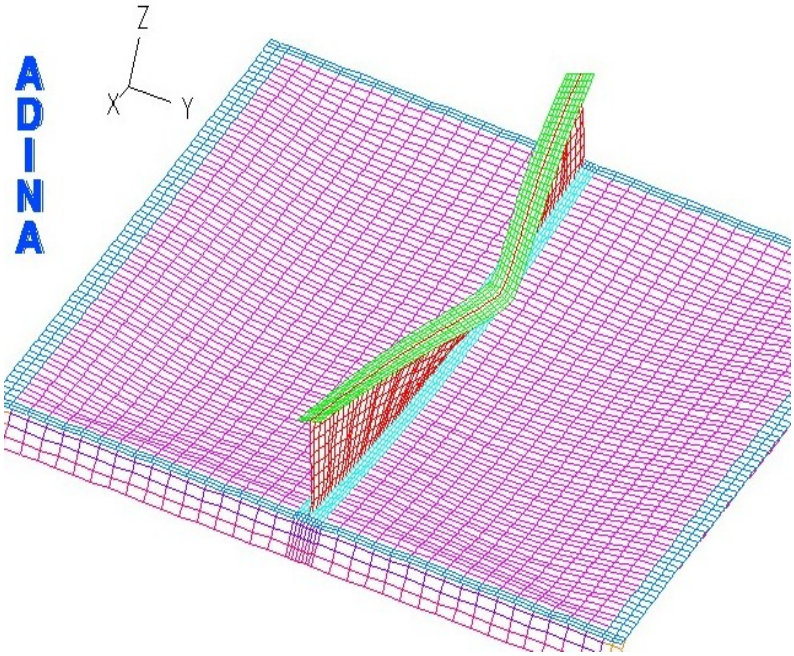

Figure 3.19 Buckling Mode of Stiffener W310X21 from Numerical Analysis

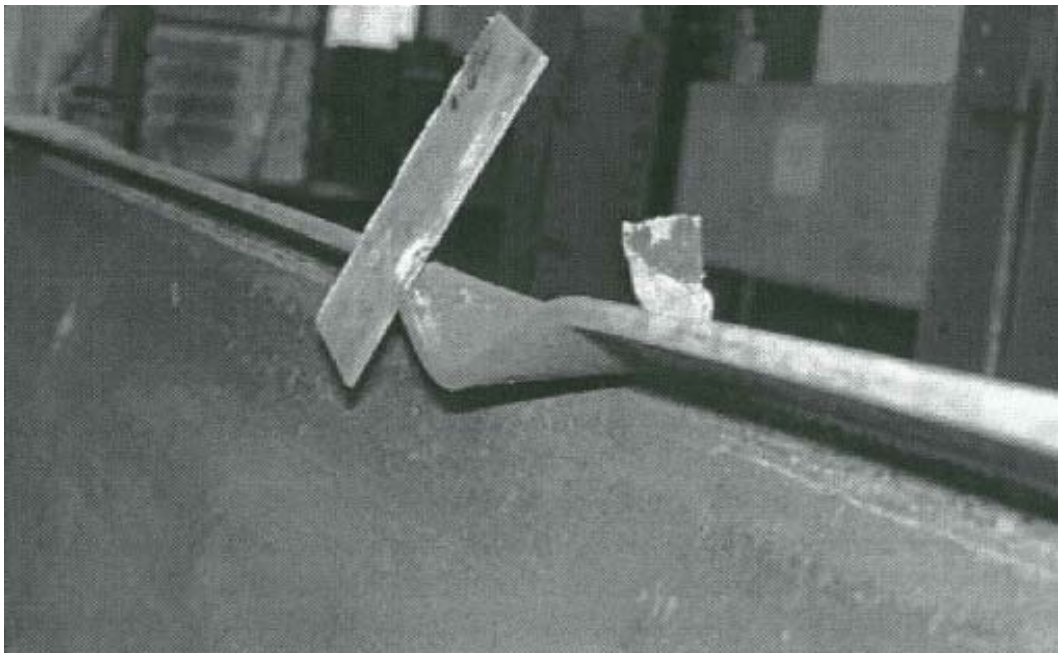

Figure 3.20 Buckling Mode of Stiffener W310X21 from Experiment

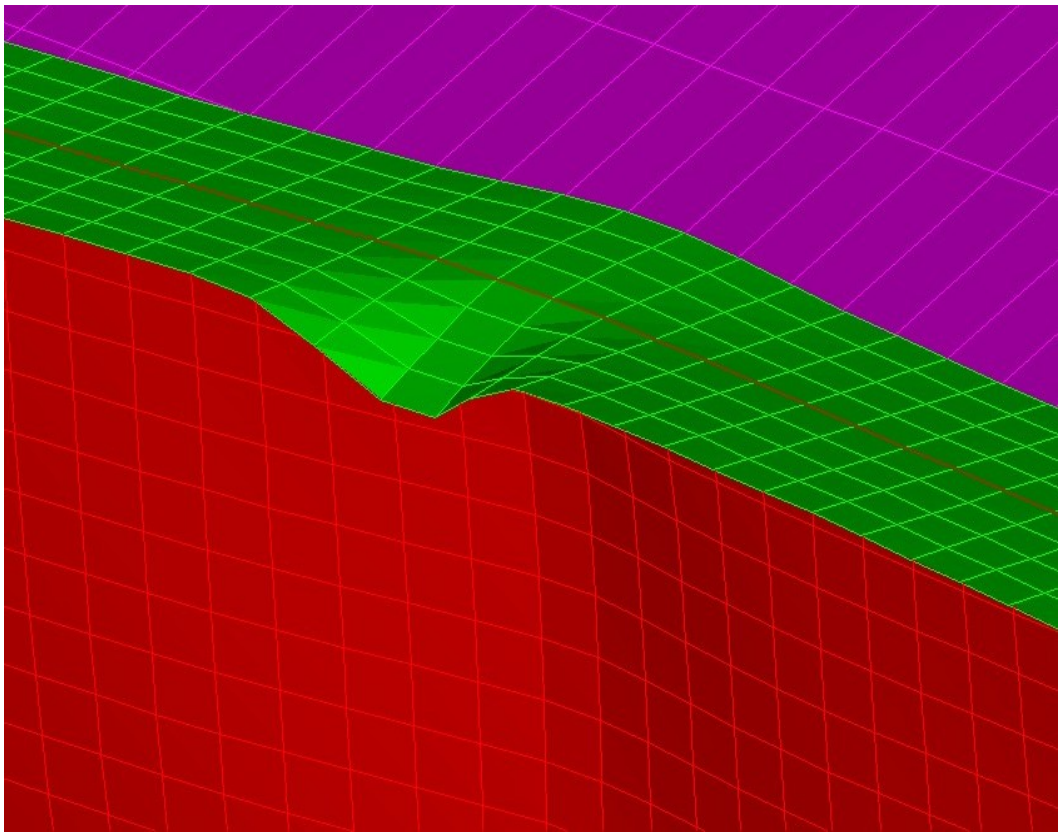

Figure 3.21 Buckling Mode of Stiffener W310X21 from Numerical Analysis

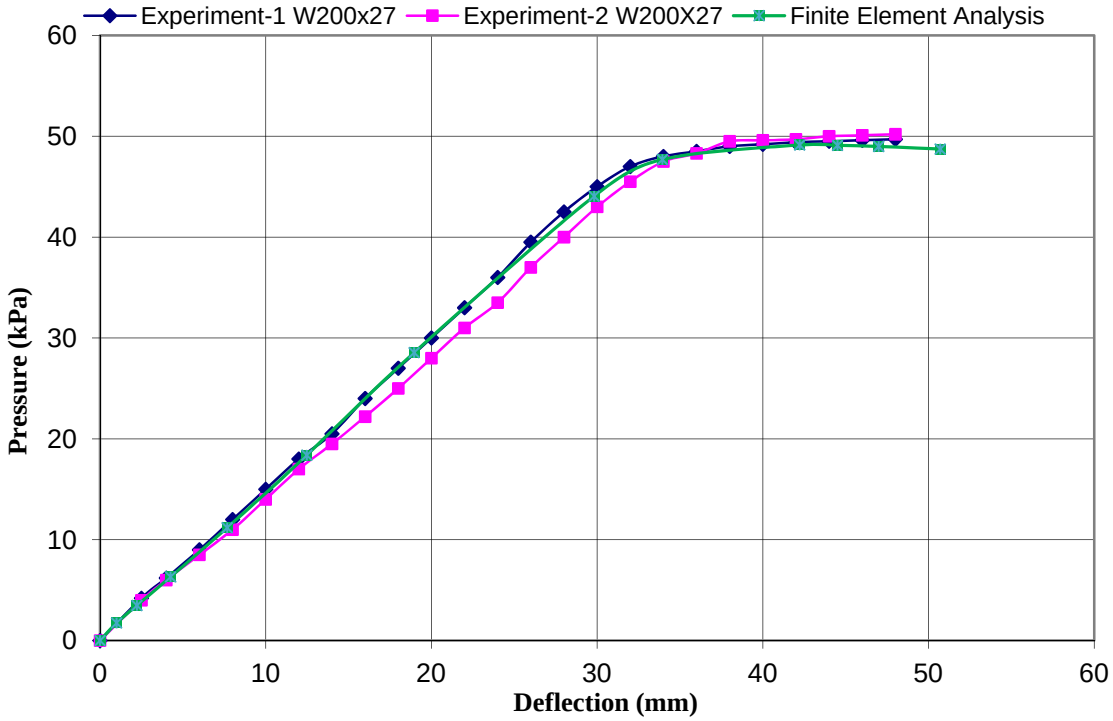

Figure 3.22 Lateral Pressure versus Vertical Deflection of Stiffened Plate Panel (W200X27)

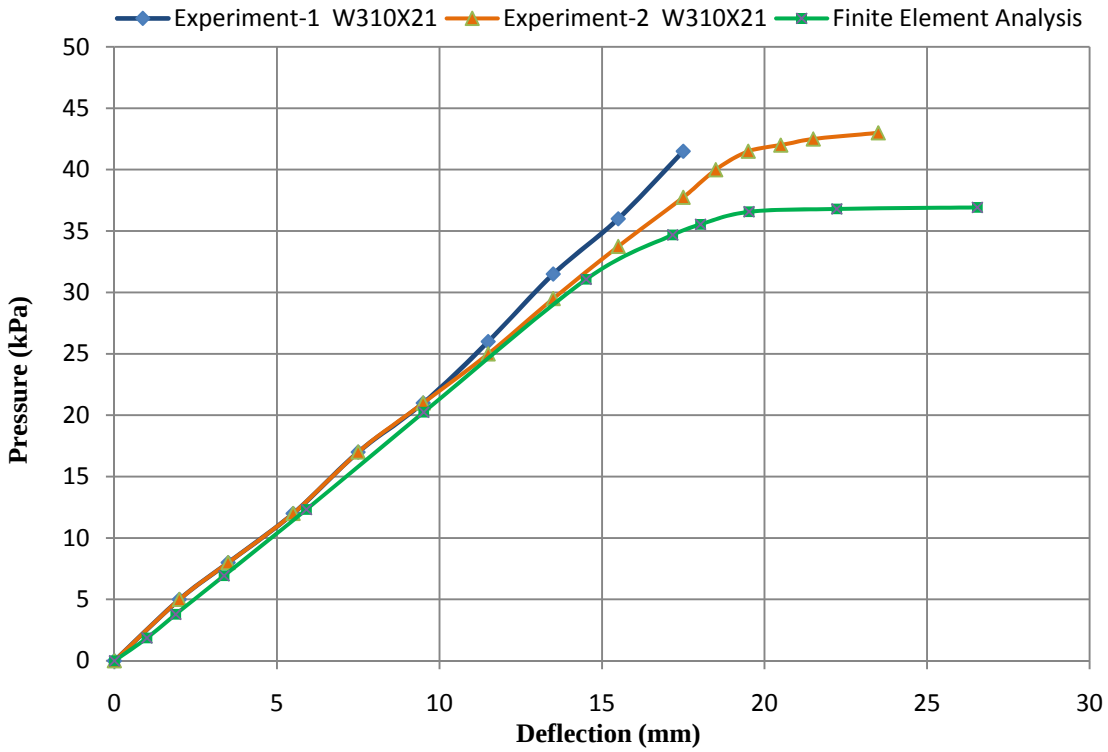

Figure 3.23 Lateral Pressure versus Vertical Deflection of Stiffened Plate Panel (W310X21)

Appendix 3.1 Notations

The following symbols are used in this chapter

b = Width of flange

C = A constant

C_w = Warping constant

d = Height of web

d' = Distance between centers of areas of flanges,

E = Young's modulus

E_{st} = Strain hardening slope

EI_F = Flexural rigidity of compression flange

f_r= Magnitude of compressive residual stress

f_y= Yield strength of plate

G = Shear modulus

h = Depth of web

I_y = Weak axis moment of inertia

I_x = Second moment of inertia about major axis

I_y = Second moment of inertia about minor axis

I_{yc} = Minor axis moment of inertia of the compression flange

I_{eff} = Effective moment of inertia

I_{yt} = Second moment of inertia of tension flange

J = Torsional constant

K_y = Effective length factor about minor axis

$K_z =$ Effective length factor about major axis

L = length of strut

$L_b =$ Distance between braced points

$M_{cr} =$ Critical moment

$M_o =$ Lateral torsional moment

$P_{ult} =$ Maximum pressure load

$N_{cr} =$ Elastic buckling load

$t =$ Thickness of web

$U_B =$ Lateral Displacement of bottom flange

$U_T =$ Lateral Displacement of top flange

$U_B{}' =$ Rate of Lateral displacement of bottom flange with respect to longitudinal axis

$U_T{}' =$ Rate of Lateral displacement of top flange with respect to longitudinal axis

$w =$ Width of web beneath support

$y_o =$ Shear centre distance

$\beta =$ Torsional stiffness per unit length

$\beta_b =$ Torsional stiffness of external bracing

$\beta_{sec} =$ Torsional stiffness of stiffener web

$\beta_t =$ Effective Torsional stiffness

$\beta_z =$ Coefficient of monosymmetry

$\varepsilon_y =$ Yield strain

$\varepsilon_{st} =$ Strain at strain hardening

$\emptyset_T =$ Twist of top flange

$\emptyset_B$ = Twist of bottom flange

$\emptyset_T{}'$ = Rate of twist of top flange

$\emptyset_B{}'$ = Rate of twist of bottom flange

δ_o = Maximum imperfection amplitude

δ = Geometric imperfection

δ_{os} = Maximum amplitude of the sinusoidal sweep

μ = A constant

Appendix 3.2 References

ADINA , 2009, "ADINA 8.5 user manual.", ADINA R & D Inc, Watertown, MA, USA

ASCE, (1995), "The structural Design of Air and Gas Ducts for Power Stations and Industrial Boiler Applications.", Air and Gas Structural Design Committee of the Energy Division of the ASCE, Reston.

AISC ASD, (1989), "Manual of Steel Construction- Allowable Stress Design.", 9th edition, American Institute of Steel Construction ,Chicago.

AISC, (2005), "Manual of Steel Construction- Load and Resistance Factor Design.", American Institute of Steel Construction, Chicago.

Arasaratnam, P., (2008), "Effect of Flange Holes on Flexural Behaviour of Steel Beams.", PhD Thesis, McMaster University, Hamilton

Bleich, F., (1952), "Buckling Strength of Metal Structures.", New York, McGraw-Hill.

Bradford, M.A., (2000), "Strength of Compact Steel Beams with Partial Restraint.", Journal of Constructional Steel Research, 53, 183-200

Bradford, M.A., (1999), "Elastic Distortional Buckling of Tee-Section Cantilevers.", Thin Walled Structures, 33, 3-17

Bradford, M.A., (1998a), "Inelastic Buckling of I-beams with Continuous Elastic Restrant.", Journal of Constructional Steel Research, 48, 63-77

Bradford, M.A., (1998b), "Distortional Buckling of Elastically Restrained Cantilevers.", Journal of Constructional Steel Research, 47, 3-18

Bradford, M.A., Ge, P., (1997), "Elastic Distortional Buckling of Continuous I-Beams.", Journal of Constructional Steel Research, 41, 249-266

Bradford M.A., Ronagh, H.R., (1997), "Generalized Elastic Buckling of Restrained I-Beams by FEM.", Journal of Structural Engineering, ASCE , 123 (15), 1631-1637

Bradford, M.A., (1992), "Lateral-Distortional Buckling of Steel I-Section Members.", Journal of Constructional Steel Research, 23, 97-116

Bradford, M.A., (1990), "Distortional Buckling Strength of Elastically Restrained Monosymmetric I-beams.", Thin Walled Structures, 9, 339-50

Bradford M.A., (1989), "Buckling Strength of Partially Restrained I-Beams.", Journal of Structural Engineering, ASCE , 115 (5), 1272-1276

Bradford M.A., Trahair, N.S., (1981), "Distortional Buckling of I-Beams.", Journal of Structural Division, ASCE , 107 (2), 355-370

Bruno, M., Chia, M., Andrew, W., (1998), "Ductile Design of Steel Structures.", 1st Edition, McGraw-Hill Book Company Inc., New York, USA.

CSA, (2010), "Handbook of Steel Construction.", Canadian Institute of Steel Construction, Willowadale, Ontario

Galambos, T.V., (1998), "Guide to Stability Design Criteria for Metal Structures.", 5th edition. Wiley, New York.

Grondin, G.Y., Elwi, A.E., Cheng, J.J.R., (1999), "Buckling of Stiffened Steel Plates-a Parametric Study.", Journal of Constructional Steel Research, 50, 151-175

Hancock, G.J., Bradford, M.A., "Trahair, N.S., (1980), Web Distortion and Flexural Torsional Buckling.", Journal of Structural Engineering, ASCE , 106(ST7), 1557-71

Hughes, O.F., Ghosh, B., Chen, Y., (2004), "Improved Prediction of simultaneous Local and Overall Buckling of Stiffened Panels.", Thin-Walled Structures, 42, 827-856

Hughes, O.F., Ma, M., (1996), "Inelastic Analysis of Panel Collapse by Stiffener Buckling.", Computers and Structutres, 61, 107-117

Kitipornchai, S., Wong-Chung, A.D., (1987), "Inelastic Buckling Welded Monosymmetric I-Beams .", ASCE Journal of Structural Engineering, 113, 740-756

Kitipornchai, S., Trahair, N.S., (1980), "Buckling Properties of Monosymmetric I-Beam.", ASCE Journal of Structural Division, 106, 941-958

Ma, M., Hughes, O., (1996), "Lateral Distortional Buckling of Monosymmetric I-Beams under Distributed Vertical Load.", Thin-Walled Structures, 26, 123-145

Milner, H.R., (1977), "The Buckling of Equal Flanged Beams Under Uniform Moment Restrained Torsionally by Stiff Brace.", Fifth Australian Conference on the Mechanics of Structures and Materials, Melbourne, 405-420

Paik, J.K., A.K., Kim, B.J., Seo, J.K., (2007), "Methods for Ultimate State Assessment of Ships and Ship Shaped Offshore Structures.", Ocean Engineering, 35, 271-280

Paik, J.K., Thayamballi, A.K., Kim, D.H., (1999), "An Analytical Method for the Ultimate Compressive Strength and Effective Plating of Stiffened Panels.", Journal of Constructional Steel Research, 49, 43-68

Paik, J.K., Thayamballi, A.K., Lee, W.H., (1998), "A Numerical Invetsigation of Tripping.", Marine Structures, 44, 51-56

Samata, A., Kumar, A., (2006), "Distortional Buckling in Monosymmetric I-beams.", Thin Walled Structures, 9, 339-50

Sheikh, I.A., Elwi, A.E., Grondin, G.Y., (2003), "Stiffened Steel Plates under Compression and bending.", Journal of Constructional Steel Research, 59, 911-930

Svensson, S.E. (1985), "Lateral Buckling of Beams Analyzed as Elastically Supported Columns Subjected to varying Axial Force.", Journal of Constructional Steel Research, 5, 179-93

Taylor, A.C., and M. Ojalvo, (1966), "Torsional Restraint of Lateral Buckling.", Journal of the Structural Division, American Society of Civil Engineers, 115-129.

Timoshenko, S.P., Gere, J.M., (1961), "Theory of Elastic Stability.", 2nd Edition, McGraw Hill, New York

Udall, J.D., (2007), "Effective Design of Stiffener on Industrial Ducts.", Master Thesis, McMaster University, Hamilton

Ugural, A.C, (1998), "Stress in Plates and Shells.", 2nd Edition, McGraw Hill, New York

Valentino, J., and Trahair. N.S., (1998), "Torsional Restraint Against Elastic Lateral Buckling", Journal of Structural Engineering, American Society of Civil Engineering, 124 (10), 1217-1225

Williams, F.W., Jemah, A.K., (1987), "Buckling Curves for Elastically Supported Columns with Axial Force, to Predict Lateral Buckling of Beams.", Journal of Constructional Steel Research, 7, 133-147

Young, W.C., (1989), "Roark's Formulas for Stress & Strain.", 6th edition. New York, McGraw Hill.

Yura, J., (2008), "Global Lateral Buckling of I-Shaped Girder Systems.", Journal of Structural Engineering, 134, 1487-1494

Yura, J.A. (2001), "Fundamentals of Beam Bracing.", Engineering Journal, American Institude of Steel Construction, 38,11-26

Chapter 4: Parametric Study on Stiffened Plate Panels

Abstract

A stiffened plate panel subjected to a lateral pressure load, which causes bending, was investigated using a finite element model. Experimentally verified finite element modeling techniques were used to develop the models. The emphasis of work presented in this chapter is to first identify the fundamental parameters that characterize the behavior and strength of the stiffened plate panels. The dimensionless parameters that govern the behavior and strength of stiffened plate panels were then identified in order to conduct a parametric study with a manageable number of models.

The parametric study was conducted using typical geometric and material parameters of general rolled stiffener sections used in an industrial duct. The numerical study indicated that the behavior and strength of the stiffened panels could be a function of web slenderness and overall slenderness of the stiffener. Also the lateral distortional buckling was identified as a dominant instability in laterally loaded stiffened plate panels. The study also identified the stiffener web slenderness limit for which the stiffener reaches the yield moment capacity. This parametric study demonstrated the conservatism of current methods used to proportion the stiffeners. Finally a method was established to calculate the moment capacity for wide flange beam stiffened plate panels subjected to lateral pressure.

Keywords: Stiffener, Plate, Finite Element, Distorsional Buckling, Dimensional Analysis

4.1. Introduction

The steel plates used in large rectangular industrial ducts are reinforced by stiffeners in one direction in the plane of the plate. The simplicity of their fabrication and their high strength-to-weight ratio make the stiffener attractive construction system in industrial ducts. The stiffened plate panels of industrial ducts are mainly loaded under internal lateral pressure. The lateral pressure might be positive or negative. This study is focused on the behavior and strength of stiffened plate panels under negative pressure.

The stiffeners of large industrial ducts are, in general, W-shaped steel sections, which have high flexural rigidity and low torsional rigidity due to their thin webs. The lateral distortional buckling of stiffeners will cause a drop in the loading capacity of stiffened panels due to loss of stiffener rigidity. However, the current method of proportioning the stiffeners is based on the use of standard steel code (AISC 2005, CSA 2001) lateral torsional buckling formula. A stiffened panel subjected to a negative (suction) pressure load experiences compressive stress on the flange that is not connected to plate. In current design practices, the unsupported length of the compression flange is assumed to be the span the stiffened panels. Due to this loading condition and the large unsupported length of the compression flange, lateral distortional instability usually governs the design of stiffened plate panels subjected to negative pressure loads.

The lateral distortional buckling of a stiffener consists of the twisting of the web and compression flange about the bottom portion of the web connected to the plate. The lateral distortional buckling is defined as the state of instability of the stiffener for which

the wavelength of the web buckling and the wavelength of flange buckling are the same, as illustrated in Figure 4.1. This occurs when the tension flange is restrained laterally and the compression flange is free.

Although the design of stiffened plate panels of large rectangular industrial ducts has been done for many years, their instability aspects and load carrying capacity are still not well understood. In a recent limited experimental study, Udall (2007) observed the instability of stiffened plate panels subjected negative pressure load. However, there are many aspects of the behavior and capacity of stiffened plate panels to be studied. Also, the range of parameters that might define the practical stiffened plate panel is too large to do experimental investigations. Thus, there is a need to conduct a large scale computer analysis parametric study in to order to discover the behavior and strength of stiffened plate panels subjected to negative pressure loads.

4.2 Objectives

In this part of the study, an extensive finite element method based parametric study will be conducted for the analysis of stiffened plate panels. The nonlinear finite element modeling techniques developed in Chapter 3 will be used in order to accurately simulate the behavior of the stiffened plate panels. The first objective of the work reported in this chapter is to identify the possible geometric and material parameters that govern the behavior and strength of stiffened plate panels and a method of determining capacity of a stiffened plate panel subjected to lateral a negative pressure load. The objectives are categorized as follows:

- To identify the fundamental parameters governing the bahaviour and capacity of stiffened plate panels
- To identify dimensionless parameters that dictate the behavior and strength of stiffened plate panels
- To understand the behavior of stiffened plate panels subjected to negative pressure loads
- To conduct a parametric non-linear finite element study to derive a method to calculate the capacity of stiffened plate panels

The stiffened plate panels subjected to static pressure loading and under ambient temperature were only considered in this study.

Section 4.3 identifies the dimensionless parameters affecting the behavior and strength of the stiffened plate panels. Section 4.4 describes the finite element model and also explains the method used to obtain the buckling moment in this parametric study. Section 4.5 proves the completeness of the dimensionless parameters identified in Section 4.3. Sections 4.6 and 4.7 analyze the effect of plate slenderness and stiffener flange slenderness. In section 4.8, the influence of the dimensionless parameters on the behavior and strength of a stiffened plate panel and its capacity are investigated through a parametric study. Conclusions and recommendations for future research are presented in Section 4.9.

4.3 Dimensionless Parameters Characterizing Stiffener Behaviour and Strength

Before a parametric study can be carried out on the laterally-loaded stiffened plate panels in rectangular industrial ducts, it is imperative to determine the dimensionless parameters that characterize the behavior and instability of the stiffeners. Theoretically these parameters should be independent of any effects of scale or material characteristics. As these parameters are a function of the governing instability and the corresponding loading condition, it is necessary to first identify the parameters for the instability. The first goal of this chapter is to identify the various dimensionless parameters that are influencing the behavior and instability of laterally loaded stiffened plate panels. These parameters will then be used to conduct a parametric study for the behavior and strength of the stiffened plate panels under negative pressure.

The instability of a stiffener with a restrained tension flange, and under lateral pressure, was identified as the lateral distortional buckling (Bradford 1998, Udall 2007). The distortional buckling is characterized by the simultaneous buckling of the stiffener compression flange and web while the tension flange remains straight. The instabilities of the flange and web of the stiffened plate panel depend on the geometric and material characteristics. The geometric parameters affecting the behavior and strength of a stiffener in a rectangular industrial duct consist of cross sectional dimensions and the length of the stiffener. These parameters namely $b_p, t_p, h_w, t_w, b_f, t_f, L$ are illustrated in Figure 4.2. The material parameters of the plate and stiffener are the elastic modulus, Poisson's ratio and the corresponding yield stresses. In addition to these geometric and

material parameters, the applied bending moment is also a parameter which measures the distortional buckling.

The fundamental parameters that are considered in the behavior and strength of laterally loaded stiffened plate panels are b_p = width of the plate (stiffener spacing), t_p = plate thickness, h_w = stiffener web height, t_w = stiffener web thickness, b_f = stiffener flange width, t_f = stiffener flange thickness, L = stiffener length, F_{ys} = yield stress of the stiffener material, F_{yp} = yield stress of the plate material, E = Young's modulus of steel and M_a = applied bending moment. The Poisson's ratio was taken as constant 0.3. The full factorial parametric study of the above fundamental parameters would results in several hundreds of runs even when only three or four values are used for each of the fundamental parameters.

It is apparent from the list of fundamental parameters above that the number of parameters is too large to run a combination of reasonable number of analysis. Therefore, it is important for the number of parameters to be reduced to do a manageable parametric study. A method of deriving dimensionless parameters from the list of governing fundamental parameters is called dimensional analysis (Harris 1999). This method can be used to reduce the number of parameters. The dimensional analysis can yield dimensionless parameters which are combination of fundamental parameters listed above.

The purpose of using a dimensional analysis is to reduce the number of parameters and to choose parameters that are scale independent and dimensionless for a manageable

parametric study. The next step is to identify the dimensionless groups of variables, i.e. the combinations of fundamental parameters. In order to identify a proper set of dimensionless parameters that characterize the behavior of laterally loaded stiffened plate panels, the Buckingham Pi-theorem can be used (Lanhaar 1951). The Pi-theorem is stated that:

"Any physical meaningful relation $\emptyset\left(R_1, \ldots R_i \ldots R_n\right) = 0$***, with*** $R_i \neq 0$ ***expressed in terms of r independent dimensions, is equivalent to a relation of the form*** $\psi\left(\beta_1, \ldots \beta_j \ldots \beta_{n-r}\right) = 0$ ***involving maximum set of independent dimensionless combinations*** β_j***."***

The important fact to notice is that the new relation involves r fewer variables than the original relations; therefore this simplifies the theoretical and experimental analysis to save significant effort and computational cost. Also, this transformation of the fundamental parameters into a set of meaningful dimensionless parameters helps not only control the scale effects in numerical analysis but also to simplify the parametric study into a manageable number of analyses.

Even though the Pi-theorem identifies the number of dimensionless parameters needed, the number of independent dimensionless combinations might be an infinite number of possibilities. The dimensionless parameters chosen should be useful in the experiment or the numerical response analysis. However, it is in fact easier to find meaningful dimensionless combinations by considering the instabilities that may arise in laterally

loaded stiffened plate panels. When the stability of a structural shape subjected to compressive stress is considered, the instability of its plate element components under compression must be first considered. Because this plate instability is limited to localized regions and does not affect the entire length of the member, this type of instability referred to as the local buckling and must be distinguished from an overall type of global buckling, such as slender column Euler buckling. The length of plate component of structural shapes can be viewed as infinite with respect to its width; therefore it is unlikely that boundary conditions of the loaded edge will affect the compressive load the plate may sustain. Consider a flat plate element of length a, width b and thickness t simply supported along the unloaded edges. During the instability of the plate element, the critical stress due to the applied load can be written as follows:

$$F_{cr} = \frac{k}{\left(\frac{b}{t}\right)^2}\left[\frac{\pi^2 E}{12(1-\nu^2)^2}\right]$$

The term k is identified as a function of the aspect ratio $\frac{a}{b}$ and the number of sine waves m that occur between loaded edges. Since the concern is the instability of long plates, the number of sine waves has no significance. The term k can be replaced for each boundary by lower bound value of k. Therefore, the slenderness of plate can be measured by a dimensionless parameter obtained by rearranging the above equation as shown below.

$$\beta = \frac{b}{t}\sqrt{\frac{F_y}{E}}$$

The square root of $\frac{F_y}{E}$ makes this dimensionless parameter material independent. The plate slenderness is well known to be one of the important factors affecting stability of plate components that are in compression. The strength of a section generally increases as the plate slenderness decreases. Therefore, the following plate slenderness can be defined for the plate components of a stiffened plate panel as listed below.

Stiffener flange flexural slenderness:

$$\beta_1 = \frac{b_f}{t_f}\sqrt{\frac{F_{ys}}{E}}$$

Stiffener web flexural slenderness:

$$\beta_2 = \frac{h_w - 2t_f}{t_w}\sqrt{\frac{F_{ys}}{E}}$$

Plate slenderness:

$$\beta_3 = \frac{b_p}{t_p}\sqrt{\frac{F_{yp}}{E}}$$

Generally the unbraced length of a stiffener in a large rectangular duct under negative transient pressure is assumed to be the span of the stiffened plate panel. The stability of the compression flange and the portion of web under compression can be assumed to be an elastically supported column with a varying axial force. The shape of the varying axial force is similar to shape of the moment diagram of the stiffened plate panel. The web of the stiffener and the duct casing may also provide some rotational restraint to the compression portion of the stiffener. However, the axial load carrying capacity will be a function of the flexural rigidity of the compression portion of the stiffener, length of the

compression flange L and the rotational stiffness provided by web of the stiffener. Therefore, the load carrying capacity of the stiffener can be shown as a function of the dimensionless overall slenderness of the compressive portion of the stiffener as given below

$$\beta_4 = \frac{L}{r}\sqrt{\frac{F_{ys}}{E}}$$

In which r is the radius of gyration of the compressive portion of the stiffener about a vertical axis parallel to the stiffener's web. The derivation of the radius of gyration is explained in Figure 4.2.

The response of a physical system through dimensional analysis should be measured by a dimensionless output parameter. Therefore for this study, the applied moment M_a is normalized relative to yield moment capacity M_y of the stiffened plate panel. The normalized moment $\frac{M_a}{M_y}$ will be the output dimensionless parameter for this parametric study and will be the control parameter used to monitor the response of laterally loaded stiffened plate panels. It is quite clear that the dimensionless parameters found are independent, since each of them contains at least one fundamental parameter which is not present in other dimensionless parameters.

As the Buckingham Pi-theorem requires, the behavior of the physical system is defined by a complete set of dimensionless parameters formed by relevant fundamental

parameters. This fact suggests that if two systems have same numerical values for all dimensionless parameters and have different scales for all fundamental parameters, then the two systems respond the same way. In order to test the suitability of the suggested dimensionless parameters, scales of the fundamental parameters can be varied while keeping the dimensionless parameters constant and checking whether the capacity and response remain the same. If the behavior and capacity are unchanged, it can be concluded that these dimensionless parameters truly characterize the laterally loaded stiffened plate panels.

4.4 Finite Element Model

As described in Chapter 3, the modeling techniques used to develop the finite element model were able to predict the behavior and strength of laterally loaded stiffened steel panels with reasonable accuracy. The same modeling techniques were applied to build the finite element models and to conduct an extensive parametric study in order to identify the behavior and capacity of stiffeners in large rectangular industrial ducts.

A large rectangular industrial duct consists of flat plates with equally spaced parallel stiffeners. Because of the symmetry in stiffener arrangement and loading condition, a portion of the plate of width b_p and one stiffener centered on that portion of plate can be modeled to represent a stiffened plate of a large rectangular duct. Figure 4.3 illustrates the extent of the typical stiffened plate panel modeled for this numerical study. In this case, it should be noted that an artificial boundary is formed along the symmetric edges (longitudinal edge of the plate). Therefore, the solution will be satisfactory if appropriate boundary conditions are used along these symmetric edges. In order to idealize the symmetry, rotation about the longitudinal direction and translation along the transverse direction were restrained for the symmetric edges to simulate the continuity of the plate. (In Figure 4.4, θ_x=0 and U_y=0 along the longitudinal edges).

The boundary conditions were introduced for the plate's other edges as the stiffener would be welded to the plate and the plates are welded to corner angles along the duct longitudinal axes. This plate –corner angle weld prevents the rotations and translation along the weld. Therefore, the translation U_y and rotations θ_x, θ_y and θ_z of the plate

edges about the transverse direction were suppressed. In order to study the bending behaviour of stiffened plate panels subjected to lateral pressure load, the vertical supports were provided along the transverse directions by restraining vertical translation U_z and by fixing the longitudinal translation U_x along one transverse direction and by freeing along other transverse direction. All the stiffener edges that are not connected to plate were set free to simulate the one flange of the stiffener welded to the plate. The boundary conditions are illustrated in Figure 4.4.

Idealized elastic-plastic-strain hardening tri-linear material models were used to represent mild carbon steel to model the material constitutive behavior of the stiffener and the plate. The typical yield strengths of $F_{ys} = 350\ MPa$ and $F_{yp} = 250\ MPa$ were used to define the stiffener and the plate material respectively. The actual stress-strain values and the description of the stress versus strain curve adopted for this parametric study are shown Figure 4.5.

The magnitude and pattern of initial geometric imperfection as described in Chapter 3 were used during modeling. The residual stress pattern as described in Chapter 3 was also incorporated into the model as initial longitudinal strains.

4.4.1 Estimation of Distortional Buckling Moment

This section provides the method of obtaining the distortional buckling moment from the finite element analysis results. The buckling loads of axially loaded plates and columns are often obtained by examining the lateral deflection versus axial loading plots. The load versus lateral deflection plots of a perfectly straight column subjected to axial load has a well defined bifurcation point. This bifurcation point has a unique value. However, for a column with imperfection, the load versus lateral deflection plot does not have a well defined bifurcation point. Therefore, it is difficult to distinguish between the pre-buckling and post-buckling paths of an axially loaded imperfect column. However, various techniques have been developed in order to experimentally determine the buckling loads of columns. These techniques approximately establish the buckling load from experimental data. Since both the experimental techniques and the current finite element study are response type problems, the techniques derived for experimental tests should be applicable here for the numerical study.

In one of those experimental techniques, the inflection point on the load-lateral deflection curve has been used to define the buckling load of an imperfect column. The important physical significance of this method is that the inflection point is a point of maximum rate of increase of lateral deflection with respect to load. However, this inflection point is very difficult to obtain from the experimental and numerical results. Thus, it becomes necessary to make use of methods such as the Southwell plot, which modifies the axial load P versus lateral deflection Δ into a linear relationship between $\frac{\Delta}{P}$ and Δ. The reciprocal of the slope of the Southwell plot represents the critical buckling load and the

Δ-intercept represents the apparent imperfection. Southwell's method can be extended to the distortional buckling of beams. As well, there are other extrapolation techniques which may be used to obtain a beam's elastic critical load from its load-lateral deflection curve. Among these techniques are the Massey method and the Modified Plots, in addition to Southwell Plots (Trahair 1969). Although these methods were developed for the elastic buckling load, these methods can be used to extrapolate the inelastic buckling load which represents the strength of beams (Bradford and Wee 1994).

Zirakian (2007) tested the applicability of the aforementioned extrapolation techniques on lateral distortional buckling of W-shape beams undergoing web distortion. The prediction provided by Sothwell, Modified and Massey Plots were compared with maximum test loads. It was found that the agreement between maximum test loads and the extrapolated loads using Southwell and Massay Plots was very good. Therefore, it was decided to use Southwell Plots for this study to obtain distortional buckling moments M_{cr}.

In order to obtain the buckling moments for the parametric study, it is necessary to check Southwell Plots used to obtain the distortional buckling moments. Two models named Model-1 and Model-2, each having the same dimensionless parameters from two different combinations of geometric and material parameters, were analyzed. Figure 4.6 shows properties of the two models and the results of applied moment $M_a$versus mid span vertical deflection Δ_Z of bottom plate. The result of Model-1 indicates the linear slope up to around 100kN.m and reaches the ultimate moment at around 113 kN.m. Therefore, the distortional buckling moment of Model-1 is expected in between 100 kN.m and 113

kN.m. Similarly, the distortional buckling moment of Model-2 is expected in between 160 kN.m and 172 kN.m.

Figure 4.7 illustrates the Southwell plots of Model-1 and Model-2 for the lateral deflection Δ_Y at mid top flange of the stiffeners. The distortional buckling moment can be obtained from relevant straight lines of best fits from the plots (Zirakian 2007). The reciprocal of the slope of linear relationship between $\frac{\Delta_y}{M_a}$ and Δ_y is the distortional buckling moment M_{cr}. The buckling moments obtained using the Southwell Plots were also included in Figure 4.7. The predicted distortional buckling moments 110.2 kN.m and 167.0kN.m were found to be within the expected ranges for Model-1 and Model-2, respectively. Therefore, the Southwell Plot can be used to predict the distortional buckling moments M_{cr} of stiffened plate panels subjected to lateral pressure load and has been used in the current study as well.

The other useful information that are extracted from this analysis are the normalized distortional buckling moments $\frac{M_{cr}}{M_y}$ and normalized ultimate moments $\frac{M_u}{M_y}$. The applied moment M_a versus mid span vertical deformation Δ_Z histories of both analysis results (Model-1 and Model-2 have same dimensionless parameters) are presented in Figure 4.8 in dimensionless form such as applied moment divided by yielding moment M_y versus mid span vertical deflection Δ_Z. It can see from Figure 4.8 that the $\frac{M_u}{M_y}$ for both Model-1 and Model-2 are to be same 1.14. In addition, the $\frac{M_{cr}}{M_y}$ were also to be same 1.11.

Therefore, the $\frac{M_{cr}}{M_y}$ and $\frac{M_u}{M_y}$ can be used to measure the performance of stiffened plate panels under lateral pressure.

4.5 Complete Set of Independent Dimensionless Parameters

The Buckingham Pi-theorem requires that all fundamental parameters that describe the mechanics of the problem are included in the set of dimensionless parameters. In this study, the dimensionless parameters were defined as β_1, β_2, β_3 and β_4. To assess whether all of the essential variable that play a role in the behavior of laterally loaded stiffened plate panel are represented in these dimensionless parameters, a preliminary investigation is carried out. For this preliminary investigation, the dimensionless parameters β_1, β_2, β_3 and β_4 were kept identical while choosing different scales for the fundamental parameters. If the output dimensionless parameter $\frac{M_a}{M_y}$ results are found to be the same, then it can be concluded that the entire set of variables that are required to define the mechanics of laterally loaded stiffened plate panels have been included. Therefore, this analysis needs to be repeated for all fundamental parameters used to define the dimensionless parameters β_1, β_2, β_3 and β_4.

Eight models of stiffened plate panels each having identical dimensionless parameters β_1, β_2, β_3 and β_4 with different scales of b_p, t_p, h_w, t_w, b_f, t_f, L, F_{ys} and F_{yp} were analyzed. The similar initial geometric imperfections and residual stresses as described in Chapter 3 were incorporated in all models. The results of each model are presented in Table 4.1. It

should be noted that one fundamental parameter can not be changed at a time because all fundamental parameters are inter-related through the dimensionless parameters.

The Southwell Method explained in Section 4.4.1 was used to obtain the distortional buckling moment M_{cr} for the rest of the study. The input dimensionless parameters selected to verify the parameters' completeness were $\beta_1 = 0.654$, $\beta_2 = 1.749$, $\beta_3 = 7.701$ and $\beta_4 = 7.889$. The first model was used as a reference for the seven other models. The seven other models were obtained by changing each of the fundamental parameters and adjusting the rest of the parameters to obtain the same dimensionless parameters mentioned above. The results of this study on scale effect are presented in Table 4.1. Table 4.1 presents the value of each of the fundamental parameters that were changed for this study. The last two columns of Table 4.1 presents the normalized output moments $\frac{M_{cr}}{M_y}$ obtained using Southwell Plots and the normalized ultimate moments $\frac{M_u}{M_y}$. The mean and standard deviation of normalized moments $\frac{M_{cr}}{M_y}$ for all analysis models were found to be 1.138 and 0.002, respectively. Similarly, the mean and Standard deviation for $\frac{M_u}{M_y}$ of all models were found to be 1.159 and 0.002. The normalized moments $\frac{M_{cr}}{M_y}$ and $\frac{M_u}{M_y}$ for all models, which have different scales while keeping constant dimensionless parameters, are within an average range and the responses also remain the same. Therefore, it can be concluded that the dimensionless parameters identified completely represent the behaviour of stiffened plate panels.

The applied bending moment M_a versus mid span vertical deflection Δ_Z responses for all models were plotted in Figure 4.9. The responses M_u of the models are different since different scales have been used. These applied moments M_a were normalized by diving the corresponding yield moments M_y and presented in dimensionless form in Figure 4.10. The comparison normalized ultimate moments $\frac{M_u}{M_y}$ in Figure 4.10 indicates to be nearly same and reveals that the change of scale did not have effect on the dimensionless response $\frac{M_u}{M_y}$ of the models as well.

In this portion of the study, the four dimensionless parameters β_1, β_2, β_3 and β_4 that characterize the behavior and strength of the stiffened plate panels were identified. The validity of these dimensionless parameters was established from the results of the analysis where the dimensions of the stiffened panel were changed by keeping the dimensionless parameters identical.

The selected dimensionless parameters β_1, β_2, β_3 and β_4 were found to be able to predict the behavior and capacity of laterally loaded stiffened plate panels. These parameters were also found to be independent of geometric and material effects.

4.6 Effect of Plate Slenderness: $\beta_3 = \frac{b_p}{t_p}\sqrt{\frac{F_{yp}}{E}}$

The stiffeners are usually oriented transverse to flow direction, spanning from one edge of panel to other and effectively wrapping around the duct. The typical stiffener spacing of a large rectangular duct varies from 0.75m to 1.5m. The design of the stiffener section is generally governed by the negative pressure load. Under the negative pressure load, the flange not connected to plate is in compression and the plate is in tension. The depth of neutral axis y_o from tension side becomes small compared to depth of stiffener for this range of stiffener spacing as wider plate is welded to the stiffener. Thus, the section modulus of the stiffened plate panel relative to its compression flange becomes nearly the same for this range of stiffener spacings. Therefore, the elastic section modulus for the range of stiffener spacing was compared in Table 4.2. The plate and tension portion of the stiffener provide enough tension before and after the instability of the compression portion of stiffener as the smaller depth of neutral axis y_o from the tension side keeps the tension very much below the yield strength. For these reasons, the effect of plate slenderness β_3 on the instability of stiffened plate panels under negative pressure was investigated.

In order to determine effect of plate slenderness β_3, five analyses of stiffened plate panels each having identical values for β_1, β_2 and β_4 but with different values for β_3 were tested. The five model cases were obtained by changing the stiffener length L and plate width b_p for each model systematically and by keeping other fundamental parameters the same in order to keep β_1, β_2 and β_4 identical and to change β_3 only.

The test model input parameters and the results for the effect plate slenderness β_3 are presented in Table 4.3. The last columns of the table presents the normalized distortional buckling moment $\frac{M_{cr}}{M_y}$ and the normalized ultimate moments $\frac{M_u}{M_y}$. The normalized applied moment versus mid span vertical deflection history for all models are presented in Figure 4.11. The variation of the normalized moments $\frac{M_a}{M_y}$ and $\frac{M_u}{M_y}$ for all analyses is less than 2%. This indicates that the effect of plate slenderness β_3 on the capacity of stiffened plate panels subjected to negative pressure is very much minimal.

4.7 Effect of Stiffener Flange Flexural Slenderness: $\beta_1 = \frac{b_f}{t_f}\sqrt{\frac{F_{ys}}{E}}$

Generally the plate components of a structural section should be capable of sustaining the stresses required to develop the capacity of the section. Plate slenderness plays a significant role in sustaining the required stress levels. The adopted method of establishing the slenderness parameter is expressed in the form of the width-to-thickness ratio of the section's plate components. Maximum width-to-thickness ratios are prescribed for plate components that make up a section. These ratios are functions of the presumed boundary conditions of the plate and the design stress to develop the required capacity of the section.

The general rolled W structural shapes are typically proportioned so as to prevent the elastic buckling of the plate components of a structural section (Class 3 or better). Thus, only plate component stresses are expected to be in plastic and inelastic states at the capacity of those sections. If a flange plate component is capable of attaining the strain associated with strain hardening without buckling prior to the plastic capacity of the section, the section can be considered as Class 1 section. Although the limiting width-to-thickness ratio for Class 2 section is less restrictive, the moment resistance developed by Class 2 section (Compact section) is equal to that of Class 1 section. The ratio of width-to-thickness ratio associated with flange of a Class 2 section is $\frac{b_f}{2t_f} < \frac{170}{F_y}$ (CSA 2010). Similarly the ratio of width-to-thickness for Compact section limit for the flange of a beam is limited as $\frac{b_f}{t_f} < 0.76\left(\frac{E}{F_y}\right)^{0.5}$ (AISC 2005). The limiting width-to-thickness ratios

are 21.6 and 18.3 for A36 and Gr50 steel respectively. When the flange width-to-thickness ratio exceeds $0.76\left(\frac{E}{F_y}\right)^{0.5}$, it is presumed that the section is non-compact. However, it is yet capable of attaining strain in excess of yield strain i.e., the capacity of a rolled section is not limited by elastic instability of the plate components. Also, inelastic behavior is understood to exist as a result of the existence of residual stresses. Most rolled sections qualify to be compact as the quantities of $\frac{b_f}{t_f}$ are provided for each structural shape in Table B4.1 of AISC (2005) and section properties table of CSA (2010).

Therefore, it can be questioned from the facts above whether the stiffener flange slenderness $\beta_1 = \frac{b_f}{t_f}\sqrt{\frac{F_{ys}}{E}}$ dictates the capacity of stiffened plate panels of practical rolled sections or not. To find the effect of dimensionless parameter $\beta_1 = \frac{b_f}{t_f}\sqrt{\frac{F_{ys}}{E}}$, five analysis of stiffened plate panels each having identical dimensionless parameter β_2, β_3 and β_4 with different scales of fundamental parameters were tested, while changing the dimensionless parameter β_1 for all five analyses. The parameter β_1 for Compact section of Gr50 steel is 0.76, the highest β_1 for available rolled section is around 0.9. Therefore, the parameter $\beta_1 = \frac{b_f}{t_f}\sqrt{\frac{F_{ys}}{E}}$ was changed from 0.6 to 1.4 in increments of 0.2. The results for each of test analyses are presented in Table 4.4. As shown in Table 4.4, the normalized moment $\frac{M_{cr}}{M_y}$ and $\frac{M_u}{M_y}$ for the first three cases of β_1=0.6, 0.8 and 1.00 were nearly same. Also, the same distortional buckling mode was observed for these three

values of β_1. The normalized moments for the cases of β_1=1.2 and 1.4 were found to be different from that above and the buckling modes were flange local buckling. The applied moments versus mid span vertical deformations history were presented in normalized form for the test cases in Figure 4.12. The differences in ultimate normalized moments and the pattern of the responses clearly show that the cases of β_1=1.2 and 1.4 were different from other three cases. Therefore, this indicates that the dimensionless parameter does not affect the capacity of stiffened plate panels with compact sections and where $\beta_1 \leq 1.00$. All rolled W shapes sections have compact flanges for $F_{ys} = 350MPa$ with exception of W530X72 (W21X48), W360X147 (W14X99), W360X134 (W14X90), W310X97 (W12X65), W200X46 (W8X31) and W200X25 (W8X10). However, the flexural flange slenderness ratios β_1 for these sections are very well below 1.00.

4.8 Parametric Study

The dimensionless parameters that characterize the strength and behavior of stiffened plate panels subjected to lateral pressure loads were established in Section 4.5. The main objective of this chapter is to carry out a detailed parametric study of the primary dimensionless parameters to find the relation among them in determining the behavior and capacity of the stiffened plate panels subjected lateral pressure load. As the number of analyses needed for the four dimensionless parameters β_1, β_2, β_3 and β_4 would result in 5^4 (625) analysis when only five values are used for each of the parameter, it became necessary to restrict the scope of the dimensionless parameters β_1, β_2, β_3 and β_4. Therefore, the dimensionless parameters β_1 and $\beta_3$were identified in the finite element analyses in Sections 4.6 and 4.7 to have a very minimal effect on the behavior and capacity of stiffened plate panels subjected to lateral pressure loads. The magnitude and initial distribution of geometric imperfections and the distribution of residual stress in the stiffened plate panels were applied as described in Chapter 3. The negative pressure load was applied incrementally so as to increase the applied bending moment M_a in the stiffened plate panel. The results of this parametric study will be used in this chapter to study the behaviour plate panels and derive a method to evaluate the capacity of stiffened plate panels subjected to lateral negative pressure.

A further study was conducted to identify the reasonable ranges for dimensionless parameters $\beta_2 = \frac{h_w - 2t_f}{t_w}\sqrt{\frac{F_{ys}}{E}}$ and $\beta_4 = \frac{L}{r}\sqrt{\frac{F_{ys}}{E}}$. It should be noted that it was not possible to change the fundamental parameters h_w, t_w and L alone to achieve the matrix for the

parametric study as the fundamental parameters are interrelated through the parameter $\beta_4 = \frac{L}{r}\sqrt{\frac{F_{ys}}{E}}$. The radius of gyration r depends on all other cross sectional geometric properties of the stiffened plate panel. A review of the geometric dimensions of rolled sections from design manuals (AISC 2005 and CSA 2010) was conducted to determine reasonable ranges for the dimensionless parameters β_2 and β_4. A parametric study was then conducted using values of β_2 and β_4 within that range. The matrix for this parametric study was obtained by examining the range of available rolled section in steel design handbooks (AISC 2005 and CSA 2010).

An examination of the slenderness of standard rolled sections indicated the possible range of web slenderness β_2. The upper limit of web slenderness β_2 was set to 2.719 which corresponds to the highest web slenderness found in the available rolled sections having a yield strength of 350MPa. The minimum value of β_2 considered was based on the lowest value found in the available standard rolled sections. The lowest value of β_2 was 0.834. Ten web slenderness β_2 values were considered ranging from 0.834 to 2.719 in increments of 0.109, i.e. the ratio $\frac{h}{t_w}$ of the stiffener made of steel with yield strength of $F_{ys} = 350$MPa is changed systematically from 20 to 65 in increments of 5. The other dimensionless parameter under consideration was $\beta_4 = \frac{L}{r}\sqrt{\frac{F_{ys}}{E}}$. The selected $\frac{L}{r}$ ranging from 120 to 300 in increments of 20 for the stiffeners which result in ten β_4 values ranged from 5.020 to 12.550. The other two dimensionless parameters $\beta_1 = \frac{b_f}{t_f}\sqrt{\frac{F_{ys}}{E}}$ and $\beta_3 =$

$\frac{b_p}{t_p}\sqrt{\frac{F_{yp}}{E}}$ were kept constant as they have minimal impact on the strength of laterally loaded stiffened plate panels. The selected constant dimensionless parameter β_1 and β_3 were 0.654 and 7.071 respectively. The matrix of selected dimensionless parameters for this parametric study is shown in Table 4.5.

The finite element modeling techniques developed for the stiffened plate panels in Chapter 3 can be used to develop a finite element model that correctly traces the equilibrium path of a laterally loaded stiffened plate panels until it collapses. Thus, this model can be used to obtain the applied bending moment versus deformation relationships even in unloading region of the response of laterally loaded stiffened plate panels. This normalized moment versus the lateral deformation of the unsupported flange of the stiffener can be used to determine the distortional buckling moment M_{cr} of stiffened plate panel as explained in Section 4.4.1. In this section, the results obtained from the parametric study for the range of dimensionless parameters β_2 and β_4 have been extensively analyzed in order to study how the strength and behavior of laterally loaded stiffened plate panels depend on the dimensionless parameters β_2 and β_4. The applied moments M_a versus mid span vertical deflections, normalized with stiffener lengths, history for one set (# 5) of the analysis results (Cases with $\beta_2 = 1.673$ and all β_4) are presented in Figure 4.13. Figure 4.14 shows the corresponding buckling modes for above cases.

The failure modes observed were lateral distortional bucking with a few exceptions in which the local instability occurred in the web at the support locations. This local instability was observed for the cases of stiffeners which have higher web slenderness and smaller spans of stiffened plate panels. As observed in Chapter 3, both ends of the top flanges move slightly in opposite direction with respect to the original location of the centerline of the top middle flange when the stiffened plate panel has a higher web slenderness β_2 and smaller span L. Movement of the top flange triggers local web instability at the support locations as shown in Figure 4.14. Also, close observation of the buckling modes indicates that both ends of the stiffener act like a support against the lateral deformation of middle the flange and web due to the lateral distortional buckling occurring at the middle of the stiffener. The web and flange that are not connected to the plate for the cases of stiffeners with higher web slenderness β_2 and smaller spans L do not provide enough support against this distorsional deformation of the web and flange. This can be observed from the change in buckling modes occurring from smaller span to higher span of stiffeners. The ends of the unsupported flange and web get twisted laterally in the opposite direction of flange distortion at the middle of the stiffener. This twisting of the ends of the unsupported flange and the web disappears as the length of the stiffener increases. This is due to the fact that the ends of the stiffener act as a support for the distortional buckling at the middle of the stiffener. This local instability results in a sharp decrease in the load carrying capacity as shown in Figure 4.13. However, this type of stiffener with higher web slenderness β_2 and smaller span L is not practical. Therefore, the results due to this local instability are omitted from the rest of the analysis.

Table 4.6 summarizes the distortional buckling moments M_{cr} obtained from the parametric study. The distortional buckling moments are non-dimensionalized relative to the corresponding yield moments. The normalized distortional buckling moments $\frac{M_{cr}}{M_y}$ are tabulated in Table 4.7. For a particular web slenderness β_2, despite the drops in strength prediction at beginning, the predicted distortional buckling moment remained the same with the increase in overall slenderness β_4. The strength drops at beginning was due to the twist of end top flanges for stiffened plate panel with small overall slenderness β_4. However, the normalized distortional buckling moments drop progressively as the web slenderness β_2 increases. The normalized ultimate moments $\frac{M_u}{M_y}$ are also reported in Table 4.8. As there was no significant post buckling strength, the predicted normalized ultimate moments $\frac{M_u}{M_y}$ were closer to respective normalized distortional buckling moments $\frac{M_{cr}}{M_y}$.

The current design methods used to proportion the stiffener in industry are adapted from structural steel codes such as CSA (2010). In order to evaluate the current method using the results obtained from the parametric study, the capacities of the matrix of stiffeners considered in this study were estimated based on the beam design method in CSA (2010). The current design practice assumes the unbraced length of the outer compression flange to be the full span of stiffener. In order to calculate the section properties, a portion of the plate welded to the stiffeners is considered to contribute for a composite action. The widths of the plate involved in this composite action are between 12 to 42 times of plate thickness (ASCE 1995). In this evaluation, 16 times of plate thickness ($32t$) on either side of flange legs, as in general practice, is considered to be effective. The bending

capacity of the composite section, assuming full span of the stiffener as the unsupported length of the compression flange, are estimated based on code formulae (CSA 2010). The code evaluation results are presented in Table 4.9 in order to compare with the results of parametric study. The comparison suggests that the code results do not predict the finite element analysis results. The code predictions are conservative as the overall slenderness increases.

Figure 4.15 graphically summarizes the normalized buckling moments obtained from the parametric study of laterally loaded stiffened plate panels. The graph shown in Figure 4.15 is three-dimensional in nature and is intended to indicate how normalized buckling moments depend on both dimensionless parameters β_2 and β_4. The two horizontal axes are associated with the web slenderness β_2 and overall slenderness β_4. The vertical axis represents the output dimensionless parameter $\frac{M_{cr}}{M_y}$ that corresponds to any given combination of dimensionless parameters β_2 and β_4. The coordinates points of $\frac{M_{cr}}{M_y}$ and the associated slenderness β_2 and β_4 were then connected in a linear fashion to provide the continuous surface as shown in Figure 4.15. The three-dimensional graphs are useful in illustrating, in a general way, how the output dimensionless parameter $\frac{M_{cr}}{M_y}$ is influenced by variations in the dimensionless parameters β_2 and β_4. It can be observed from Figure 4.15 that the normalized moment $\frac{M_{cr}}{M_y}$ does not change significantly as the overall slenderness β_4 increases for a particular web slenderness β_2. However, the normalized moment $\frac{M_{cr}}{M_y}$ decreases as the web slenderness β_2 increases. Also it should be noted that

the applied moment M_{cr} reaches the yield moment M_y of the cross section indicated by $\frac{M_{cr}}{M_y} = 1$ for the web slenderness of practical wide flange stiffeners used in industry. This can be explained by the fact that symmetrical loading, loading height and the smaller height of the tension side of the web (height of neutral axis from tension side) provide enough rotational resistance to the compression portion of laterally loaded stiffened plate panels to reach the yield stress before experiencing elastic buckling. The symmetrical negative pressure loading with respect to an axis parallel to the web create a fixed support condition of the web connected to the plate as shown in Figure 4.16. Also, the height of the applied load with respect to a beam centroid is known to affect the buckling capacity of the beam in flexure. The general lateral torsional buckling formula was developed without considering any external torsional forces on the beam. Such forces can be presented by a load applied away from the centroid of the beam section. When the unsupported flange remains vertical, the load applied away from centroid does not provide any torsional forces. As the unsupported flange begins to distort, the load no longer acts through the centroid and the load height up or down with respect to centroid of the section increases or decreases the torsional forces leading to buckling. The SSRC guide (Galambus 1998) addresses the load height by incorporating it within the moment gradient factor in calculating the lateral torsional buckling moment of a section. In the case of laterally loaded stiffened plate panels, the load is applied below the centroid, therefore the negative pressure load also provides restorative forces against distortional buckling.

In an industrial duct stiffener, the tension flange is held rotationally fixed about its longitudinal axis, and the compression portion of the stiffener is also held rotationally fixed through the tension portion of the web. Thus the torsional restraint for the compression portion of stiffener is provided by the tension portion of the web. If the rotational restraint provided by the tension portion of the web is effective enough, this can restraint the unsupported compression portion of the stiffener until yielding. To act effectively as a rotational bracing, the tension portion of the web must have enough strength and stiffness. The rotational stiffness of web is inversely proportional to the height of the tension portion of the web. This can be derived assuming that the height of tension portion of web acts like a cantilever beam supported at the plate. The height of tension portion of stiffened plate panels is very small compared with depth of stiffeners. This small height of the tension portion of the web may provide high torsional restraint for the compression portion of the stiffener. Therefore, the fixed support condition of the web due to symmetrical loading, smaller height of the tension portion of web that provides higher rotational stiffness and the load height that provides a restorative force against twisting of the unsupported compression flange provide substantial resistance for the distortional buckling. Therefore, these factors lead the laterally loaded plate, stiffened with general rolled wide flange shape structural steel sections, to reach the yielding moment before buckling.

The three-dimensional graphs provide a general summary of the available normalized moment $\frac{M_{cr}}{M_y}$ for laterally loaded stiffened plate panels. However, in order to obtain a method to evaluate the strength of laterally loaded stiffened plate panels, the results must

be presented in a different way. It is generally desired to obtain the available normalized moment $\frac{M_{cr}}{M_y}$ for various values of the dimensionless parameters β_2 and β_4. With this in mind, Figure 4.17, which illustrates the normalized distortional buckling moment, was presented in two dimensional contour plots. The contours of normalized distortional buckling moments and ultimate moments are plotted as shown in Figure 4.17 and Figure 4.18, respectively. These contours were taken from the three dimensional surface plot. An inspection of the contour plots also reveals that the normalized moment for a particular dimensionless parameters β_2 does not change significantly when β_4 changes. This may be explained by the shape of the buckling mode. The wave length of the distortional buckling of the flange seems to be nearly the same as the overall slenderness parameter β_4 increases for particular web slenderness β_2. The same wavelength indicates that the compression portion of the stiffener undergoes the same mode of buckling and requires the same amount of energy. Therefore, it is reasonable to conclude that the buckling moment capacity of an industrial duct stiffener was not significantly affected by the overall slenderness parameter β_4, except the cases with higher web slenderness and smaller spans.

Even though the above conclusions can be reached, it is anticipated to propose a useful and practical design method of quantifying the available capacity of the stiffened plate panel subjected to negative pressure loading. An inspection of the contour of the available capacity of a stiffened plate panel as depicted in Figure 4.17 shows clearly that the normalized moment capacities depend mainly on the dimensionless web slenderness parameter β_2. Also It can be concluded from the results that the general rolled stiffeners

used in rectangular large industrial duct can reach their top flange fibre yielding moment M_y, if their dimensionless slenderness β_2 is less than or equal to 2.0. However, this should satisfy one condition to avoid local web instability at the support for stiffeners with high depth to span ratio. A boundary between lateral distortional buckling and local web instability was established. The proposed boundary for the lateral distortional buckling can be described as:

$$\beta_4 \geq 3.33\,\beta_2 + 0.145 \tag{3.1}$$

This proposed boundary can also be written as

$$\frac{L}{r}\sqrt{\frac{F_{ys}}{E}} \geq 3.33\,\frac{h_w - 2t_f}{t_w}\sqrt{\frac{F_{ys}}{E}} + 0.145 \tag{3.2}$$

The applied bending moment M_a can reach the cross sectional yield moment M_y for the stiffener section of which the dimensionless parameter β_2 is less than or equal to 2.0.

$$M_{cr} \geq M_y \;\; for \;\; \beta_2 \leq 2.0 \;\; and \;\; \beta_4 \geq 3.33\,\beta_2 + 0.145 \tag{3.3}$$

This rule can also be written as

$$M_{cr} \geq M_y \;\; for \;\; \frac{h_w - 2t_f}{t_w}\sqrt{\frac{F_{ys}}{E}} \leq 2.0 \;\; and \;\; \frac{L}{r}\sqrt{\frac{F_{ys}}{E}} \geq 3.33\,\frac{h_w - 2t_f}{t_w}\sqrt{\frac{F_{ys}}{E}} + 0.145 \tag{3.4}$$

A close inspection of these results and contours reveals that the trend of normalized distortional buckling moment capacity $\frac{M_{cr}}{M_y}$ can be a function of $\beta_2 = \frac{h_w - 2t_f}{t_w}\sqrt{\frac{F_{ys}}{E}}$. Therefore, approximate values of $\beta_2 = \frac{h_w - 2t_f}{t_w}\sqrt{\frac{F_{ys}}{E}}$ for each contour line of the normalized moment $\frac{M_{cr}}{M_y}$ were established in order to drive a relation between the normalized moment capacity $\frac{M_{cr}}{M_y}$ and dimensionless web slenderness $\beta_2 = \frac{h_w - 2t_f}{t_w}\sqrt{\frac{F_{ys}}{E}}$.

In order to propose this relation, the data points corresponding to each contour line were derived from the contour plots and plotted in scattered form as shown in Figure 4.19. Then, a linear line was established so that the line included all data points in order to derive a best approximate relation in between the normalized moment capacity $\frac{M_{cr}}{M_y}$ and dimensionless web slenderness $\beta_2 = \frac{h_w - 2t_f}{t_w}\sqrt{\frac{F_{ys}}{E}}$. In this derivation, the points due to local instabilities were exempted. Therefore, this relation can be applicable if it satisfies the condition that excludes the local instability. The summary of proposed relation is:

$$\frac{M_{cr}}{M_y} = 1.51 - 0.275\,\beta_2 \qquad for\ \frac{L}{r}\sqrt{\frac{F_{ys}}{E}} \geq 3.33\left(\frac{h_w - 2t_f}{t_w}\sqrt{\frac{F_{ys}}{E}}\right) + 0.145 \tag{3.5}$$

This rule also can also be written as:

$$\frac{M_{cr}}{M_y} = 1.51 - 0.275\left(\frac{h_w - 2t_f}{t_w}\sqrt{\frac{F_{ys}}{E}}\right) \quad for\ \frac{L}{r}\sqrt{\frac{F_{ys}}{E}} \geq 3.33\left(\frac{h_w - 2t_f}{t_w}\sqrt{\frac{F_{ys}}{E}}\right) + 0.145 \tag{3.6}$$

It should be noted here that these results are valid only for the stiffened plate panels subjected to static pressure loading and ambient temperature.

4.9 Conclusions and Further Recommendations

This study has shown that the standard beam method used to estimate the capacity of stiffened plate panel was inappropriate for this type failure mode of the stiffeners. The standard beam method leads to excessive conservatism in designing stiffener sections. The failure mode observed for the stiffened plate panels subjected to bending was the lateral distortional buckling of the stiffener. The lateral distortional buckling is characterized as simultaneous buckling of the web and flange with same wavelength. This type of failure mode does not result in progressive loss in buckling strength of the stiffened plate panels as overall slenderness $\beta_4 = \frac{L}{r}\sqrt{\frac{F_{ys}}{E}}$ increases.

The stiffener web slenderness $\beta_2 = \frac{h_w - 2t_f}{t_w}\sqrt{\frac{F_{ys}}{E}}$ was found to be the most influential dimensionless parameter affecting the strength and behavior of stiffened plate panels under bending. The stiffener overall dimensionless slenderness $\beta_4 = \frac{L}{r}\sqrt{\frac{F_{ys}}{E}}$ did not show a significant effect on the capacity of stiffened plate panels due to distortional buckling. However, stiffeners with higher web depth slenderness β_2 and smaller span L lead to local web failure at support locations. A local failure of the web is triggered when the web slenderness is higher and the span of stiffener is small. The boundary between the local web crippling was defined in order to provide a design guideline that can predict the lateral distortional buckling capacity of stiffened plate panels. Based on the parametric study, the design equation was provided in terms of stiffener web slenderness $\beta_2 = \frac{h_w - 2t_f}{t_w}\sqrt{\frac{F_{ys}}{E}}$.

The flange slenderness $\beta_1 = \frac{b_f}{t_f}\sqrt{\frac{F_{ys}}{E}}$ of a rolled section stiffener has no effect on the behavior and strength the stiffened plate panel. The practical range of the plate slenderness affected neither the behavior nor the strength of the stiffened plate panel subjected to lateral pressure loading.

The practical range of plate slenderness $\beta_3 = \frac{b_p}{t_p}\sqrt{\frac{F_{yp}}{E}}$ also does not affect the behavior and strength of the stiffener.

4.9.1 Further Recommendations

Through this numerical parametric study, a significant progress in understanding the behavior of stiffened plates has been achieved. However, there are several items that need further investigation:

1. This parametric study concentrates only on the negative pressure loading that causes bending on the stiffened panel. Although, the lateral pressure load is the significant loading, the stiffened panel can be subjected to compression arising from negative pressure on top and bottom panels, self weight, dust weight, refractory weight etc. Therefore, the effect of additional compression should be investigated.
2. Although wide flange beam stiffeners are widely used in large rectangular industrial ducts, there are rectangular duct for which the plates are stiffened with other shapes such as channels and angles. The shear centers of these shapes are

offset from their centeroid. The effect of this offset shear center for these shapes stiffeners should be investigated.

3. This study assumed the temperature of the stiffened plate panel to be ambient. However, generally, industrial ducts transport flue gases at elevated temperatures. These elevated temperatures may introduce a temperature gradient across the depth of the stiffened plate panel. The centre of temperature gradient and the location of the neutral axis are offset. This offset will introduce additional stresses. Therefore, the combining effect of the temperature gradient and the lateral load need to be investigated.
4. The dimensionless parameters proposed should be tested experimentally for the scale effects.
5. The dimensionless parameters with material independent were established for the idealized elastic-plastic-strain hardening tri-linear material model representing mild carbon steel. The material independency of the dimensionless parameters for the material models representing high strength steel should be established.

Table 4.1 Completeness of Dimensional Parameters

($\beta_1 = 0.654,\ \beta_2 = 1.749,\ \beta_3 = 7.889,\ \beta_4 = 7.071$)

Model #	b_f	t_f	h_w	t_w	L	b_p	t_p	E	F_{ys}	F_{yp}	M_y (kN.m)	$\frac{M_{cr}}{M_y}$	$\frac{M_u}{M_y}$
1	125.00	8.00	225.00	5.00	5000.00	1000	5	200000	350	250	99.7	1.138	1.160
2	150.00	9.60	210.00	4.56	6710.47	1000	5	200000	350	250	118.5	1.134	1.158
3	160.00	10.23	250.00	5.49	6905.36	1000	5	200000	350	250	166.5	1.136	1.158
4	109.44	7.00	230.00	5.17	4010.44	1000	5	200000	350	250	86.3	1.137	1.158
5	187.60	12.00	224.94	4.81	8818.00	1200	6	200000	350	250	188.3	1.135	1.158
6	168.86	10.00	242.97	4.94	8101.89	1000	5	200000	300	250	139.2	1.141	1.157
7	166.48	9.00	319.39	6.09	7728.30	1000	5	200000	250	250	155.6	1.139	1.164
8	132.89	8.50	202.45	4.44	5727.34	1000	5	200000	350	250	93.4	1.140	1.159
										Mean		1.138	1.159
										Std. Dev		0.002	0.002

Table 4.2 Section Modulus for Various Plate Widths

$b_p(mm)$	$I_s(in^4)$	$y_o(mm)$	$S_s(in^3)$	$\%\ Change$
500	103.54	62.65	17.26	
				1.37%
750	112.44	51.80	17.50	
				0.85%
1000	118.62	44.26	17.65	
				0.57%
1250	123.17	38.72	17.75	
				0.41%
1500	126.64	34.48	17.82	
				0.31%
1750	129.40	31.13	17.87	
				0.24%
2000	131.62	28.41	17.92	
				0.20%
2250	133.46	26.17	17.95	
				0.16%
2500	135.01	24.48	17.98	

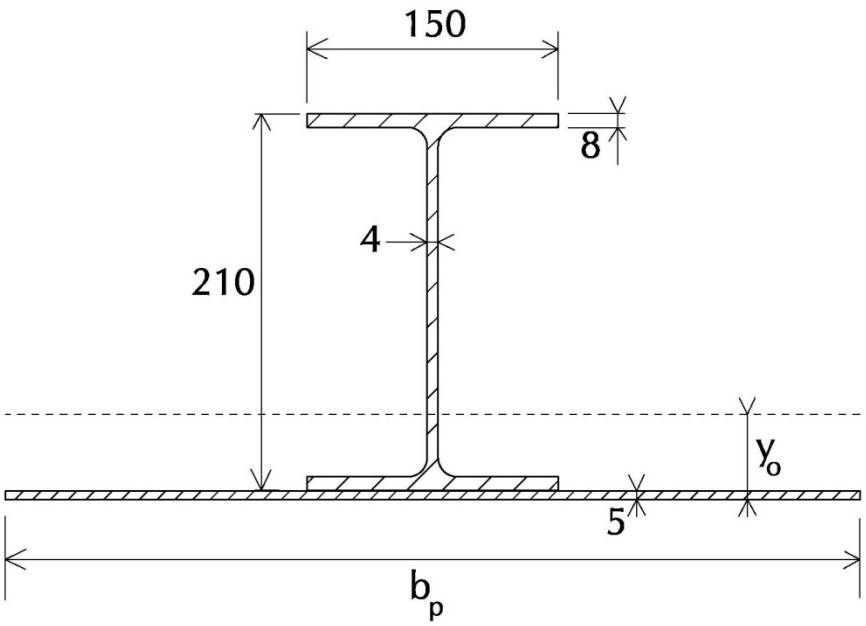

Table 4.3 Effect of Plate Slenderness $\beta_3 = \frac{b_p}{t_p}\sqrt{\frac{F_{yp}}{E}}$

($\beta_1 = 0.784,\ \beta_2 = 2.029,\ \beta_4 = 7.880,\ F_{ys} = 350MPa, F_{yp} = 250MPa, E = 200000MPa$)

$Model$	b_f	t_f	h_w	t_w	L	b_p	t_p	β_3	M_y (kN.m)	$\frac{M_{cr}}{M_y}$	$\frac{M_u}{M_y}$
1	150	8	210	4	6512	1750	5	12.374	102.6	1.117	1.132
2	150	8	210	4	6535	1500	5	10.607	102.2	1.108	1.118
3	150	8	210	4	6565	1250	5	8.839	101.8	1.103	1.112
4	150	8	210	4	6605	1000	5	7.071	101.2	1.096	1.109
5	150	8	210	4	6660	750	5	5.303	100.4	1.098	1.108

Table 4.4 Effect of Stiffener Flange Flexural Slenderness $\beta_1 = \frac{b_f}{t_f}\sqrt{\frac{F_{ys}}{E}}$

($\beta_2 = 1.527,\ \beta_3 = 7.071,\ \beta_4 = 7.524, F_{ys} = 350MPa, F_{yp} = 250MPa, E = 200000MPa$)

$Model$	b_f	t_f	h_w	t_w	L	b_p	t_p	β_1	M_y (kN.m)	$\frac{M_{cr}}{M_y}$	$\frac{M_u}{M_y}$
1	125	8.72	200	5.00	5000	1000	5	0.600	91.2	1.163	1.189
2	150	7.84	215	5.46	5904	1000	5	0.800	108.5	1.167	1.187
3	160	6.69	225	5.80	6002	1000	5	1.000	109.6	1.168	1.187
4	175	6.10	230	5.97	6477	1000	5	1.200	113.9	1.081	1.160
5	200	5.98	240	6.25	7472	1000	5	1.400	131.9	1.085	1.097

Flange Slenderness of Compact Section as per AISC LRFD 2005

$$\beta_1 = \frac{b_f}{t_f}\sqrt{\frac{F_{ys}}{E}} = 0.76\ for\ F_{ys} = 350MPa$$

Flange Slenderness of Class 2 Section as per CSA 2010

$$\frac{b_f}{2t_f} < \frac{170}{\sqrt{F_{ys}}}$$

For $F_{ys} = 350MPa$:

$$\beta_1 = \frac{b_f}{t_f}\sqrt{\frac{F_{ys}}{E}} = 0.76$$

Table 4.5 Matrix of Dimensionless Parameters

Set	#	$F_{ys} = 350MPa,\ F_{yp} = 250MPa,\ E = 200000MPa,$ $\beta_1 = 0.654\ ,\ \beta_3 = 7.071$ $b_f = 125,\ t_f = 8,\ b_p = 1000,\ t_p = 5,\ h_w = 250$ in mm	L(mm)	$\frac{L}{r_f}$	β_4
1	1	$\beta_2 = 0.837$ $\frac{h_w}{t_w} = 20,\quad t_w = 11.70mm$ $M_y = 149.5kN.m\ ,\ M_p = 210.6kN.m*$	2491	120	5.020
	2		2906	140	5.857
	3		3322	160	6.693
	4		3737	180	7.530
	5		4152	200	8.367
	6		4567	220	9.203
	7		4982	240	10.040
	8		5397	260	10.877
	9		5813	280	11.713
	10		6228	300	12.550
2	1	$\beta_2 = 1.046$ $\frac{h_w}{t_w} = 25,\quad t_w = 9.36mm$ $M_y = 137.5kN.m, M_p = 187.0kN.m*$	2649	120	5.020
	2		3090	140	5.857
	3		3532	160	6.693
	4		3973	180	7.530
	5		4415	200	8.367
	6		4856	220	9.203
	7		5298	240	10.040
	8		5739	260	10.877
	9		6181	280	11.713
	10		6622	300	12.550
3	1	$\beta_2 = 1.255$ $\frac{h_w}{t_w} = 30,\quad t_w = 7.80mm$ $M_y = 129.3kN.m, M_p = 171.3kN.m*$	2782	120	5.020
	2		3245	140	5.857
	3		3709	160	6.693
	4		4172	180	7.530
	5		4636	200	8.367
	6		5099	220	9.203
	7		5563	240	10.040
	8		6027	260	10.877
	9		6490	280	11.713
	10		6954	300	12.550

Table 4.5 Matrix of Dimensionless Parameters continues..

4	1	$\beta_2 = 1.464$ $\frac{h_w}{t_w} = 35, \quad t_w = 6.69mm$ $M_y = 123.3kN.m, M_p = 160.0kN.m^*$	2894	120	5.020
	2		3377	140	5.857
	3		3859	160	6.693
	4		4341	180	7.530
	5		4824	200	8.367
	6		5306	220	9.203
	7		5788	240	10.040
	8		6271	260	10.877
	9		6753	280	11.713
	10		7235	300	12.550
5	1	$\beta_2 = 1.673$ $\frac{h_w}{t_w} = 40, \quad t_w = 5.85mm$ $M_y = 118.8kN.m, M_p = 151.5kN.m^*$	2991	120	5.020
	2		3490	140	5.857
	3		3988	160	6.693
	4		4487	180	7.530
	5		4985	200	8.367
	6		5484	220	9.203
	7		5982	240	10.040
	8		6481	260	10.877
	9		6979	280	11.713
	10		7478	300	12.550
6	1	$\beta_2 = 1.882$ $\frac{h_w}{t_w} = 45, \quad t_w = 5.20mm$ $M_y = 115.2kN.m, M_p = 144.9kN.m^*$	3075	120	5.020
	2		3588	140	5.857
	3		4101	160	6.693
	4		4613	180	7.530
	5		5126	200	8.367
	6		5638	220	9.203
	7		6151	240	10.040
	8		6663	260	10.877
	9		7176	280	11.713
	10		7688	300	12.550
7	1	$\beta_2 = 2.092$ $\frac{h_w}{t_w} = 50, \quad t_w = 4.68mm$ $M_y = 112.3kN.m, M_p = 139.6kN.m^*$	3149	120	5.020
	2		3674	140	5.857
	3		4199	160	6.693
	4		4724	180	7.530
	5		5249	200	8.367
	6		5774	220	9.203
	7		6299	240	10.040
	8		6824	260	10.877
	9		7349	280	11.713
	10		7874	300	12.550

Table 4.5 Matrix of Dimensionless Parameters continues..

8	1	$\beta_2 = 2.031$ $\frac{h_w}{t_w} = 55, \quad t_w = 4.25mm$ $M_y = 109.9kN.m, M_p = 135.2kN.m$*	3215	120	5.020
	2		3751	140	5.857
	3		4287	160	6.693
	4		4822	180	7.530
	5		5358	200	8.367
	6		5894	220	9.203
	7		6430	240	10.040
	8		6966	260	10.877
	9		7502	280	11.713
	10		8037	300	12.550
9	1	$\beta_2 = 2.510$ $\frac{h_w}{t_w} = 60, \quad t_w = 3.90mm$ $M_y = 107.9kN.m, M_p = 131.6kN.m$*	3274	120	5.020
	2		3819	140	5.857
	3		4365	160	6.693
	4		4910	180	7.530
	5		5456	200	8.367
	6		6001	220	9.203
	7		6547	240	10.040
	8		7093	260	10.877
	9		7638	280	11.713
	10		8184	300	12.550
10	1	$\beta_2 = 2.719$ $\frac{h_w}{t_w} = 65, \quad t_w = 3.60mm$ $M_y = 106.2kN.m, M_p = 128.6kN.m$*	3326	120	5.020
	2		3880	140	5.857
	3		4435	160	6.693
	4		4989	180	7.530
	5		5543	200	8.367
	6		6098	220	9.203
	7		6652	240	10.040
	8		7207	260	10.877
	9		7761	280	11.713
	10		8315	300	12.550

*Plastic moments are based on elastic-perfectly plastic material models.

Table 4.6 Distortional Buckling Moments of Parametric Study

($F_{ys} = 350MPa$, $F_{yp} = 250MPa, E = 200GPa$)

M_{cr}		$\frac{L}{r_f}$									
		120	140	160	180	200	220	240	260	280	300
$\frac{h_w}{t_w}$	20	190.1	203.0	204.9	203.2	188.5	197.5	191.2	197.2	196.0	187.8
	25	171.6	175.3	173.9	169.0	172.1	171.0	170.6	167.8	167.1	165.9
	30	149.3	153.8	153.8	154.2	151.9	152.5	151.1	150.7	148.3	147.5
	35	166.7	177.7	182.0	183.6	183.5	183.4	178.9	177.7	179.6	174.9
	40	xxx	123.1	125.8	128.5	127.8	127.9	127.7	125.6	125.7	125.1
	45	xxx	104.0	114.4	118.0	120.0	118.2	118.5	118.8	117.2	117.4
	50	xxx	xxx	99.2	108.2	112.1	113.7	111.9	112.5	111.3	111.6
	55	xxx	xxx	xxx	93.8	103.2	105.7	105.5	106.4	105.3	105.2
	60	xxx	xxx	xxx	xxx	88.7	98.9	101.9	101.9	102.0	101.3
	65	xxx	xxx	xxx	xxx	81.8	92.2	94.0	96.3	97.8	97.7

Table 4.7 Normalized Distortional Buckling Moments of Parametric Study

($F_{ys} = 350MPa, F_{yp} = 250MPa, E = 200GPa$)

$\frac{M_{cr}}{M_y}$		β_4									
		5.020	5.860	6.690	7.530	8.370	9.200	10.040	10.880	11.710	12.550
β_2	0.837	1.201	1.358	1.371	1.359	1.261	1.321	1.279	1.320	1.311	1.256
	1.046	1.248	1.275	1.264	1.229	1.252	1.243	1.240	1.220	1.215	1.207
	1.255	1.155	1.190	1.190	1.193	1.175	1.179	1.169	1.165	1.147	1.141
	1.464	1.042	1.111	1.137	1.147	1.147	1.146	1.118	1.111	1.122	1.093
	1.673	xxx	1.037	1.059	1.082	1.076	1.077	1.075	1.058	1.058	1.053
	1.882	xxx	0.902	0.993	1.025	1.042	1.026	1.029	1.031	1.017	1.019
	2.092	xxx	xxx	0.883	0.964	0.998	1.012	0.996	1.001	0.991	0.994
	2.301	xxx	xxx	xxx	0.854	0.939	0.962	0.960	0.968	0.958	0.957
	2.510	xxx	xxx	xxx	xxx	0.822	0.917	0.944	0.945	0.945	0.938
	2.719	xxx	xxx	xxx	xxx	0.770	0.868	0.885	0.907	0.921	0.919

Table 4.8 Normalized Ultimate Moment of Parametric Study

($F_{ys} = 350MPa, F_{yp} = 250MPa, E = 200GPa$)

$\frac{M_u}{M_y}$		β_4									
		5.020	5.860	6.690	7.530	8.370	9.200	10.040	10.880	11.710	12.550
β_2	0.837	1.218	1.382	1.383	1.380	1.366	1.354	1.340	1.332	1.322	1.316
	1.046	1.268	1.286	1.290	1.271	1.271	1.261	1.252	1.241	1.236	1.230
	1.255	1.183	1.196	1.209	1.204	1.195	1.186	1.180	1.172	1.160	1.158
	1.464	1.063	1.121	1.152	1.163	1.159	1.154	1.146	1.138	1.131	1.121
	1.673	xxx	1.048	1.071	1.093	1.093	1.096	1.087	1.086	1.083	1.078
	1.882	xxx	0.912	1.011	1.038	1.053	1.056	1.051	1.044	1.036	1.039
	2.092	xxx	xxx	0.899	0.976	1.006	1.020	1.018	1.015	1.004	1.004
	2.301	xxx	xxx	xxx	0.863	0.950	0.975	0.987	0.987	0.982	0.980
	2.510	xxx	xxx	xxx	xxx	0.834	0.925	0.951	0.956	0.957	0.954
	2.719	xxx	xxx	xxx	xxx	0.781	0.874	0.903	0.923	0.928	0.928

Table 4.9 Normalized Stiffener Capacity Based on CSA 2010

($F_{ys} = 350MPa, F_{yp} = 250MPa, E = 200GPa$)

$\left(\frac{M_{cr}}{M_y}\right)_{S16}$		β_4									
		5.020	5.860	6.690	7.530	8.370	9.200	10.040	10.880	11.710	12.550
β_2	0.837	1.41	1.34	1.28	1.21	1.14	1.07	1.01	0.93	0.85	0.79
	1.046	1.33	1.26	1.18	1.11	1.04	0.96	0.88	0.80	0.73	0.68
	1.255	1.27	1.20	1.12	1.05	0.97	0.89	0.80	0.73	0.66	0.61
	1.464	1.23	1.16	1.08	1.00	0.93	0.84	0.75	0.68	0.63	0.58
	1.673	1.20	1.13	1.05	0.97	0.90	0.81	0.72	0.66	0.60	0.55
	1.882	1.18	1.10	1.03	0.95	0.87	0.78	0.70	0.64	0.58	0.54
	2.092	1.16	1.08	1.01	0.93	0.86	0.77	0.69	0.62	0.57	0.53
	2.301	1.14	1.07	0.99	0.92	0.84	0.75	0.68	0.61	0.56	0.52
	2.510	1.13	1.05	0.98	0.91	0.83	0.74	0.67	0.61	0.56	0.51
	2.719	1.11	1.04	0.97	0.90	0.82	0.73	0.66	0.60	0.55	0.51

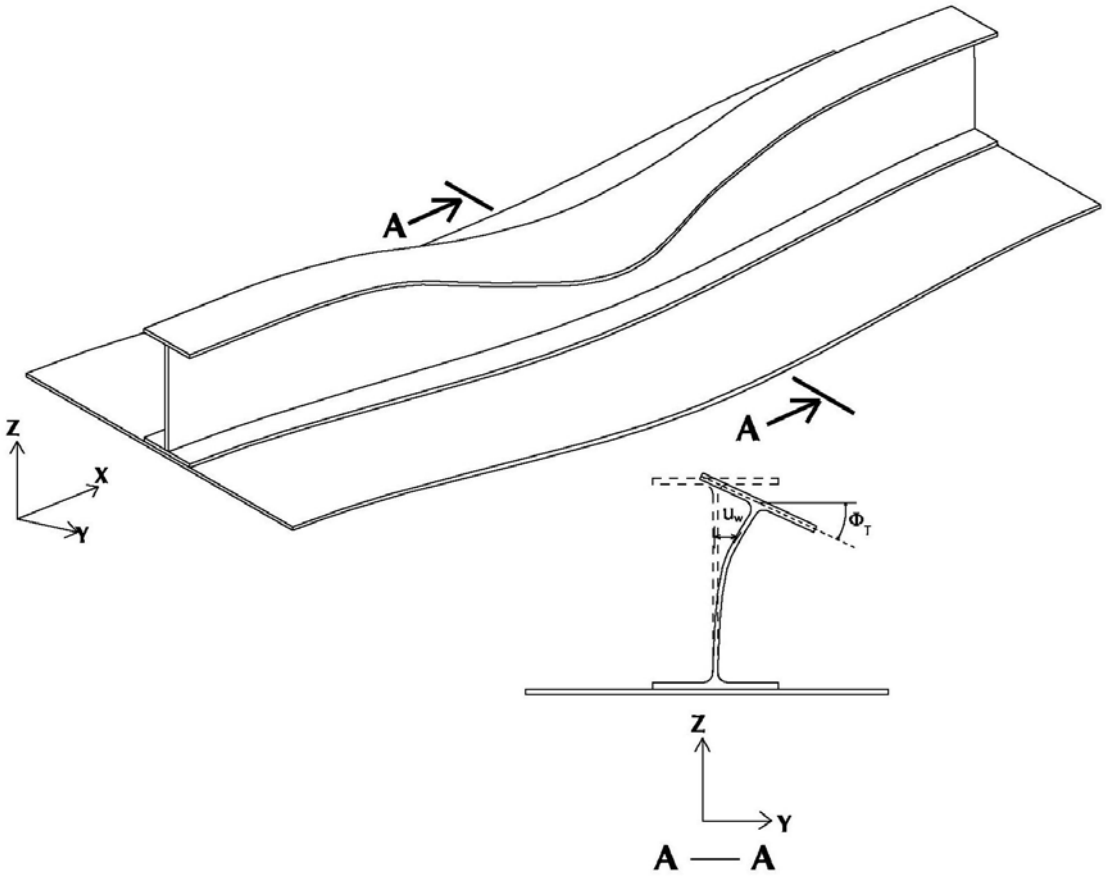

Figure 4.1 Distortional Buckling of Stiffened Plate Panel

Figure 4.2 Fundamental Parameters

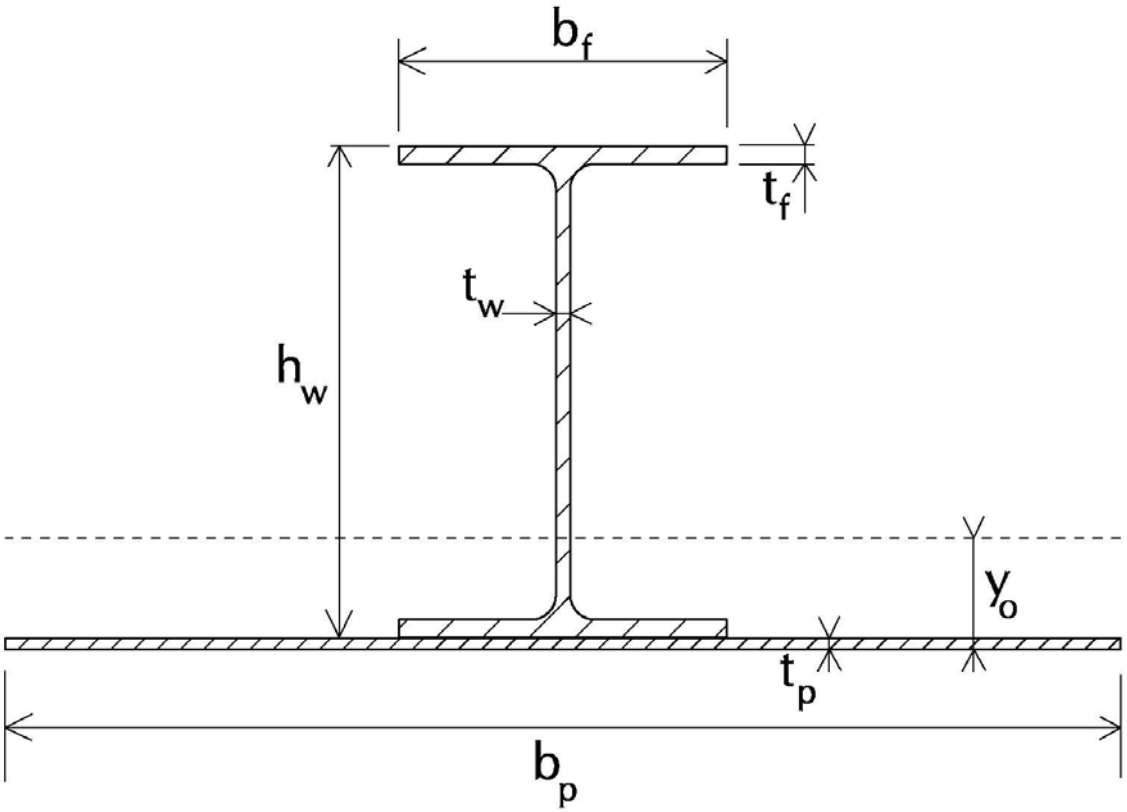

Area of stiffener:

$$A_s = 2b_f t_f + (h_w - 2t_f)t_w$$

Depth of neutral axis from the bottom plate:

$$y_o = \frac{A_s\left(\frac{h_w}{2} + t_p\right) + b_p t_p \frac{t_p}{2}}{A_s + b_p t_p}$$

Second moment of area of compression portion with respect to vertical axis:

$$I_{sf} = \frac{1}{12} {b_f}^3 t_f + \frac{1}{12}(h_w + t_p - t_f - y_o){t_w}^3$$

Area of compression portion:

$$A_f = b_f t_f + (h_w + t_p - t_f - y_o)t_w$$

Radius of gyration of compression portion with respect to vertical axis:

Figure 4.2 Fundamental Parameters Continues

$$r = \sqrt{\frac{I_{sf}}{A_f}}$$

Second moment of area of stiffener with respect to major axis:

$$I_s = \frac{1}{6}{t_f}^3 b_f + 2 b_f t_f \left(\frac{h_w}{2} - \frac{t_f}{2}\right)^2 + \frac{1}{12}\left(h_w - 2t_f\right)^3 t_w$$

Second moment of area of stiffened plate panel with respect to neutral axis:

$$I_{sp} = I_s + A_s \left(\frac{h_w}{2} + t_p - y_o\right)^2 + \frac{1}{12}{t_p}^3 b_p + b_p t_p \left(y_o - \frac{t_p}{2}\right)^2$$

Section modulus with respect to top compression flange:

$$S_t = \frac{I_{sp}}{\left(h_w + t_p - y_o\right)}$$

Moment at which top flange begins to yield:

$$M_y = S_t F_{ys}$$

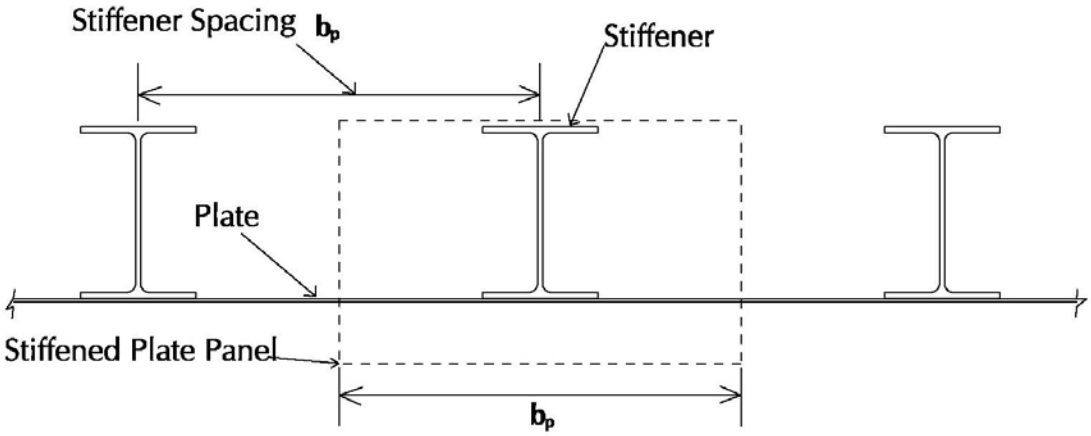

Figure 4.3 Typical Stiffened Plate Panel

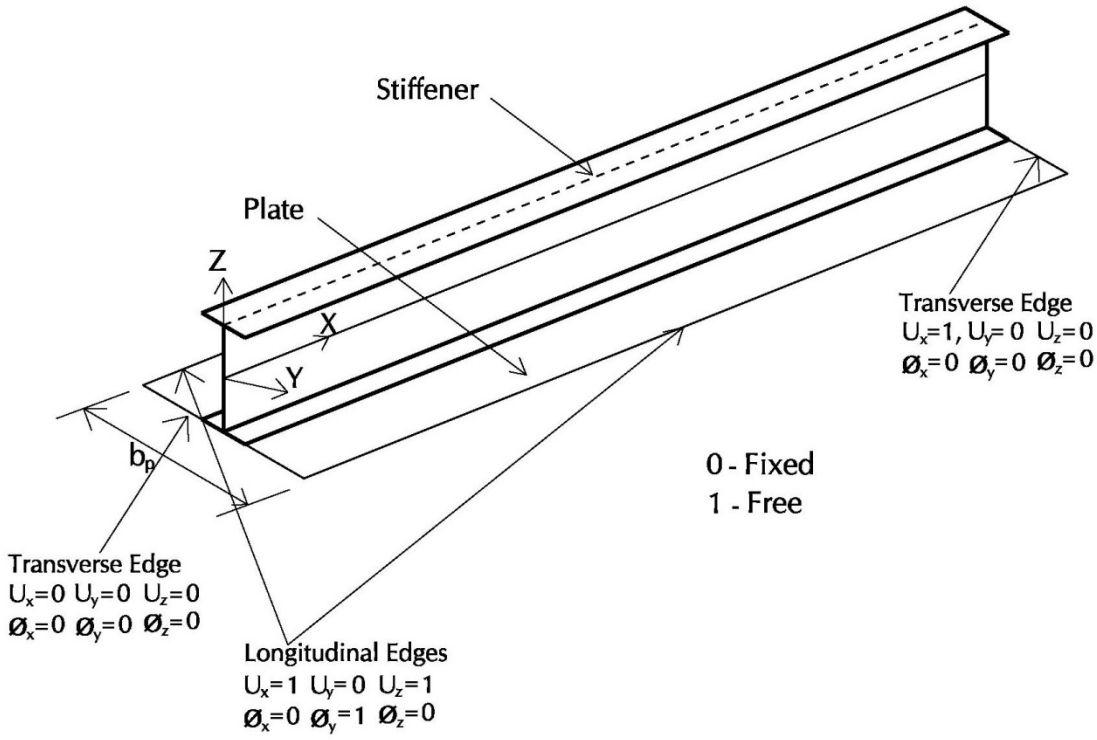

Figure 4.4 Boundary Conditions

Stiffener	Strain	ε_y	ε_{st}	ε_u	ε_l
		0.00175	0.0175	0.033	0.1
	Stress (MPa)	F_y	F_{st}	F_u	F_u
		350	350	450	450
Plate	Strain	ε_y	ε_{st}	ε_u	ε_l
		0.0025	0.025	0.035	0.1
	Stress (MPa)	F_y	F_{st}	F_u	F_u
		250	250	400	400

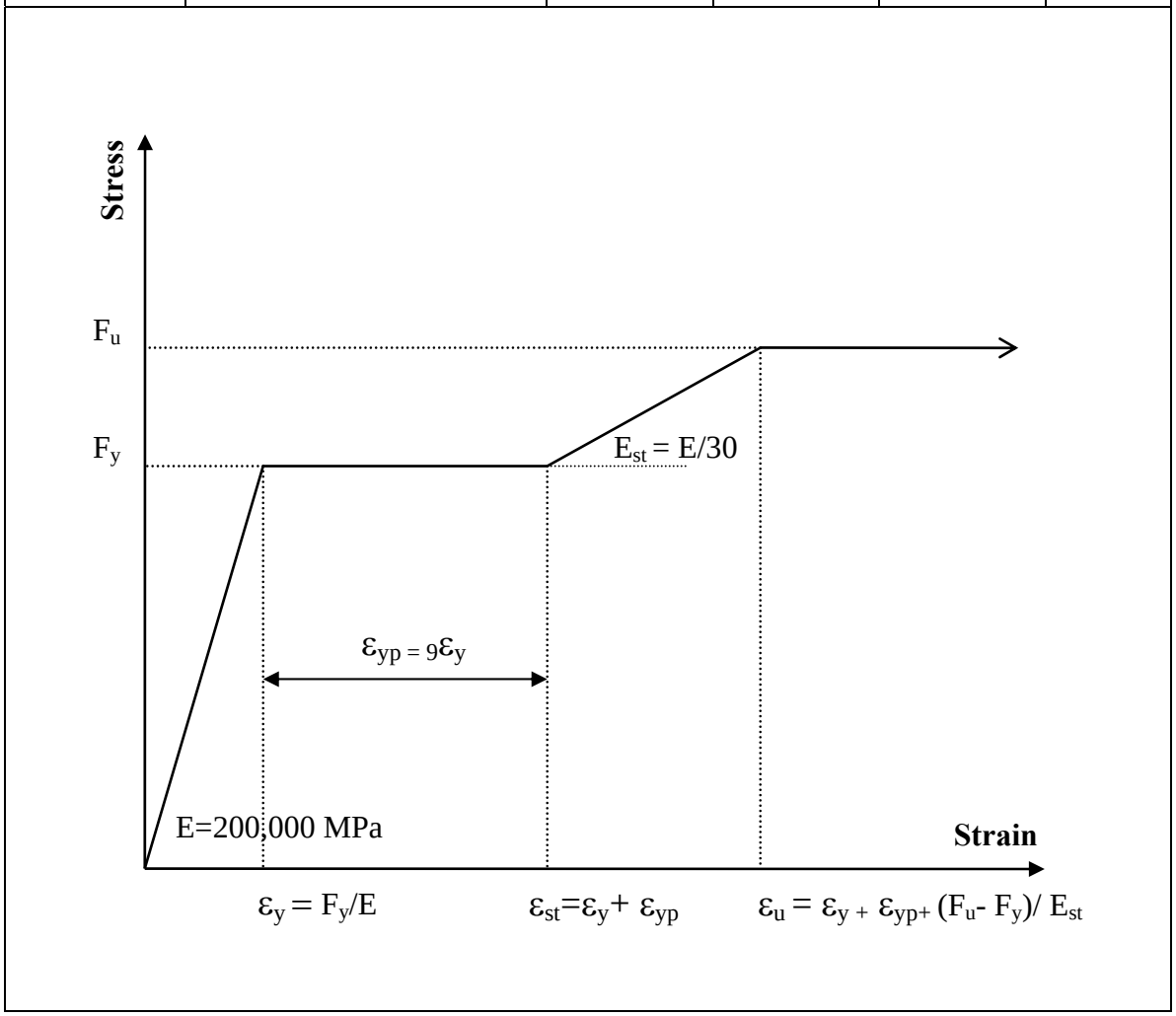

Figure 4.5 Idealized Material Models

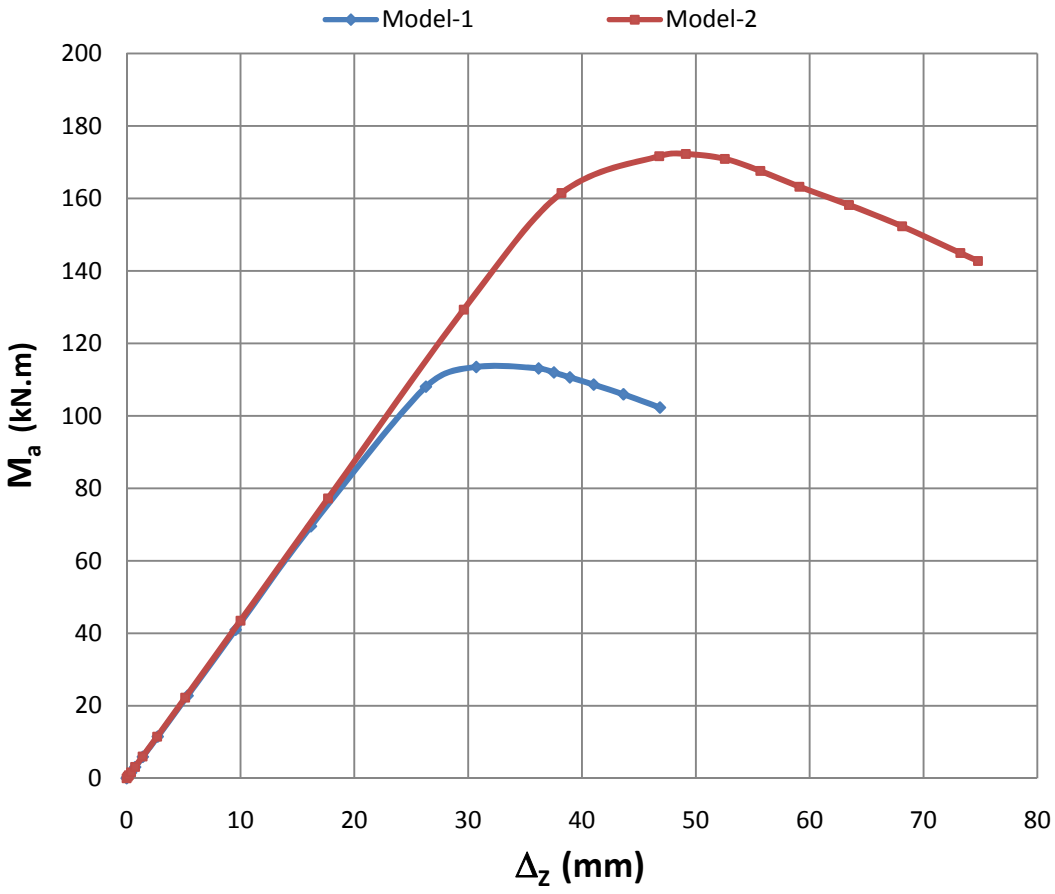

$\boldsymbol{Model-1}$: $b_f = 125, t_f = 8, h_w = 225, t_w = 5, b_p = 1000, t_p = 5, L = 5000$
$\boldsymbol{Model-2}$: $b_f = 150, t_f = 9.6, h_w = 250, t_w = 5.52, b_p = 1000, t_p = 5$, L=6284
Units are in mm

Figure 4.6 Applied Moment versus Mid Span Vertical Deflection

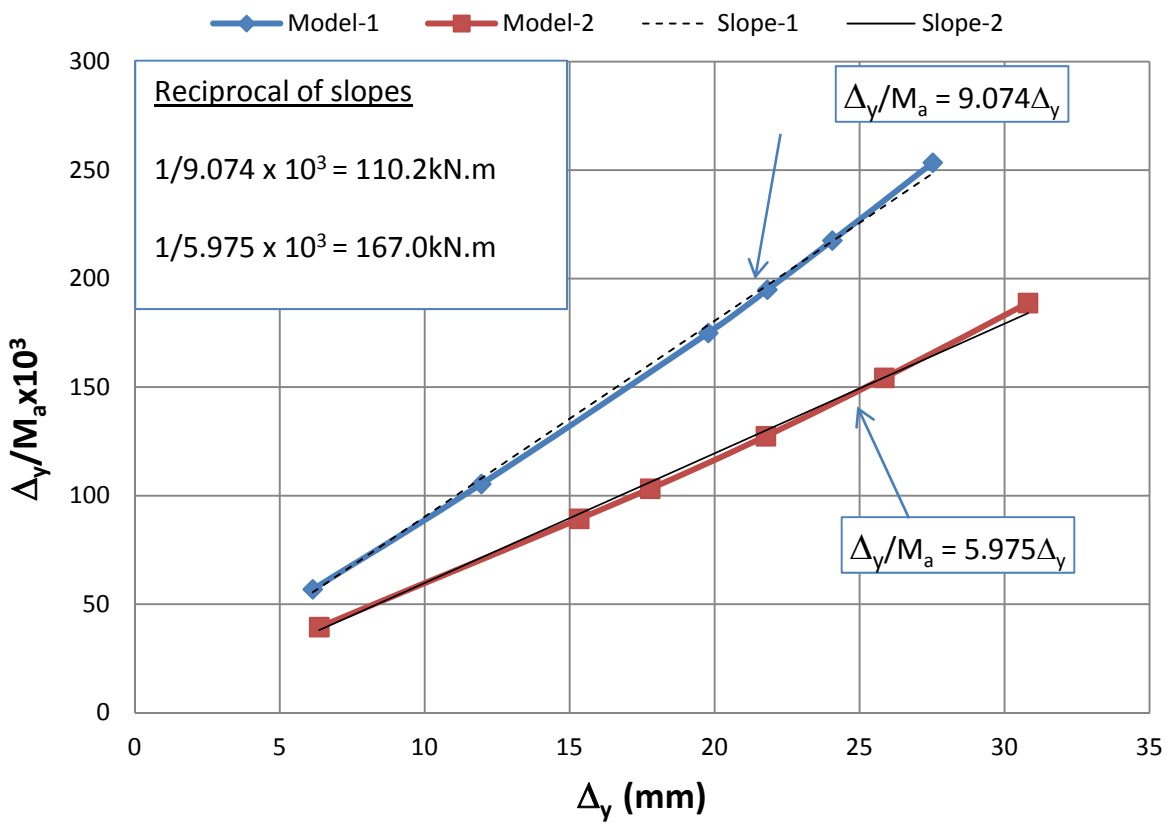

Figure 4.7 Lateral Deflection over Applied Moment (Δ_Y/M_a) versus Lateral Deflection (Δ_Y)

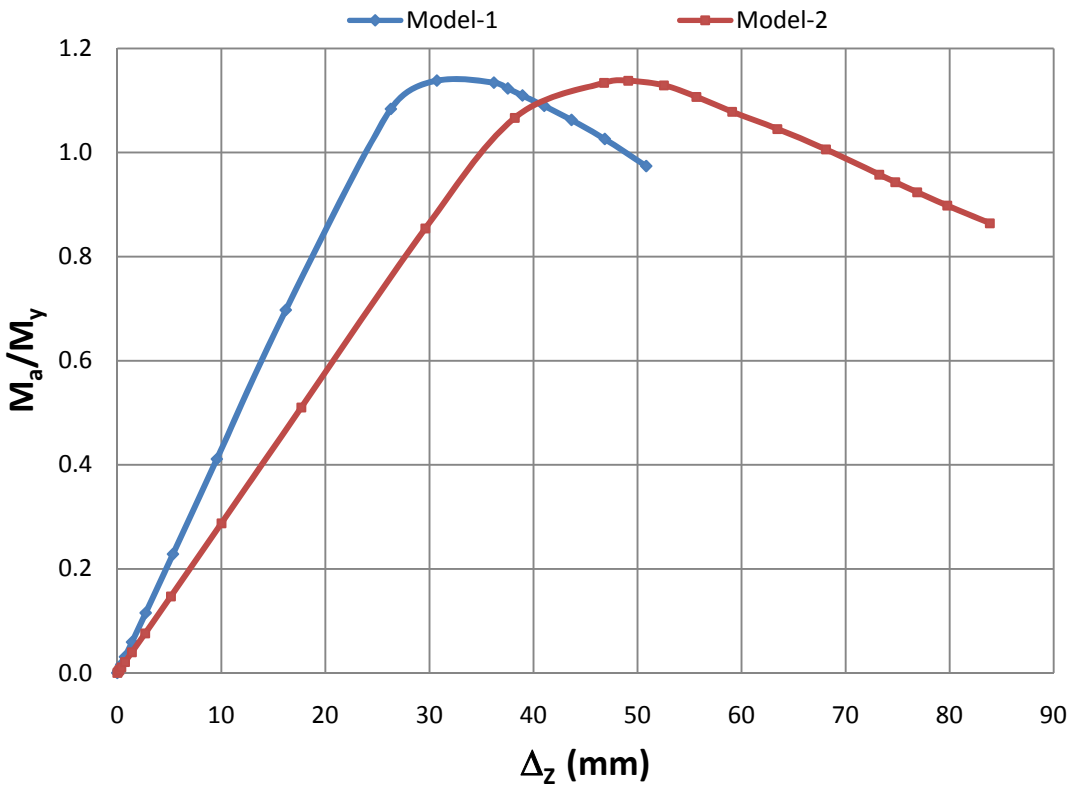

Figure 4.8 Normalized Applied Moment versus Mid Span Vertical Deflection (Δ_z)

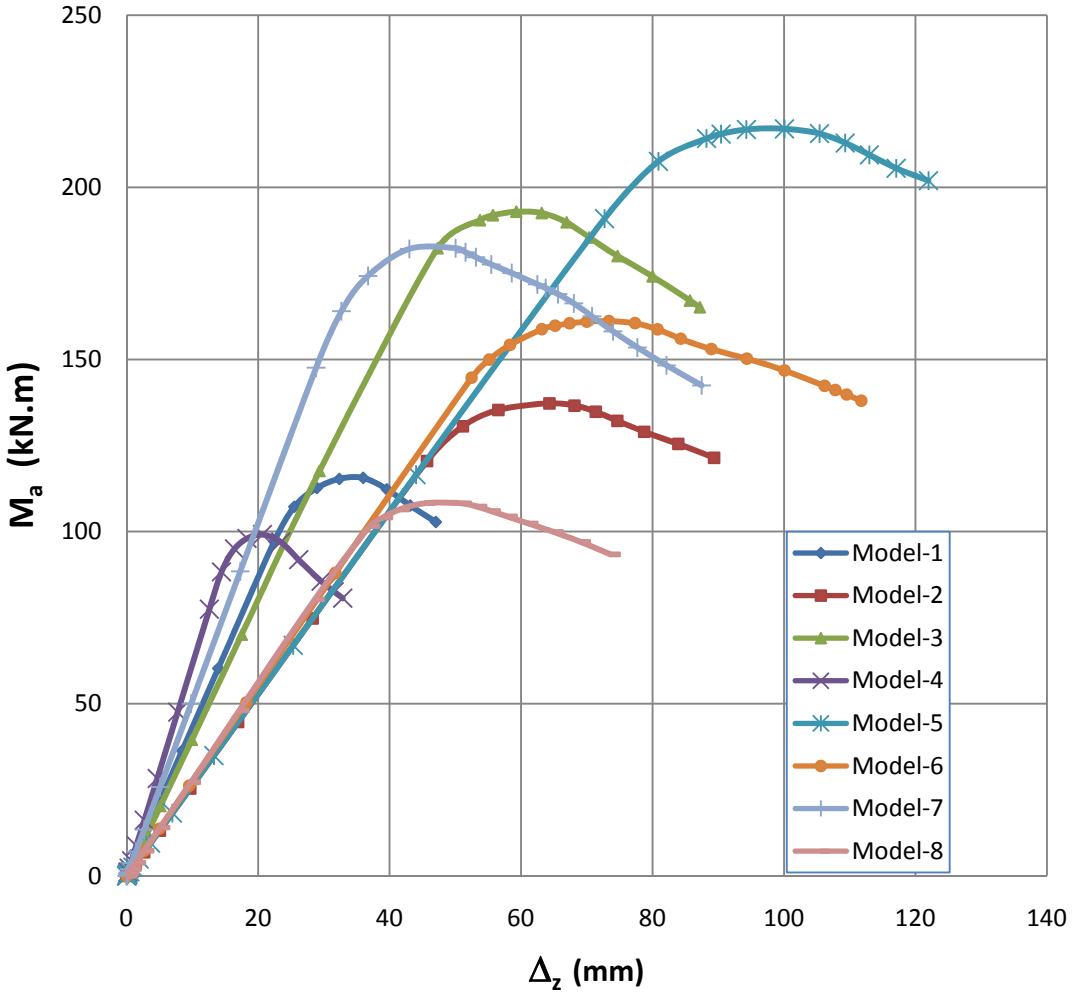

Figure 4.9 Applied Moment versus Mid Span Vertical Deflection (Δ_z) Histories of Models

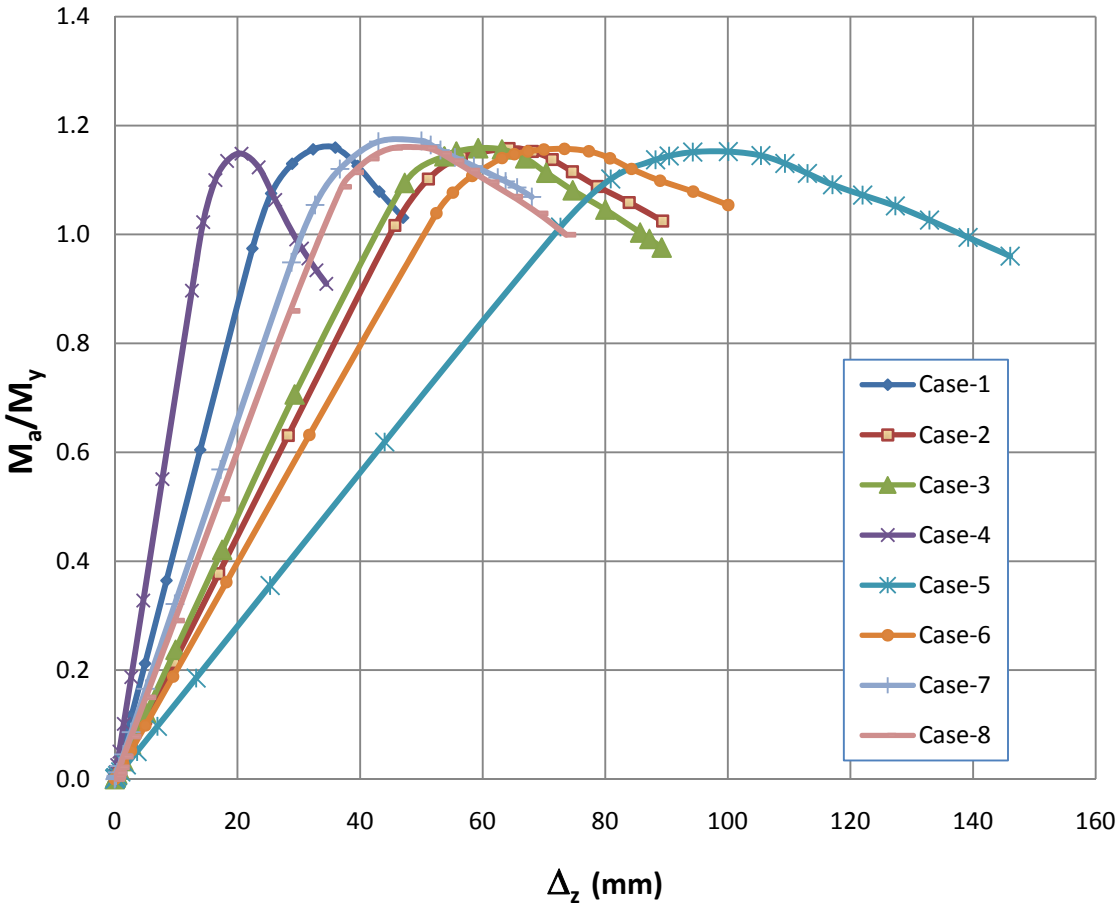

Figure 4.10 Normalized Applied Moment versus Mid Span Vertical Deflection (Δ_z) Histories of Models

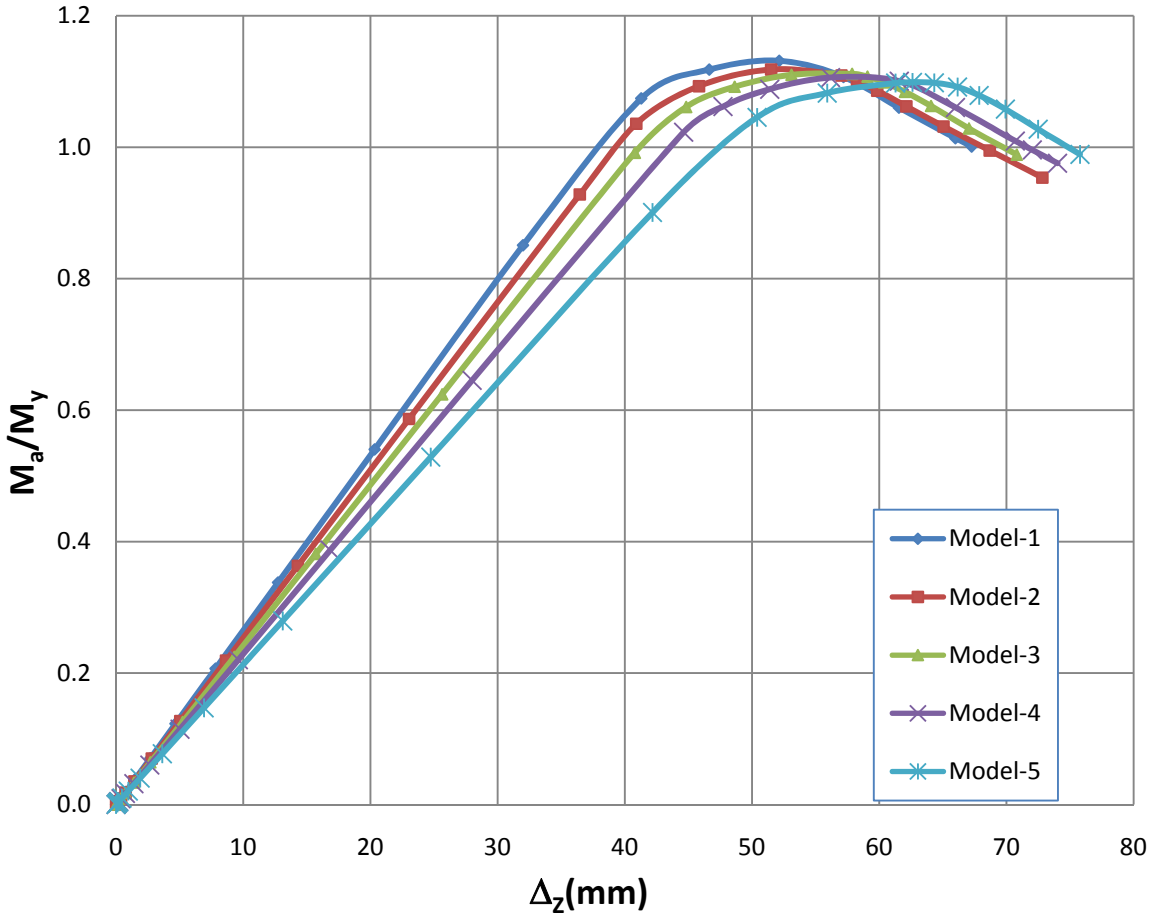

Figure 4.11 Normalized Applied Moment versus Mid Span Vertical Deflection (Δ_z) : Effect of β_3

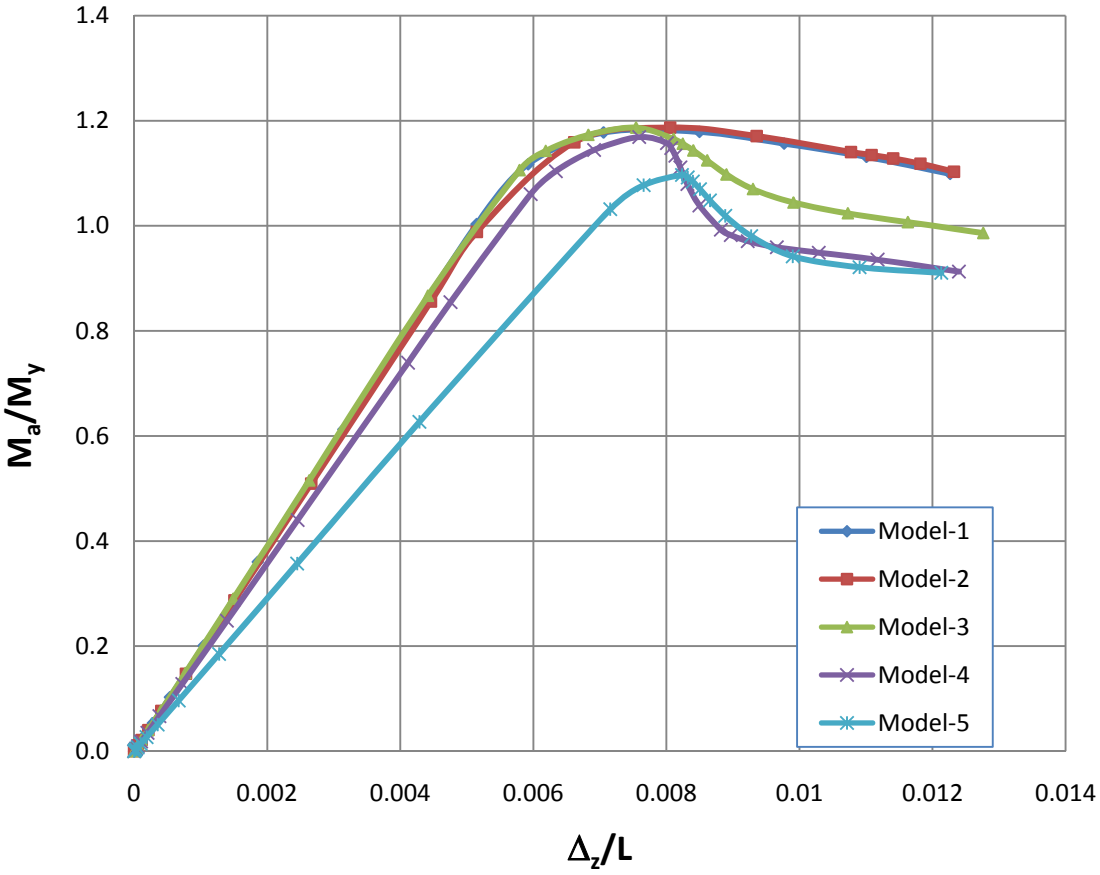

Figure 4.12 Normalized Applied Moment versus Deformation **:** Effect of β_1

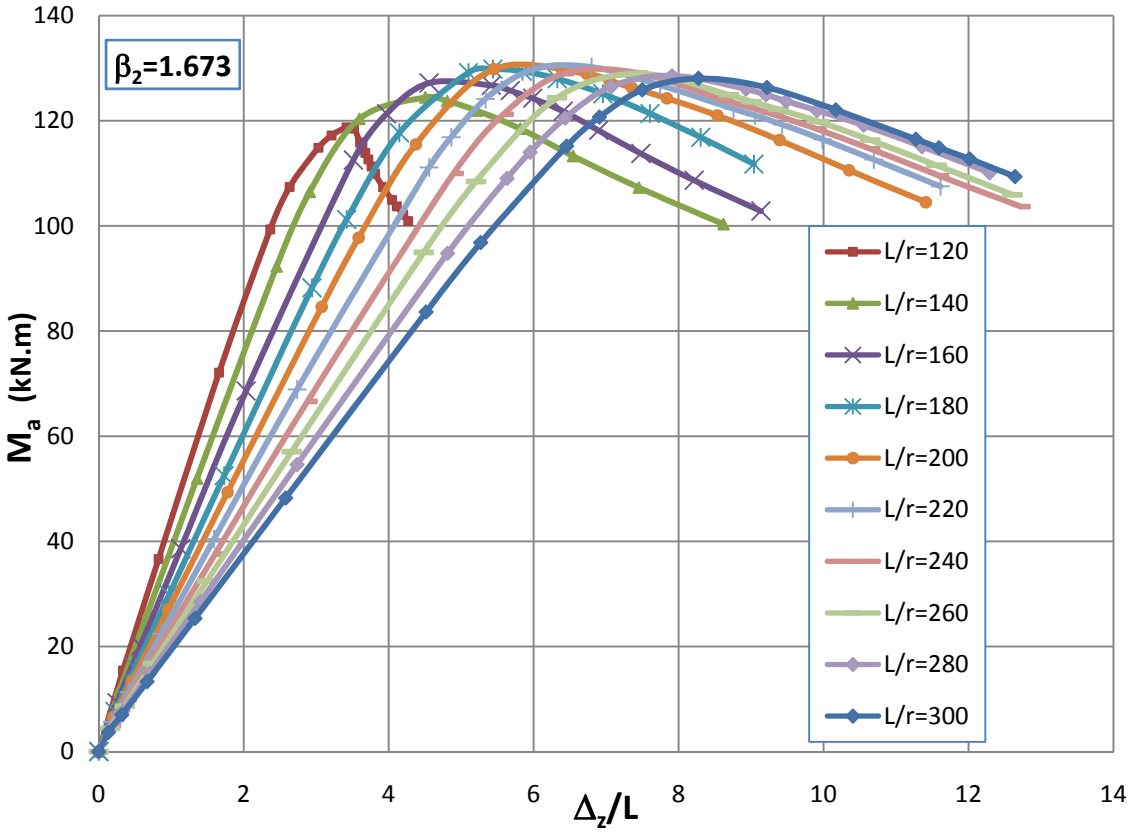

Figure 4.13 Applied Moment versus Deformation History: $\boldsymbol{\beta_2 = 1.673}$

Figure 4.14 Buckling Modes of Stiffened Plate Panels

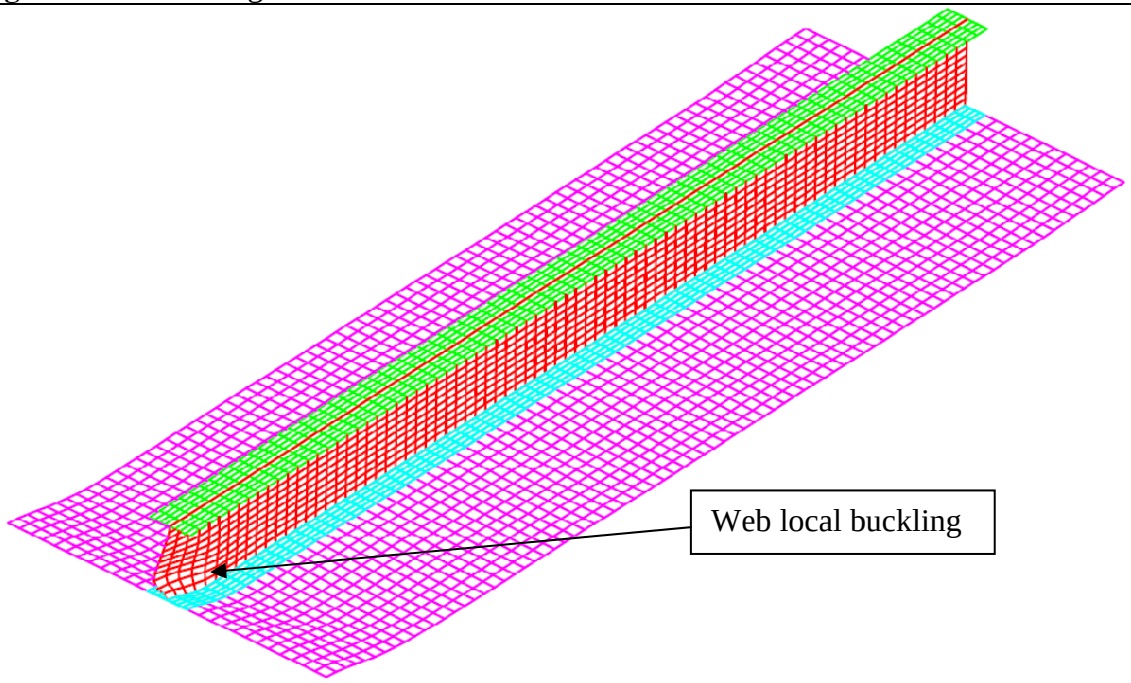

($F_{ys} = 350MPa, F_{yp} = 250MPa, E = 200GPa, \beta_2 = 1.673, \beta_4 = 5.020$ ($\frac{L}{r_f}$=120))

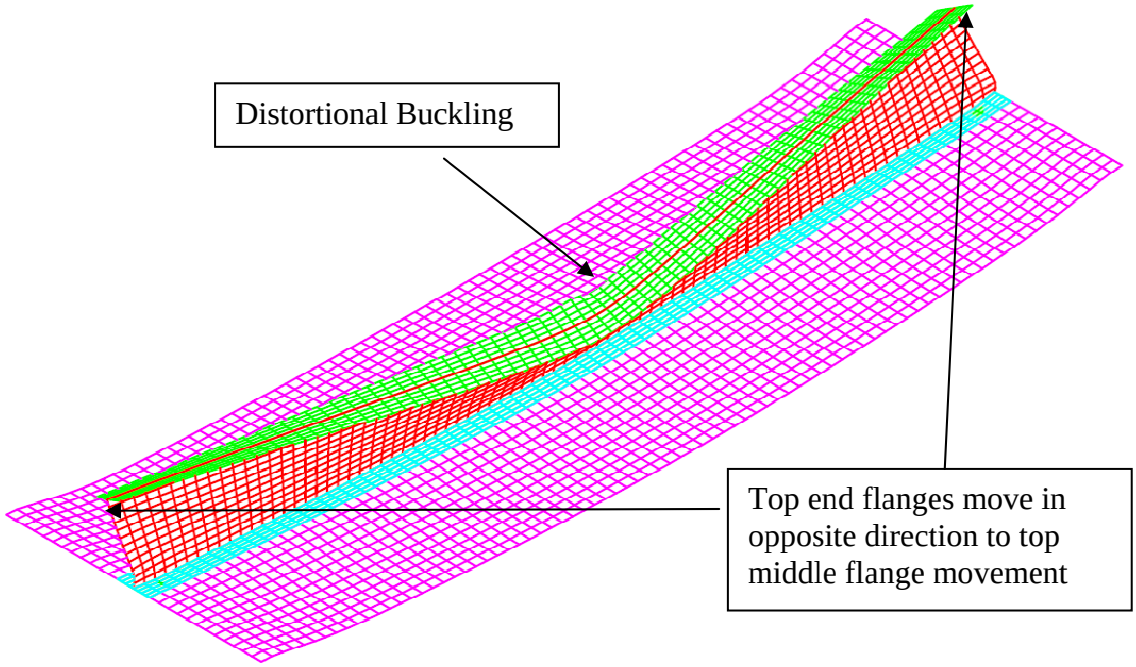

($F_{ys} = 350MPa,\ F_{yp} = 250MPa, E = 200GPa, \beta_2 = 1.673, \beta_4 = 5.860$ ($\frac{L}{r_f}$=140))

Figure 4.14 Buckling Modes of Stiffened Plate Panels (cont'd)

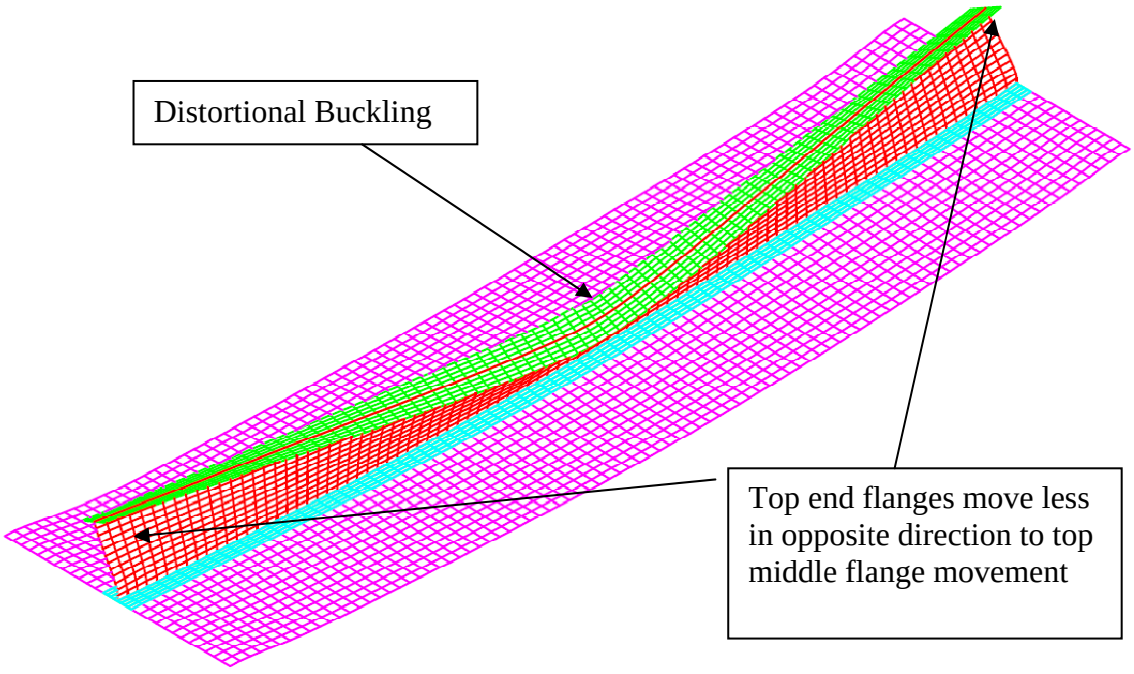

($F_{ys} = 350MPa, F_{yp} = 250MPa, E = 200GPa, \beta_2 = 1.673, \beta_4 = 6.690$ ($\frac{L}{r_f}$=160))

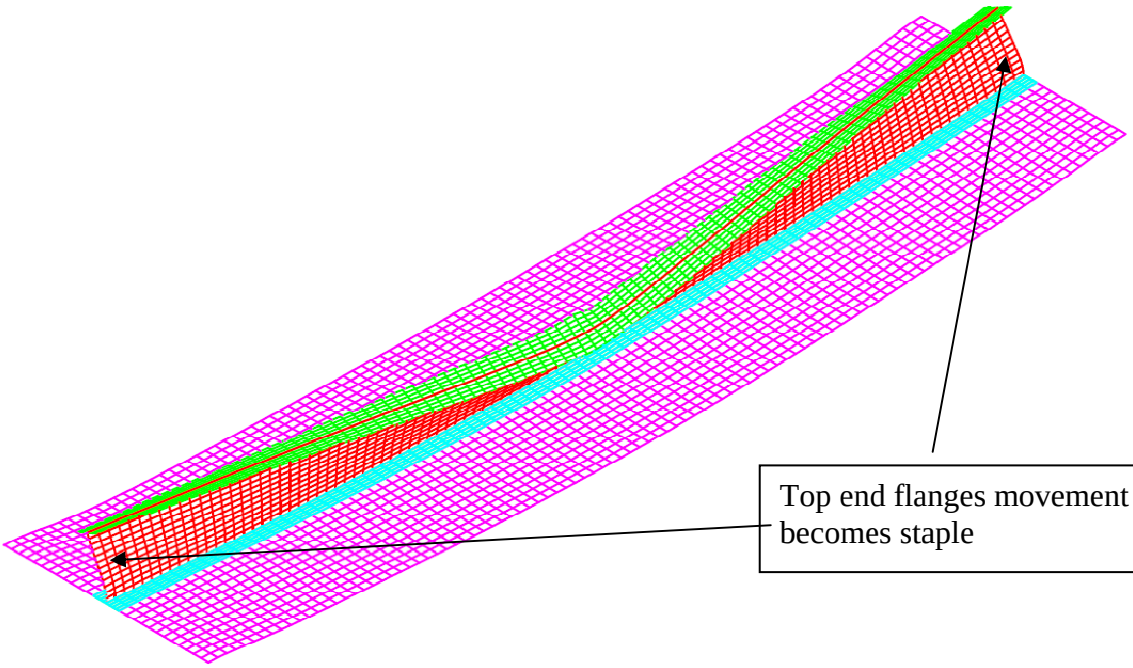

($F_{ys} = 350MPa, F_{yp} = 250MPa, E = 200GPa, \beta_2 = 1.673, \beta_4 = 7.530$ ($\frac{L}{r_f}$=180))

Figure 4.14 Buckling Modes of Stiffened Plate Panels (cont'd)

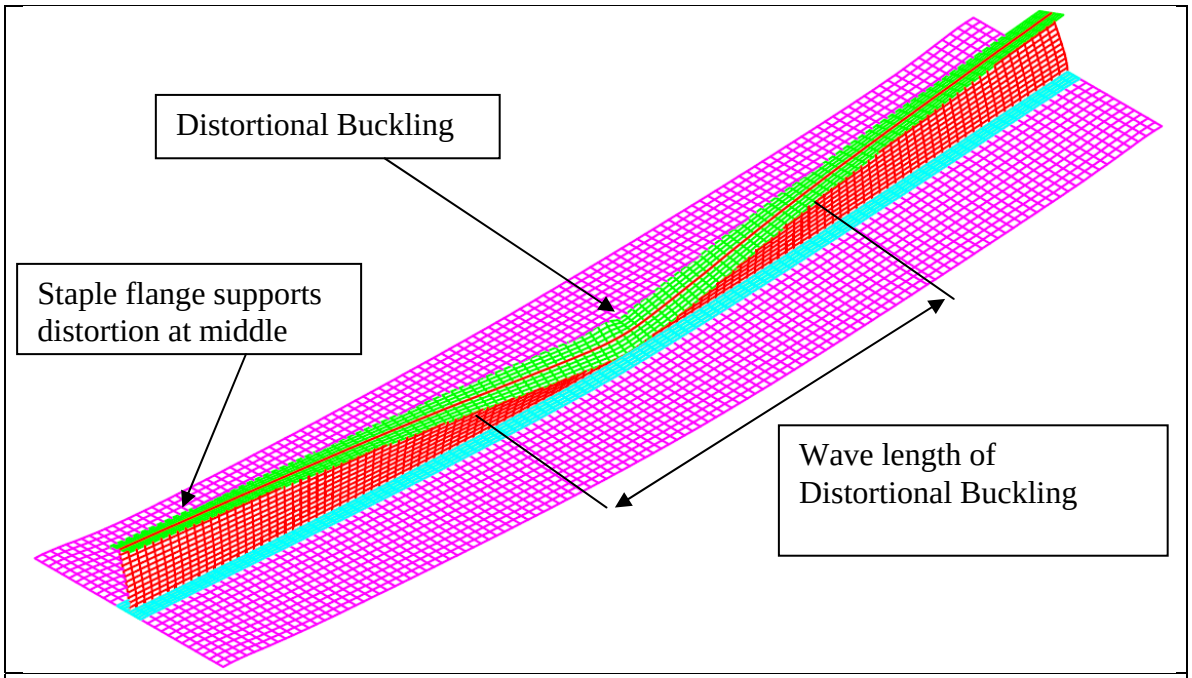

($F_{ys} = 350MPa, F_{yp} = 250MPa, E = 200GPa, \beta_2 = 1.673, \beta_4 = 8.370$ ($\frac{L}{r_f}$=200))

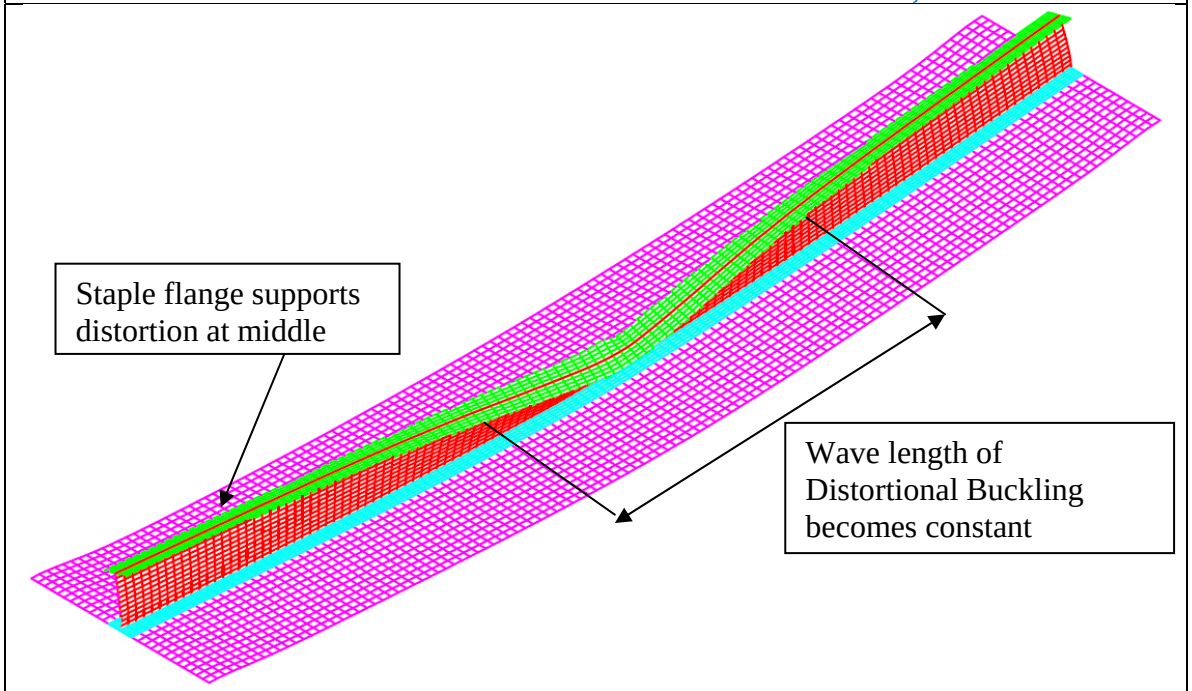

($F_{ys} = 350MPa, F_{yp} = 250MPa, E = 200GPa, \beta_2 = 1.673, \beta_4 = 9.200$ ($\frac{L}{r_f}$=220))

Figure 4.14 Buckling Modes of Stiffened Plate Panels (cont'd)

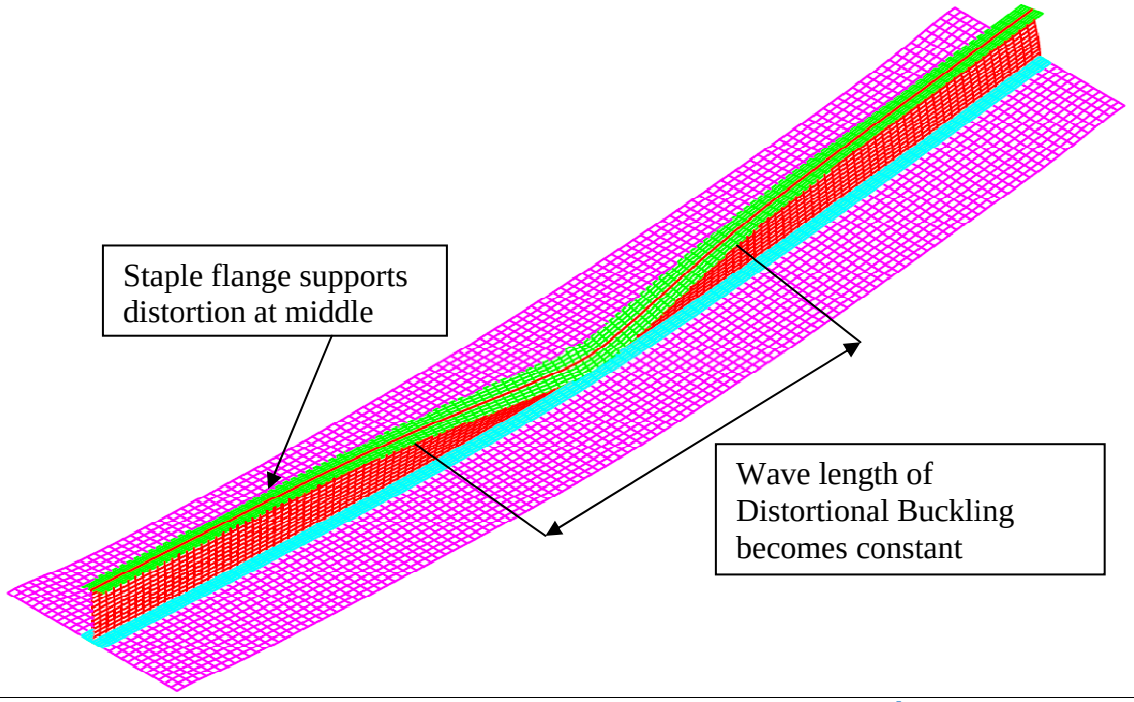

($F_{ys} = 350MPa, F_{yp} = 250MPa, E = 200GPa, \beta_2 = 1.673, \beta_4 = 10.040$ ($\frac{L}{r_f}$=240))

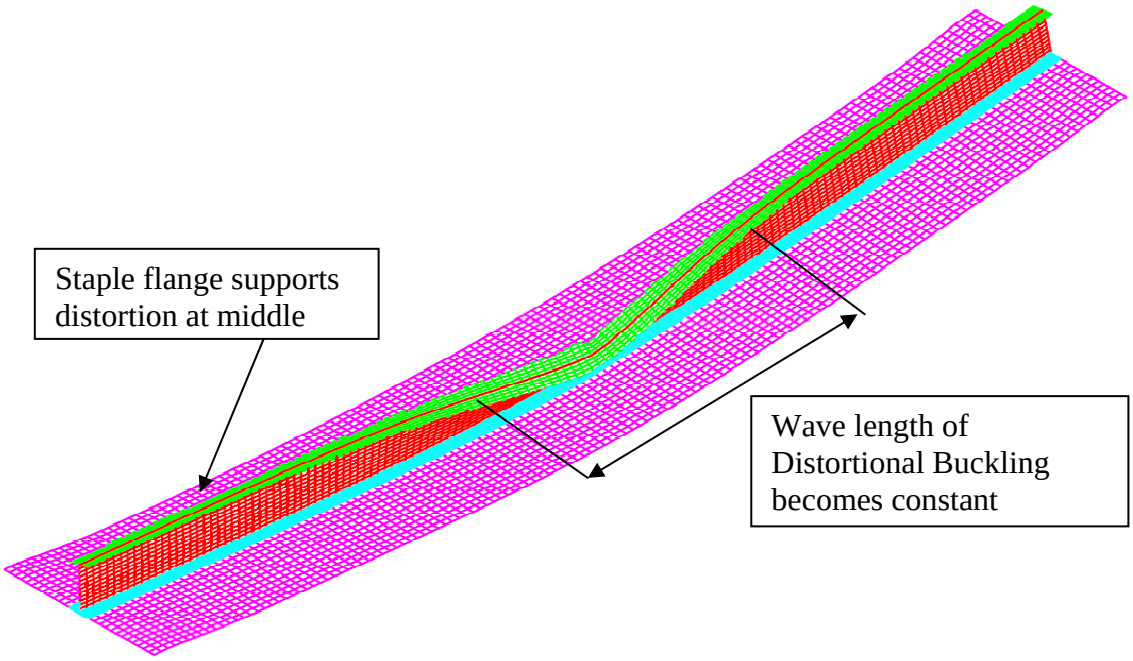

($F_{ys} = 350MPa, F_{yp} = 250MPa, E = 200GPa, \beta_2 = 1.673, \beta_4 = 10.880$ ($\frac{L}{r_f}$=260))

Figure 4.14 Buckling Modes of Stiffened Plate Panels (cont'd)

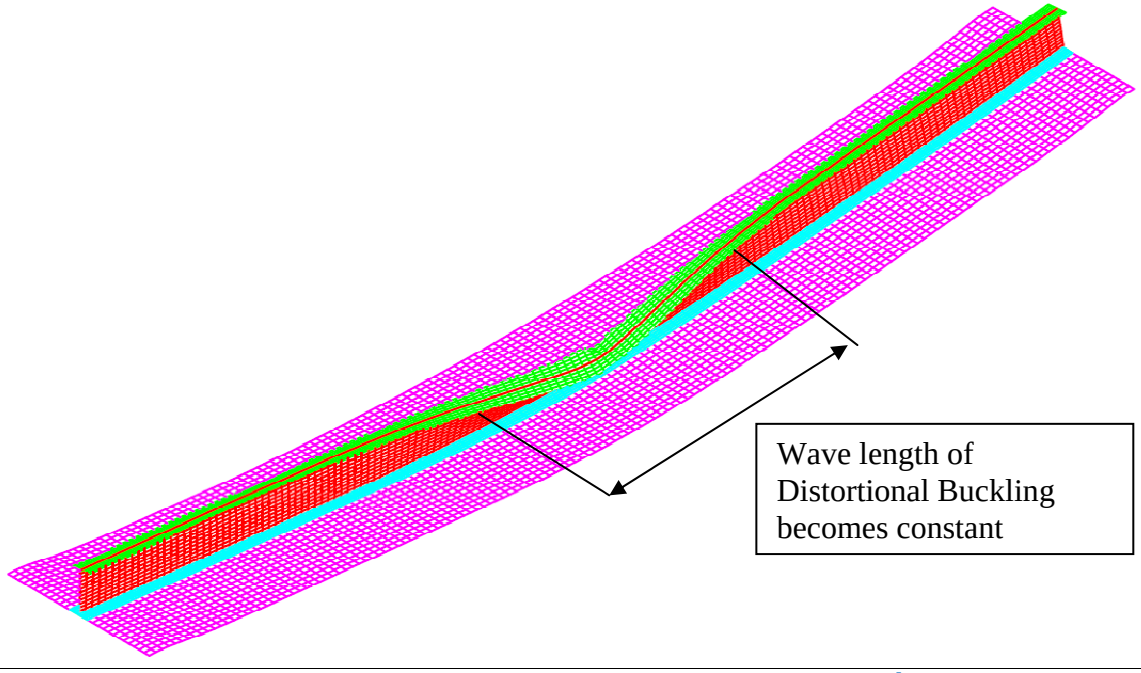

($F_{ys} = 350MPa, F_{yp} = 250MPa, E = 200GPa, \beta_2 = 1.673, \beta_4 = 11.710$ ($\frac{L}{r_f}$=280))

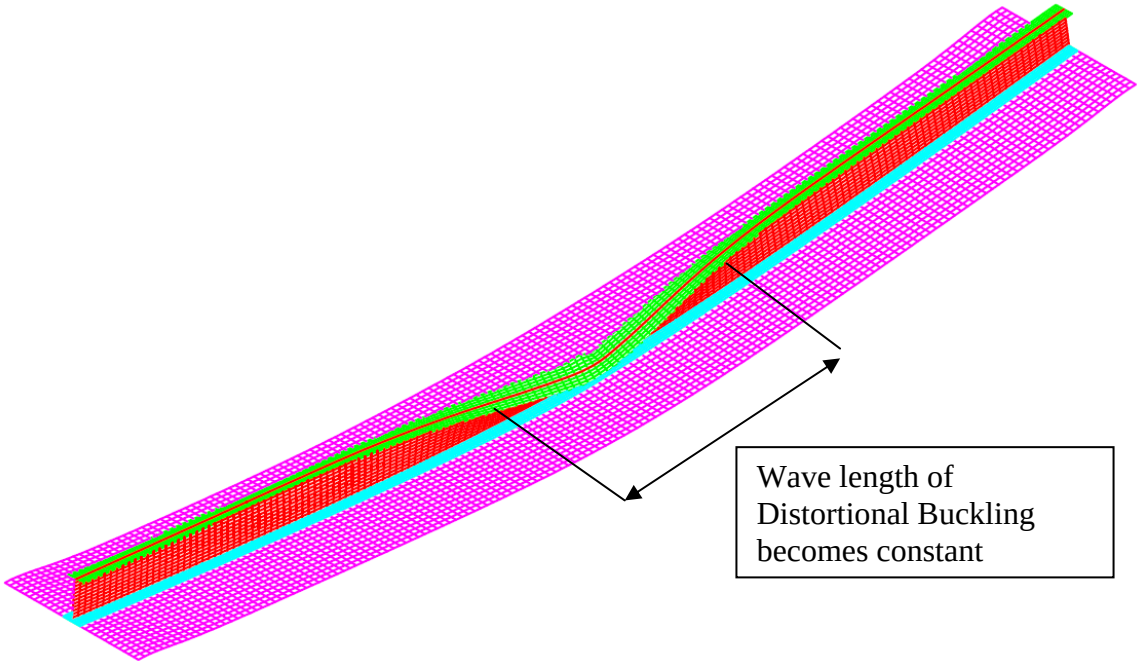

($F_{ys} = 350MPa, F_{yp} = 250MPa, E = 200GPa, \beta_2 = 1.673, \beta_4 = 12.550$ ($\frac{L}{r_f}$=300))

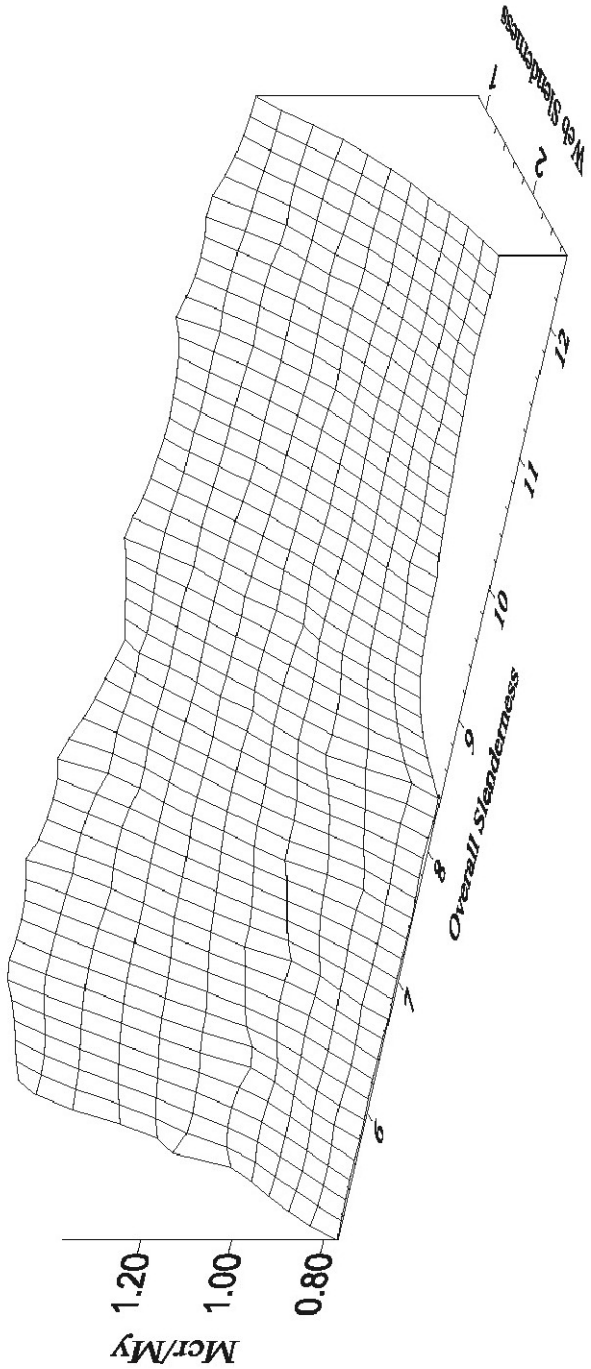

Figure 4.15 Normalized Distortional Moments versus Slenderness

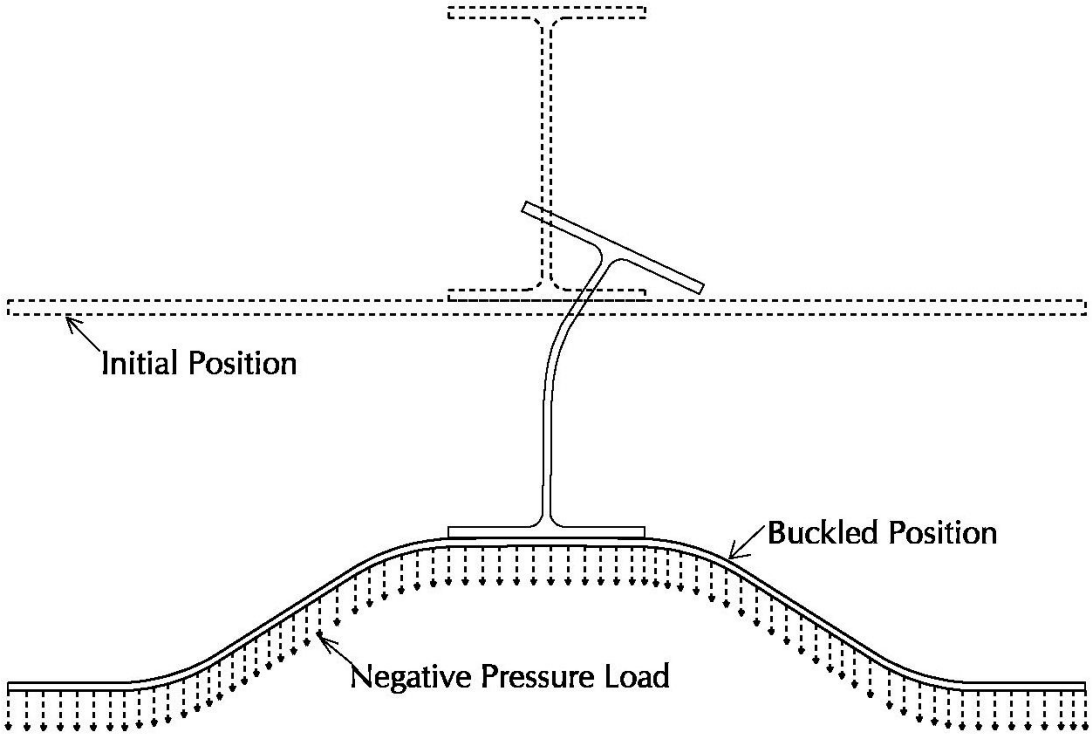

Figure 4.16 Deformed Shape of Stiffened Plate Panel

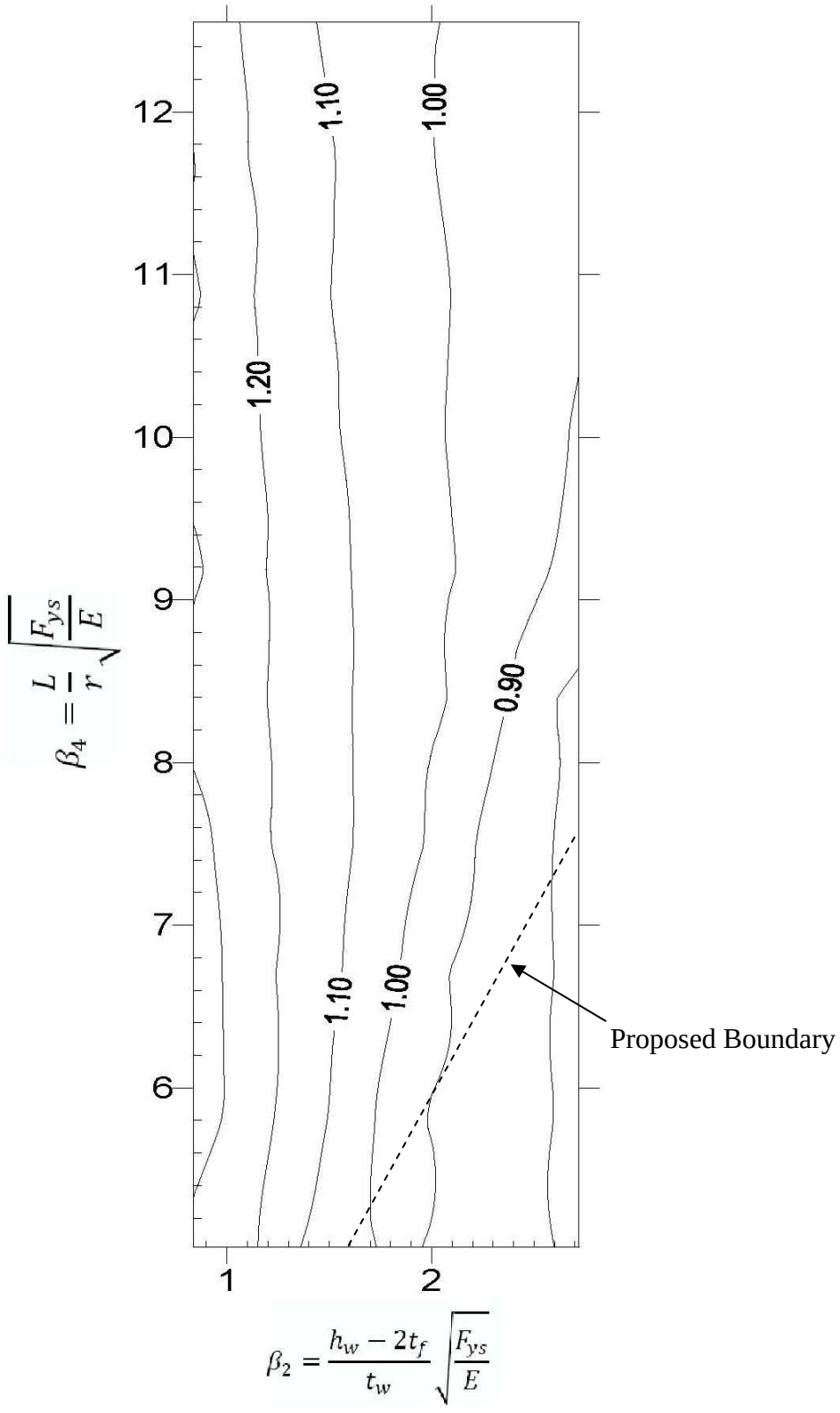

Figure 4.17 Contours of Normalized Distortional Moments versus Slenderness

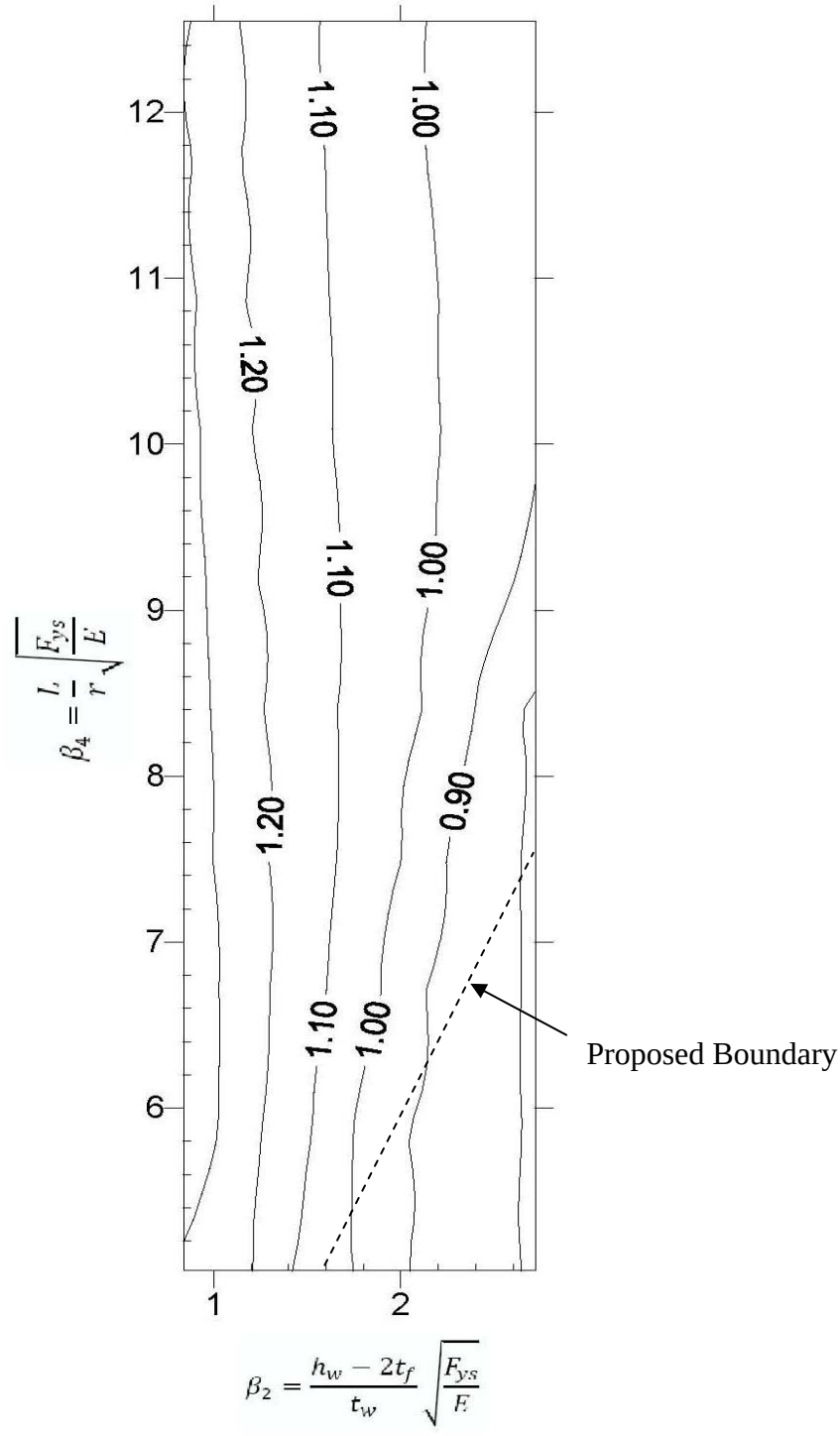

Figure 4.18 Contours of Normalized Ultimate Moments versus Slenderness

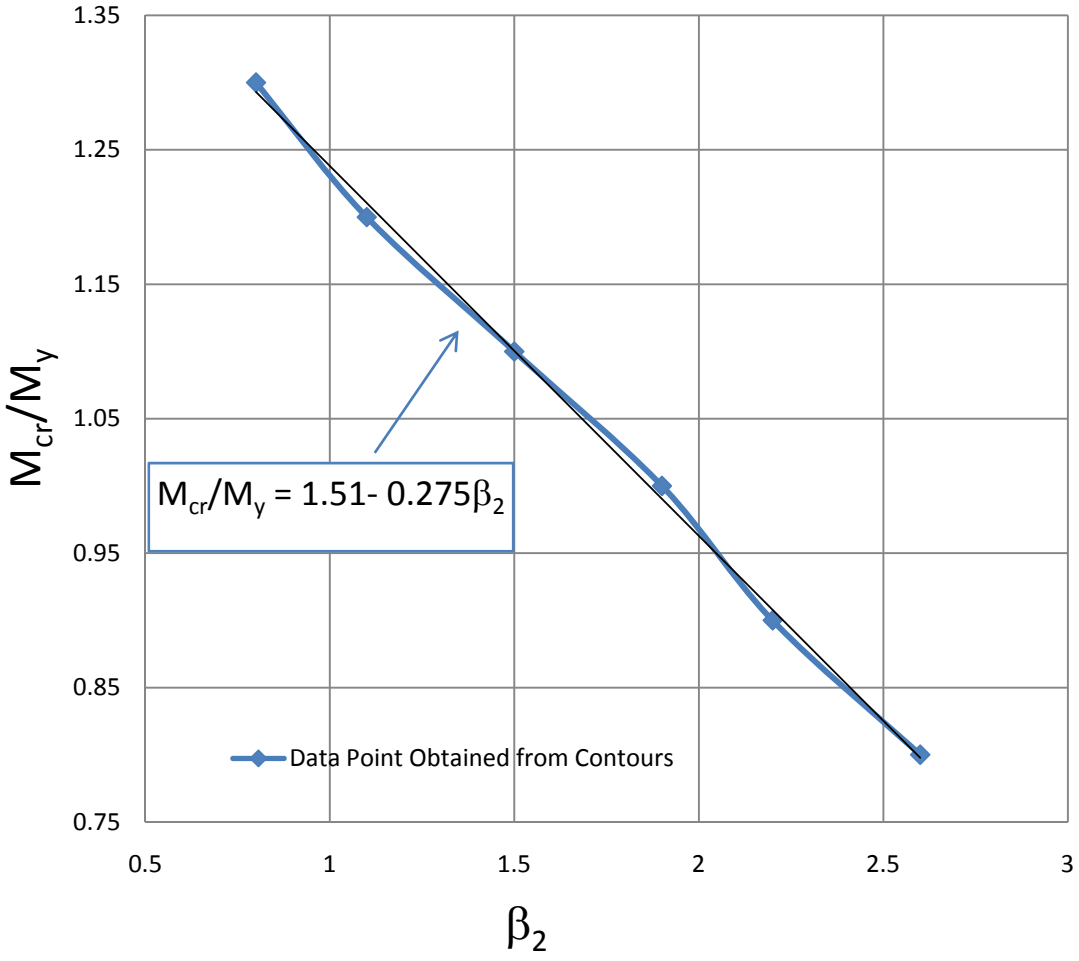

Figure 4.19 Proposed Normalized Moment Capacity

Appendix 4.1 Notations

The following symbols are used in this chapter.

A = Cross sectional area of stiffener

A_f = Area of compression portion of stiffener

b = Width of Plate under compression

b_f = Stiffener flange width

b_p = Width of the plate (stiffener spacing)

E = Young's modulus of steel

F_{cr} = Plate buckling stress

F_{yp} = Yield stress of plate material

F_{ys} = Yield stress of stiffener material

h_w = Stiffener web height

I_s = Second moment of area of stiffener with respect to major axis

I_{sf} = Second moment of area of compression portion with respect to vertical axis

I_{sp} = Second moment of area of stiffened plate panel with respect to neutral axis

L = Stiffener length

M_a = Applied bending moment

M_{cr} = Distortional buckling moment

M_y = Yield moment

M_p = Plastic moment

M_u = Ultimate moment

r = Radius of gyration of compressive portion of stiffener

S_t = Section modulus with respect to top compression flange

t = Thickness of Plate under compression

t_f = Stiffener flange thickness

t_p = Plate thickness

t_w = Stiffener web thickness

y_o = Depth of neutral axis from bottom plate

$\beta = \frac{b}{t}\sqrt{\frac{F_y}{E}}$ = Slenderness of a plate

$\beta_1 = \frac{b_f}{t_f}\sqrt{\frac{F_{ys}}{E}}$ = Stiffener flange flexural slenderness

$\beta_2 = \frac{h_w - 2t_f}{t_w}\sqrt{\frac{F_{ys}}{E}}$ = Stiffener web flexural slenderness

$\beta_3 = \frac{b_p}{t_p}\sqrt{\frac{F_{yp}}{E}}$ = Plate slenderness

$\beta_4 = \frac{L}{r}\sqrt{\frac{F_{ys}}{E}} =$ Slenderness of compressive portion of stiffener

Δ_z= Mid span vertical deflection

Δ_y= Lateral deflection at mid top flange

ν = Poisson's ratio

Appendix 4.2 References

ADINA , 2009, "ADINA 8.5 user manual.", ADINA R & D Inc, Watertown, MA, USA

ASCE, (1995), "The structural Design of Air and Gas Ducts for Power Stations and Industrial Boiler Applications.", Air and Gas Structural Design Committee of the Energy Division of the ASCE, Reston.

AISC ASD, (1989), "Manual of Steel Construction- Allowable Stress Design.", 9th edition, American Institute of Steel Construction ,Chicago.

AISC LRFD, (2005), "Manual of Steel Construction- Load and Resistance Factor Design.", American Institute of Steel Construction, Chicago.

Arasaratnam, P., (2008), "Effect of Flange Holes on Flexural Behaviour of Steel Beams.", PhD Thesis, McMaster University, Hamilton

Bleich, F., (1952), "Buckling Strength of Metal Structures.", New York, McGraw-Hill.

Bradford, M.A., (2000), "Strength of Compact Steel Beams with Partial Restraint.", Journal of Constructional Steel Research, 53, 183-200

Bradford, M.A., (1999), "Elastic Distortional Buckling of Tee-Section Cantilevers.", Thin Walled Structures, 33, 3-17

Bradford, M.A., (1998a), "Inelastic Buckling of I-beams with Continuous Elastic Restrant.", Journal of Constructional Steel Research, 48, 63-77

Bradford, M.A., (1998b), "Distortional Buckling of Elastically Restrained Cantilevers.", Journal of Constructional Steel Research, 47, 3-18

Bradford, M.A., Ge, P., (1997), "Elastic Distortional Buckling of Continuous I-Beams.", Journal of Constructional Steel Research, 41, 249-266

Bradford M.A., Ronagh, H.R., (1997), "Generalized Elastic Buckling of Restrained I-Beams by FEM.", Journal of Structural Engineering, ASCE , 123 (15), 1631-1637

Bradford, M.A., (1992), "Lateral-Distortional Buckling of Steel I-Section Members.", Journal of Constructional Steel Research, 23, 97-116

Bradford, M.A., (1990), "Distortional Buckling Strength of Elastically Restrained Monosymmetric I-beams.", Thin Walled Structures, 9, 339-50

Bradford M.A., (1989), "Buckling Strength of Partially Restrained I-Beams.", Journal of Structural Engineering, ASCE , 115 (5), 1272-1276

Bradford M.A., Trahair, N.S., (1981), "Distortional Buckling of I-Beams.", Journal of Structural Division, ASCE , 107 (2), 355-370

Bruno, M., Chia, M., Andrew, W., (1998), "Ductile Design of Steel Structures.", 1st Edition, McGraw-Hill Book Company Inc., New York, USA.

CSA, (2010), "Handbook of Steel Construction.", Canadian Institute of Steel Construction, Willowadale, Ontario

Galambos, T.V., (1998), "Guide to Stability Design Criteria for Metal Structures.", 5th edition. Wiley, New York.

Grondin, G.Y., Elwi, A.E., Cheng, J.J.R., (1999), "Buckling of Stiffened Steel Plates-a Parametric Study.", Journal of Constructional Steel Research, 50, 151-175

Hancock, G.J., Bradford, M.A., "Trahair, N.S., (1980), Web Distortion and Flexural Torsional Buckling.", Journal of Structural Engineering, ASCE , 106(ST7), 1557-71

Harris, H.G., Sabnis, G., (1999), "Structural Modeling and Experimental Techniques." 2nd edition. CRC Press, New York.

Hughes, O.F., Ghosh, B., Chen, Y., (2004), "Improved Prediction of simultaneous Local and Overall Buckling of Stiffened Panels.", Thin-Walled Structures, 42, 827-856

Hughes, O.F., Ma, M., (1996), "Inelastic Analysis of Panel Collapse by Stiffener Buckling.", Computers and Structutres, 61, 107-117

Kitipornchai, S., Wong-Chung, A.D., (1987), "Inelastic Buckling Welded Monosymmetric I-Beams .", ASCE Journal of Structural Engineering, 113, 740-756

Kitipornchai, S., Trahair, N.S., (1980), "Buckling Properties of Monosymmetric I-Beam.", ASCE Journal of Structural Division, 106, 941-958

Langhaar, H.L., (1951), "Dimensional Analysis and Theory of Models." John Wiley, N.Y

Ma, M., Hughes, O., (1996), "Lateral Distortional Buckling of Monosymmetric I-Beams under Distributed Vertical Load.", Thin-Walled Structures, 26, 123-145

Milner, H.R., (1977), "The Buckling of Equal Flanged Beams Under Uniform Moment Restrained Torsionally by Stiff Brace.", Fifth Australian Conference on the Mechanics of Structures and Materials, Melbourne, 405-420

Paik, J.K., A.K., Kim, B.J., Seo, J.K., (2007), "Methods for Ultimate State Assessment of Ships and Ship Shaped Offshore Structures.", Ocean Engineering, 35, 271-280

Paik, J.K., Thayamballi, A.K., Kim, D.H., (1999), "An Analytical Method for the Ultimate Compressive Strength and Effective Plating of Stiffened Panels.", Journal of Constructional Steel Research, 49, 43-68

Paik, J.K., Thayamballi, A.K., Lee, W.H., (1998), "A Numerical Invetsigation of Tripping.", Marine Structures, 44, 51-56

Samata, A., Kumar, A., (2006), "Distortional Buckling in Monosymmetric I-beams.", Thin Walled Structures, 9, 339-50

Sheikh, I.A., Elwi, A.E., Grondin, G.Y., (2003), "Stiffened Steel Plates under Compression and bending.", Journal of Constructional Steel Research, 59, 911-930

Svensson, S.E. (1985), "Lateral Buckling of Beams Analyzed as Elastically Supported Columns Subjected to varying Axial Force.", Journal of Constructional Steel Research, 5, 179-93

Taylor, A.C., and M. Ojalvo, (1966), "Torsional Restraint of Lateral Buckling.", Journal of the Structural Division, American Society of Civil Engineers, 115-129.

Trahair, N.S., (1969), "Deformation of Geometrically imperfect Beams.", Proceedings of ASCE, Journal of the Structural Division, 95(ST7), 1475-1496.

Timoshenko, S.P., Gere, J.M., (1961), "Theory of Elastic Stability.", 2nd Edition, McGraw Hill, New York

Udall, J.D., (2007), "Effective Design of Stiffener on Industrial Ducts.", Master Thesis, McMaster University, Hamilton

Ugural, A.C, (1998), "Stress in Plates and Shells.", 2nd Edition, McGraw Hill, New York

Valentino, J., and Trahair. N.S., (1998), "Torsional Restraint Against Elastic Lateral Buckling", Journal of Structural Engineering, American Society of Civil Engineering, 124 (10), 1217-1225

Williams, F.W., Jemah, A.K., (1987), "Buckling Curves for Elastically Supported Columns with Axial Force, to Predict Lateral Buckling of Beams.", Journal of Constructional Steel Research, 7, 133-147

Young, W.C., (1989), "Roark's Formulas for Stress & Strain.", 6th edition. New York, McGraw Hill.

Yura, J., (2008), "Global Lateral Buckling of I-Shaped Girder Systems.", Journal of Structural Engineering, 134, 1487-1494

Yura, J.A., (2001), "Fundamentals of Beam Bracing.", Engineering Journal, American Institude of Steel Construction, 38,11-26

Zirakian, T., (2007), "Lateral-distortional Buckling and the Extrapolation Techniques.", Journal of Constructional Steel Research, 64, 1-11

Chapter 5: Shear Capacity of Side Panel of Large Rectangular Industrial Ducts

Abstract

Side panels of a large rectangular industrial duct transfer the gravity loads to the supports by transverse shear and, in addition, carry internal pressure. Currently the design practice of plate panels for shear load is based on the methods used for the web of the plate girders. The behaviour and the characteristics between the web of plate girder and the thin side panels are significantly different. The large aspect ratio of the side panels develops multiple bands of tension fields, whereas the methods for plate girders are based on one tension field. In addition to shear, the side panels are subjected to internal pressure which in turn produces membrane action. Minimal research has been done dealing with industrial duct plate panel subjected to shear load. Therefore, a study was undertaken to review current methods of analysis and design and to propose a comprehensive method of designing industrial duct side panel for shear resistance.

A nonlinear finite element model was developed to simulate the behavior of industrial duct side panel subjected to transverse shear. In order to carry out a parametric study, six scale independent dimensionless parameters that govern the behavior of plate panel were identified. An extensive parametric study was then done. It was concluded that the plate slenderness dominates the normalized shear strength of stockier side panels. The aspect ratio and plate slenderness influence the normalized shear strength of slender side panels. Design equation and aids for estimating the shear strength of industrial duct side panels subjected to shear were proposed.

Keywords: Plate, Shear, Diagonal Tension Field, Finite Element, Dimensional Analysis

5.1 Introduction

Large rectangular industrial duct and its supports are unique structures which require local and global analysis to predict their performance and to verify the safety in preventing catastrophic failure. The paramount importance of the analysis and the design of this unique rectangular duct system for an engineer is to apply available analytical and design tools. The fundamental in this analytical process is the need to verify the strength of every element in the path of transferring all loadings down to supports. The vertical loads such as dead load, weight of insulation, dust load, etc., must be transferred to the side walls (which act as web) and then to the supports. These side walls consist of thin plate panels between parallel stiffeners. The plate panels transfer the loads to the supports by shear. The plate panels of the side walls adjacent to the support legs are subjected to large shear loads. In addition these panels are under internal pressure.

Currently, the plate panels of rectangular ducts for carrying shear loads are designed based on methods used in plate girder web design. The side walls of the large industrial rectangular duct can be considered to be similar to the web of a large fabricated plate girder with transverse stiffeners. The plate girder web design is often based on a combination of both web shear buckling and tension field action between stiffeners (post buckling strength). The web of the plate girders, however, may have relatively thicker plate compared to the side panel of the large rectangular duct. The large aspect ratio of the side panels develops multiple bands of tension fields, whereas the methods for plate girders are based on one tension field. Furthermore, plate girders are not subjected concurrent pressure load. For a thin plate panel, the web shear buckling capacity will be

lower; as a result, the proportion of tension field action will be higher in carrying the shear. There are several theories available to estimate the shear capacity of the girder web. However, it is necessary to examine the applicability of these theories for the side walls of the large rectangular duct and to provide analysis and design guides for such panels. Note that the design of the large industrial duct is not covered by any design standards. Therefore, it is necessary to conduct a detailed study of the behavior and to quantify the capacity of the industrial plate panels subjected to shear load so that relevant design standards may be established. In order to include all the parameters that affect the behavior of the plate panels and to avoid the expenses involved with the experiments, a numerical parametric study based on the finite element model may be done.

In the study described herein, firstly, a nonlinear finite element model for the industrial duct plate panel subjected to uniform shear was developed and validated. Secondly, dimensionless parameters that affect the behavior of the plate panel were identified. Thirdly, an extensive parametric study was done to establish the impact of above parameters on the shear resistance of such plate panels.

5.2 Objectives

The objectives of this part of the study presented in this chapter are to study the behaviour of the industrial duct plate panels subjected to uniform transverse shear and to propose a comprehensive method of estimating their shear capacity. In order to achieve these objectives, a suitable finite element model that includes material and geometric nonlinearities was developed in order to capture the shear buckling and the diagonal tension field action of plate panel when the panels are under uniform pressure load. It is also necessary to do a detailed parametric study. This phase would identify the dimensionless parameters those dominate the behavior of the plate panel subjected to transverse uniform shear. The side plate panels subjected to static loading and under ambient temperature were only considered in this study.

Section 5.3 reviews the available literature on the plates subjected to uniform shear. This review examines the available theories and their applicability for the industrial duct side plate panels. Section 5.4 describes the nonlinear finite element analysis model developed and validated to study the behaviour of the thin plate panels. The current method in design practice is evaluated in Section 5.5. In Section 5.6, the dimensionless parameters are identified in order to conduct the parametric study. The influence of the identified dimensionless parameters on the behavior and strength of the plate panels are investigated in Section 5.7. The conclusions and further recommendations are presented in Section 5.8.

5.3 Literature Review

Analytical and experimental researches on this topic have been conducted for more than last fifty years in order to improve the understandings of the behavior of the plate subjected to shear load. Consider a thin plate panel with width b , height h and thickness t. Such a plate panel when subjected to shear stress τ as shown in Fig 5.1 experiences in-plane tensile and compressive stresses σ. This compressive stress σ is equal to the applied shear stress τ and acts at 45^o to the shear axis. This compressive stress σ can causes buckling of the plate when the applied shear stress τ reaches the shear buckling load τ_{cr}. Therefore, it could be expected that the resulting formulae for critical shear stress τ_{cr} would closely resemble the critical load for the in-plane compression. The critical shear buckling stress τ_{cr} for a long rectangular plate with height h, width b and thickness t, when subjected to uniform shearing stress was provided by Timoshenko and Gere (1961) as follows

$$\tau_{cr} = \frac{k\,\pi^2\,E}{12(1-v^2)\left(\frac{b}{t}\right)^2} \tag{5.1}$$

Where E = elastic modulus , v = Poisson`s ratio and k = shear buckling coefficient. In this derivation, b is the width of short dimension of the long plate. The following formulas can be used to establish approximate values of the k in Equation 5.1 when $\frac{h}{b} > 1$ (Timoshenko and Gere (1961)).

$k = 5.35 + 4\left(\frac{b}{h}\right)^2$ for the simply supported plates (5.2)

$k = 8.98 + 5.6\left(\frac{b}{h}\right)^2$ for the clamped plates (5.3)

It can be seen that the critical buckling stress τ_{cr} is a function of the plate slenderness $\frac{b}{t}$ and the aspect ratio $\frac{b}{h}$ for a plate with given material properties and boundary conditions. Theoretically, the critical buckling stress τ_{cr} can be as high as the shear yield stress τ_y for a perfectly elastic-plastic material. The buckling stress τ_{cr} increases as the plate slenderness $\frac{b}{t}$ decreases. When the plate is stocky, it is considered to fail by yielding in shear equal to the theoretical shear yield stress $\tau_y = \frac{F_y}{\sqrt{3}}$. The limiting plate slenderness $\frac{b}{t}$ for the shear yielding can be obtained by substituting τ_y into Equation 5.1 for the τ_{cr}.

$$\frac{b}{t} = \sqrt{\frac{k\,\pi^2\,E}{12(1-v^2)\tau_y}} \tag{5.4}$$

Therefore, the plates will yield first before it buckles if the plate slenderness $\frac{b}{t}$ is less than the limiting plate slenderness given in Equation 5.4. Substituting Poisson's ratio $v = 0.3$ and $\tau_y = \frac{F_y}{\sqrt{3}}$, the Equation 5.4 becomes:

$$\frac{b}{t} = \sqrt{\frac{k\,\pi^2\,E}{12(1-0.3^2)\frac{F_y}{\sqrt{3}}}} \approx 1.25\sqrt{\frac{Ek}{F_y}} \tag{5.5}$$

The limiting $\frac{b}{t}$ for a simply supported plate with material properties of elastic modulus $E = 200{,}000$ MPa and yield strength of $F_y = 350$ MPa and with the aspect ratio $\frac{b}{h} = 1$ will be 90. However, for the plate of a side wall of large industrial duct, the ratio of the stiffener spacing to the plate thickness $\frac{b}{t}$ will be much higher than this value. In actual large rectangular duct, the plate slenderness $\frac{b}{t}$ may be in the range of 125 to 350. The applied shear stress will cause elastic buckling for these slender plates. However, beyond buckling, the plate has the capacity to carry additional shear load because stable tensile stresses may be generated in diagonal direction. Therefore, the plate can carry additional shear load until yielding occurs in the plate. This is referred to as tension-field action. Even though, the tension field action in a web carrying shear was identified by Wagnar (1939), Basler (1961) first introduced this tension field theory for civil engineering applications.

Based on the extensive studies on the post buckling behavior of the web panels by Basler (1961), AISC (1963) first included the post buckling strength in addition to elastic buckling shear capacity in its specification. In Basler (1961) tension field idealization of the post buckling contribution to the strength, the flanges were assumed to provide no

anchorage to the tension field. In later stages of Basler's derivation (1963), the web of the plate girders bounded by flanges and by the transverse stiffeners on each side was assumed to be capable of carrying load in excess of buckling load. In the latest approach used by Basler (1963), equilibrium of section taken vertically midway between two adjacent stiffeners and horizontally at mid-depth was considered (See Figure 5.2). The additional post buckling strength V_{tf} was given as follows:

$$V_{tf} = \frac{F_y h t (1 - C_v)}{2\sqrt{1 + \left(\frac{b}{h}\right)^2}} \tag{5.6}$$

Where $C_v = \frac{\tau_{cr}}{F_y/\sqrt{3}} =$ web shear coefficient. The angle of the tension field providing maximum vertical shear component from the tension field was given by:

$$\tan(2\theta) = \frac{h}{b} \tag{5.7}$$

Therefore, the tension field contribution to the shear strength is based on uniform yielding throughout the web panel. The shear strength of web panel in the current AISC (2005) is based on this Basler's model. The ultimate shear strength for the slender web panel in the current AISC (2005) is given by:

$$V_u = 0.6F_y ht\left[C_v + \frac{(1 - C_v)}{1.15\sqrt{1 + \left(\frac{b}{h}\right)^2}}\right] \tag{5.8}$$

The first term in the bracket represents the relative contribution of the buckling strength V_{cr}. The second term in the bracket represents the increase of the plate shear strength due to the diagonal tension field action. Equation 5.8 is the same fundamental form for the ultimate shear strength of the slender web panel in the current CSA (2010).

Numerous models for the diagonal tension contribution have been developed. Another model developed by Porter et al. (1975) was adopted in the British standards. In this model, a similar tension field was assumed for only limited portion of the web. However, the flanges were assumed to contribute to the post buckling strength by absorbing normal stresses from tension field. As a result, girder collapses when plastic hinge is formed in the flanges. However, both models assume that the compressive stresses that developed perpendicular to the diagonal tension field do not increase after the elastic buckling.

In current design practice in heavy industries, the side wall of the duct is assumed to be the web of the large fabricated girder. The panel stiffeners are serving as the girder web stiffeners. The current methods in AISC (2005) and CSA (2010), which are based on Basler's model (1963), is then used to design the plate panels of the side wall for shear

resistance. In this model, the tension field contribution to the shear strength as per Equation 5.8 is based on uniform yielding throughout the web panel.

In large industrial rectangular ducts, the width of the plate b between the stiffeners is smaller compared with the length of the plate h. The plate panel under consideration is a long rectangular plate with the aspect ratio $\frac{h}{b}$ higher than 2. The diagonal tension field depends on the wave length and other details of buckled shape. The wave length and the buckled shape will depend on the aspect ratio and the boundary conditions. In the case of plate with higher aspect ratio $\frac{h}{b}$ and simply supported boundary condition, the buckled shape is illustrated in Figure 5.3 (Bruhn 1973). This buckled shape consists of a half wave in the transverse direction (b) and a series of half waves in the longitudinal direction (h). The long plate subjected to uniform shear will develop internal compressive stresses on the plane 45^o with the edge and thus these compressive stresses cause buckling pattern at an angle to the plate edges as shown in Figure 5.3(a). The buckled pattern has a half wave length of $1.25b$ (Bruhn 1965). As the shear load increases, the long plate buckles between the stiffeners in above manner with the remaining load being resisted by the tension field action. For this buckled shape, the long plate subjected to uniform shear develops several bands of tension fields across the length of the plate as illustrated in Figure 5.3(b). In contrast, the current AISC (2005) method based on Basler (1963) model represents only one band of uniform tension field across the web between stiffeners. This raises the concern of the applicability of the current

AISC (2005) or CSA (2010) methods to the plate panel of side wall of the duct when designing for shear load.

In the derivation of the second term of Equation 5.8 by Basler (1963), the contribution of tension field action was limited by the failure state of the plate element subjected to shear τ in combination with the inclined tension σ_t . The actual state of stresses considered in this derivation was only the shear τ_{cr} and the inclined tension σ_t as shown in Figure 5.4. There are two assumptions involved in determining this inclined tension σ_t. The τ_{cr} was assumed to be constant from buckling load to post buckling strength and therefore the inclined tension σ_t acts in addition to the principal stresses τ_{cr}. Also, the angle θ , the inclination of the tension σ_t , was conservatively taken as 45^o . At this state of stress, the principal stresses are $(\tau_{cr} + \sigma_t)$ and $(-\tau_{cr})$. Then, the von-Mises yield criterion was used to determine the inclined tension σ_t when a yield zone develops. The vertical component of this inclined tension σ_t contributed to the post buckling strength V_{tf}.

The contribution of buckling shear depends mainly on the plate slenderness $\frac{b}{t}$. The plate slenderness $\frac{b}{t}$ of side panels of large industrial ducts are very high (in the range of 125 to 350). Therefore, the relative contribution of buckling shear will be minimal.

In large industrial duct, the plate panel between stiffeners is subjected to lateral pressure load in addition to the shear loads. The current industrial practice of designing the plate, thus the spacing the stiffeners, is based on large deflection plate theory. The plate

between stiffeners can be assumed as one way bending of a long plate subjected to lateral pressure load because the typical aspect ratio $\frac{h}{b}$ for a plate panel of industrial duct is more than 2. As explained in Chapter 2, a strip of the long plate that is perpendicular to the stiffeners and restrained by the stiffeners, when analyzed with large deflection plate bending theory, produces the bending stresses σ_b and the diaphragm stresses σ_m perpendicular to the stiffener direction. The second term in the brackets of Equation of 5.8, the contribution of the tension field action, does not account for these bending stresses σ_b and diaphragm stresses σ_m in its derivation. Lee and Yoo (1998) suggested that the Basler's model does not consider bending stresses of the web developed perpendicular to the tension line of web due to out of plane deflections of web panels. However, the bending stresses vary across thickness of the plate. i.e, while one side is tension, the other side is in compression. Therefore, the effect on the effective tension field due to bending stresses will be minimal. White et al. (2008) noted the flaws in the Lee and Yoo's suggestion.

However, the uniform diaphragm stress σ_m which is perpendicular to the stiffener direction and in the plane of the plate will affect the diagonal tension field. Basler's model can be extended to include the effect of diaphragm σ_m. The state of the stresses at shear buckling is shown in Figure 5.5. Before the shear buckling occurs, the state of the stresses contains the applied shear τ, horizontal diaphragm stress σ_m and the transverse stress $v\sigma_m$. The application of Mohr's circle for this state of the stresses is shown in Figure 5.5(b). It can be noted that the horizontal diaphragm stress σ_m and the transverse stress $v\sigma_m$ change the principal stresses and the principal plane. σ_1 and σ_2 represent the

tensile and the compressive principal stresses. Compared to the Mohr's circle of pure shear (Figure 5.5(a)), the introduction of diaphragm σ_m stress lowers the compressive principal stress σ_2 and the inclination of the principal plane associated with the principal stress σ_2 becomes less than 45^o. Therefore, the applied shear τ should be increased to τ'_{cr} in order raise the σ_2 to the buckling shear stress τ_{cr}. From the above facts, it is obvious that the diaphragm stress σ_m increases the contribution of buckling shear V_{cr} to the ultimate shear strength V_u. After the web has buckled, the bands of inclined tensile forces from the tension field action develop. The equilibrium is maintained between these applied shear force, the bands of tensile forces and the compressive forces (σ_2) at buckling. As the load increases, the angle of the bands of tension forces changes to accommodate the greatest carrying capacity. At the ultimate state, the angle of the bands of the tension forces θ for a long plate is unknown. The current method for shear capacity of web girder (Basler's method) does not include the effects of the diaphragm stress σ_m and is based on one complete tensile band between the stiffeners.

The Basler's work (1963) and Porter's work (1975) have been widely accepted and have formed the basis for estimating the shear capacity of the web of the plate girder in North American and European standards, respectively. Both models assumed that the web panel was simply supported at the edges. The actual boundary condition in the web of plate girder will most likely be intermediate between simply supported and clamped condition. Kuhn et al. (1952) proposed a correction factor based on their test data of thin web with different vertical structural angle stiffeners. This correction factor was applied to the buckling coefficient k of the simply supported boundary condition. The correction factor

was function of the aspect ratio of the plate and the relative thickness of the plate and the leg of the angle stiffeners. Lee et al. (1996) studied the influence of the end restraint of the web plate between the stiffeners using finite element models. Two equations were proposed by them to be used to determine the shear buckling coefficient for plate girder web. These equations addressed the fixity of boundary between the flange and the web, based on the relative thickness of the web and the flange.

It is recognized that the frame action of flanges also contributes to the shear resistance of transversely stiffened large plate girders (White et al. 2008). The model from Porter's work (1975) highlights the contribution of the frame action of flanges. Large plate girders with heavy flanges develop larger shear strengths as the girder flanges, in addition to transverse stiffeners, also provides substantial anchorage to the tension field developed (White et al. 2008). The anchorage provided by heavy flanges for one tension field developed in large plate girders will be significant. The multiple tension fields developed along the duct side plate panel will be mostly anchored by the stiffeners. The vertical components of the tension fields in industrial ducts are transferred at the stiffeners. The wide flange stiffeners have enough capacity to carry the necessary compressive forces. Therefore, there will be minimal effect by the stiffeners on the shear capacity of side plate panel.

To date, the shear capacity of the plate panel of large rectangular industrial duct is based on the numerous researches on the behavior of the web panel of the large plate girder. Also there are no codified design guidelines for the design of elements of the large

industrial rectangular duct. Considering the cost associated with large scale experiments, a parametric study became necessary.

5.4 Finite Element Model

Most of the researchers, Lee et al. (1995, 1998, 2002, 2003, 2008, 2009), Yoo et al. (2006), White et al.(2008), Marsh et al. (1998), Shanmugam et al.(2003) and Alinia et al.(2009, 2011), successfully carried out finite element analysis on the buckling behavior of the plate girder web panel with the transverse stiffeners. The review of these research studies indicated that the finite element method is able to accurately predict the behavior and the ultimate strength of the plate panel. To the author's knowledge, no finite element study has been attempted for shear resistance of a plate panel of the large rectangular duct. Furthermore, the limited number of experiments does not cover all the practical cases. Therefore, a finite element based parametric study is necessary to study the behavior of the industrial duct plate panel with all possible parameters. In this section, a nonlinear finite element model to capture the shear buckling and the diagonal tension field action of a long rectangular plate subjected uniform shear was developed. The finite element model will be validated with available theoretical results.

A schematic of duct side panel selected for the parametric study presented in Section 5.7 is shown Figure 5.6. The duct side panel consists of a plate panel bounded by two adjacent stiffeners and the corner angles at its top and bottom. Typical angle L76X76X7.9 (3X3X5/16) and stiffener W200x27 (W8X18) were selected for this study.

To simulate the behaviour of the plate panel with shear, the finite element model was developed using a commercial general purpose nonlinear finite element program ADINA(2009). It has an extensive element library, material models and modeling capabilities of any nonlinear problem. As the shear load increases on the plate panel, initially the shear buckling creates local instability, then the diagonal tension field develops at an angle, which is considered to be optimum, and the equilibrium path goes beyond the ultimate capacity. These nonlinear changes require the finite element model to be able to trace the equilibrium path beyond the shear buckling state up to and beyond the ultimate state. Therefore, the solution should be obtained incrementally. To reach the convergence of the equilibrium of the nonlinear load-displacement path, a displacement control analysis method was used. For each increment of displacement, the solution process needs an iterative process to obtain the equilibrium load vector. The arc length iterative method used for these analyses was able to reach the convergence throughout the nonlinear equilibrium path.

In order to capture the out-of-plane movement due to instabilities and the nonlinear equilibrium path, a 4-node shall element from ADINA element library was used to model the entire plate panel. The 4-node shell element is based on updated Lagrangian formulation (Bathe 1996). The nodal coordinates are updated to reflect the current position in space and all the shape functions and derivatives are updated based on current updated coordinates. Also, this element can be used for large displacement and small strain problems. Each node has six degrees of freedom: three translations and three rotations. The 4-node shell element can be used to model for both thick and thin shell

problems that require the Mindlin plate theory to describe their behaviour. The available maximum of seven integration points through thickness were used for this analysis in order to capture the stress variation across the thickness, and thus to ensure accurate initiation and development of tension field across the plate.

5.4.1 Initial Geometric Imperfection

Geometric imperfections such as out-of-flatness of the plate and camber or sweep of structural members exist in their unloaded condition. The behavior of plate panel subjected to in plane forces is affected by initial out-of-flatness. In finite element analysis, the perfectly flat plate will not make buckling response as its in-plane stiffness is high. Therefore, some form of disturbance should be introduced on a perfectly flat plate in order to evoke the buckling response. In this finite element analysis, the initial geometric imperfection was introduced to the plate panel. The magnitude and shape of initial geometric imperfection play a significant role in response behavior. Generally the initial geometric imperfection is either similar to that of buckling mode shape or shape of existing out of flatness measured on the plate panel. The shape of the buckling mode is generally assumed because it gives lower bound even after collapse.

A long rectangular plate subjected to pure shear buckled in a pattern as illustrated in Figure 5.3(a). Incorporating this buckling pattern into the finite element models was not practical. A pattern consisting of a half sine wave in transverse direction and a series of half waves in the longitudinal direction was introduced in order to initiate the buckling.

Therefore, a double sine function is used to represent the out of flatness of the plate panel. The double sine function is as follows:

$$\Delta_{imp} = \Delta_o \sin\left(\pi\frac{x}{b}\right)\left(\pi\frac{y}{b}\right) \tag{5.9}$$

Where Δ_{imp}= initial geometric imperfection distribution, Δ_o= maximum amplitude of the initial geometric imperfection, b = width of the plate panel, h = height of the plate panel, x = coordinate in the transverse direction of the plate panel and y = coordinate in the longitudinal direction of the plate panel. The maximum permissible variation of out of flatness of a steel plate for fabrication related initial imperfections was given in Paik et al. (2003) as follows:

$$\frac{\Delta_o}{t} = 0.025\left(\left(\frac{b}{t}\right)\sqrt{\frac{F_y}{E}}\right)^2 \tag{5.10}$$

$$\frac{\Delta_o}{t} = 0.005\left(\frac{b}{t}\right) \tag{5.11}$$

Equation 5.10 gives better representation of the plate characteristics. Equation 5.11 is a function of plate width b only. The use of latter does not represent the slenderness of the plate. Therefore, the present study used the maximum values of imperfection given by Equation 5.10.

In a large industrial duct, the deflected shape of the plate panel subjected to transverse pressure load should be incorporated as the plate panel considered is subjected to in plane shear and transverse pressure load as well at the ultimate states. The deflected shape of the long plate panel due to transverse pressure can be assumed to be cylindrical. The relation between the plate slenderness $\frac{b}{t}\sqrt{\frac{F_y}{E}}$ and the normalized deflection $\frac{\Delta}{t}$,when the top fibre yields due to lateral pressure, was established in Chapter 2. Therefore, the pattern of initial geometric imperfection assumed for this study was the summation of the cylindrical deformation due to lateral pressure and the double sine function of out of flatness. This pattern was then mapped onto the finite element mesh in order to model accurately the plate panel. The initial geometric imperfection pattern used for this study is depicted in Figure 5.7.

5.4.2 Material Model

The coupon test gives the relationship between stress and strain, covering elastic, yielding, ultimate and necking states. However, often the current industrial practice for the ultimate limit state of the structural members uses idealized material model. The Idealized elastic-plastic-strain hardening tri-linear material model representing mild carbon steel was used to model the material constitutive behavior of the plate panel. The yield strength of 250MPa (F_y) and modulus of elasticity of 200000MPa (E) were used to define the material of the plate panel. This represents the most common structural steel for plates, ASTM A36. The strain and the stress values are listed in Figure 5.8. In order to describe the various features of steel, the strain values are presented in terms of

characteristic stresses in Figure 5.8. The nominal strain at yield, ε_y, is $\frac{F_y}{E}$ or 0.00125 for A36 steel. The strain hardening can be anticipated at a strain of around 10 times the ε_y. A constant proportionality is also presumed in the strain hardening range. The accepted strain hardening modulus E_{st} for mild carbon steels is $\frac{E}{30}$. The minimum tensile strength, F_u, for A36 steel is 400MPa. The plate, stiffener sections and corner angles are assumed to be made by A36 steel for this study.

The material models in ADINA (2009) are based on incremental theories in which the total strain increment is decomposed into an elastic strain increment and a plastic strain increment. An incremental plasticity model is formulated in terms of yield surface, flow rule and a hardening rule. The von Mises yield surface is used to specify the state of stresses corresponding to start of plastic flow. The von Mises yield surface assumes that yielding metal has the form of a cylinder in three dimensional principal stress space. The von Mises criterion uses the associated flow rule for the development of plastics stress-strain relations of metals. The associated flow is the plastic flow developed along the direction normal to yield surfaces. A hardening rule specifies the yield surface during plastic flow. In this study, the isotropic hardening rule was selected. In the isotropic hardening rule, the size of the yield surface changes uniformly in all directions as plastic straining occurs. The isotropic hardening rule is more suitable for a static nonlinear analysis of this plate panel subjected to shear.

5.4.3 Loading and Boundary Conditions

It is very important that the boundaries must be incorporated realistically in numerical simulation. The boundary conditions of a plate in large rectangular duct may be taken as restrained against rotation and restrained against pulling in along longitudinal direction (edges with stiffeners). As discussed in Chapter 2, the plate between stiffeners is designed based on bending of large deflection plate theory. Such a plate design is governed by transient pressure. These boundary conditions are reasonable as the plate is welded to thick flange of stiffener and symmetrical uniform transient pressure load prevents any relative rotation of plate panel with respect the flange edge.

However, the rotational stiffness of the longer edges of the plate panel depends on the rotational stiffness of the flange of the stiffener connected to the plate. Therefore, the edge boundary condition of plate panel at its ultimate shear capacity can be expected to be between fixed and simple. In order to represent the rotation stiffeners of the flange of practical stiffeners, typical stiffener W200X27 (W8X18) was modeled on along the both longer edges of the plate panel for this study. The opposite transverse edges were not restrained against the rotation along the transverse direction.

In large industrial duct, side plate panels, adjacent to the support stiffener ring transfer large amount of shear. During the ultimate state, the horizontal components of tension fields could not be anchored by the adjacent side panel that is outside of support rings as one support ring in industrial duct is allowed to slide toward the duct longitudinal axis. Also the panel on outside of the support has lesser shear load, thus no tension field to

anchor the horizontal components. Therefore, the translations of longer edges along the transverse direction are not restrained. In addition, this translation of longer edges will be uniform as the plate is continuous on either side of the side panel considered.

In order to simulate plate panel between the stiffeners, the following boundary conditions were incorporated into the model. Figure 5.9 shows the geometry of the plate panel, the loadings applied and the boundary conditions considered. The $x-y$ plane coincides with the middle plane of the plate panel. The z-axis is perpendicular to the plate and originating from the centre of the plate panel. In this figure, u_1, u_2, and u_3 are the translations along the x, y, and z directions, respectively and θ_1, θ_2, and θ_3 are the rotations about the x, y, and z directions, respectively. The edges of the plate panel are labeled L_1, L_2, L_3 and L_4 the four corners of the plate panel are marked as P_1, P_2, P_3 and P_4 as shown in Figure 5.9. In order to provide the rotational stiffness along the plate and flange juncture, the rotation about the y direction and the translation along the z direction were restrained along the edges L_1 and L_3. In order to simulate the uniform translation of longer edges due to continuous plate, the translation along the x direction were constrained to be the same along the edges L_1 and L_3. The translation in z direction was restrained along the all edges. The translation along x direction was restrained at the point P_1 while the translation along x and y directions were restrained at the point P_2 to avoid any rigid body rotation. The boundary conditions are indicated in Figure 5.9. To simulate shear loading, uniformly distributed line loads are applied along plate edges as shown in Figure 5.9.

5.4.4 Validation of Modeling Techniques

To determine how accurately the proposed modeling techniques applied to a nonlinear finite element model are able predict the behavior of plate panel subjected to shear, the modeling techniques will be applied to a square plate in this portion of the study. Then, the results of the analysis are compared to theoretical results of the square plate subjected to uniform shear.

Before the validation study is done, a convergence study is usually carried out to determine the best size of finite element mesh. Therefore, a convergence study was performed. In this convergence study, one meter length of square plate with different mesh density was subjected to a uniform shear load.

The geometry, the loadings and the boundary conditions for the model are as shown in Figure 5.11. The dimension of the plate are: b $= 1000mm$, $h = 1000mm$ and $t = 5mm$. The plate is subjected to uniform shear load. The plate material is assumed to be the material model descried in Section 5.4.2. The initial geometric imperfection imposed to the model was only the shape of the buckling mode as described in Section 5.4.1, with the amplitude of initial imperfection calculated as per Equation 5.10. The amplitude of double sine function of out of flatness of the plate is 6.25mm.

The analysis includes 5 identical plate models with different mesh densities. The density of the coarse mesh is 5x5, while the density of the finer mesh is 26x26. The ultimate strength for corresponding mesh densities are tabulated in Table 5.1. The percentage

changes in ultimate strength of each model were compared and included in the Table 5.1 as the mesh was being refined. The percentage change in ultimate strength between mesh density of 1 to 2, 2 to 3, 3 to 4 and 4 to 5 were 7.4%, 3.0%, 2.2% and 1.1%, respectively. It can be noted here that a reasonable degree of accuracy can be attained with coarser mesh density. In general, the percentage change less than 5 % may be considered acceptable. Therefore, mesh density 2, 3, 4 and 5 may be acceptable. However, due to the severe nature of the material and geometric nonlinearities involved the plate panel subjected to shear, a very dense mesh of shell elements was desirable in order to trace the nonlinear equilibrium path into the unloading regime. Thus, mesh density 3 was selected as the most suitable mesh and this mesh density was used for rest of the studies presented in this chapter. In Physical dimensions, each element size is approximately 62.5 mm x 62.5 mm.

The finite element model developed for the convergence study was used for the comparison of theoretical buckling strength with results of analysis. The square plate with $b = 1000mm$, $h = 1000mm$ and $t = 5mm$ was subjected to uniform shear load. The mesh density was 16x16. The material model and the boundary conditions were same as in the convergence study. The theoretical buckling load calculated for the plate from Equation 5.1 and 5.2 was 211kN.

The applied shear and the out of plane deflection at the middle of the plate were obtained from the results of the analysis for each time step. The graph of the applied shear versus the out of plane deflection was plotted as shown in Figure 5.11. It is difficult to

distinguish between the pre buckling and post-buckling response paths of an imperfect plate subjected to uniform shear. However various techniques have been developed in order to obtain buckling load from experimental and numerical results. In one of those techniques, two tangent lines are drawn from two points where the slope changes with maximum rate and the intersection of the two tangents gives the buckling load. The buckling load obtained from Figure 5.11 was around 210kN which was in very close agreement to the theoretical results. From the above comparison, it can be concluded the finite element modeling techniques applied to simulate the plate panel subjected to shear load will predict an accurate buckling behavior.

5.5 An Evaluation of Current Method

Before a parametric study on side plate panel subjected shear was carried out, an example calculation was done to compare the results from the method in current design practice and the nonlinear finite element model. The intent of this comparison was to evaluate the method in current design practice and demonstrate the inconsistency of the current design method for the side panel of large ducts. The current design practice in heavy industries uses the method based on plate girder web design. This calculation uses the provisions in AISC (2005) for the design of web of large plate girders. This method accounts the enhanced strength of webs of built-up plate girders due to tension field action.

The following design parameters were used for this comparison:

Width of plate panel	$b = 1000\ mm$
Height of plate panel	$h = 4000\ mm$
Thickness of plate	$t = 5\ mm$
Modulus of elasticity	$E = 200\ GPa$
Yield stress of plate material	$F_y = 250\ MPa$

The actual panel aspect ratio:

$$\frac{b}{h} = 0.25$$

Hence, the panel plate buckling coefficient given by AISC-05 Section G2.1(b) (ii):

$$k_v = 5 + \frac{5}{\left(\frac{b}{h}\right)^2} = 85$$

When the panel depth to thickness ratio is greater than the limiting ratio;

$$\frac{h}{t} = 800 \; > \; 1.10\left(k_v \frac{E}{F_y}\right)^{0.5} = 69.6$$

The nominal shear capacity is then given by Equation ASIC-05 G3.2.

Therefore, the shear coefficient C_v is:

$$C_v = 1.51\frac{k_v \frac{E}{F_y}}{\left(\frac{h}{t}\right)^2} = 0.16$$

The normalized nominal ultimate shear capacity as given by Equation AISC-05 G3.2 is:

$$\frac{V_u}{0.6F_y ht} = \left(C_v + \frac{(1 - C_v)}{1.15\left(1 + \left(\frac{b}{h}\right)^2\right)^{0.5}}\right) = 0.9$$

As noted earlier in Section 5.3, the slender plate panels have less contribution from shear buckling (C_v) compared with the contribution of tension field action.

In order to compare this current design practice with the nonlinear finite element model developed in Section 5.4, a test run was done for the design parameters mentioned above. The result of normalized ultimate shear capacity obtained from the test run was 0.63. The current method estimates around 42% greater than the strength predicted by the finite element model.

A close observation of this Equation 5.8 raises the concern on the applicability of this for large rectangular industrial duct. Equation 5.8 is a more fundamental form of design guide line in AISC (2005) and CSA (2010) to establish the shear strength of web or plate (between stiffeners) with large depth to thickness ratio $\frac{h}{t}$. The total ultimate shear capacity V_u will be additive of the web shear buckling V_{cr} and tension field action V_{tf} represented by the first and second term of Equation 5.8, respectively. The contribution of the web shear buckling V_{cr} (C_v) is minimal for a plate with large slenderness. Therefore, the larger contribution to the estimated shear capacity of the side panel of large rectangular ducts comes from the second term referred to the tension field action V_{tf}. The second term in the bracket of Equation 5.8 is

$$\frac{V_{tf}}{0.6F_y ht} = \frac{(1 - C_v)}{1.15\sqrt{1 + \left(\frac{b}{h}\right)^2}}$$

The aspect ratio $\frac{h}{b}$ of the side panels of large rectangular ducts are generally in the range of 2 to 10 ($\frac{b}{h} \ll$).

For the smaller $\frac{b}{h}$ ratio of the side panels,

$$\sqrt{1 + \left(\frac{b}{h}\right)^2} \approx 1$$

Therefore, the second term referred to the tension field action V_{tf} becomes approximately:

$$\frac{V_{tf}}{0.6F_y ht} \approx \frac{(1 - C_v)}{1.15}$$

Taking the minimal contribution of C_v of the side panels of large industrial duct, the total normalized ultimate shear V_u approximately becomes:

$$\frac{V_u}{0.6F_y ht} \approx C_v + \frac{(1 - C_v)}{1.15} \approx \frac{1}{1.15} \approx 0.9$$

This indicates that the current method based on the design of large plate girder web always predicts nearly the same normalized shear capacity for the side plate panels with all practical range of plate slenderness and aspect ratios. Therefore, it is imperative to study all the parameters that uniquely characterize the behaviour and strength of plate panel subjected to shear load.

As described in Section 5.4, a precise modeling of side plate panels can be achieved. Factors such as pattern of geometric imperfections and initial stresses can be incorporated into finite element model in order to accurately simulate the side panels subjected to shear. The finite element models can be used to perform an extensive parametric study of the behavior of side panels.

5.6 Dimensionless Parameters

The finite element model was developed in Section 5.4 for the analysis of the plate panel subjected to uniform shear load. The main objective of this section is to identify the fundamental parameters that affect the behavior and the ultimate strength of the plate panel. To do a parametric study, dimensionless parameters that define the behavior and ultimate strength will be identified and then be used to conduct a parametric study.

Before a parametric study of plate panel subjected to uniform shear is done, it is important to determine the parameters that characterize the behavior and the shearing capacity of the plate panel. These parameters should be independent of any scale and material characteristic.

The fundamental parameters that affect the behavior and ultimate shear capacity of the side plate panel can be geometric parameters, loading parameters, output parameters and material characteristics. The fundamental geometric parameters of plate panel are illustrated in Figure 5.12. The geometric parameters are: $b =$ width of the side plate panel, $h =$ height of the side plate panel , $t =$ thickness of the plate , $\Delta =$ deflection and $\sigma_m =$ diaphragm stress. The loading parameter is the applied shear V. The output variable is selected as the in-plane drift δ. The material parameters are: $E =$ modulus of elasticity, $G =$ elastic shear modulus , $v =$ Poisson ratio and $F_y =$ yield strength of the plate material. It should be noted here the Δ is the algebraic sum of magnitude of initial geometric imperfection Δ_o and the deflection Δ due to pressure.

It can be seen from the above list of 11 fundamental parameters that the numbers of combinations of analysis models for practical range of each parameter would be very large. It is therefore necessary to reduce the number of parameters for a manageable parametric study, in the same time to cover all the practical range of each parameter. The suitable tool to reduce the number of the parameters into manageable number of dimensionless parameter is dimensional analysis which would yield number of dimensionless parameters (Harris 1999). The independent scale effect should be checked later.

This can be done by using the Buckingham Pi-theorem (Lanhaar 1951). The Pi-theorem is stated as:

"The number of independent dimensionless parameters arising from n fundamental independent parameters in m dimensions is n-r, where r is the order of largest non-zero determinant of a matrix which is formed from the fundamental parameters and their dimensions."

The independent dimensionless parameters are defined as those which can be formed by combinations of any number of fundamental parameters, but none of them can be formed by any combination of others. Rank of a matrix is order of the largest non-zero determinant.

The behavior of the plate panel subjected to uniform shear is a function of 11 fundamental parameters: $b, h, t, V, \delta, \Delta, F_y, E, G, v$ and σ_m. The E, G and v are dependent on each other and v is dimensionless. Therefore, only one of these three parameters should be independent. The modulus of elasticity E is generally considered as an independent fundamental parameter. Therefore the behavior of the side plate panel is a function of 9 independent fundamental parameters: $b, h, t, V, \delta, \Delta, F_y, E$ and σ_m. These parameters have the dimensions: $M =$ mass, $L =$ length and $T =$ time. To apply the Buckingham Pi theorem, the matrix by the fundamental parameters and their dimensions is formed as shown below.

Fundamental Parameters	b	h	t	V	δ	Δ	F_y	E	σ_m
M	0	0	0	1	0	0	1	1	1
L	1	1	1	1	1	1	-1	-1	-1
T	0	0	0	-2	0	0	-2	-2	-2

The rank of above matrix is 2 i.e., the highest order of determinant would be second order. Therefore, the number of dimensionless parameters expected in this case would be 7.

Having determined the number of dimensionless parameters as described above, the next step is to combine the fundamental parameters to form the desired dimensionless parameters. Even though the Pi-theorem identifies the number of dimensionless

parameters, the independent dimensionless parameters might be an infinite number of possibilities. However, the dimensionless parameters should be useful choice for an experiment or for a parametric study or for design perspective.

As described in Section 5.3, the slender plate panels subjected to a uniform shear, as per Equation 5.8, have the contribution for the shear capacity from the pre buckling strength of plate and from the diagonal tension field. Therefore, the dimensionless parameter $\frac{b}{t}$ can be a variable to measure the contribution of pre buckling strength. This dimensionless parameter is termed as plate slenderness:

$$\frac{b}{t} = \text{Plate Slenderness} \tag{5.12}$$

By inspection of Equation 5.2, 5.3 and 5.1, the aspect ratio $\frac{h}{b}$ can also be a variable to measure the contribution of the pre buckling strength. The aspect ratio $\frac{h}{b}$ influence not only the inclination of the diagonal tension field as per Equation 5.7. but also the number of bands of tension fields. Therefore, the aspect ratio $\frac{h}{b}$ is an important dimensionless parameter to measure the both pre buckling and diagonal tension field contribution.

$$\frac{h}{b} = \text{Aspect ratio of side plate panel} \tag{5.13}$$

The shear loading parameter V can be normalized by the yielding capacity of whole cross section of the plate panel. By applying the von Mises yield criteria for uni-axial and pure shear yielding, the yielding shear capacity of the cross section can be obtained as $\frac{F_y}{\sqrt{3}}ht \approx 0.577htF_y$. Therefore, the normalized shear loading parameter is defined as:

$$\frac{V}{0.577htF_y} = \text{Normalized shear} \tag{5.14}$$

The response of the side plate panel subjected to uniform shear can be measured by the normalized drift obtained by dividing the in plane drift δ by the width b of the plate panel. Therefore, the output parameter is defined as

$$\frac{\delta}{b} = \text{Normalized drift} \tag{5.15}$$

The plate panel subjected to shear loading is also resisting the lateral pressure load which causes the plate to undergo large deflection. The maximum deflection Δ of this long plate panel subjected to lateral pressure is measured at the middle of the cylindrical deflected shape. The relations between the plate slenderness $\frac{b}{t}\sqrt{\frac{F_y}{E}}$ and the normalized deflection $\frac{\Delta}{t}$, when the plate edges begin to yield, have been derived in Chapter 2. Therefore, the dimensionless parameter Δ normalized with the plate thickness t can be another dimensionless parameter.

$$\frac{\Delta}{t} = \text{Normalized deflection} \tag{5.16}$$

The yield strain of the plate is important because they affect the capacity of the plate panel under shear. Therefore normalized yield stress $\frac{F_y}{E}$ will be another dimensionless parameter. Equation 5.4 for the contribution of the pre buckling strength can be re-arranged as:

$$\frac{b}{t}\sqrt{\frac{\tau_y}{E}} = \sqrt{\frac{k\,\pi^2}{12(1-v^2)}} \tag{5.17}$$

Also, by substituting the $\tau_y = \frac{F_y}{\sqrt{3}}$ into Equation 5.17:

$$\frac{b}{t}\sqrt{\frac{F_y}{E}} = \sqrt{\frac{3k\,\pi^2}{12(1-v^2)}} \tag{5.18}$$

Therefore, the geometric plate slenderness $\frac{b}{t}$ and the normalized yield stress $\frac{F_y}{E}$ were combined into $\frac{b}{t}\sqrt{\frac{F_y}{E}}$ to make it material strength independent.

$$\frac{b}{t}\sqrt{\frac{F_y}{E}} = \text{Plate slenderness} \tag{5.19}$$

The diaphragm stress σ_m can also be normalized by yield stress F_y of the plate material.

$$\frac{\sigma_m}{F_y} = \text{Normalized diaphragm stress} \tag{5.20}$$

The application of the dimensional analysis to an experiment or to a parametric study requires an understanding of significance of the dimensionless parameters identified. In this case, the dimensionless parameters that affect the behavior of the plate panel subjected to shear were $\frac{b}{t}\sqrt{\frac{F_y}{E}}$, $\frac{h}{b}$, $\frac{V}{0.577htF_y}$, $\frac{\delta}{b}$, $\frac{\Delta}{t}$ and $\frac{\sigma_m}{F_y}$. In Chapter 2, the relation between $\frac{b}{t}\sqrt{\frac{F_y}{E}}$ and the dimensionless load parameter $\frac{pE}{{F_y}^2}$ were developed for the strip of plate subjected lateral pressure load when the top fibre of plate at support begins to yield. Similarly, the relation between $\frac{\Delta}{t}$ and $\frac{b}{t}\sqrt{\frac{F_y}{E}}$ was established in Chapter 2. In the meantime, the diaphragm stress σ_m was also known for a particular $\frac{b}{t}\sqrt{\frac{F_y}{E}}$ when the top fibre begins to yield. Therefore, for a particular plate slenderness $\frac{b}{t}\sqrt{\frac{F_y}{E}}$, the $\frac{\Delta}{t}$ and $\frac{\sigma_m}{F_y}$ are known quantities from the studies in Chapter 2. Therefore, the dimensionless parameters $\frac{\Delta}{t}$ and $\frac{\sigma_m}{F_y}$ are constant for a plate panel with particular $\frac{b}{t}\sqrt{\frac{F_y}{E}}$ when it is subjected uniform

shear, the parameters $\frac{b}{t}\sqrt{\frac{F_y}{E}}$ and $\frac{h}{b}$ are the input parameters, $\frac{\delta}{b}$ is the output parameter and $\frac{V}{0.577htF_y}$ will be the loading parameter applied to measure the response of the plate panel subjected to the shear load.

5.6.1 Completeness of Dimensionless Parameters

To verify the completeness and the scale independent of the dimensionless parameters identified, the Buckingham Pi-theorem requires all the fundamental parameters should be included into the dimensionless parameters. Therefore, a preliminary study was conducted to determine that all the fundamental parameters that govern the behavior of the plate panel subjected shear are included in the dimensionless parameters. This will confirm scale independency of the dimensionless parameters chosen. The preliminary study contains three plate panels having same dimensionless parameters $\frac{b}{t}\sqrt{\frac{F_y}{E}}$ and $\frac{h}{b}$ but with different scale. The corresponding dimensionless parameters $\frac{\Delta}{t}$ and $\frac{\sigma_m}{F_y}$ were applied for this analysis even though these would be constant for the plate panels with the same $\frac{b}{t}\sqrt{\frac{F_y}{E}}$. If the plots of the dimensionless parameters $\frac{V}{0.577htF_y}$ versus $\frac{\delta}{b}$ are identical for the three plate panels chosen, then it can be concluded that the dimensionless parameters are complete and scale independent.

Table 5.2 presents the three plate panels considered for this analysis. All three cases contains different scales, however the dimensionless plate slenderness and aspect ratio are same for three cases. The applied shear versus the vertical drift was plotted in Figure

5.13 for the three cases. These plots are different as the scale of fundamental parameters the shear and the vertical drift are not dimensionless. However, the plots of normalized applied shear versus normalized drift became identical as shown in Figure 5.14. Therefore, it can be concluded that the change of scale fundamental parameters does not affect the response if the models have same dimensionless parameters.

It can be concluded from the above study that the dimensionless parameter chosen fully govern the behavior of plate panel subjected shear and have no scale effect. Therefore, these parameters can be used for this parametric study.

5.7 Parametric Study

The dimensionless parameters identified in Section 5.6 can be used to simulate the behavior of the side plate panel subjected to shear. The primary objective of this study was to carry out a detailed parametric study to establish a comprehensive method for estimating ultimate shear capacity of the side plate panels.

The reasonable ranges of input dimensionless parameters $\frac{b}{t}\sqrt{\frac{F_y}{E}}$ and $\frac{h}{b}$ for large rectangular industrial duct were established here to complete the matrix of analysis models. As identified in Chapter 2, the range of the plate slenderness $\frac{b}{t}$ for the side plate panels considered were from 125 to 350 in steps of 25. As the yield strength $F_y = 250MPa$ and the modulus of elasticity $E = 200000MPa$ were chosen for the idealized material model, the dimensionless parameters $\frac{b}{t}\sqrt{\frac{F_y}{E}}$ for this study were 4.419, 5.303, 6.187, 7.7071, 7.955, 8.839, 9.723, 10.607, 11.490 and 12.374 to complete the analysis matrix. An examination of the aspect ratio $\frac{h}{b}$ of the practical duct reveals that the range of the aspect ratio $\frac{h}{b}$ is approximately from 3 to 10. However, a lower bound of the aspect ratio of 2 was assumed in addition to 3 to 10. Therefore, the dimensionless parameters $\frac{h}{b}$ selected for this study were from 2 to 10 in step of 1.

The complete set of input dimensionless parameters $\frac{b}{t}\sqrt{\frac{F_y}{E}}$ and $\frac{h}{b}$ are summarized in Table 5.3. In addition to $\frac{b}{t}\sqrt{\frac{F_y}{E}}$ and $\frac{h}{b}$, the corresponding dimensionless parameters $\frac{\Delta}{t}$ and

$\frac{\sigma_m}{F_y}$ were also included in Table 5.3. Therefore, the total number of analysis models needed for this parametric study will be 90.

The finite element models developed for the analysis of industrial duct side panels subjected to shear was presented in Section 5.4. This model can be used to simulate the behaviour of the side panel and to obtain the equilibrium path beyond its ultimate state. The intention of this simulation was to obtain ultimate strength of the side panels subjected to shear load. The shear load V versus in plane drift δ history of each analysis was obtained from the analysis results. For each analysis model, the load versus drift history was converted into dimensionless form of normalized shear $\frac{V}{0.577htF_y}$ versus normalized drift $\frac{\delta}{b}$ history. The normalized ultimate shear capacity $\frac{V_u}{0.577htF_y}$ was taken as the peak load point from the normalized shear versus normalized drift history plot.

A typical representative finite element model of the side plate panel with $\frac{b}{t}\sqrt{\frac{F_y}{E}} = 7.071$ and $\frac{h}{b} = 5$ is shown in Figure 5.15. Figure 5.16 represents the deformed shape of the corresponding finite element model at the peak shear load.

Figure 5.17 shows the normalized shear versus normalized drift history plots of the side plate panels with $\frac{b}{t}\sqrt{\frac{F_y}{E}} = 7.955$ and aspect ratios $\frac{h}{b}$ considered. For each panel aspect ratio, the slope of the linear portion of the responses represents a non-dimensional

stiffness. The initial non-dimensional stiffnesses were same. As the aspect ratio increases, the predicted normalized ultimate shear strength $\frac{V_u}{0.577htF_y}$ slightly decreases.

In order to explain how the number of bands of tension fields on a side panel varies with the increase in aspect ratios $\frac{h}{b}$, the stress vector plots of the side panels with dimensionless slenderness $\frac{b}{t}\sqrt{\frac{F_y}{E}} = 7.071$ were chosen. The representative stress vector plots of the side panels chosen were illustrated in Figure 5.18. These vector plots show how the number of bands of tension fields developed in resisting the shear applied as the aspect ratio $\frac{h}{b}$ increases from 2 to 10. It can be observed that the angles of the tension field within the stiffeners are same. However, the top and bottom tension fields incline towards the intersection of the angle and stiffener. This is because the boundary members should have enough flexural stiffness to anchor the tension fields. The low flexural stiffness of the angles at top and bottom of side panel does not provide enough rigidity to anchor the tension fields.

It should noted that the current methods in AISC 2005 and CSA 2010 are based on the model representing one band of inclined uniform tension field (across the side panel) extending from top to bottom of the web between stiffeners (one wide band of tension field). The current methods in AISC (2005) and CSA (2010) use the vertical component of the one wide band of inclined uniform tension field to make the additional contribution to the ultimate shear resistance. The one wide band of tension field resulted high shear

resistance. However, in a narrow and long side panel (with large aspect ratios $\frac{h}{b}$), the tension field contribution comes from several bands of inclined tension fields as shown in Figure 5.18. The vertical component of the several band of tension field reduced the contribution to ultimate shear resistance significantly less than that of predicted by Equation 5.8.

The results of the finite element analysis for the side plate panel subjected to shear were tabulated in Table 5.4. The peak normalized ultimate shear strengths $\frac{V_u}{0.577htF_y}$ obtained from shear load V versus in plane drift δ plots were tabulated with respect to the dimensionless parameters $\frac{b}{t}\sqrt{\frac{F_y}{E}}$ and $\frac{h}{b}$. The normalized ultimate shear strengths $\frac{V_u}{0.577htF_y}$ were observed to decrease slightly with the increase in aspect ratio $\frac{h}{b}$ for a particular plate slenderness of stockier side panels $\left(\frac{b}{t}\sqrt{\frac{F_y}{E}} \leq 6.187\right)$. However, the decrease in $\frac{V_u}{0.577htF_y}$ with the increase in $\frac{h}{b}$ was more gradual for slender side panels $\left(\frac{b}{t}\sqrt{\frac{F_y}{E}} > 6.187\right)$. The stockier side plate panels show gradual loss in normalized shear capacity $\frac{V_u}{0.577htF_y}$ with the increase in the plate slenderness $\frac{b}{t}\sqrt{\frac{F_y}{E}}$ for a particular aspect ratio $\frac{h}{b}$. However, the $\frac{V_u}{0.577htF_y}$ became approximately constant for slender side panels for a particular aspect ratio $\frac{h}{b}$. The mean and standard deviation of normalized shear capacities $\frac{V_u}{0.577htF_y}$ for each plate slenderness are presented in the last column. The

values of standard deviation indicate that the mean normalized ultimate shear $\frac{V_u}{0.577htF_y}$ for the side panels with plate slenderness $\frac{b}{t}\sqrt{\frac{F_y}{E}}$ up to 6.187 are reasonable values to predict the shear capacities of those side panels $\left(\frac{b}{t}\sqrt{\frac{F_y}{E}} \leq 6.187\right)$.

The ultimate shear strength V_u will be additive of the web shear buckling strength V_{cr} and the contribution from the tension field action V_{tf}. The former is simply the capacity attained at the point of theoretical plate (web) buckling. This shear buckling strength for slender plates was established well. Therefore, the contribution of the shear buckling strength for the side panels considered in this study can be estimated using the first part of the Equation 5.8.

Using the first part of Equation 5.8, the shear buckling strengths V_{cr} are calculated and tabulated in Table 5.5 with respect to the corresponding dimensionless parameters $\frac{b}{t}\sqrt{\frac{F_y}{E}}$ and $\frac{h}{b}$. Therefore, the additional contribution provided by the tension field action can be calculated for the each analysis model by subtracting the shear buckling strength V_{cr} in Table 5.5 from the corresponding ultimate shear strength V_u in Table 5.4. The additional contributions from the tension field action V_{tf} are tabulated in Table 5.6.

A closed observation of the normalized contribution of the tension field action $\frac{V_{tf}}{0.577htF_y}$ in Table 5.6 indicates that $\frac{V_{tf}}{0.577htF_y}$ are nearly constant with the increase in the aspect ratio $\frac{h}{b}$

for each plate slenderness $\frac{b}{t}\sqrt{\frac{F_y}{E}}$ up to 6.187. However, the normalized contribution of tension fields $\frac{V_{tf}}{0.577htF_y}$ gradually increases with the increase in plate slenderness $\frac{b}{t}\sqrt{\frac{F_y}{E}}$. The aspect ratio has minimal effect on the normalized contribution of the tension fields for plate slenderness up to 6.187.

The last columns of Table 5.6 indicate the average normalized contributions of the tension field $\frac{V_{tf}}{0.577htF_y}$ and corresponding standard deviations for the each plate slenderness considered in this study. The standard deviations indicate that the normalized contributions of the tension field $\frac{V_{tf}}{0.577htF_y}$ can be considered as the average values for each plate panel with plate slenderness up to 6.187. The normalized contributions of the tension field $\frac{V_{tf}}{0.577htF_y}$ for each plate panel with plate slenderness above 6.187 can be expressed function of aspect ratio and plate slenderness. Therefore, by modifying Equation 5.8, a simple relation to estimate the ultimate shear capacity of the side plate panels can obtained by adding the first term in Equation 5.8 for the contribution of the shear buckling and the corresponding contribution of tension field action. Approximate normalized ultimate shear for the side panels considered in this study can be obtained from the modified Equation 5.8 as follows:

$$V_u = 0.577htF_y\left(C_v + C_{tf}\right) \tag{5.21}$$

Where C_{tf} is:

$$C_{tf} = 0.033\frac{b}{t}\sqrt{\frac{F_y}{E}} + 0.236 \qquad if \ \ \frac{b}{t}\sqrt{\frac{F_y}{E}} \leq 6.187 \tag{5.22}$$

$$C_{tf} = 0.013\frac{b}{t}\sqrt{\frac{F_y}{E}} + 0.351 - 0.01\left(\frac{h}{b} - 7\right) \qquad if \ \ \frac{b}{t}\sqrt{\frac{F_y}{E}} > 6.187 \tag{5.23}$$

The first term in Equation 5.8 is based on the simply supported boundary conditions for all four edges. However, in this numerical analysis, the longitudinal edges are provided a rotational stiffness by the flange of the stiffeners and the transverse edges are modeled to be simply supported. This support conditions along the longitudinal edges of the side panels will most likely be intermediate between the simply supported and clamped condition. Kuhn(1952), based on experiments with angle stiffeners, showed that the boundary conditions can be assumed to be simply supported for shear buckling when the leg thickness of the angle stiffeners are at least the thickness of the side plate panels. In addition, the shear buckling coefficients k (Equation 5.2 and 5.3 that account the boundary conditions) are not influenced by the large aspect ratio $\frac{h}{b}$. These facts make it difficult specify the exact boundary conditions of the industrial duct side panel under shear. However, Equation 5.21 can be applicable to obtain the ultimate normalized shear buckling strength $\frac{V_u}{0.577htF_y}$ of the side plate panel with plate slenderness up to 6.187, even though the relation does not fully represents the rational behind the ultimate strength. Therefore, in order to study the relation between the normalized ultimate shear

$\frac{V_u}{0.577htF_y}$, plate slenderness $\frac{b}{t}\sqrt{\frac{F_y}{E}}$ and aspect ratio $\frac{h}{b}$, the results of ultimate strengths (Table 5.4) obtained directly from the numerical analysis models were considered.

The aim of the parametric study was to investigate the influence of dimensionless parameters on ultimate shear strengths and to propose a method for estimating ultimate shear strength of given duct side plate panel. It should be noted here that the plate slenderness $\frac{b}{t}\sqrt{\frac{F_y}{E}}$ is the dominant dimensionless parameter that affects the normalized ultimate shear strength $\frac{V_u}{0.577htF_y}$ of the industrial duct side panels with lower plate slenderness up to 6.187. However, the aspect ratios $\frac{h}{b}$ have minimal effect on the normalized ultimate shear strength of plate panels with plate slenderness up to 6.187. For side plate panels with plate slenderness more than 6.187, the normalized ultimate shear strength depends on both aspect ratios $\frac{h}{b}$ and plate slenderness $\frac{b}{t}\sqrt{\frac{F_y}{E}}$. Therefore, it is intended to derive relation between the normalized shear strength $\frac{V_u}{0.577htF_y}$, aspect ratio $\frac{h}{b}$ and plate slenderness $\frac{b}{t}\sqrt{\frac{F_y}{E}}$ in order to propose a useful and practical design method.

It was obvious from above facts that the trend between $\frac{V_u}{0.577htF_y}$, $\frac{b}{t}\sqrt{\frac{F_y}{E}}$ and $\frac{h}{b}$ can be used to develop a set of graphs for different ultimate shear levels in order to aid the design. A set of such design curves would enable the designer to calculate the ultimate shear capacity of industrial duct side panels. In order to develop a complete set of design

curves, the ultimate normalized shear strengths $\frac{V_u}{0.577htF_y}$ with respect to $\frac{b}{t}\sqrt{\frac{F_y}{E}}$ and $\frac{h}{b}$ were plotted in a three-dimensional plot as shown in Figure 5.19. Figure 5.19 graphically illustrates how the normalized shear capacity $\frac{V_u}{0.577htF_y}$ varies with respect to the plate slenderness $\frac{b}{t}\sqrt{\frac{F_y}{E}}$ and aspect ratio $\frac{h}{b}$. The horizontal axes are associated with the plate slenderness $\frac{b}{t}\sqrt{\frac{F_y}{E}}$ and aspect ratio $\frac{h}{b}$. The vertical axis represents the normalized shear strength $\frac{V_u}{0.577htF_y}$. This three-dimensional graph illustrates how the dimensionless parameters $\frac{b}{t}\sqrt{\frac{F_y}{E}}$ and $\frac{h}{b}$ influence the normalized shear $\frac{V_u}{0.577htF_y}$. It is obvious that the normalized shear strengths are influenced by both aspect ratio and plate slenderness for slender side panels (with higher $\frac{b}{t}\sqrt{\frac{F_y}{E}}$). The aspect ratio $\frac{h}{b}$ has minimal effect on the normalized shear strengths for stockier side plate panel (with lower $\frac{b}{t}\sqrt{\frac{F_y}{E}}$).

Although the three-dimensional graphs provide the general pattern how the normalized shear strength is influenced by dimensionless parameters $\frac{b}{t}\sqrt{\frac{F_y}{E}}$ and $\frac{h}{b}$, the contours of $\frac{V_u}{0.577htF_y}$ should be generated in order to obtain the different level of normalized shear strengths' curves with respect to parameters $\frac{b}{t}\sqrt{\frac{F_y}{E}}$ and $\frac{h}{b}$. With this in mind, Figure 5.20, which provides the contours of normalized ultimate shear strengths, was generated from the three-dimensional plot. The pattern of the contour indicates that the normalized

ultimate shear strength $\frac{V_u}{0.577htF_y}$ with values more than 0.65 is not influenced by the aspect ratio and depends on plate slenderness $\frac{b}{t}\sqrt{\frac{F_y}{E}}$. For the normalized ultimate shear strength $\frac{V_u}{0.577htF_y}$ up to 0.65, it is influenced by both aspect ratio and plate slenderness.

In order to calculate the ultimate shear capacity V_u of a side plate panel with given plate slenderness $\frac{b}{t}\sqrt{\frac{F_y}{E}}$ and aspect ratio $\frac{h}{b}$, the set of design curves (contours) in Figure 5.20 can be used. Above set of design curves, in addition to Table 5.4, can be used to calculate the ultimate shear strength V_u of a large industrial duct side panel subjected shear for the range of plate slenderness and aspect ratios considered in this study. It should be noted here that these results are valid only for the side plate panels subjected to static loading and ambient temperature.

5.8 Conclusions and Further Recommendations

The ultimate shear resistance V_u of the slender side plate panels of large rectangular industrial ducts consists of plate shear buckling and contribution of the tension field action. In order to estimate the ultimate shear resistance in the current industrial duct design practice, the methods used to design the web of large plate girder from the design standards such as AISC (2005) and CSA (2010) are used. These methods are based on Basler's theory (1963) in which the contribution of the tension field is assumed to form one wide band of tension field. In contrast to this method, it has been demonstrated that several bands of tension fields contribute to the ultimate shear strength of the side panel

with large aspect ratio. In addition, it was observed that the methods based on the web of large girder design predict higher and approximately same ultimate shear capacity for all practical geometric dimensions of the side panels of large industrial ducts. However, it has been shown that the side plate panel have less shear resistance compared to the results of current design method. The dimensionless parameters affecting the behaviour of the side panel subjected to shear were identified. A parametric study was conducted for all the practical range of the dimensionless parameters. The plate slenderness $\frac{b}{t}\sqrt{\frac{F_y}{E}}$ was found to be dominant dimensionless parameter dictating the normalized ultimate shear capacity $\frac{V_u}{0.577htF_y}$ of the large industrial duct stockier side panels. The dimensionless aspect ratio $\frac{h}{b}$ and plate slenderness $\frac{b}{t}\sqrt{\frac{F_y}{E}}$ influenced the normalized ultimate shear capacity of slender side plate panels. Design aids for estimating the ultimate shear capacity of the industrial duct side plate panel were proposed.

5.8.1 Further Recommendations

Considerable understanding of the behaviour of the side plate panel subjected to shear has been made through this parametric study. The scope of the current study can be broadened to include the following further investigations:

1. Although, in Chapter 2, the relations between $\frac{b}{t}\sqrt{\frac{F_y}{E}}$ and $\frac{\Delta}{t}$ and $\frac{b}{t}\sqrt{\frac{F_y}{E}}$ and $\frac{\sigma_m}{F_y}$ were derived when top fibre begins to yield and 16.5% and 33% of the thickness of plate yield, only the values of $\frac{\Delta}{t}$ and $\frac{\sigma_m}{F_y}$ for the case of top fibre beginning to yield were considered in this study. This was because these relations were

obtained to design the plate (thickness or spacing) for the excursion internal pressure load and the operating pressure load are very low. Therefore, the effects of $\frac{\Delta}{t}$ and $\frac{\sigma_m}{F_y}$,when 16.5% and 33% of the thickness of plate yield, should be investigated.

2. In the industrial duct slender side panel with large aspect ratio $\frac{h}{b}$, the majority of the shear capacity comes from several band of tension fields. The vertical component of tension fields is anchored by stiffener and effective corner elements. Most of the tension fields will be anchored by stiffeners. In this study, a practical corner angle L76XL76X7.9 (L3X3X5/16) was modeled. Therefore, the effect of corner angle should be investigated.
3. In this parametric study, the completeness and scale effect of dimensionless parameters were established by numerical analysis. The completeness and scale effect should be investigated experimentally. In addition, the results obtained from the numerical study should be compared with experimental results for one or two random cases.
4. The bands of tension fields may cause additional forces and moments of stiffeners. This effect should be investigated.
5. The dimensionless parameters with material independent were established for the idealized elastic-plastic-strain hardening tri-linear material model representing mild carbon steel. The material independency of the dimensionless parameters for the material models representing high strength steel should be established.

Table 5.1 Ultimate Strengths of Different Mesh Densities

Mesh Density	Total Elements	Ultimate Load (kN)	% Difference
6x6	36	490.5	
			7.4
10x10	100	456.7	
			3.0
16x16	256	434.04	
			2.2
20x20	400	424.69	
			1.1
26x26	676	420.12	

Table 5.2 Plate Panels for Completeness and Scale effect

	$b\ (mm)$	$t\ (mm)$	$h\ (mm)$	$\frac{b}{t}\sqrt{\frac{F_y}{E}}$	$\frac{h}{b}$	$\frac{V_u}{0.577htF_y}$
Case 1	1000	5	4000	7.071	4	0.64
Case 2	1250	6.25	5000	7.071	4	0.63
Case 3	1400	7	5600	7.071	4	0.63

Table 5.3 Matrix of Parameters

#	($b = 1000mm, F_y = 250MPa, E = 200000MPa$)	h	$\frac{h}{b}$
1		2000	2
2		3000	3
3	$\frac{b}{t}\sqrt{\frac{F_y}{E}} = 4.419,\ t = 8mm$	4000	4
4		5000	5
5		6000	6
6		7000	7
7	$\frac{\Delta}{t} = 0.86,\ \Delta_0 = 3.91mm,\ \sigma_m = 22.0MPa$	8000	8
8		9000	9
9		10000	10
10		2000	2
11		3000	3
12	$\frac{b}{t}\sqrt{\frac{F_y}{E}} = 5.303, t = 6.667mm$	4000	4
13		5000	5
14		6000	6
15		7000	7
16	$\frac{\Delta}{t} = 1.13,\ \Delta_0 = 4.69mm,\ \sigma_m = 25.0MPa$	8000	8
17		9000	9
18		10000	10
19		2000	2
20		3000	3
21	$\frac{b}{t}\sqrt{\frac{F_y}{E}} = 6.187, t = 5.714mm$	4000	4
22		5000	5
23		6000	6
24		7000	7
25	$\frac{\Delta}{t} = 1.38,\ \Delta_0 = 5.47mm,\ \sigma_m = 29.3MPa$	8000	8
26		9000	9
27		10000	10
28		2000	2
29		3000	3
30	$\frac{b}{t}\sqrt{\frac{F_y}{E}} = 7.071\ , t = 5mm$	4000	4
31		5000	5
32		6000	6
33		7000	7
34	$\frac{\Delta}{t} = 1.65,\ \Delta_0 = 6.25mm,\ \sigma_m = 31.8MPa$	8000	8
35		9000	9
36		1000	10

Table 5.3 Matrix of Parameters Continues….

37		2000	2
38		3000	3
39	$\frac{b}{t}\sqrt{\frac{F_y}{E}} = 7.955, t = 4.444mm$	4000	4
40		5000	5
41		6000	6
42		7000	7
43	$\frac{\Delta}{t} = 1.91, \quad \Delta_0 = 7.03mm, \quad \sigma_m = 33.9\ MPa$	8000	8
44		9000	9
45		10000	10
46		2000	2
47		3000	3
48	$\frac{b}{t}\sqrt{\frac{F_y}{E}} = 8.839\ , t = 4.0mm$	4000	4
49		5000	5
50		6000	6
51		7000	7
52	$\frac{\Delta}{t} = 2.17, \quad \Delta_0 = 7.81mm, \quad \sigma_m = \ 35.2\ MPa$	8000	8
53		9000	9
54		10000	10
55		2000	2
56	$\frac{b}{t}\sqrt{\frac{F_y}{E}} = 9.723, \quad t = 3.636mm$	3000	3
57		4000	4
58		5000	5
59		6000	6
60	$\frac{\Delta}{t} = 2.42, \quad \Delta_0 = 8.60mm, \quad \sigma_m = 36.6\ MPa$	7000	7
61		8000	8
62		9000	9
63		10000	10
64		2000	2
65		3000	3
66	$\frac{b}{t}\sqrt{\frac{F_y}{E}} = 10.607, t = 3.333mm$	4000	4
67		5000	5
68		6000	6
69		7000	7
70	$\frac{\Delta}{t} = 2.67, \quad \Delta_0 = 9.38mm, \quad \sigma_m = 37.8MPa$	8000	8
71		9000	9
72		10000	10

Table 5.3 Matrix of Parameters Continues….

73		2000	2
74		3000	3
75	$\frac{b}{t}\sqrt{\frac{F_y}{E}} = 11.490, t = 3.077mm$	4000	4
76		5000	5
77		6000	6
78		7000	7
79	$\frac{\Delta}{t} = 2.91, \quad \Delta_0 = 10.16mm, \quad \sigma_m = 38.6MPa$	8000	8
80		9000	9
81		10000	10
82		2000	2
83	$\frac{b}{t}\sqrt{\frac{F_y}{E}} = 12.374, \quad t = 2.857mm$	3000	3
84		4000	4
85		5000	5
86		6000	6
87	$\frac{\Delta}{t} = 3.15, \quad \Delta_0 = 10.94mm, \quad \sigma_m = \quad 39.4MPa$	7000	7
88		8000	8
89		9000	9
90		10000	10

Table 5.4 Results of Parametric Study

($F_y = 250MPa,\ E = 200GPa$)

$\frac{V_u}{0.577htF_y}$		$\frac{h}{b}$										
		2	3	4	5	6	7	8	9	10	Average	Std Dev
$\frac{b}{t}\sqrt{\frac{F_y}{E}}$	4.419	0.85	0.82	0.81	0.81	0.80	0.80	0.79	0.79	0.79	*0.81*	*0.02*
	5.303	0.75	0.73	0.73	0.72	0.71	0.71	0.71	0.70	0.70	*0.72*	*0.02*
	6.187	0.71	0.68	0.67	0.66	0.65	0.64	0.63	0.63	0.64	*0.66*	*0.03*
	7.071	0.67	0.66	0.63	0.62	0.61	0.60	0.60	0.57	0.56	*0.62*	*0.04*
	7.955	0.65	0.64	0.61	0.59	0.58	0.57	0.56	0.56	0.55	*0.59*	*0.04*
	8.839	0.65	0.62	0.59	0.58	0.56	0.55	0.54	0.53	0.53	*0.57*	*0.04*
	9.725	0.66	0.63	0.59	0.57	0.55	0.54	0.53	0.52	0.52	*0.57*	*0.05*
	10.607	0.65	0.63	0.59	0.58	0.55	0.54	0.52	0.52	0.51	*0.56*	*0.05*
	11.490	0.66	0.63	0.60	0.58	0.55	0.54	0.52	0.52	0.50	*0.56*	*0.05*
	12.374	0.66	0.64	0.60	0.58	0.55	0.52	0.52	0.52	0.50	*0.56*	*0.06*

Table 5.5 Shear Buckling Strengths

($F_y = 250MPa,\ E = 200GPa$)

$\frac{V_{cr}}{0.577htF_y}$		$\frac{h}{b}$								
		2	3	4	5	6	7	8	9	10
$\frac{b}{t}\sqrt{\frac{F_y}{E}}$	4.419	0.50	0.45	0.43	0.42	0.41	0.41	0.41	0.41	0.41
	5.303	0.36	0.31	0.30	0.29	0.29	0.28	0.28	0.28	0.28
	6.187	0.26	0.23	0.22	0.21	0.21	0.21	0.21	0.21	0.21
	7.071	0.20	0.17	0.17	0.17	0.16	0.16	0.16	0.16	0.16
	7.955	0.16	0.14	0.13	0.13	0.13	0.13	0.13	0.13	0.13
	8.839	0.13	0.11	0.11	0.11	0.10	0.10	0.10	0.10	0.10
	9.725	0.10	0.09	0.09	0.09	0.09	0.09	0.09	0.09	0.09
	10.607	0.09	0.08	0.08	0.07	0.07	0.07	0.07	0.07	0.07
	11.490	0.07	0.07	0.06	0.06	0.06	0.06	0.06	0.06	0.06
	12.374	0.06	0.06	0.06	0.05	0.05	0.05	0.05	0.05	0.05

Table 5.6 Contributions from Tension Field Actions
($F_y = 250MPa,\ E = 200GPa$)

$\frac{V_{tf}}{0.577htF_y}$		$\frac{h}{b}$										
		2	3	4	5	6	7	8	9	10	Average	Std Dev
$\frac{b}{t}\sqrt{\frac{F_y}{E}}$	4.419	0.35	0.37	0.38	0.39	0.39	0.39	0.38	0.38	0.38	*0.38*	*0.01*
	5.303	0.39	0.42	0.43	0.43	0.42	0.43	0.43	0.42	0.42	*0.42*	*0.01*
	6.187	0.45	0.45	0.45	0.45	0.44	0.43	0.42	0.42	0.43	*0.44*	*0.01*
	7.071	0.47	0.49	0.46	0.45	0.45	0.44	0.44	0.41	0.40	*0.45*	*0.03*
	7.955	0.49	0.50	0.48	0.46	0.45	0.44	0.43	0.43	0.42	*0.46*	*0.03*
	8.839	0.52	0.51	0.48	0.47	0.46	0.45	0.44	0.43	0.43	*0.47*	*0.03*
	9.725	0.56	0.54	0.50	0.48	0.46	0.45	0.44	0.43	0.43	*0.48*	*0.05*
	10.607	0.56	0.55	0.51	0.51	0.48	0.47	0.45	0.45	0.44	*0.49*	*0.04*
	11.490	0.59	0.56	0.54	0.52	0.49	0.48	0.46	0.46	0.44	*0.50*	*0.05*
	12.374	0.60	0.58	0.54	0.53	0.50	0.47	0.47	0.47	0.45	*0.51*	*0.05*

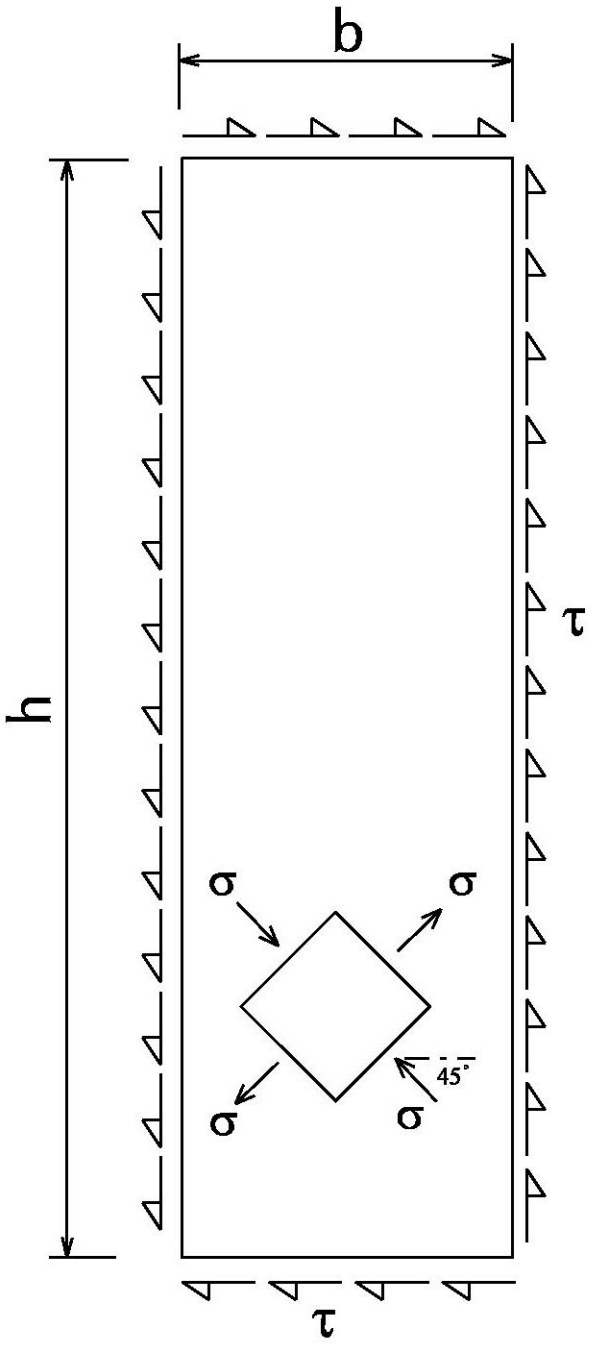

Figure 5.1 Rectangular Plate with Uniform Shear

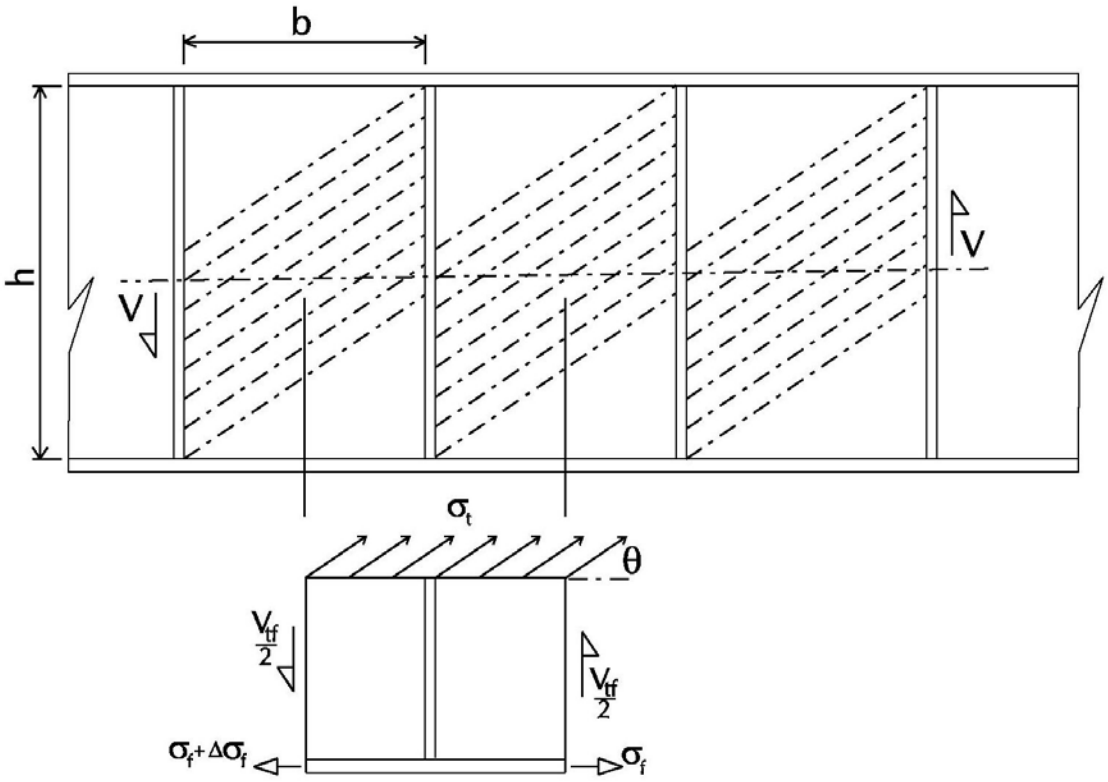

Figure 5.2 Complete Tension Field

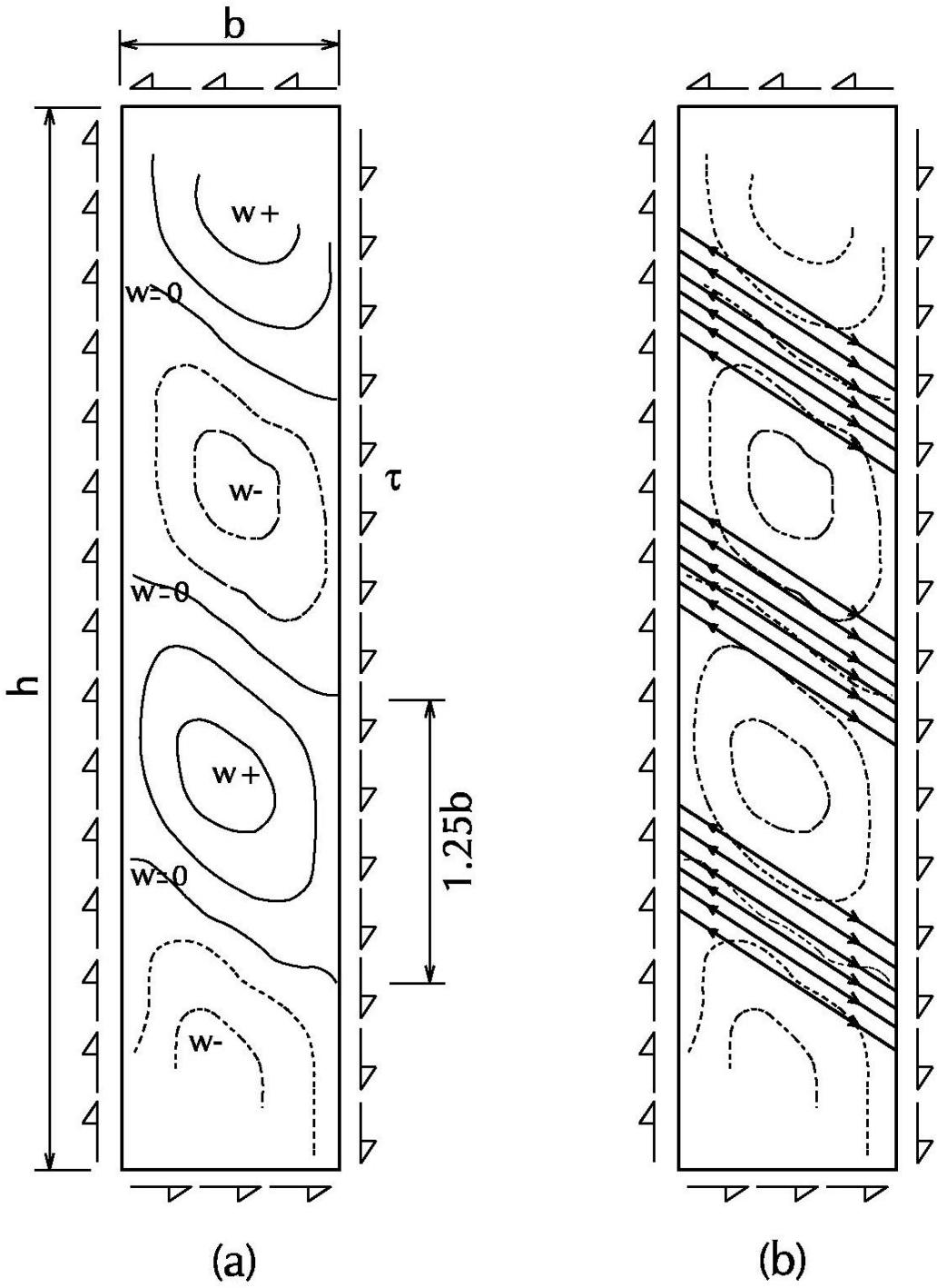

Figure 5.3 Buckling Shape of Long Plate and Bands of Tension Fields (Bruhn 1973)

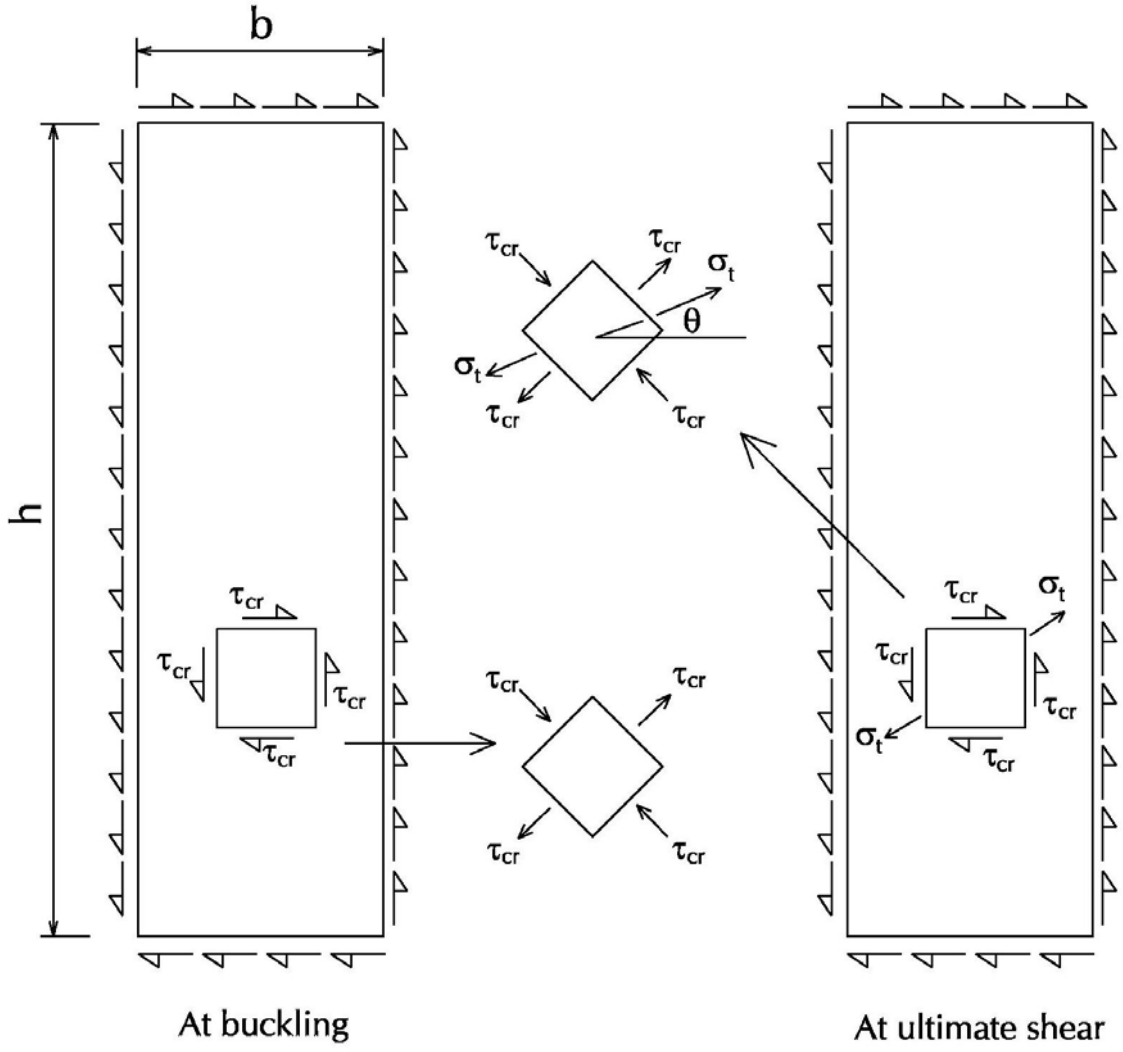

Figure 5.4 Stresses at Buckling and Ultimate State (Charles 1997)

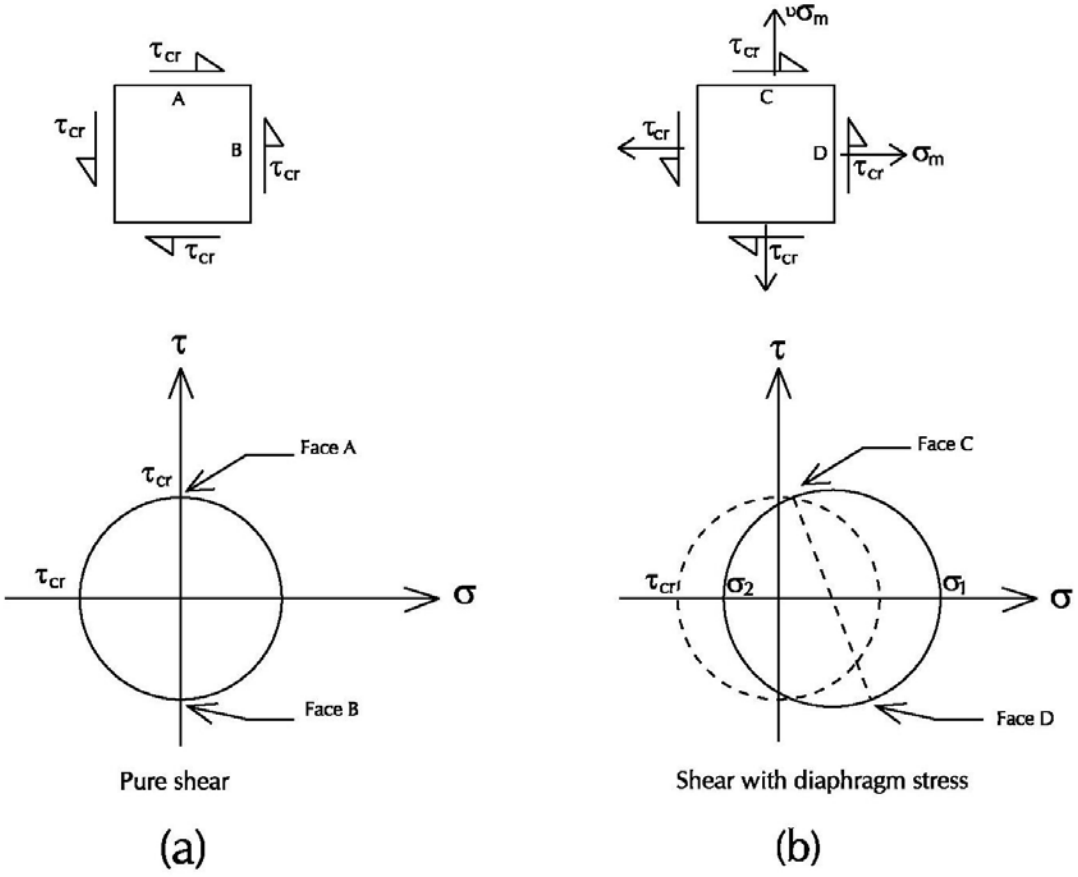

Figure 5.5 Effect of Diaphragm Stresses

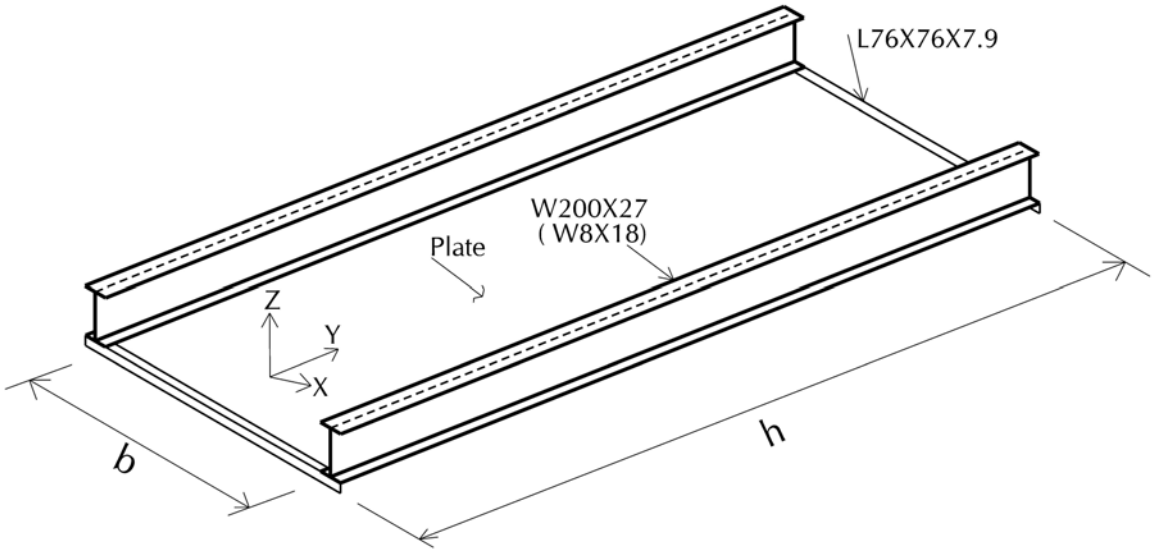

Figure 5.6 Schematic of Duct Side Panel

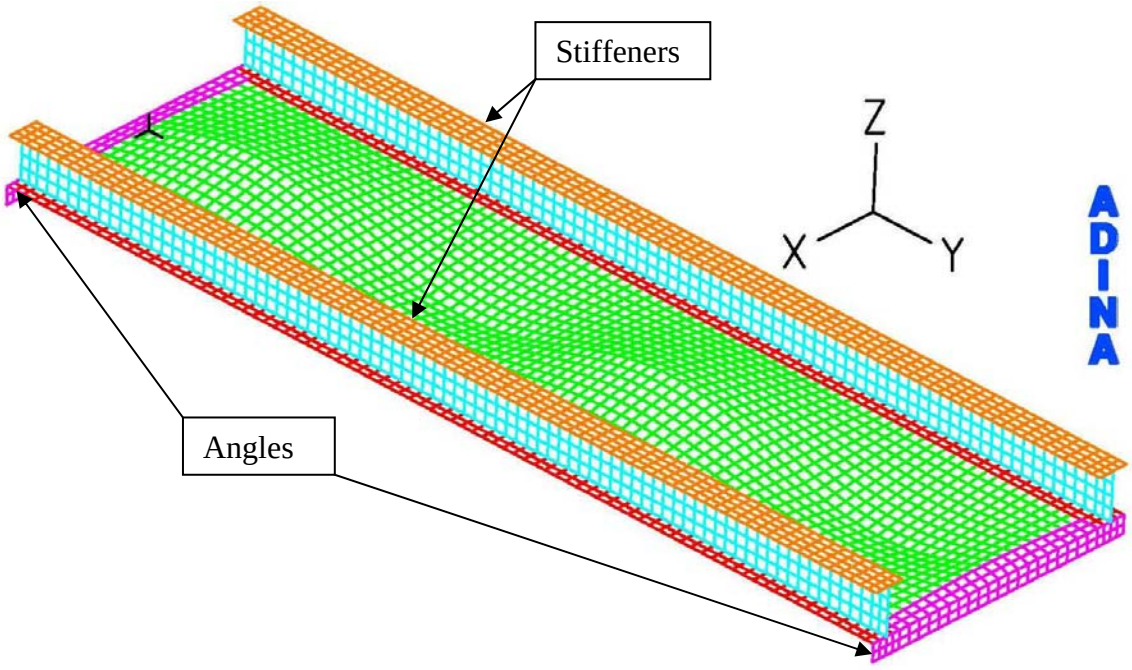

Figure 5.7 Exaggerated Initial Geometric Imperfections

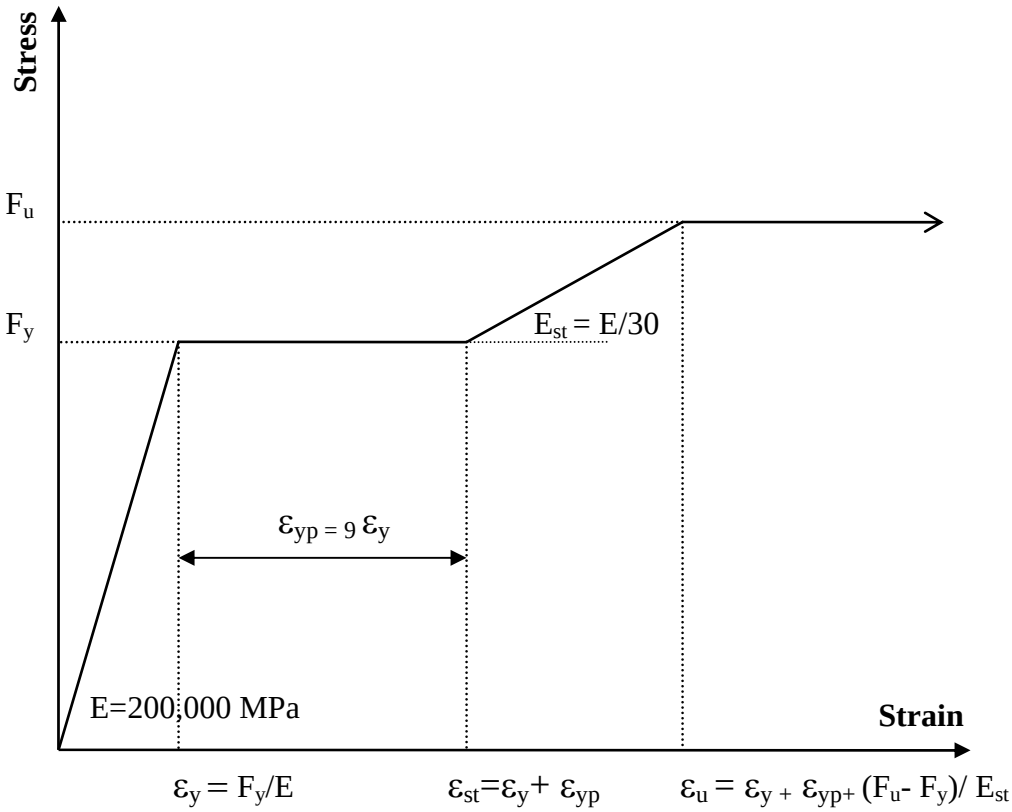

Grade A36 Steel	Strain	ε_y	ε_{st}	ε_u	ε_l
		0.00125	0.0125	0.03500	0.1
	Stress (MPa)	F_y	F_{st}	F_u	F_u
		250	250	400	400

Figure 5.8 Idealized Material Model

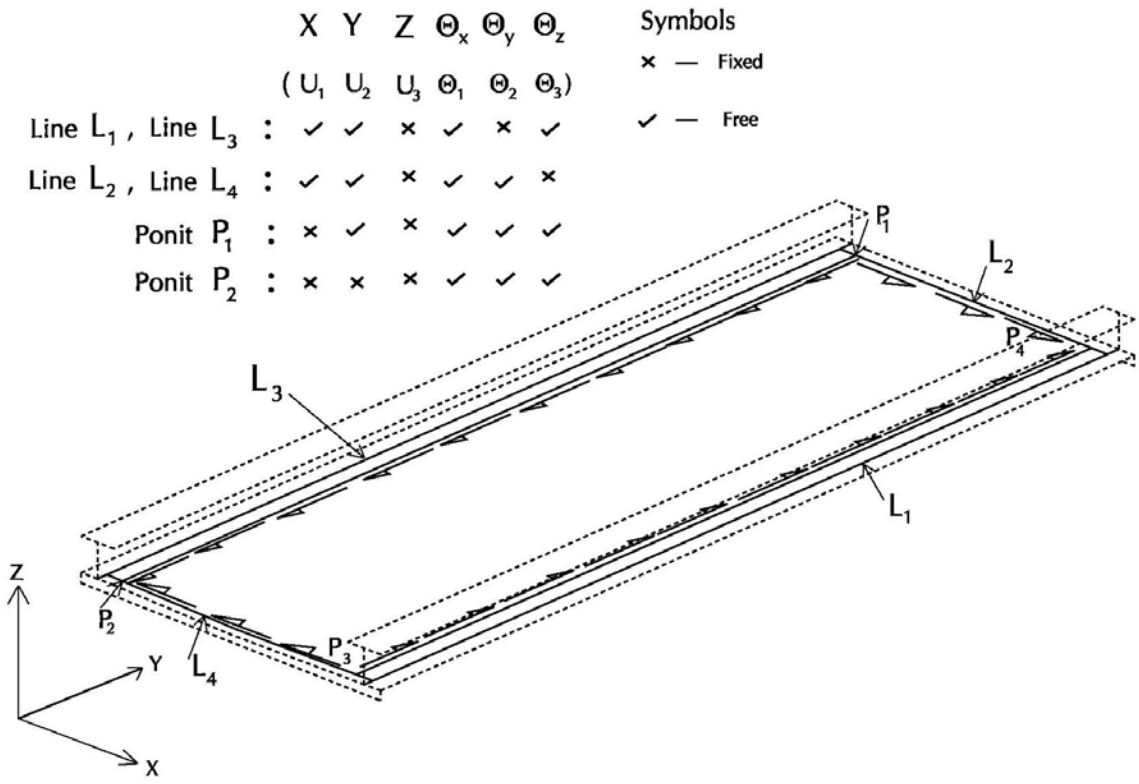

Figure 5.9 Boundary Conditions

	U_1	U_2	U_3	Θ_1	Θ_2	Θ_3
Line L_1 :	✓	✓	×	✓	✓	✓
Line L_2 :	✓	✓	×	✓	✓	✓
Line L_3 :	✓	✓	×	✓	✓	✓
Line L_4 :	✓	✓	×	✓	✓	✓
Ponit P_1 :	×	✓	×	✓	✓	✓
Ponit P_2 :	×	×	×	✓	✓	✓

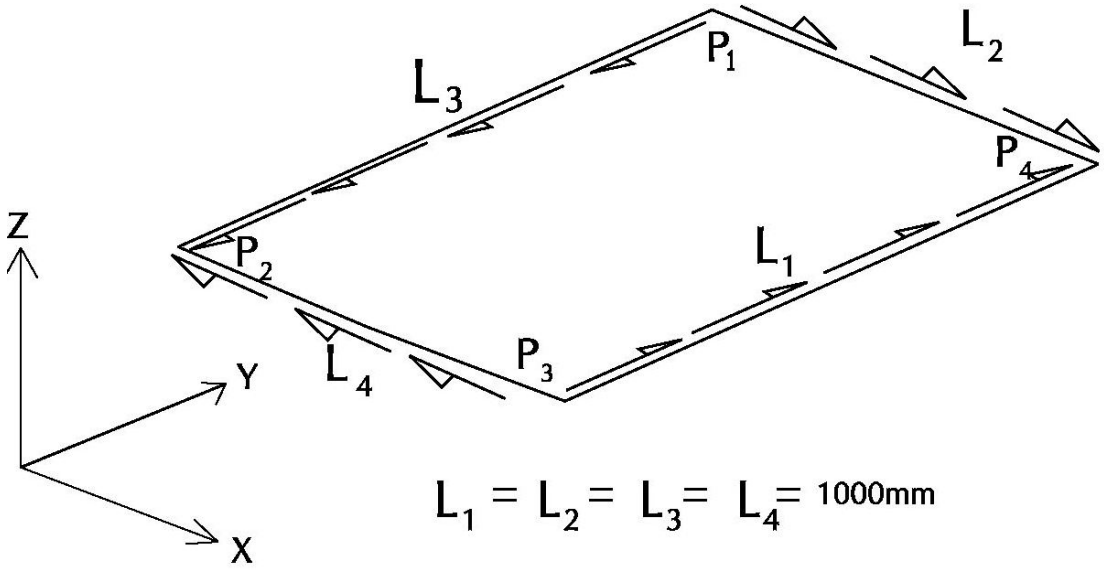

Figure 5.10 Model for Verification Study

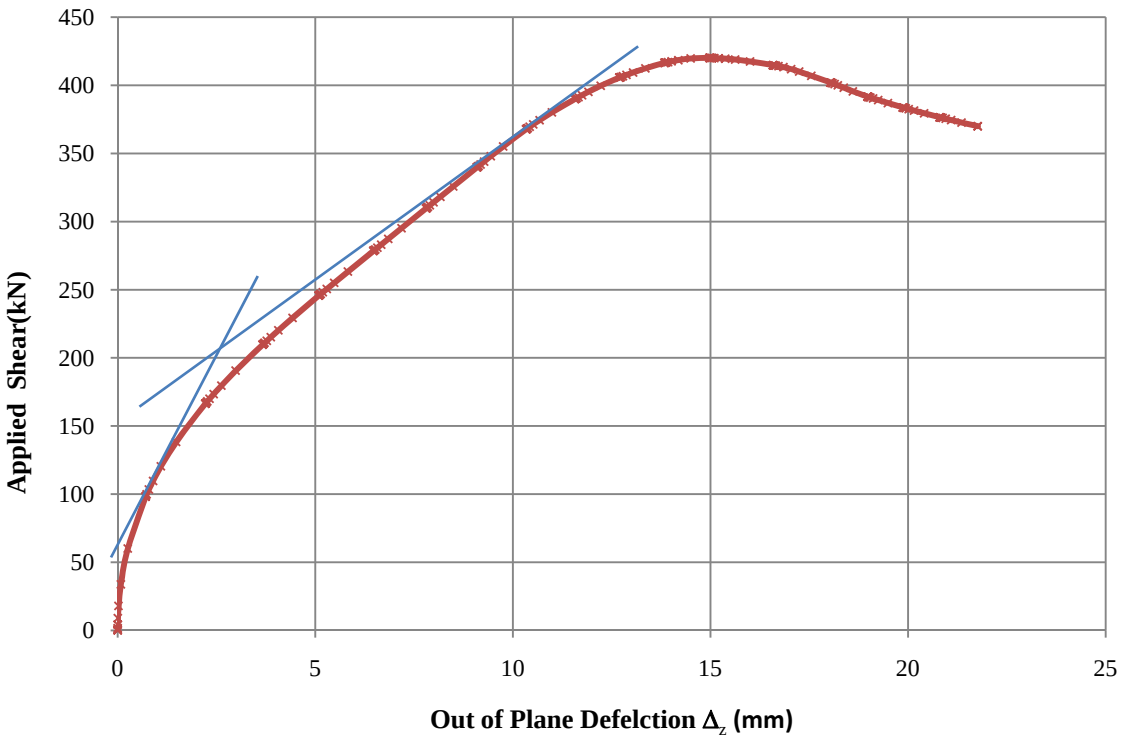

Figure 5.11 Bucking Strength of Square Plate

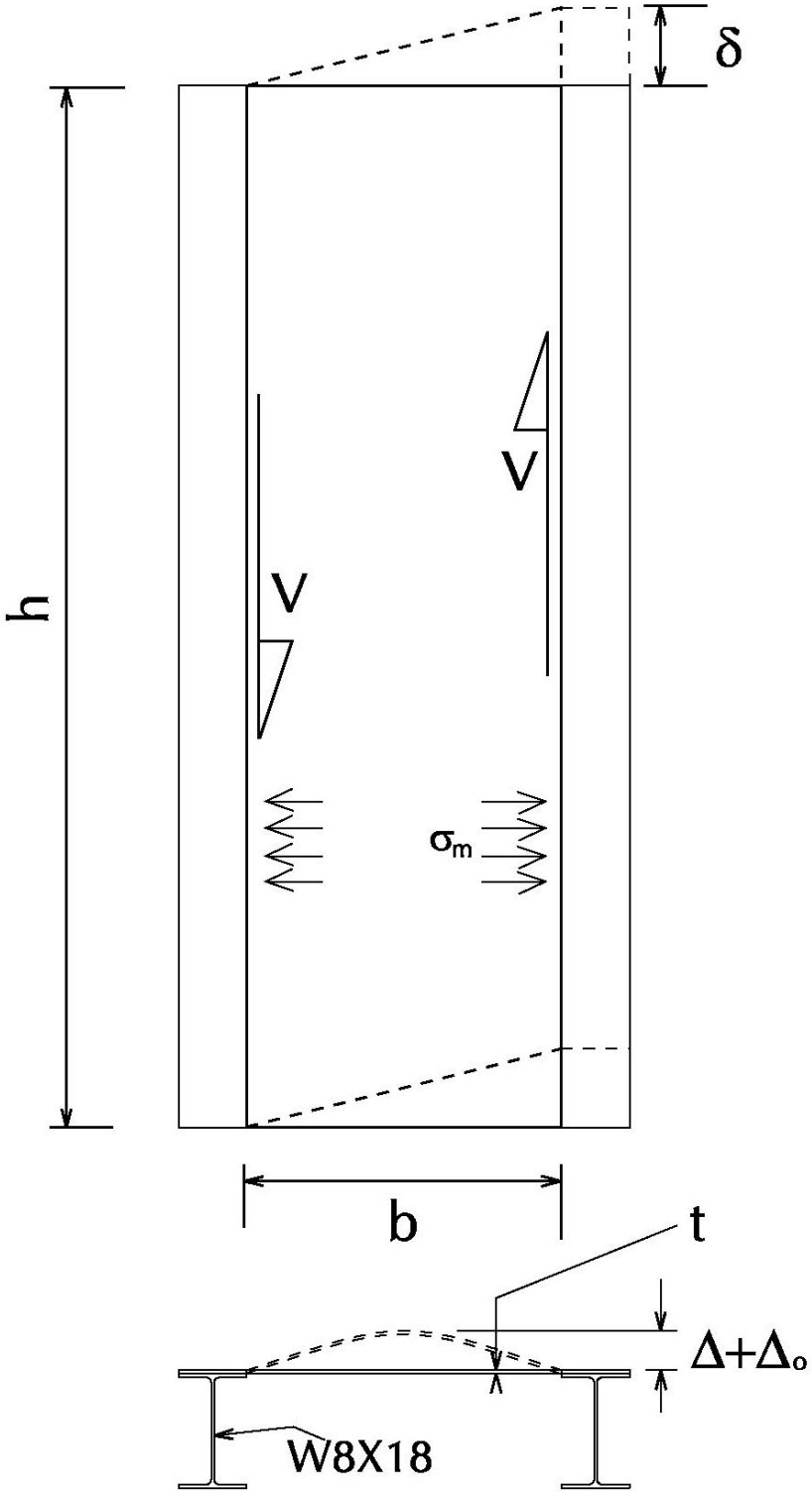

Figure 5.12 Fundamental Parameters

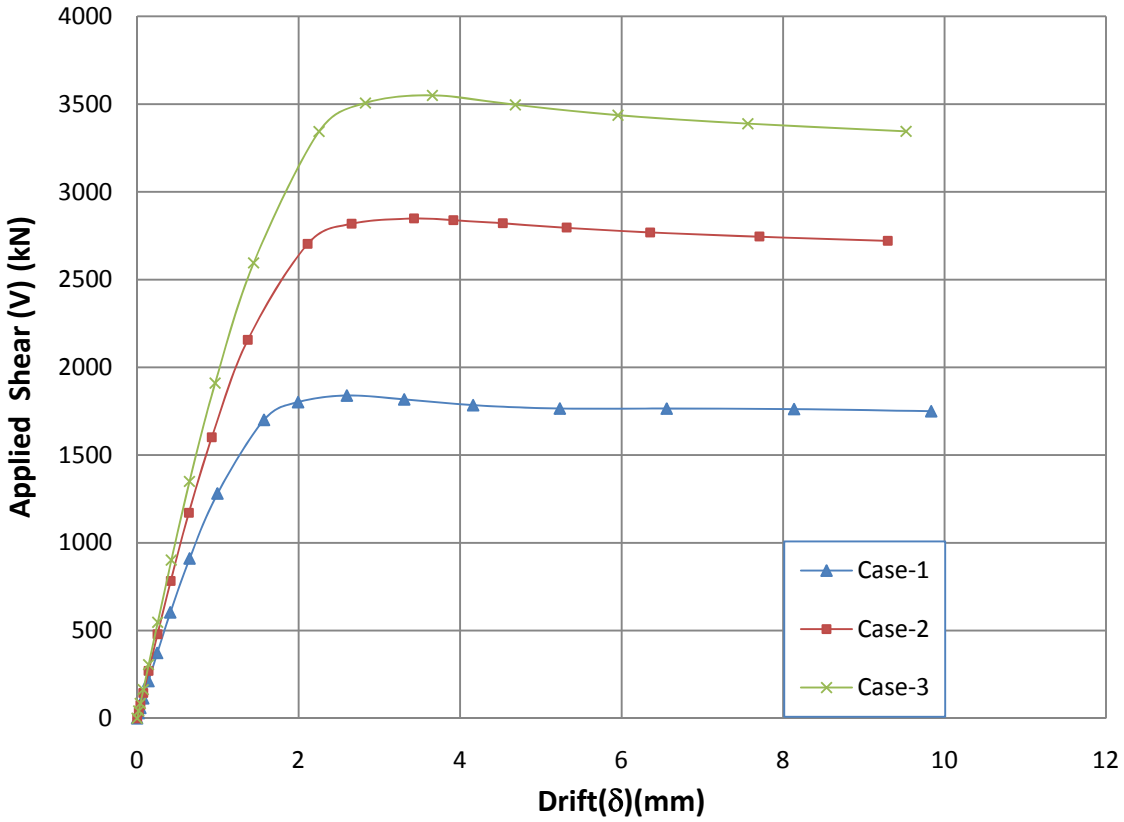

Figure 5.13 Applied shear versus drift

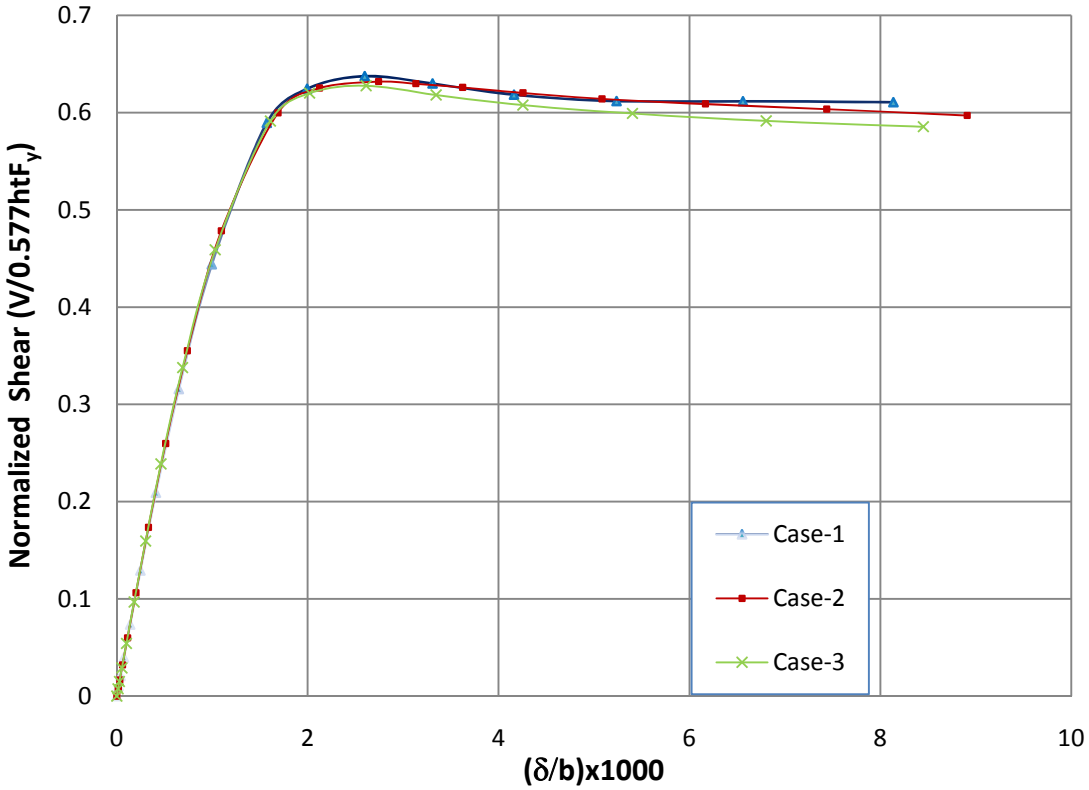

Figure 5.14 Normalized shear versus normalized drift

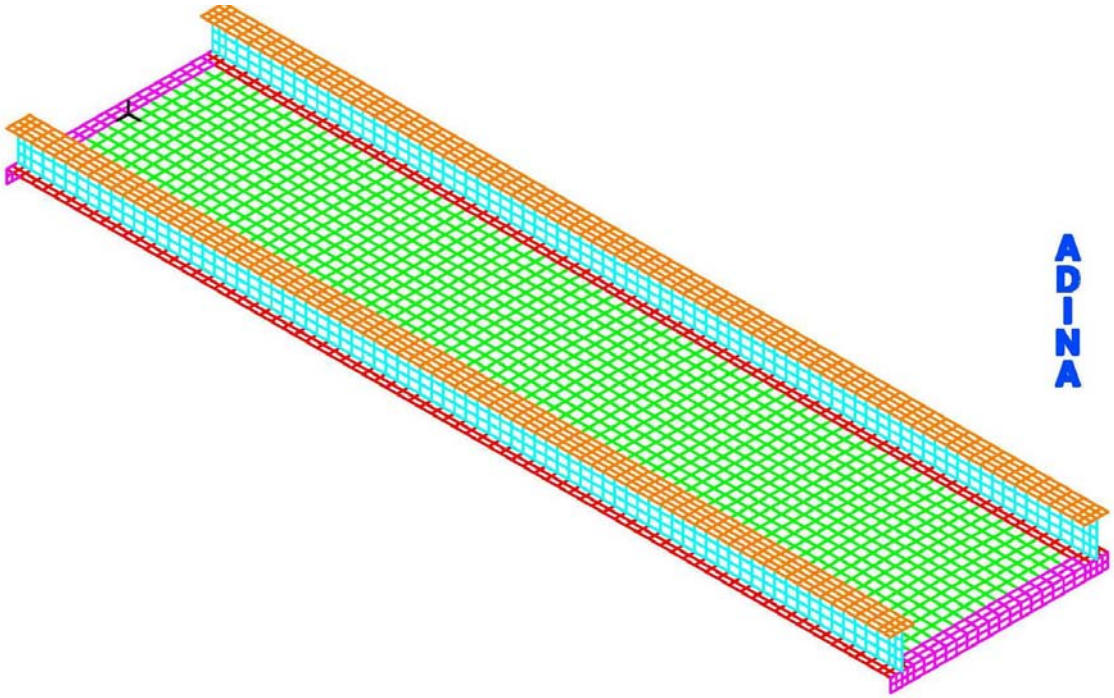

Figure 5.15 Finite Element Model of $\frac{h}{b} = 5$ and $\frac{b}{t}\sqrt{\frac{F_y}{E}} = 7.071$

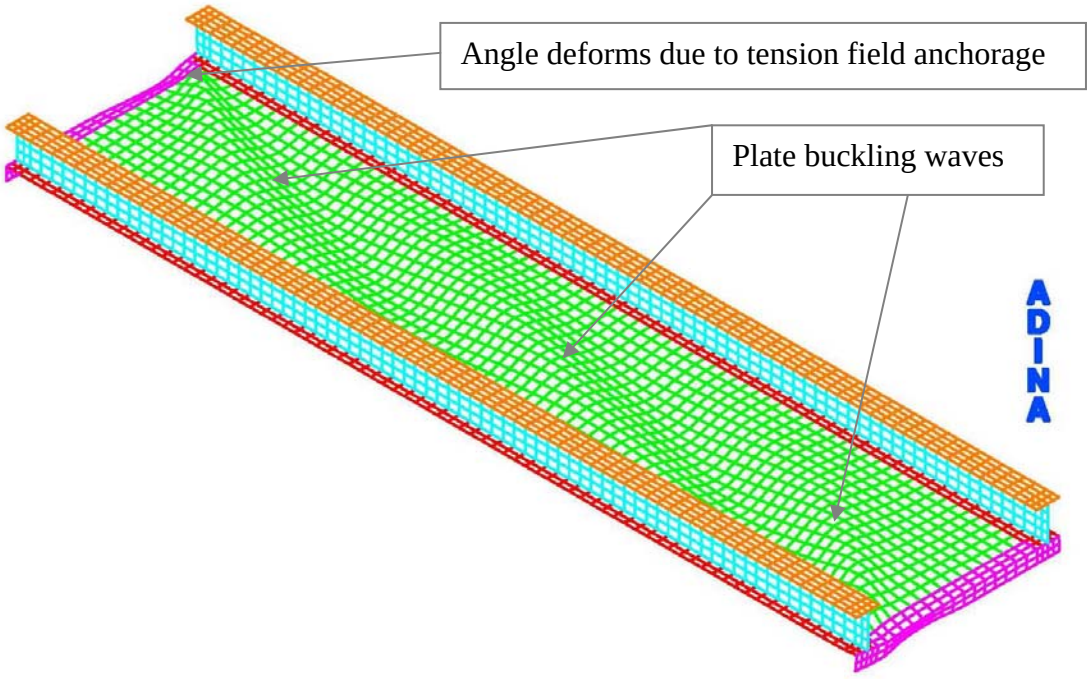

Figure 5.16 Deformed Shape of Model of $\frac{h}{b} = 5$ and $\frac{b}{t}\sqrt{\frac{F_y}{E}} = 7.071$

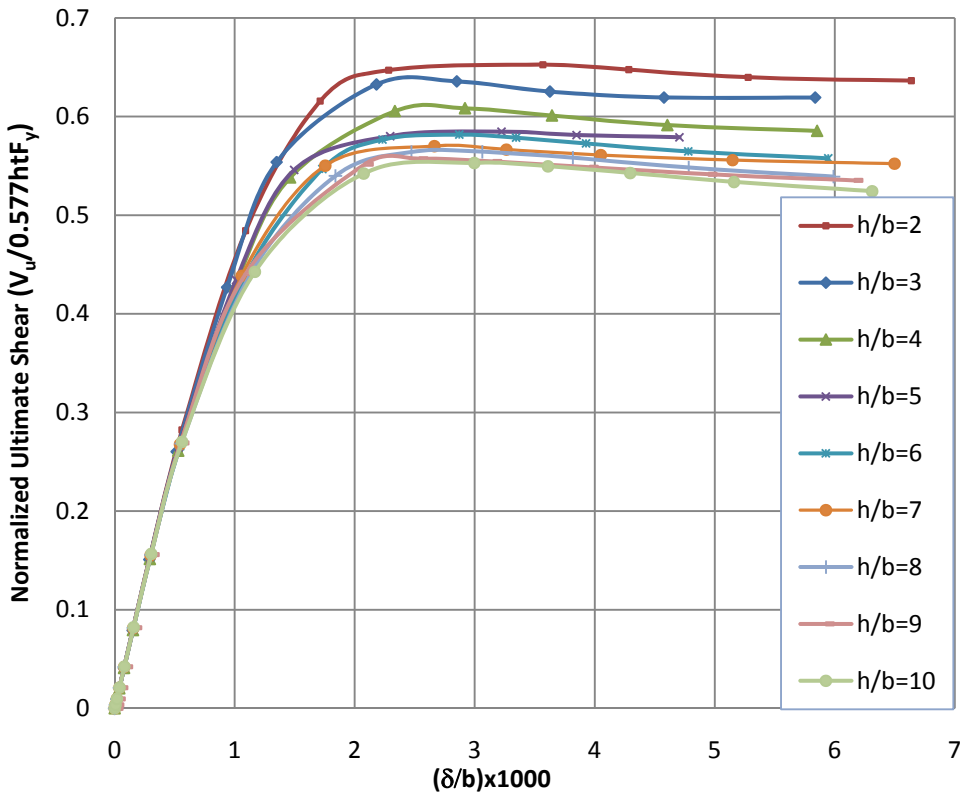

Figure 5.17 Normalized Shear versus Drift of Cases with $\frac{b}{t}\sqrt{\frac{F_y}{E}} = 7.955$

Figure 5.18 Bands of Tension Field Action of Side Panel with $\frac{b}{t}\sqrt{\frac{F_y}{E}} = 7.071$

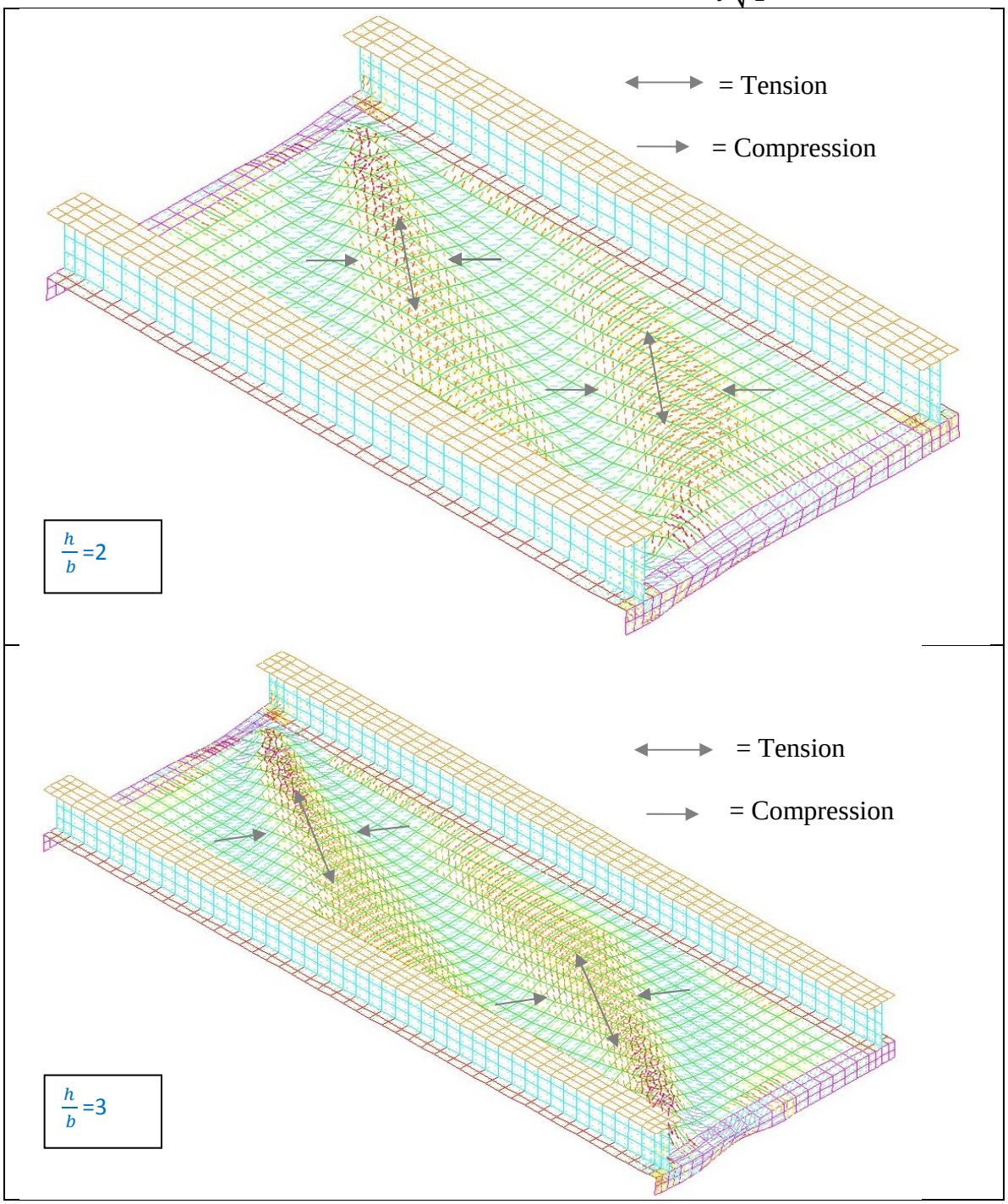

Figure 5.18 Continues….

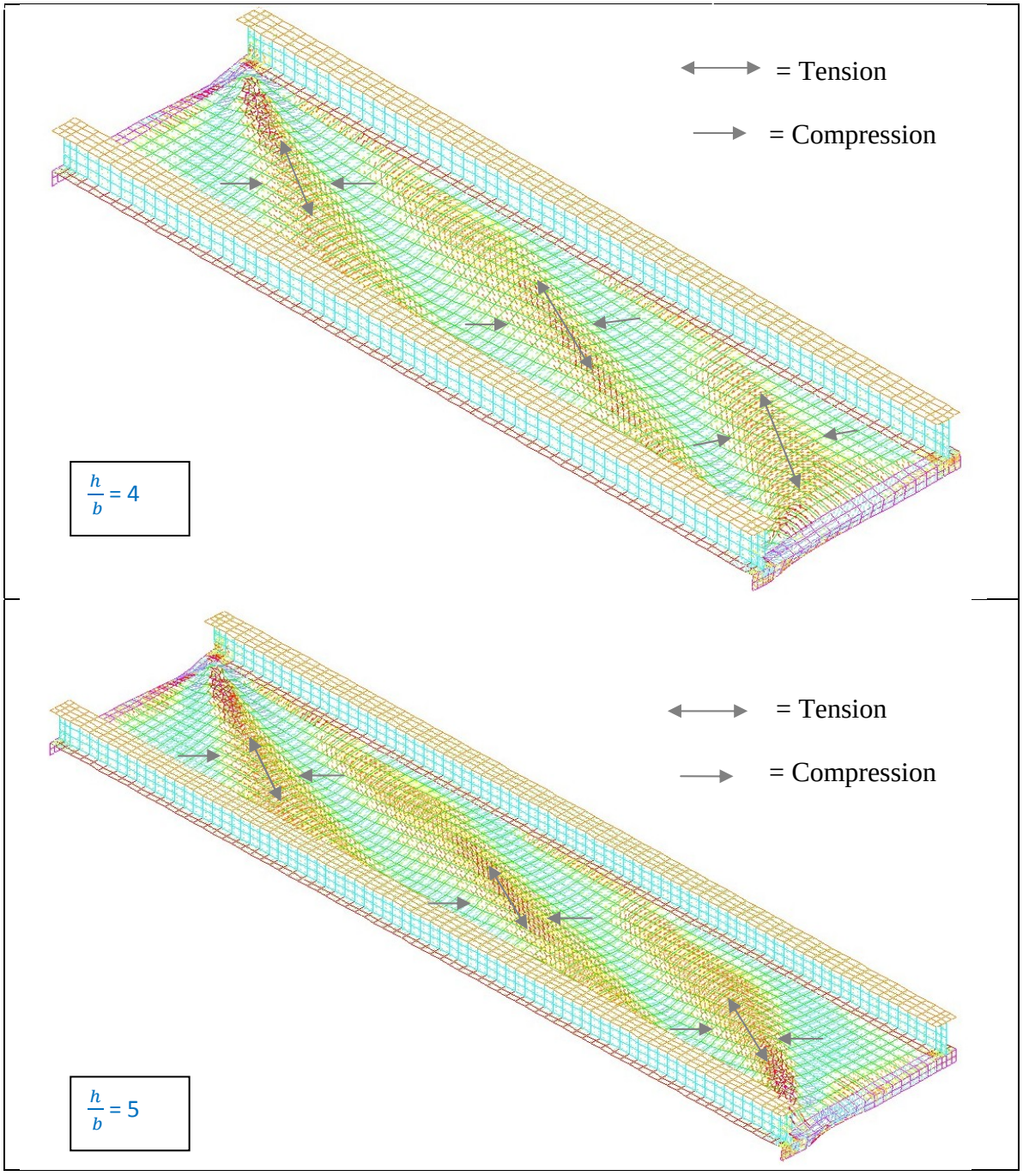

Figure 5.18 Continues….

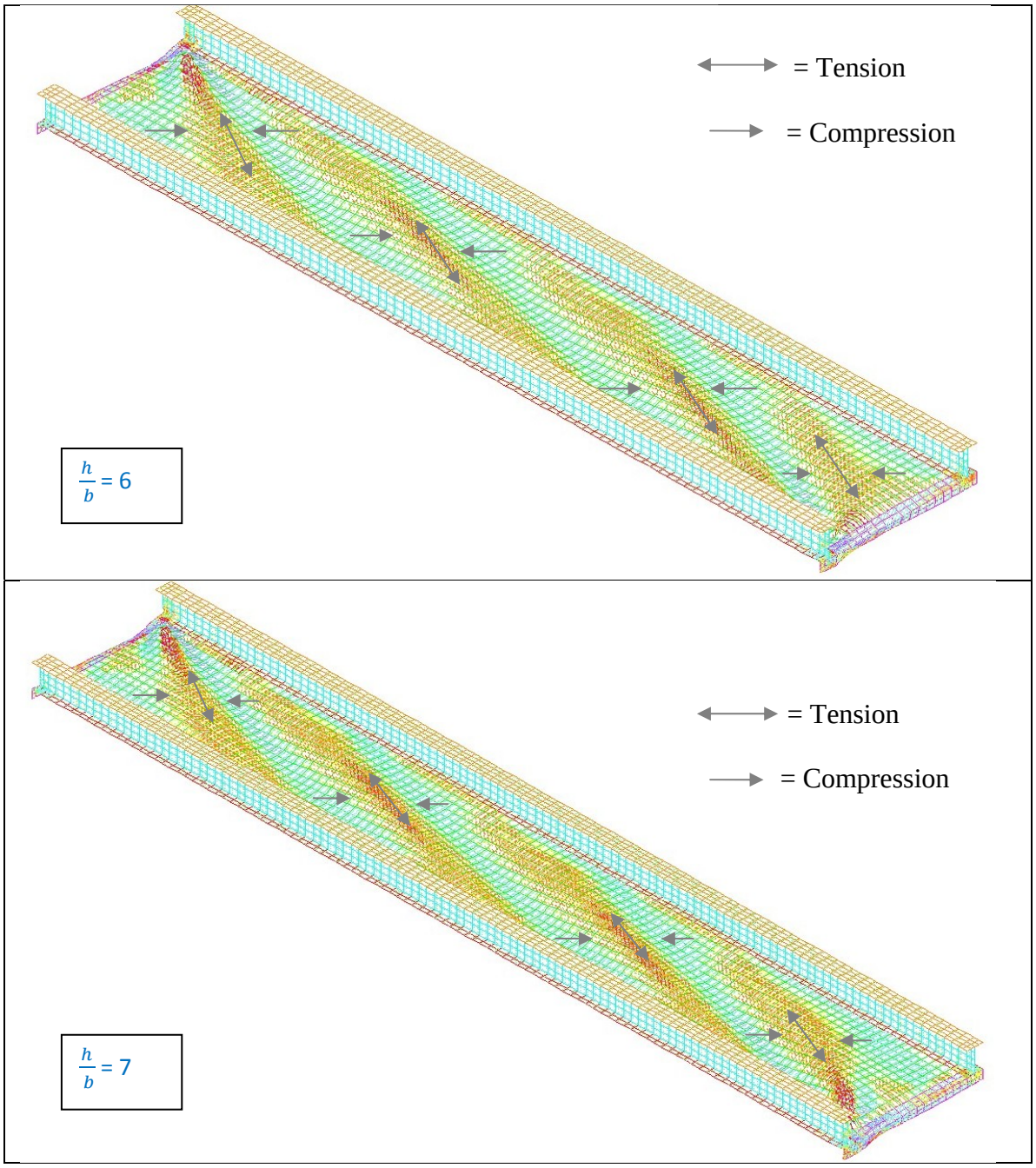

Figure 5.18 Continues….

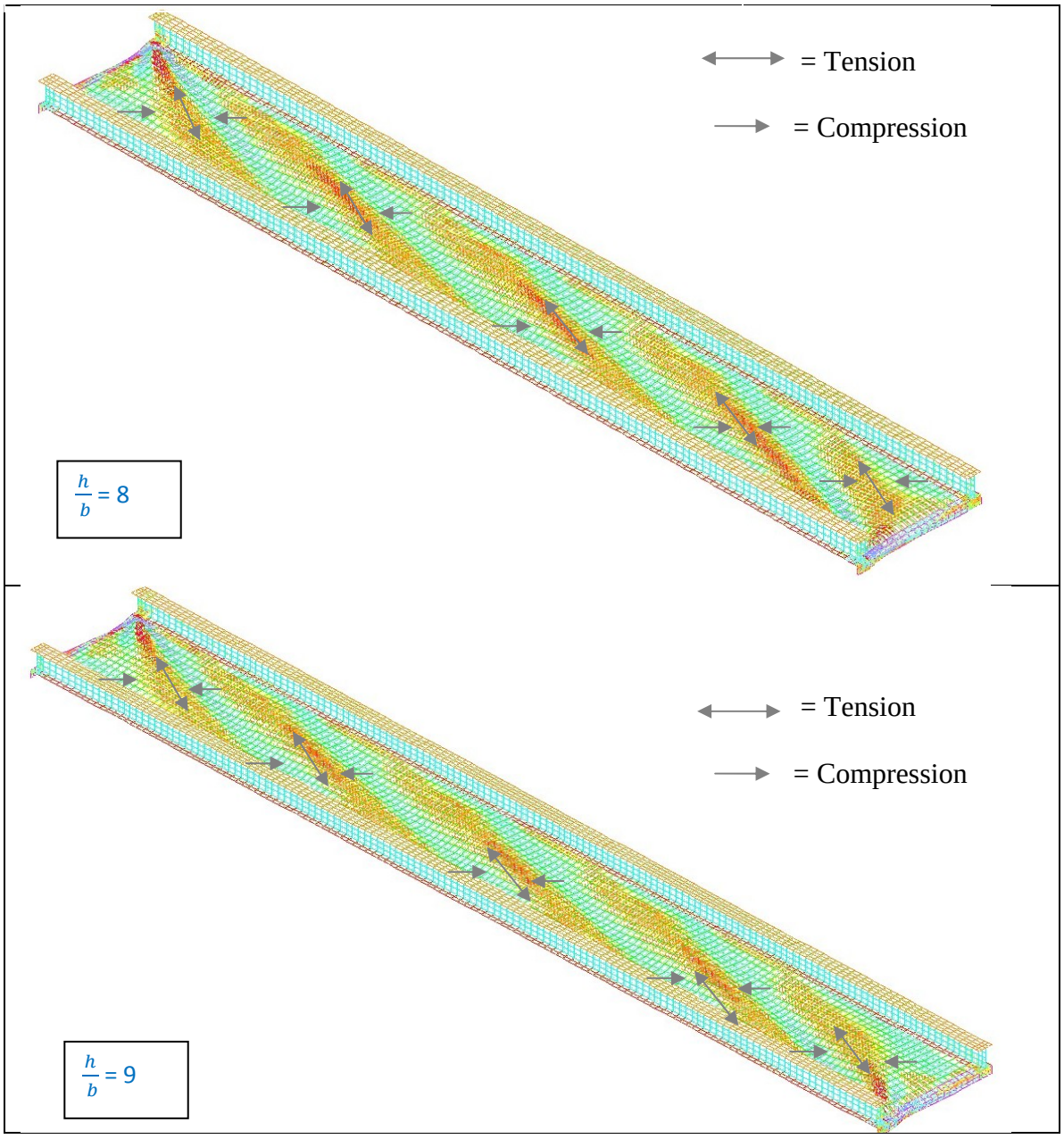

Figure 5.18 Continues….

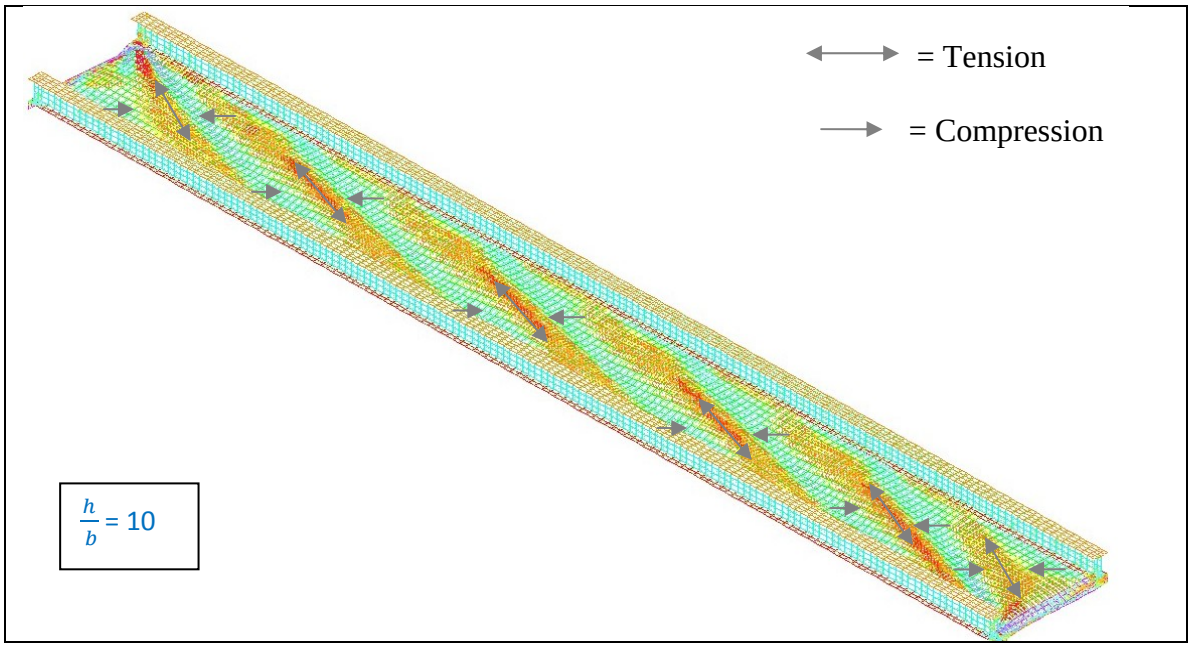

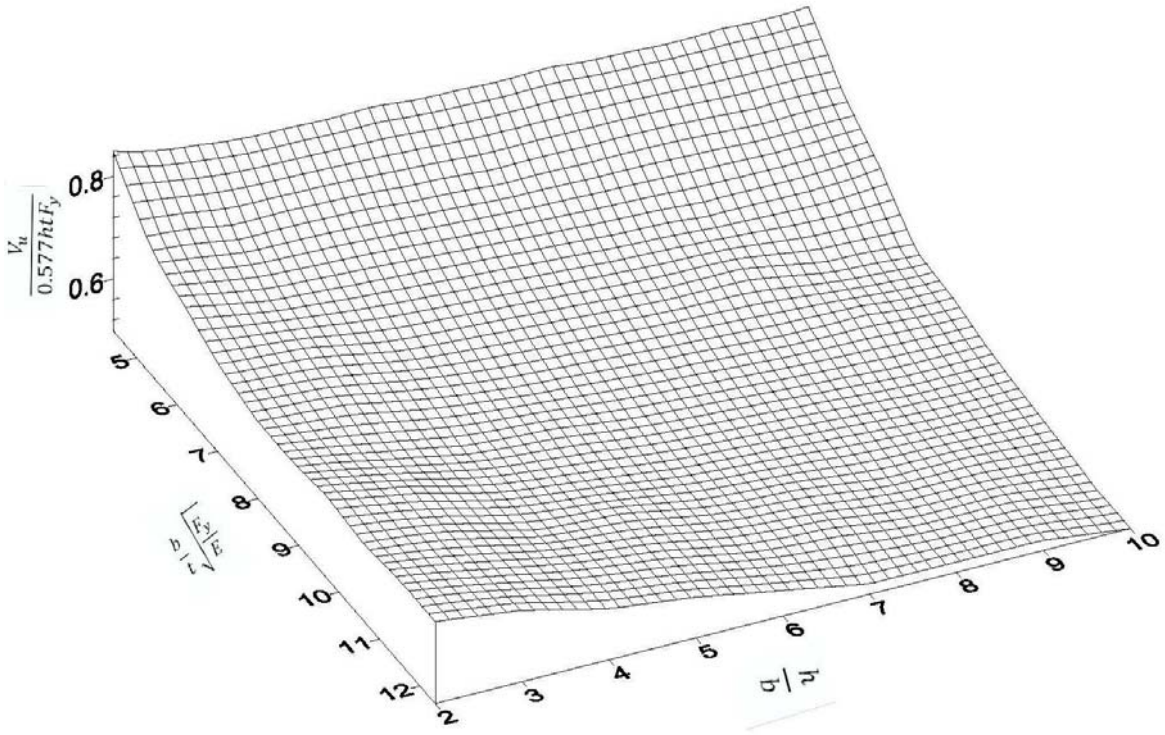

Figure 5.19 Normalized Shear versus Dimensionless Parameters

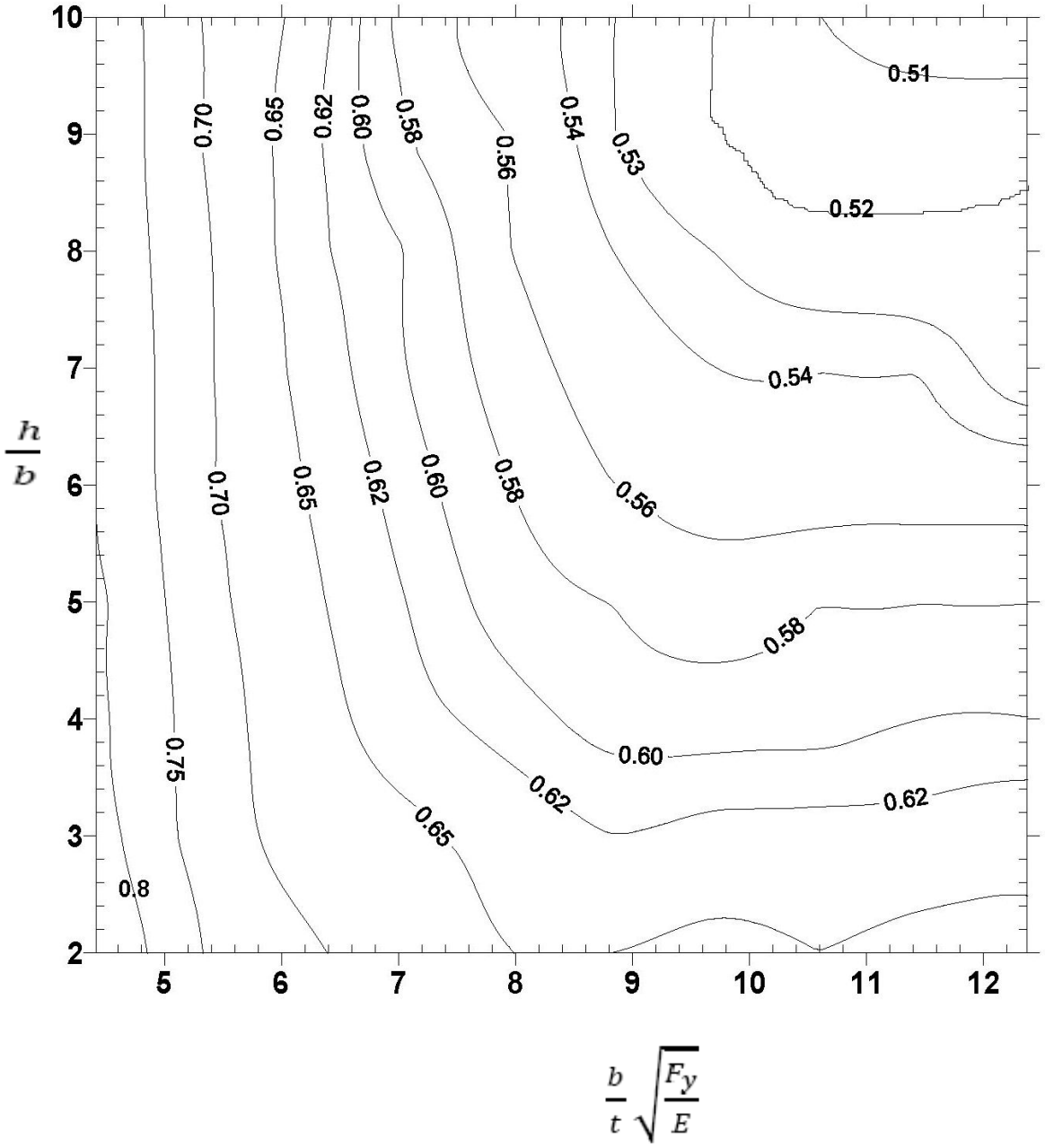

Figure 5.20 Contour of Normalized Shear versus Dimensionless Parameters

Appendix 5.1 Notations

The following symbols are used in this chapter

b = Width of plate panel

C_v = Shear coefficient

E = Young`s modulus

E_{st} = Modulus of strain hardening

F_y = Yield stress

F_u = Tensile stress

G = Modulus of shear

h = height of plate panel

k = Shear buckling coefficient

t = Thickness of plate

V = Applied shear

V_{cr} = Shear buckling strength

V_{tf} = Tension field post buckling shear strength

V_u = Ultimate shear strength

ε_y = Nominal strain at yield

δ = In-plane drift

σ = Compressive stress

σ_t = Inclined tension

σ_m = Diaphragm stress

σ_1 = Major principal stress

σ_2 = Minor principal stress

θ = Inclination of tension field

Δ_{imp}= Initial geometric imperfection distribution

Δ_o= Maximum amplitude of the initial geometric imperfection

Δ_z= Out of plane deflection

τ = Shear stress

τ_{cr} = Buckling shear stress

τ_y = Yield shear stress

τ'_{cr} = Shear stress increased

ν = Poisson's ratio

Appendix 5.2 References

ADINA , (2009), "ADINA 8.5 User Manual." ADINA R & D Inc, Watertown, MA, USA.

ASCE, (1995), "The structural Design of Air and Gas Ducts for Power Stations and Industrial Boiler Applications." Air and Gas Structural Design Committee of the Energy Division of the ASCE, Reston.

AISC ASD, (1989), "Manual of Steel Construction- Allowable Stress Design, 9th edition." American Institute of Steel Construction ,Chicago.

AISC LRFD, (2005), "Manual of Steel Construction- Load and Resistance Factor Design." American Institute of Steel Construction, Chicago.

Alinia, M. M. and Dastfan, M. (2006), "Behavior of Thin Steel Plate Shear Walls Regarding Frame Members." Journal of Constructional Research, 62 (2006), 730-738.

Alinia, M. M. , Habashi, H.R. and Khorram, A., (2009), "Nonlinearity in the postbuckling behaviour of thin Steel Shear Panels." Thin Walled Structures, 47, 412-420.

Alinia, M. M. , Gheitasi, A. and Shakiba, M., (2011), "Postbuckling and Ultimate State of Stresses in Steel Plate Girders." Thin Walled Structures, 49, 455-464.

Alinia, M. M., Shakiba,M. and Habashi, H.R., (2009), "Shear Failure Characteristics of Steel Plate Girders." Thin Walled Structures, 47, 1498-1506.

Azizinamini, A. , Hash, J.B., Yakel, A.J.and Farimani, R., (2007), "Shear Capacity of Hybrid Plate Girders." Journal of Bridge Engineering, 12(5), 535-543.

Basler, K. (1961), "Strength of Plate Girders in Shear." Journal of the Structural Division, In Proceedings of the American Society of Civil Engineers 87 (ST7), 151-180.

Basler, K. (1963), "Strength of Plate Girders in Shear." Trans. ASCE 128, pp. 683-719.

Bathe, K.J (1996), "Finite Element Procedures." Prentice Hall, 5th Edition.

Bleich, F., (1952), "Buckling Strength of Metal Structures." New York: McGraw-Hill.

Bradfored, M. A. , (1996), "Improved Shear Strength of Webs Designed in Accordance with the LRFD Specification." Engineering Journal , 33(3), 95-100.

Bruhn, E.F., (1973), "Analysis and Design of Flight Vehicle Structures." Jacobs Publication.

Charles, G.S., John, E.J.,(1997) "Steel Structures: Design and Behaviour", 4th Edition, Prentice Hall, Newyork.

CSA, (2010), "Handbook of Steel Construction." Canadian Institute of Steel Construction, Willowadale, Ontario

Daniel, V., Nicolau, M., Dimache, A. and Modiga, M. (2004), "Ultimate Strength of Plate Girders in Shear." University of Galati.

Dawson, R. G. and Walker, A. C.,(1972), "Post-buckling of Geometrically Imperfect Plates." Journal of the Structural Division. ASCE, 98(1), pp. 75-94.

Galambos, T.V., (1998), "Guide to Stability Design Criteria for Metal Structures." 5th edition. Structural Stability Council, Rolla.

Harris, H.G. and Sabnis, G., (1999), "Structural Modeling and Experimental Techniques." 2nd edition. CRC Press, New York.

Hagen, N. C. (2005), "On the Shear Capacity of Steel Plate Girders with Large Web Openings, Doctoral Thesis." Norwegian University of Science and Technology.

Hagen, N. C. and Larsen, P. K ,(2009), "Shear Capacity of Steel Plate Girders with Large Web Openings, Part 1: Modeling and Simulations." Journal of Constructional Steel Research, 65, 151-158.

Hoglund, T. (1997), "Shear Buckling Resistance of Steel and Aluminum Plate Girders." Journal of Thin-Walled Structures, 29 (14), 13-30.

John, W. and Sons, New York (1979), "Thin Plate Design for in-Plane Loading."

Kuhn, P., Peterson, J.P., Levin, I.R., (1952), "A Summary of Diagonal tension", Part 1 and Part 2, U.S. National Advisory Committee for Aeronautics, Technical Notes 2661, 2662.

Larson, M. A. and Shah, K. N., (1976), "Plastic Design of Web Openings." Journal of Structural Division, 102 (ST5, May), 1031-1041.

Langhaar, H.L., (1951), "Dimensional Analysis and Theory of Models." John Wiley, N.Y

Lee, S. c., Davidson, J. S. and Yoo, C. H., (1996), "Shear Buckling Coefficients of Plate Girder Web Panels." Computer and Structures, 56 (5), 789-795.

Lee, S. C. and Yoo, C. H., (1998), "Strength of Plate Girder Web Panels under Pure Shear." Journal of Structural Engineering, 124 (2), February, 1998, 184-194.

Lee, S. C. and Yoo, C. H. (1999), "Experimental Study on Ultimate Shear Strength of Web Panels." Journal of Structural Engineering, 125 (8), 838-846.

Lee, S. C., Lee, D.S. and Yoo, C. H. (2008), "Ultimate Shear Strength of Long Web Panels." Journal of Constructional Steel Research, Volume 64, 1357-1365.

Lee, S. C., Yoo, C. H. and Yoon, D. Y. (2002), "Behavior of Intermediate Transverse Stiffeners Attached on Web Panels." Journal of Structural Engineering ASCE 2002; 128 (3), 337-345.

Lee, S. C., Lee, D.S., Yoo, C. H. and Park, C. S. (2009), "Further Insights into Postbuckling of Web Panles. 11: Experiments and Verification of New Theory." Journal of Structural Engineering ASCE 2009; 135 (1), 11-18.

Marsh, C., Ajam, W., and Ha, H. K., (1988), "Finite Element Analysis of Postbuckled Shear Webs." Journal of Structural Engineering ASCE; 114 (7), 1571-1587.

Olaru, V. D., Nocolau, M., Dimache, A. and Modiga, M. (2004), "Ultimate Strength of Plate Girders in Shear." The Annals of 'Dunarea De Jos' University of Galati, pp. 59-64.

Paik, K. J., Thayamballi, A.K., (2003), "Ultimate Limit State Design of Steel-Plated Structures." Wiley, Edition 1.

Pellegrino, c., Maiorana, E. and Modena, C. (2008), "Linear and Non-Linear Behavior of Steel Plates with Circular and Rectangular Holes under Shear Loading." Thin-Walled Structures (2008)

Porter, D. M., Rocket, K C. and Evans, H. R. (1975), "The Collapse behavior of Plate Girders Loaded in Shear." The Structural Engineer. Vo1.53.

Salmon, G.C., Johnson, E.Y., Malhas A.F., (2008), "Steel Structures: Design and Behaviour." 5th edition. Prentice Hall, New York.

Shanmugam, N. E. and Basker, K., (2003), "Steel-Concrete Composite Plate Girders Subjected to Shear Loading." Journal of Structural Engineering , 129(9), 1230-1242.

Stein, M. N. (1947), "Buckling Stresses of Simply Supported Rectangular Flat Plates in Shear." NACA Tech. Note No. 1222.

Timoshenko, S. and Krieger, S.W.,(1959), "Theory of Plates and Shells." McGraw-Hill, Tokyo.

Timoshenko, S. P., Gere, J. M., (1961), "Theory of Elastic Stability." 2nd Edition. McGraw-Hill, New York.

Ugural, A. C., (1981), "Stresses in plates and shell." Mcgraw Hill Companies. FL. USA.

Wagner, H. (1931), "Flat Sheet Metal Girders with Very Thin Metal Web." Washington, DC, NACA TM.

White, D. W. and Barker, M. G., (2008), "Shear Resistance of Transversely Stiffened Steel I-Girders." Journal of Structural Engineering ASCE 134 (9), 1425-1436.

Young, W.C., (1989), "Roark's Formulas for Stress & Strain, 6th edition." McGraw Hill, New York.

Yoo, C. H and Lee, S. C., (2006), "Mechanics of Web Plate Postbuckling Behaviour in Shear." Journal of Structural Engineering, ASCE 132 (10), 1580-1589.

Chapter 6: Summary and Conclusions

It should be noted that a considerable progress has been made towards understanding of the behaviours of the components of large rectangular industrial ducts through these studies. The components considered in these studies were stiffener spacing and strength of plate, behaviour and strength of stiffened plate panels and shear capacity of industrial duct side panels. The following sections provide the summary and conclusions drawn from the studies for each component mentioned above. Further recommendations for future studies for each component were provided at the end of each respective chapter. Also, it should be noted here that these finding were valid for the components subjected static loading conditions and at ambient temperature.

6.1 Stiffener Spacing and Strength of Plates

Large industrial duct system is often rectangular and consists of stiffened plates, where the plates along with stiffeners act to resist the pressure loads. Since the parallel stiffeners are often closely spaced, the plate element between the pair of parallel stiffeners is often idealized as a long plate spanning between and fixed supported by those stiffeners. The internal pressure and serviceability limit determine the plate thickness and the stiffener spacing. Currently, the engineers determine the plate thickness and the stiffener spacing based on elastic large deflection plate theory in which bending and membrane actions both dictate the strength and deflection of the plate. This study postulates that the plate design allowing for partial yielding may result in economical and efficient duct system. The objective of this study is to establish relations between loads and stiffener spacing recognizing the available ductility and the true capacity of steel plates associated with

large industrial ducts. Since, large displacement analysis of plates beyond yielding is quite complicated due to nonlinearities; this investigation is based on finite element analysis of long plates made of elastic-plastic steel. A numerical parametric study was conducted. The model uses a four-node nonlinear shell element based on Mindlin/Reissner plate theory. Newton-Cotes integration scheme with seven integration points through thickness was chosen in order to trace the yielding of plate through thickness.

In order to do a manageable parametric study and to have parameters that are independent of material characteristics, a dimensional analysis was performed. Through the dimensional analysis identified the meaningful dimensionless parameters that characterize the behaviour of plate laterally loaded even into the plastic range. The dimensionless parameters selected were plate slenderness $\beta = \frac{b}{t}\sqrt{\frac{F_y}{E}}$, load parameter $Q = \frac{pE}{{F_y}^2}$, normalized deflection $\frac{\Delta}{t}$, normalized total stress $\frac{\sigma_t}{F_y}$ and normalized diaphragm stress $\frac{\sigma_m}{F_y}$. The independency of any scale and material characteristic of the dimensionless parameters was established by conducting sample analysis.

The parametric study considered the plates having various slenderness values, and the results were established for pressure $\frac{pE}{{F_y}^2}$ versus slenderness $\frac{b}{t}\sqrt{\frac{F_y}{E}}$ relations and out-of-plane deflection $\frac{\Delta}{t}$ versus slenderness $\frac{b}{t}\sqrt{\frac{F_y}{E}}$ relations for three cases namely; 0%, 16.5% and 33% of through thickness yielding of the plate. Design equations were established for

the above three cases. Results show that approximately 55% and 110% increase in load carrying capacities when 16.5% and 33% yielding is permitted. However, such yielding results in 30% and 50% increase in deflections as well. Partially yielding plates can easily satisfy the serviceability limit states and lead to economical stiffened plate system for industrial duct. The study established the design equations for industrial plates for three design scenarios namely; 0%, 16.5% and 33% of through thickness yielding of the plate as indicated below.

Cases	**Limiting Load Parameter** $\boldsymbol{Q = \frac{pE}{F_y^2}}$	**Normalized Deflection** $\boldsymbol{\frac{\Delta}{t}}$
Top fiber yields	$Q = 0.580\left(\frac{b}{t}\sqrt{\frac{F_y}{E}}\right)^{-1.10}$	$\frac{\Delta}{t} = 0.288\left(\frac{b}{t}\sqrt{\frac{F_y}{E}}\right) - 0.399$
16.5% of thickness yields	$Q = 0.864\left(\frac{b}{t}\sqrt{\frac{F_y}{E}}\right)^{-1.08}$	$\frac{\Delta}{t} = 0.330\left(\frac{b}{t}\sqrt{\frac{F_y}{E}}\right) - 0.356$
33% of thickness yields	$Q = 1.112\left(\frac{b}{t}\sqrt{\frac{F_y}{E}}\right)^{-1.05}$	$\frac{\Delta}{t} = 0.367\left(\frac{b}{t}\sqrt{\frac{F_y}{E}}\right) - 0.328$

Chapter 2 addressed the additional in-plane forces developed due to the membrane stress σ_m. The in-plane forces at end panels will be transmitted by shear to the duct effective corner elements. This shear causes additional compressive forces on the duct effective corner elements. The effective corner elements should be designed to this additional compression together with the forces due to the global bending.

An example calculation was carried out to verify and compare the proposed design method of spacing stiffeners.

6.2 Behaviour and Capacity of Stiffened Plate Panels

Large rectangular industrial duct wall panels often require regularly spaced parallel stiffeners which strengthen the thin wall plates in one direction. In the design, an appropriate stiffener member and its spacing are chosen to achieve adequate overall capacity of stiffened plate panel. In view of enormous size and the loadings associated with such duct work, generally wide flanged steel beam sections are used as stiffeners. One flange is welded to the steel plate and other flange is unsupported and unbraced. Under negative pressure loading, the unconnected flange is in compression and the other flange and duct panel are in tension. In theory, the bending capacity of wide flanged section depends on the unbraced length of compression flange. However, the web and duct plate may provide a rotational stiffness to the compression flange. This may lead to a web distorational buckling. Current design codes do not adequately address the capacity of the distortional buckling of the stiffeners. The objective of this study concerns with the behaviour, bending capacity and the design of such stiffened plate panels.

In the first step in achieving this objective, nonlinear finite element modeling techniques for stiffened plate panel were developed using finite element software ADINA. The material model selected was elastic-plastic-multilinear material model with von Mises yield criterion, associated flow plasticity based on isotropic hardening rule. The model

included the pattern of geometric imperfections and residual stresses. The Load Displacement Control incremental method was used to capture the pressure load versus displacement history even into unloading regions. Based on the comparison of the corresponding full scale test results, it was concluded that modeling techniques applied can reliably establish the behaviour and response of the stiffened plate panel subjected lateral pressure load.

In the next step in order to do a parametric study, a dimensional analysis was performed to identify the meaningful dimensionless parameters that characterize the behaviour and strength of the stiffened plate panel subjected to lateral pressure load. The dimensionless parameters include all geometric details, material characteristics, applied loading and deformation response. The dimensionless parameters were stiffener flange slenderness $\beta_1 = \frac{b_f}{t_f}\sqrt{\frac{F_{ys}}{E}}$, stiffener web slenderness $\beta_2 = \frac{h_w - 2t_f}{t_w}\sqrt{\frac{F_{ys}}{E}}$, plate slenderness $\beta_3 = \frac{b_p}{t_p}\sqrt{\frac{F_{yp}}{E}}$, stiffener overall slenderness $\beta_4 = \frac{L}{r}\sqrt{\frac{F_{ys}}{E}}$ and normalized moment capacity $\frac{M_a}{M_y}$. The completeness of the dimensionless parameters was established. Thus, the selected dimensionless parameters were found to characterize the behaviour and strength of stiffened plate panel without scale effect.

The practical range of the dimensional parameters resulted in one hundred finite element analysis models for this parametric study. As each model took considerable amount of labour to build and taking into account that manual modeling may lead accidental error

during the modeling, an external computer program that creates finite element models based on scales of fundamental parameters was developed.

Before the parametric study was done, the effect of selected dimensionless parameters was analysed. It was found that the plate slenderness $\beta_3 = \frac{b_p}{t_p}\sqrt{\frac{F_{yp}}{E}}$ and stiffener flange slenderness $\beta_1 = \frac{b_f}{t_f}\sqrt{\frac{F_{ys}}{E}}$ has very minimal effect of on the strength of the stiffened plate under bending. Then the matrix of the models was analyzed and the behaviour of the each model was observed. The failure mode observed for the stiffened plate panels subjected to bending was lateral distortional buckling of the stiffener. This type of failure mode did not result in progressive loss in buckling strength of the stiffened plate panels as overall slenderness $\beta_4 = \frac{L}{r}\sqrt{\frac{F_{ys}}{E}}$ increases.

The stiffener web slenderness $\beta_2 = \frac{h_w - 2t_f}{t_w}\sqrt{\frac{F_{ys}}{E}}$ was found to be the most influential dimensionless parameter affecting the strength and behavior of stiffened plate panel under bending. The stiffener overall dimensionless slenderness $\beta_4 = \frac{L}{r}\sqrt{\frac{F_{ys}}{E}}$ has minimal effect on the capacity of stiffened plate panel due to distortional buckling. However, the higher ratio of web depth to stiffener span leads to some local web failure at support locations. A local failure of web was triggered when the span of stiffened plate panel with higher web slenderness becomes small. The boundary between the local web crippling was defined in order to provide a design guideline that can predict the lateral distortional buckling capacity of stiffened plate panel. Based on the parametric study, design

equation was provided in terms of stiffener web slenderness $\beta_2 = \frac{h_w - 2t_f}{t_w}\sqrt{\frac{F_{ys}}{E}}$. This study has shown that the standard beam method used to estimate the capacity of stiffened plate panel was inappropriate for this type failure mode of the stiffeners. The standard beam method leads to excessive conservatism in designing stiffener sections.

It was found that the applied bending moment M_a can reach the cross sectional yield moment M_y if stiffener web slenderss $\frac{h_w - 2t_f}{t_w}\sqrt{\frac{F_{ys}}{E}}$ is less than or equal to 2.0.

This rule can be written as

$$M_a \geq M_y \ for \ \frac{h_w - 2t_f}{t_w}\sqrt{\frac{F_{ys}}{E}} \leq 2.0 \ and \ \frac{L}{r}\sqrt{\frac{F_{ys}}{E}} \geq 3.33\frac{h_w - 2t_f}{t_w}\sqrt{\frac{F_{ys}}{E}} + 0.145$$

The proposed relation between applied bending moment and stiffener web slenderness is as follows.

$$\frac{M_{cr}}{M_y} = 1.51 - 0.275\left(\frac{h_w - 2t_f}{t_w}\sqrt{\frac{F_{ys}}{E}}\right) \quad for \ \frac{L}{r}\sqrt{\frac{F_{ys}}{E}} \geq 3.33\left(\frac{h_w - 2t_f}{t_w}\sqrt{\frac{F_{ys}}{E}}\right) + 0.145$$

6.3 Shear Capacity of Side Panel of Large Industrial Ducts

In large rectangular ducts, the plate acts in conjunction with stiffeners to balance the pressure loads and to carry the dead loads and external loads to the supports. The duct side panels transmit the gravity loads to the supports by shear. Currently the plate panels for shear load are designed based on the methods used for the web of the plate girders. The behaviors and the characteristics between the web of plate girder and the plate panels are significantly different. The large aspect ratio of the side panels develops multiple bands of tension fields, whereas the methods for plate girders are based on one tension field action. In addition to carrying shear, the slender side panels are subjected to congruent pressure load. Very little research has been done dealing with industrial duct plate panel subjected to shear load. A study therefore was undertaken to review current methods of analysis and design and to propose a comprehensive method of designing industrial duct side panel for shear resistance.

A nonlinear finite element model was developed to simulate the behavior of industrial duct side panel subjected to transverse shear. Geometric and material nonlinearity, initial imperfections and initial stresses were incorporated into the model. To reach the convergence of the equilibrium of the nonlinear load-displacement path, a displacement control analysis method was used. The idealized elastic-plastic-strain hardening tri-linear material model representing mild carbon steel was used.

In order to carry out a manageable parametric study, a dimensional analysis was performed to identify the dimensionless parameters describing the behaviour of the

industrial side panel subjected to uniform shear. The identified dimensionless parameters were plate slenderness $\frac{b}{t}\sqrt{\frac{F_y}{E}}$, aspect ratio $\frac{h}{b}$, normalized shear $\frac{V}{0.577htF_y}$, normalized drift $\frac{\delta}{b}$, normalized out of plane deflection $\frac{\Delta}{t}$ and normalized diaphragm stress $\frac{\sigma_m}{F_y}$. The completeness and scale independent of the parameters identified were established through a preliminary finite element analysis. The reasonable ranges of input dimensionless parameters $\frac{b}{t}\sqrt{\frac{F_y}{E}}$ and $\frac{h}{b}$ for practical large rectangular industrial duct were established to complete the matrix of analysis models. The dimensionless parameters $\frac{\Delta}{t}$ and $\frac{\sigma_m}{F_y}$ established in Chapter 2 with respect to plate slenderness $\frac{b}{t}\sqrt{\frac{F_y}{E}}$,when the top fibre begins to yield, were used for the range of $\frac{b}{t}\sqrt{\frac{F_y}{E}}$ and $\frac{h}{b}$.

The analysis matrix considered for this study contained total of ninety analysis models. Considering the amount of labour to build each model and the possibility of accidental error during the modeling, an external computer program that create a finite element model based on scales of fundamental parameters was developed.

From the vector plots of the results, the increase in the number of bands of tension fields on the side panels were observed as the aspect ratio $\frac{b}{h}$ increases. This observation proved that the ultimate shear capacity of the side plate panel depends on the number of inclined tension fields; however on the other hand, the current method for web of large plate girder is based on one band of uniform inclined tension field. Therefore, the vertical

component of the number of bands of tension field results in contribution to the ultimate shear resistance significantly less compared to the contribution predicted by one band of tension field.

The current method used to design the web of large plate girder was modified and a method was proposed to calculate normalized ultimate shear for the side panels considered in this study.

In order to obtain the ultimate shear strengths, the peak load points from the normalized shear versus normalized drift history plots were obtained for each analysis model. The plate slenderness $\frac{b}{t}\sqrt{\frac{F_y}{E}}$ and aspect ratios $\frac{h}{b}$ were found to be the influential dimensionless parameter dictating the normalized ultimate shear capacity $\frac{V_u}{0.577htF_y}$ of slender side panels. The plate slenderness $\frac{b}{t}\sqrt{\frac{F_y}{E}}$ dominates the normalized shear strength of stockier side panels.

In order to calculate the ultimate shear capacity V_u of a side plate panel with given plate slenderness $\frac{b}{t}\sqrt{\frac{F_y}{E}}$ and aspect ratio $\frac{h}{b}$, the set of design curves (contours) were proposed. The set of design curves can be used to calculate the ultimate shear strength V_u of a large industrial duct side panel subjected shear for the range of plate slenderness and aspect ratios considered in this study.